Influence of Phosphorylation on the Pathological Conformation of Human Microtubule Associated Protein Tau

Thesis submitted to the University of Hamburg in partial fulfillment of the requirements for the award of the degree of Ph.D.

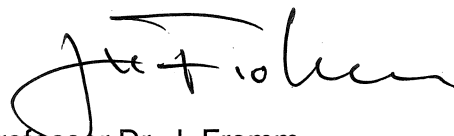Submitted by

Subashchandrabose Chinnathambi

Born in India

July, 2011

Hamburg

Genehmigt vom Fachbereich Biologie
der Fakultät für Mathematik, Informatik und Naturwissenschaften
an der Universität Hamburg
auf Antrag von Prof. Dr. E. MANDELKOW
Weiterer Gutachter der Dissertation:
Prof. Dr. M. KNEUSSEL
Tag der Disputation: 02. September 2011

Hamburg, den 28. Juli 2011

Professor Dr. J. Fromm
Vorsitzender des Promotionsausschusses
Biologie

1 Introduction

1.1 Protein misfolding diseases

The native conformation of a protein is essential for its function; however, under certain circumstances a protein loses its structural identity which may lead to aggregation. Such aggregates are causative agents of several diseases collectively known as protein misfolding diseases. These diseases can be broadly grouped into (1) neurodegenerative; aggregation occurs in the brain, (2) non-neuropathic localized; aggregation occurs in a single type of tissue other than the brain and (3) non-neuropathic systemic; aggregation occurs in multiple tissues. Some of the diseases such as Alzheimer's and Parkinson's diseases are predominantly sporadic, however hereditary forms of these disease are also reported (Chiti and Dobson, 2006). Neurodegenerative diseases include neuronal pathologic forms in which a progressive loss of structure or function of neurons is found, ultimately leading to the death of neurons. Some of the proteins that aggregate in neurodegenerative diseases are α-synuclein (in Parkinson disease), Aβ peptide and tau (in Alzheimer's disease), Huntington (in Huntington's disease) and prion protein (in Prion disease).

The aggregates of tau occur in a group of neurodegenerative diseases such as progressive supranuclear palsy, corticobasal degeneration, Pick disease, and frontotemporal dementia and parkinsonism linked to chromosome 17 (FTDP-17). These diseases, together with AD are collectively known as neurodegenerative tauopathies. The mechanisms of the formation of aggregates from soluble tau have been studied in great detail, particularly in AD and FTDP-17 (Esmaeli et al., 1994; Lee et al., 2001).

1.1.1 Alzheimer disease (AD)

In 1907, Alois Alzheimer, a German psychiatrist reported a case of a 51 year old female patient, who had been suffering from strong feelings of jealousy, increased memory impairment, disorientation, hallucinations, and often loud and aggressive behavior. After four and a half years of rapidly deteriorating mental illness, she died in a completely demented state (Alzheimer, 1970). Now this disease carries the doctor's name – Alzheimer's disease (AD). AD is the most common cause of dementia that is characterized by persistent decline of cognitive function, alterations in judgment, perception and finally personality. The occurrence of dementia is age related because the prevalence of dementia is below 1% in individuals aged 60-64 years, but increases almost exponentially in people aged 85 years or above. The prevalence of dementia was reported between 24% and 33% in the western countries (Ferri et al., 2005). On average, patients with AD live for 8-10 years after they are diagnosed, though the disease can last for up to 20 years.

Two abnormal structures in the brain are the hallmarks of AD, (i) intracellular neurofibrillary tangles (NFT) and (ii) extracellular amyloid plaques (Fig. 1.1). NFTs are composed of microtubule associated protein-tau filaments, often referred to as paired helical filaments
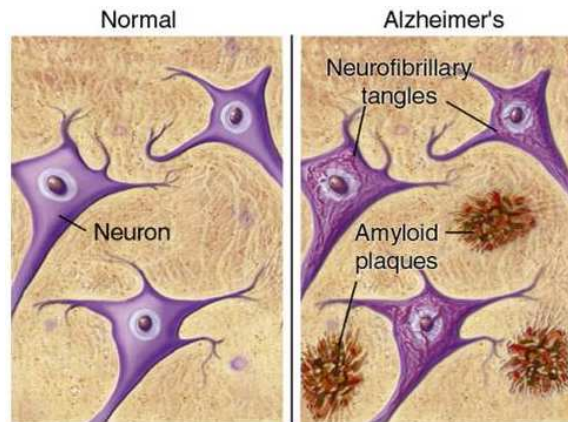
Figure 1.1: Pathological hallmarks of AD. Extracellular plaques which are deposits of Aß peptide produced from APP and the intracellular tangles which are aggregates composed of microtubule associated protein-tau are found together in AD. The formation of amyloid plaques and tangles contribute to the dysfunction and ultimately the degradation of the brain and the subsequent symptoms of AD. (http://www.ahaf.org/alzheimers/about/understanding/plaques-and-tangles.html)

(PHFs) due to their appearance in the electron microscope (EM). The extracellular plaques are composed of aggregated amyloid peptide (Aß) (Lee et al., 2001). They contain degenerated neurites and a 34-43 amino acid peptide called ß-amyloid (Aß), which has a natural tendency to form insoluble fibrils (Vickers et al., 2000). The amyloid plaques are extracellular deposits mainly located in the cortex. The Aß peptide is processed from the ß-amyloid precursor protein (ß-APP) by the enzymes ß-secretase (or ß-amyloid cleaving enzyme, BACE) and γ-secretase (Hardly and Selkoe, 2002; Cummings, 2004). Though tangles and plaques are found in conjunction, the appearance and distribution of Aß deposits are difficult to correlate with the progression of disease whereas the appearance and distribution of tangles are well correlated ("Braak stages", Braak and Braak, 1995).

1.1.1.1 Tau hypothesis in AD

Tau belongs to a class of proteins called microtubule-associated proteins (MAPs) whose major function is to stabilize microtubules (MT) that serve as cytoskeleton. Microtubules are important for cell viability, particularly for growth development of neurons. The main known biological function of tau is to stimulate microtubule assembly and to stabilize the structure of microtubules. Tau is a phosphoprotein and its phosphorylation state is developmentally regulated (Kopke et al., 1993). In AD, tau is hyperphosphorylated at many sites (Gong et al., 2005) probably due to the disturbance in the regulation of tau phosphorylation which is achieved by the

balanced activity of multiple kinases and phosphatases. The phosphorylation sites of tau are mainly localized in the proline-rich (residues 172-251) and C-terminal tail (residues 368-441)
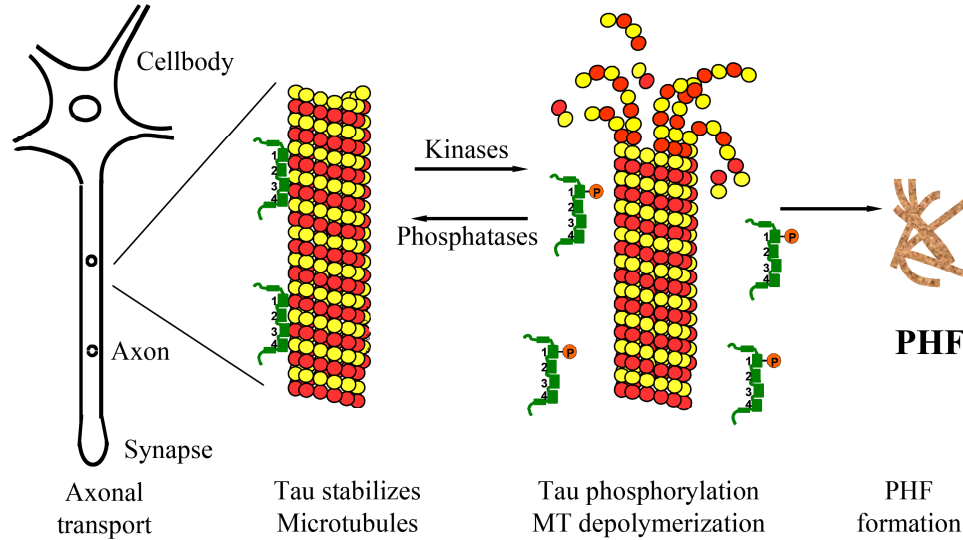
Figure 1.1: Tau hypothesis of AD. Hyperphosphorylation of tau due to the disturbances in the regulation of activity of kinases and phosphatases results in the detachment of tau from microtubules. Subsequent failure of microtubules stabilization causes disturbance in the axonal transport. Accumulation of hyperphosphorylated tau in cytosol might favor the aggregation into PHFs which can further augment the obstruction of axonal transport. Ultimately, normal neuronal functions are deceased leading to neurodegeneration (reproduced from Mandelkow and Mandelkow, 1998).

regions, which flank the repeat domain. Hyperphosphorylated tau can no longer bind to microtubules and fails to stabilize them causing a disturbance of normal function in neurons (Fig. 1.2) (Mandelkow and Mandelkow, 1998). Because of phosphorylation the local concentration of tau may be increased in the cytosol which might favor the aggregation of tau into PHFs and larger aggregates. In addition, both the loss of microtubule stabilization and the tangle formation could compromise neuronal and synaptic function (Thies and Mandelkow, 2007). Loss of microtubule stabilization and the tangle formation due to aggregation could compromise neuronal and synaptic function.

1.1.2 Frontotemporal dementia and Parkinsonism linked to chromosome 17

The microtubule-associated protein tau is necessary for the establishment of neuronal polarity, axonal outgrowth, axonal transport, and the maintenance of axonal morphology (Stamer et al., 2002). Tau dysfunction has long been correlated with a variety of neurodegenerative diseases, including Alzheimer's disease, frontotemporal dementia, and parkinsonism associated with chromosome-17 (FTDP-17) (Esmaeli Azad et al., 1994). Each of these diseases is characterized by extensive neuronal cell death and the presence of abnormal pathological fibers composed primarily of hyperphosphorylated tau (Buee et al., 2000; Lee et al., 2001; Gamblin et al., 2003). In 1998, direct genetic linkages between mutations in the tau gene and FTDP-17 were reported

(Hutton et al., 1998; Hong et al., 1998; Spillantini et al., 1998). Frontotemporal dementias are characterized by a confined atrophy of frontal and temporal lobes of the cerebral cortex. This occurs rarely as familial but more commonly as sporadic form of diseases. Many forms of familial frontotemporal dementia with Parkinsonism are linked to chromosome 17q21-22, hence their name FTDP-17 (Wilhelmsen et at., 1994; Hutton et al., 1998; Poorkaj et al., 1998; Spillantini et al., 1998). The gene coding tau protein is localized to chromosome 17q21-22 and all cases of FTDP-17 that has been characterized showed pathology caused by tau filaments. Presently, 32 different mutations in the tau gene are known to occur in FTDP-17. These mutations include either missense, deletion or silent mutation in the coding region (Fig. 1.3) or intronic mutations located close to the splice-donor site of the intron following the alternatively spliced exon 10 (R2) (van Swieten and Spillantini, 2007).

Tau mutations in FTDP-17 fall largely into two categories: those that affect (i) the alternative splicing of pre-mRNA and (ii) the normal function of tau (e.g. binding to microtubules or aggregation propensity). Most of the missense mutations that occur in repeat domains reduce the binding ability of tau to microtubules (Hasegawa et al., 1998; Hong et al., 1998; Barghorn et al., 2000). A number of other missense mutations may promote the aggregation of tau
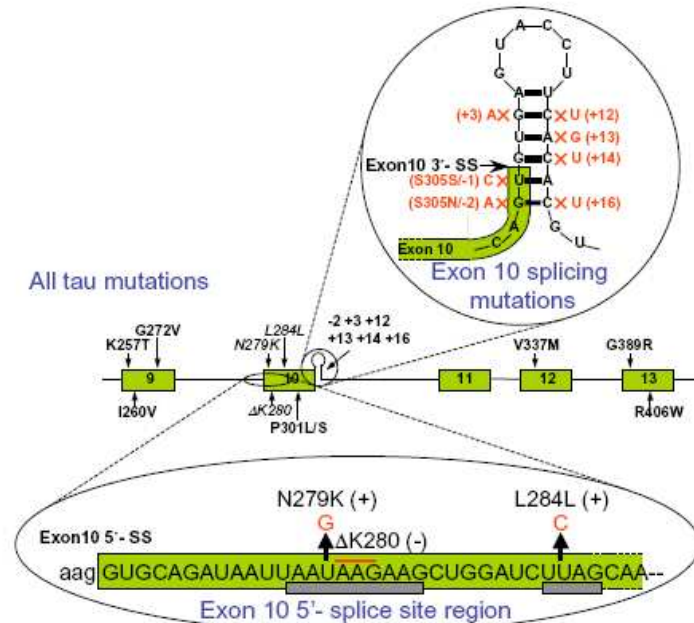
Figure 1.3: Mutations in the tau gene in FTDP-17. Tau mutations that occur in FTDP-17 are shown. Mutations influence either the splicing of exon 10 (alternating ration of 3R and 4R isoforms) or function of tau (mostly by increasing aggregation ability or reducing microtubules binding ability). The mutations are numbered according to the longest isoform-htau40 (441 amino acids) and are located in the coding region (reproduced from Hutton et al., 1998).

 (Goedert et al., 1999; Barghorn et al., 2000; von Bergen et al., 2001). Mutations such as R5L, K257T, I260V, G272V, ΔK280, P301L, Q336R, V337M, and R406W are shown to accelerate the tau aggregation compared to the wild type in the presence of aggregation-inducing cofactors (heparin or arachidonic acid). The intronic mutations as well as most of the coding region mutations in exon 10 (N279K, L284L ΔN296, N296N, N296H, S305N, and S305S) increase the splicing of exon 10, thus decreasing the ratio of 3R to 4R (Hutton et al., 1998; D'Souza et al., 1999; Yoshida et al., 2002). Mechanistically, both 3-repeat and 4-repeat tau bind directly to microtubules, stimulate microtubule polymerization, and regulate microtubule dynamics (Trinczek et al., 1995). Both quantitative and qualitative mechanistic differences exist between the two isoform classes, with 4-repeat tau generally being more potent than 3-repeat tau (Goode et al., 2000).

1.2 Tau: A neuronal microtubule associated protein

The establishment of the intricate wiring of the nervous system requires terminal neuronal differentiation, an event that is characterized by the formation of specialized cytoplasmic domains e.g. axons and dendrites. Microtubules have spatially and temporally distinct properties within each subcellular compartment (Ahmad et al., 1993). For example, within the body of elongating axonal projections, stable microtubules are organized in a polarized array. The structural integrity of microtubules provides scaffolding for the transport of membranous organelles and/or cytoskeletal elements to the active growing tips of the neuronal processes. In contrast to the stable microtubules in the axonal projections, growth cone microtubules are highly dynamic structures that rapidly extend and retract. The distinctive properties of microtubules in selected neuronal compartments arise in part from the regulated expression and subcellular localization of the structural microtubule associated protein families, for example tau, MAP1, and MAP2 (Caceres et al., 1992; Gordon-Weeks, 1993; Esmaeli-Azad et al., 1994).

Tau was initially identified in 1975 by Weingarten and co-workers as a protein belonging to a heat stable family of microtubule-associated proteins that co-purify with tubulin. Furthermore, they found that tau restores the microtubule assembly competence of phosphocellulose-purified (PC) tubulin that is essentially devoid of MAPs. They also found that tau functions stoichiometrically rather than catalytically. In other words the ability of tau to promote microtubule assembly is a characteristic of the binding of tau to tubulin (Weingarten et al., 1975). A single gene encoding tau generates six main isoforms ranging from 325 to 441 amino acid residues, in the human central nervous system by alternative splicing, and several further variants in peripheral nerves (Goedert, 1996; Andreaidis, 2005). Tau isoforms are categorized on

the basis of alternatively spliced domains near the N-terminus (insert domains denoted as I) and in the C-terminal half (second repeat domain denoted as R2).

Tau domains are further defined based on the character of the primary sequence (Fig. 1.4). The part of N-terminal with amino acids The establishment of the intricate wiring of the nervous system requires terminal neuronal differentiation, an event that is characterized by the formation of specialized cytoplasmic domains e.g. axons and dendrites. Microtubules have spatially and temporally distinct properties within each subcellular compartment (Ahmad et al., 1993). For example, within the body of elongating axonal projections, stable microtubules are organized in a polarized array. The structural integrity of microtubules provides scaffolding for the transport of membranous organelles and/or cytoskeletal elements to the active growing tips of the neuronal processes. In contrast to the stable microtubules in the axonal projections, growth cone microtubules are highly dynamic structures that rapidly extend and retract. The distinctive properties of microtubules in selected neuronal compartments arise in part from the regulated expression and subcellular localization of the structural microtubule associated protein families, for example tau, MAP1, and MAP2 (Caceres et al., 1992; Gordon-Weeks, 1993; Esmaeli-Azad et al., 1994).

Tau isoform	Denotation	Number of Amino Acids	Molecular Weight (Da)
hTau23	0I/3R	352	36750
hTau37	1I/3R	381	39720
hTau39	2I/3R	410	42603
hTau24	0I/4R	383	40007
hTau34	1I/4R	412	42967
hTau40	2I/4R	441	45850

Table 1.1: List of tau isoforms present in CNS. This table shows tau isoforms present in CNS listed by name, denotation based on the presence or absence of I and R domains, number of amino acids and the molecular weight (this table reproduced from Goedert et al., 1989).

The domains of tau are broadly divided into an acidic N-terminal 'Projection domain' (M1-Y197) and a C-terminal 'assembly domain' (S198- L441) based on limited proteolysis and microtubule binding ability (Gustke et al., 1994). Tau domains are further defined based on the character of the primary sequence (Fig. 1.4). The part of N-terminal with amino acids M1-G120 constitutes the acidic domain. This domain includes two insert domains that are alternatively spliced (I1 and I2; E42-A103). The region G120-Q244 is basic in nature, but in addition proline is a prominent feature in the region (hence named proline rich region with further subdivision into P1and P2 at Y197).The region T244-K368 is characterized by three or four imperfect repeats (R1-R4) of 31or 32 residues.
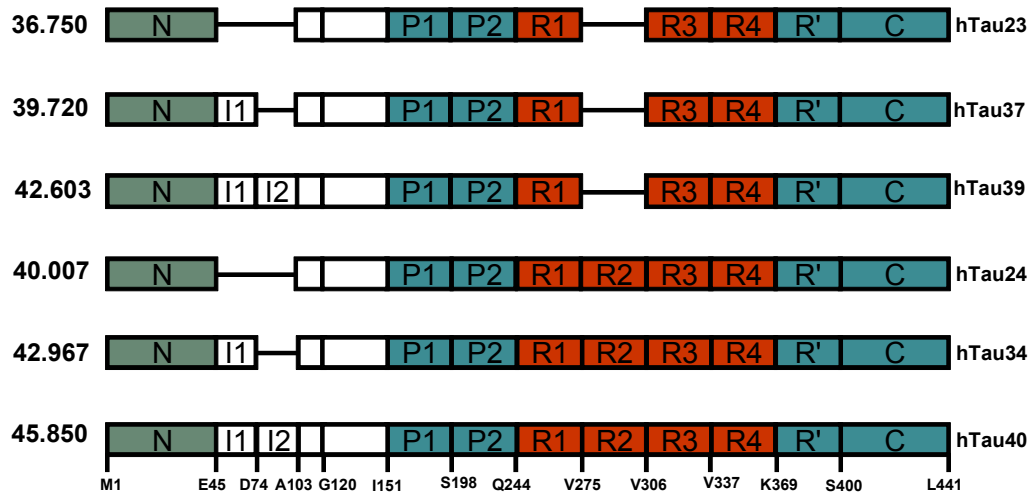
Figure 1.4: Domain organization of Tau. Tau isoforms in the CNS are represented with the organization of domains.Tau domains are broadly divided into N-terminal 'projection domain' (amino acids M1-Y197) and C-terminal 'assembly domain' (amino acids S198-L441).The C-terminal assembly domain includes three or four pseudo-repeats (~31 residues each, R1-R4), which together with their proline-rich flanking regions (P1 and P2) constitute the microtubule binding region. Repeat domain R2 and the two near N-terminal inserts (I1 and I2) may be absent due to alternative splicing (reproduced from Gustke et al., 1994 with modification).

1.2.1 Role of Tau in the Normal developmental and Maintenance of the Nervous System

Early evidence supported the role of tau in regulating assembly, stabilization, and bundling of microtubules. For example, microinjection of tau into rat fibroblasts increased the microtubule mass and enhanced microtubule stability (Drubin and Kirschner, 1986). Microtubules that serve as tracks for motor proteins are important for the intracellular transport of vesicles, organelles, and protein complexes by motor proteins (Hirokawa, 1993, 1994; Garcia and Cleveland 2001). Over-expression of tau in Chinese hamster ovary (CHO) cells causes a change in cell shape, retarded cell growth and dramatically altered the distribution of various organelles that are known to be transported via microtubule-dependent motor proteins (Ebneth et al., 1998). Mitochondria fail to be transported to peripheral cell compartments and cluster in the vicinity of the microtubule-organizing center. The endoplasmic reticulum becomes less dense and no longer extends to the cell periphery. In differentiated N2a cells, the over expression of tau leads to disappearance of mitochondria from the neurites. These effects are caused by tau's binding to microtubules and slowing down intracellular transport by preferential impairment of plus-end-directed transport mediated by kinesin like motor proteins. (Ebneth et al., 1998). Furthermore, primary cerebellar neurons treated with antisense oligonucleotides complementary to the 5' sequences of the tau gene, show a role for tau in the establishment of neuronal polarity, axonal outgrowth and process stability (Caceres and Kosik, 1990). Neuronal polarity is also established by the transport of tau mRNA to the proximal axon where translation occurs (Litman et al., 1994).

On the other hand, definitively unraveling the physiological role of tau in whole animal models has been more challenging. Since tau was initially isolated due to its microtubule assembly and stabilizing properties, it was assumed that tau plays a pivotal role in axonal stability *in vivo*. Although cell culture evidence (as detailed above) appears to demonstrate an essential role in axonal morphogenesis, the original tau knockout mouse exhibited only subtle differences in neuronal organization (Harada et al., 1994; Dawson et al., 2001). In addition, the primary hippocampal cultures from the original tau knockout strain failed to show any deficiencies in axonogenesis. However, in comparison to normal cultures, tau deficient neurons from this stain exhibit a delay in development, which is not compensated for by non-tau MAPs (Dawson et al., 2001). Results from a mouse line with knockouts of both MAP1and tau (Takei et al., 2000) indicate that tau is functionally redundant with the ubiquitously expressed neuronal MAP1 since homozygous double knockouts exhibit a very strong lethal phenotype, as would be expected from ablating essential neuronal functions (reviewed in Garcia and Cleveland, 2001). Tau and MAP1 appear to act cooperatively to regulate axonal elongation of both commissural fibers and of noncommissural long tracts in the cerebellum and the spinal cord. Tau and MAP1 also display an integral role in neuronal migration as evidenced by the disruption of the neuronal layer formation in the mutant mice. In culture, neurons from the double knockout mice exhibit a delay in neuronal migration along with a concurrent suppression of the elongation step of the leading process. Cultures from the double knockout heterozygotes also show abnormalities in the shape and cytoskeletal organization of growth cones. It is not yet known whether this is due to the lack of tau or MAP1 gene function or a secondary result of altered microtubule properties.

1.2.2 Tau phosphorylation and pseudophosphorylation

Tau can be phosphorylated by multiple kinases at multiple sites (Fig. 1.5) (Johnson and Stoothoff, 2004). The phosphorylation sites can be broadly subdivided into three classes: (i) Several SP/TP motifs in the flanking regions of the repeats that are targets of proline-directed kinases such as glycogen synthase kinase-3ß (Ishiguro et al., 1993), cyclin-dependent kinase 5 (CDK5) (Baumann et al., 1993) or mitogen activated kinase (MAPK) (Drewes et al., 1992; Lu et al., 1993). (ii) KXGS motifs in the repeats that are targets of non-proline directed kinases such as protein kinase-A (PKA), microtubule affinity regulating kinase (MARK) (Drewes et al., 1997) and synapses of amphids defective family kinases (SADK) (Kishi et al., 2005). (iii) Tyrosine residues at Y18 and Y394 that are targets of src family kinases (SFK) such as fyn (Lee et al., 1998: Lee, 2005) and c-Abl (Derkinderen et al 2005). Tau is dephosphorylated by several protein phosphatases, most notably PP1, PP2, PP2B, and PP5 (Tian and Wang, 2002; Gong et al., 2004). Nonetheless, PP2A is believed to be the major tau phosphatase. Specific PP2A isoforms bind to

MTs with distinct affinities *in vitro*, and these interactions differentially inhibit the ability of PP2A to dephosphorylate various substrates including tau (Sontag et al., 1999).

The SP/TP phosphorylation has only a moderate influence on tau-MT interaction but is strongly up-regulated in AD and other tauopathies and is therefore used for post-mortem diagnosis of AD patient (Mandelkow et al., 2007). Other phosphorylation sites include targets of non-proline directed kinases – PKA (214), MARK (KXGS motifs including Ser^{262}, Ser^{356}), SADK (Ser^{262}) or Ca2+/ calmodulin-dependent protein kinase II (S^{416}) (Fig. 1.5).

Phosphorylation at Ser^{262} or Ser^{214} result in strong reduction of tau's ability to bind microtubules (Brandt et al., 1994; Drewes et al., 1997; Ebneth et al., 1999) and phosphorylations at these sites are features of AD (Gustke et al., 1992; Mandelkow et al., 1995; Mandelkow and Mandelkow, 1998). Enhanced phosphorylation at several SP/TP motifs and at S214 has been shown in mitotic cells (Illenberger et al., 1996). In addition, phosphorylation of Ser^{214}, the major protein kinase-A target site in the proline-rich domain of tau, decreases the MT-stabilizing and MT-nucleating effects exerted by tau. This S214 phosphorylation catalyzes the detachment of tau from microtubules and thereby, increases the dynamics of MTs. These studies underline the role of tau and its phosphorylation in the regulation of microtubule dynamics.
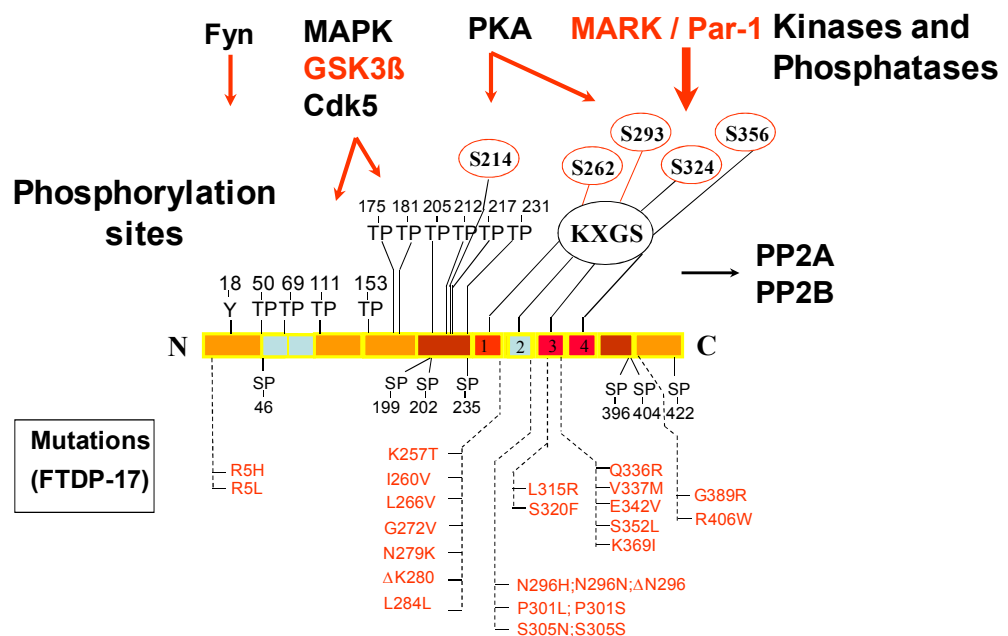
Figure 1.5: Tau domains, mutations and phosphorylation sites of tau: Full length isoform htau40 is shown with phosphorylation targets of many different kinases. The SP/TP motifs are the main targets for proline directed kinases such as GSK3ß, CDK5 and MAPK. S214 and KXGS motifs are targets of non-proline directed kinases such as PKA, MARK and SADK (Illenberger et al., 1996). Tyrosine residues at 18 and 394 are targets of src family kinases such as fyn and c-Abl. The phosphorylated tau can be dephosphorylated by phosphatases such as PP2A and PP2B (Sontag et al., 1999).

The activity of GSK-3ß is furthermore regulated by its own phosphorylation. Phosphorylation of GSK-3ß on Tyr-216 increases its activity, and can occur in an autocatalytic process (Wang QM et al 1994). *In vivo* as well as *in vitro*, tau becomes a more favorable substrate for GSK-3ß when it is pre-phosphorylated either by a non-proline dependent kinase (Liu et al., 2004; Wang et al., 1998) such as the cAMP-dependent protein kinase (PKA) or by another proline-dependent kinase such as the CDK5 cyclin-dependent kinase (Sengupta et al. 1997; Landrieu et al., 2010). Tau is phosphorylated by PKA at Ser208, Ser214**,** Ser324, Ser416, Ser356, and Ser409 sites, with a clear preference for the Ser214 site (Landrieu et al., 2006; Scott et al., 1993), whereas CDK5 phosphorylates tau at the S235 site (Landrieu et al., 2010; Peterson et al., 2010). The GSK-3ß phosphorylation of full length tau 441residues has been unraveled or depicted by two dimensional phosphopeptide mapping, immunuoblotting with phosphorylation-sensitive antibodies and phosphopeptide sequencing. From these studies it has been shown that GSK-3ß phosphorylates predominantly Ser/Thr-Pro motifs in tau protein which exist as closely spaced pairs, in the order Ser396/Ser404, Ser46/Thr50 and Ser202/Thr205, but not at the Ser262 position. In HEK-293 cells co-transfected with GSK3ß and tau, a direct phosphorylation of tau at the Ser202 position was observed but no phosphorylation for the Ser262, Ser235 and Ser404 was found (Li et al., 2006b). The *in vivo* phosphorylation of Ser396 would hence occur sequentially, with a priming kinase phosphorylating Ser404 first, followed by GSK3ß that sequentially phosphorylates Ser400 and then Ser396. By transfecting the same HEK-293 cells with tau, GSK3ß and CDK5, it was found that CDK5 could play the role of the priming kinase as it phosphorylates the Ser202, Ser235, and Ser404 sites (Li et al., 2006a). The Ser235 phosphorylation by CDK5 thereby enhances GSK3ß-catalyzed Thr231 phosphorylation and the Ser404 phosphorylation by CDK5 enhances sequential phosphorylation of Ser400 and Ser396 by GSK3ß (Li et al., 2006b). However these three residues (Ser396, Ser400, and Ser404) can be phosphorylated by GSK3ß alone, without priming. Ser404 is essential in this process, as its mutation to Alanine prevents further phosphorylation by GSK-3ß.

The highly phosphorylated status of the tau protein in embryonic stage and abnormal tau phosphorylation at Ser^{396} in AD recapitulates development and contributes to reduced microtubule binding (Bramblett et al., 1993). The embryonic stage of tau demonstrates hyper-phosphorylation of the shortest tau isoform containing the majority of PHF-like epitopes (Matsuo et al., 1994). In torpor during hibernation in animal brain (European ground squirrels), highly phosphorylated tau containing a number of PHF-like epitopes is generated. PHF-like phosphorylation of tau was not associated with fibril formation and it was fully reversible after arousal. The distribution of PHF-like tau follows a consistent pattern, being most intense in the entorhinal cortex, hippocampus, and isocortical areas and lesser reactivity was present in CA1

neurons while dentate gyrus cells are not reactive. Formation of PHF-like tau in CA3 neurons is paralleled by the regression of synaptic contacts the mossy fiber system terminating on CA3 apical dendrites. Mossy fiber afferentation was re-established during arousal, concomitantly with the decrease of PHF-like tau in CA3 neurons.

These findings implicate an essential link between neuronal plasticity and PHF-like phosphorylation of tau. The repeated formation and degradation of PHF-like tau might, thus, represent a physiological mechanism not necessarily associated with pathological effects (Arendt et al., 2003).

Finally, Planel and coworkers (Planel et al., 2007) reported that anesthesia induced tau hyperphosphorylation but did not affect APP metabolism. Hyperphosphorylated tau was not relocalized to the somodendritic region. Anesthesia induced tau phosphorylation was mediated by hypothermia and by inhibition of IPP2A is an inhibitor of PP2A (Planel et al., 2007). Recently the same group (Planel et al., 2008) reported that hyperphosphorylation impaired tau ability to bind and polymerize MTs, but did not detach it from MTs in normal mice. Neither normal nor human Tau (hTau) expressed in transgenic mice however, displayed a breakdown of MTs. These results demonstrate that 4R tau was tightly bound to MTs and did not readily dissociate, whereas 3R was more sensitive to the effects of phosphorylation, resulting in its dissociation from the MTs. However, this dissociation did not lead to collapse the MT network (Planel et al., 2008). In these normal physiological situations, tau occurs in highly phosphorylated, so called PHF similar phosphorylation form which can be reversibly dephosphorylated, and without any pathological consequences tau protein exerts its cellular function in a new basal degree of phosphorylation.

On the other hand in Alzheimer's disease the hyperphosphorylated tau was found in abnormal fibers, which are one of the histopathological hallmarks of this type of dementia in brain (Lee et al., 2001; Delacourte et al., 2000). The hyperphosphorylation of tau protein in physiological situations runs on a fine line, and some unknown factors in the pathological conditions of Alzheimer's disease are able to direct hyperphosphorylated protein tau into abnormal fibers.

The protein kinase MARK can phosphorylate several sites within the repeats (notably the KXGS motifs including Ser^{262}, Ser^{324}, and Ser^{356}). The KXGS sites are not exclusively the targets of MARK as SAD can also phosphorylate tau at S262, which has been shown to be required for neuronal polarity (Kishi et al., 2005).
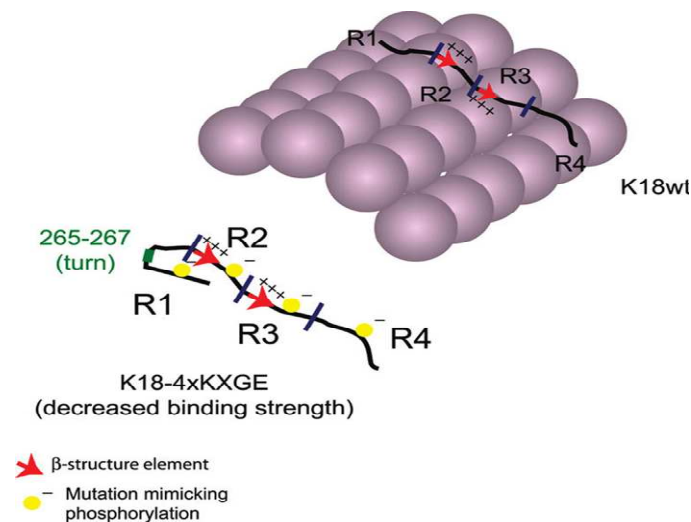
Figure 1.6: The conformational changes induced by pseudo-phosphorylation of the repeat domain of tau: Wild-type tau can bind to microtubules, whereas the construct mutated at repeat domain (4X KXGE) can no longer bind due to the formation of a turn and the resulting contact between repeat domains R1 and R2, which interferes with MT binding. Phosphorylated groups are shown as yellow dots (reproduced from Fischer et al., 2009).

Phosphorylation at these sites appears early in AD brain (Augustinack et al., 2002) and MARK phosphorylation sites on tau are elevated in transgenic mouse models of tauopathy (Mocanu et al., 2008). Phosphorylation of tau or related MAPs by MARK appears to be important for the establishment of cell polarity and for the outgrowth of neurites (Kosik and McConlogue, 1994; Biernat and Mandelkow, 1999), but overactivity of MARK leads to cell death due to microtubule destabilization caused by phosphorylation of tau at the KXGS motifs in the repeat domain (Drewes et al., 1998 and fig. 1.6).

The interaction between tau and src family non-receptor tyrosine kinases represents a new function of tau mediated by the proline-rich region of tau and the SH3 domain of fyn or src. This interaction has the potential to confer novel cellular activities for tau in the growth cone and in the membrane. The subsequent finding that tau is tyrosine phosphorylated has led to the observation that tau in neurofibrillary tangles is tyrosine phosphorylated (Y18) (Lee et al., 1998; Lee, 2005), lck (Y29) (Williamson et al., 2002) and c-Abl (Y394) (Derkinderen et al., 2005). In addition, upregulation of fyn was shown to occur in AD brain (Shirazi and Wood, 1993). It is believed that the phosphorylation of tyrosine residues in tau may play an important role in both physiological (e.g. cell signaling) and pathological conditions (e.g. AD).

1.2.3 Pathological modifications of tau

In AD, the properties of tau change in several ways leading to loss of its normal cellular function followed by its aggregation. The modifications of tau in AD and their consequences are the following:

(i) Tau undergoes an abnormal 'hyperphosphorylation' at many sites, mostly at SP/TP motifs. Analysis of brain tissue and cell models of AD revealed that abnormal phosphorylation occurs before aggregation (Mandelkow et al., 1995; Trojanowski and Lee 1995).

(ii) Tau is hyperphosphorylated at a number of sites and does not bind to microtubules resulting in disassembly of microtubules and subsequent decrease in axonal transport (Mandelkow et al., 2007). In addition, hyperphosphorylated tau gets aggregated into PHFs, despite tau being a highly soluble protein. Nevertheless, there is still a debate over the influence of hyperphosphorylation on the aggregation of tau.

(iii) It appears that tau self-assembles by association of the microtubule binding domains/repeats and that the abnormal hyperphosphorylation promotes the self-assembly of tau into PHFs by neutralizing the inhibitory basic charges of the flanking regions (Alonso et al., 2001).

(iv) A possible hypothesis can be that hyperphosphorylation changes tau properties in some ways (e.g., its conformation, binding) such that aggregation into PHFs is promoted. In fact we have shown that pseudo-phosphorylation at certain combinations of epitopes induce changes in the global conformation of tau and are responsible for increased aggregation propensity (Jeganathan et al., 2008). The effects of tau phosphorylation on microtubule interactions may or may not be parallel to the effects on self-assembly of tau into PHFs. This same phosphorylation that prevents tau binding to microtubules may increase or protect tau from self-assembling into PHFs (Jeganathan et al., 2008).

(v) Tau shows a loss of microtubule binding which is probably due to hyperphosphorylation at sites (e.g. S262 or S214) that detach tau from microtubules (Drewes et al., 1997). This could account for the disappearance of microtubules causing the breakdown of intracellular traffic which would result in the death of neuron.

(vi) Tau aggregates into 'paired helical filaments' (PHFs) which show a two-stranded appearance, with a width of 10-20 nm (Crowther, 1991). The PHFs in turn bundle into neurofibrillary tangles.

(vii) Proteolysis and ubiquitination are post-translational modifications of tau that probably represent cellular attempts to degrade the aberrant protein via the proteasome or calpain pathway (Litersky and Johnson, 1995). The truncations of tau at the C-terminus (E391) by unidentified proteases (Novak et al., 1993) and at D421 by members of the caspase family (Gamblin et al., 2003b; Rissman et al., 2004) have been shown to increase the rate of polymerization. This could be due to nucleation of the aggregation by some proteolytic fragments and exposure of certain residues with increased seeding capacity. Caspase-cleaved tau (Δtau) may initiate or accelerate the development of tangle pathology. Tau, when cleaved by caspases at Asp^{421}, forms filamentous aggregates *in vitro*. Caspase-cleaved tau also adopts the MC1-conformation, one of

the earliest pathologic events in tangle formation. Importantly, Δtau occurs early in the development of tangle pathology within AD brains and in a transgenic mouse model of AD (Cotman et al., 2005). In neurons treated with amyloid-ß (1-42) peptide, tau gets rapidly cleaved at Asp[421] and this proteolysis appears to precede the apoptotic destruction of the nucleus. Furthermore, the caspase cleavage of tau generates a truncated protein that lacks its C-terminal 20 amino acids and assembles more rapidly and more extensively into tau filaments *in vitro* than the wild type tau (Gamblin et al., 2003b)

(viii) Nitration and glycation are the other post-translational modifications of tau in AD. Nitration of tau is shown to be a salient feature of diverse tauopathies (Horiguchi et al., 2003) and antibodies against site specific nitration in tau stains AD brain but not the normal brain (Reynolds et al., 2005).

(ix) Pseudophosphorylation and glycation of tau protein enhance but do not trigger fibrillization *in vitro* (Necula et al., 2004). Glycated tau and pseudophosphorylation of single site tau mutants (S199E, T212E and S214E), a double mutant (T212E/S214E) and a triple mutant (S199E/S202E/S205E) yielded increased filament mass at equilibrium relative to wild-type tau. Increases in filament mass correlated strongly with decreases in critical concentration, indicating that both pseudophosphorylation and glycation promoted fibrillization by shifting equilibrium toward the fibrillized state. The site-specific post-translational modifications can stabilize filaments once they nucleate (Necula et al., 2004).

(x) The acetylation of tau inhibits its function and promotes pathological conformation of tau and aggregation in AD and related tauopathies. Acetylation of tau aggregates was associated with hyperphosphorylated, ThS positive tau inclusions on both transgenic mouse models and human tauopathies. This implies that negative regulation of tau function could occur via phosphorylation and acetylation events either separately or in combination. Tau is extensively phosphorylated on at least 25 distinct serines/threonines. In contrast, tau acetylation in cells was specifically detected on four lysine residues, three of which are located within the MT-binding repeats (Cohen et al., 2010).

(xi) Tau acquires pathological conformation before its aggregation in AD brain as determined by tau's immunoreactivity with certain antibodies that detect an early conformational change of tau in AD (e.g. Alz-50, MC1, and Tau-66) (Carmel et al., 1996; Jicha et al., 1977a).

1.2.4 Structural properties of tau

1.2.4.1 Structure of soluble tau

Tau when first isolated from brain showed surprising heat stability (Weingarten et al., 1975). Later analysis by sedimentation and circular dichroism (CD) showed tau to be a highly

asymmetric molecule with very little secondary structure (Cleveland et al., 1977). Analysis by proton NMR revealed that tau has flexibility reminiscent of denatured and unfolded proteins (Woody et al., 1983). Efforts to visualize tau in EM suffered from its low contrast due to its hydrophilic nature (Zingsheim et al., 1979), but the glycerol-spray technique revealed the structure of tau to be an elongated and flexible rod, about 35 nm in length (Wille et al., 1992).

The heat stability of tau was exploited for its purification from *E.coli* and the purified tau surprisingly retained its ability to assemble microtubules (Fellous et al., 1977; Biernat et al., 1992). A detailed investigation of tau structure in solution using solution X-ray scattering and CD revealed that tau behaves as a random Gaussian coil with persistence length of ~ 2 nm (Schweers et al., 1994). Intrinsic fluorescence analysis of tryptophan mutants of tau confirmed that residues along the polypeptide chain were indeed completely solvent exposed, supporting the lack of structure (Li et al., 2002). All these observations show that tau in solution does not contain any secondary structure and can be regarded as 'natively unfolded' (Schweers et al., 1994; Barghorn et al., 2004).

Analysis of repeat domain constructs by NMR confirmed the paucity of secondary structural elements, but there are hexapeptide motifs in R2 and R3 showing inherent ß-structure propensity (Mukrasch et al., 2005). Tau construct K32 (repeat domains plus its flanking regions; S198-Y314) showed a lack of well ordered structure by NMR analysis. However, the presence of some more structural elements was revealed particularly in flanking regions. The residues V256-S262 (in the core of R1) and Q351-L357 (in the center of R4) as well as residues in the flanking regions of the repeat domains (K224-R230 in P2, V363-E372 in R4 and R`) also showed preferential ß-structure (Mukrasch et al., 2007). The short stretches of amino acids showing ß-structure in the beginning of R2 and R3 coincide with the sequences PHF6 (VQIVYK in R3) and PHF6* (VQIINK in R2; see Fig.1.7, residues in boxes), and are involved in PHF formation (von Bergen et al., 2000; von Bergen et al., 2001). As tau mainly binds to and stabilizes microtubules, it was expected that the binding to microtubules can induce some structure. Some reports stated that tau becomes more compact upon binding with microtubules (Butner and Kirschner, 1991) whereas other studies indicated that even tau bound to microtubules retains much of its disordered state (Al-Bassam et al., 2002; Santarella et al., 2004). Nevertheless, NMR analysis of tau-microtubule interactions highlighted binding
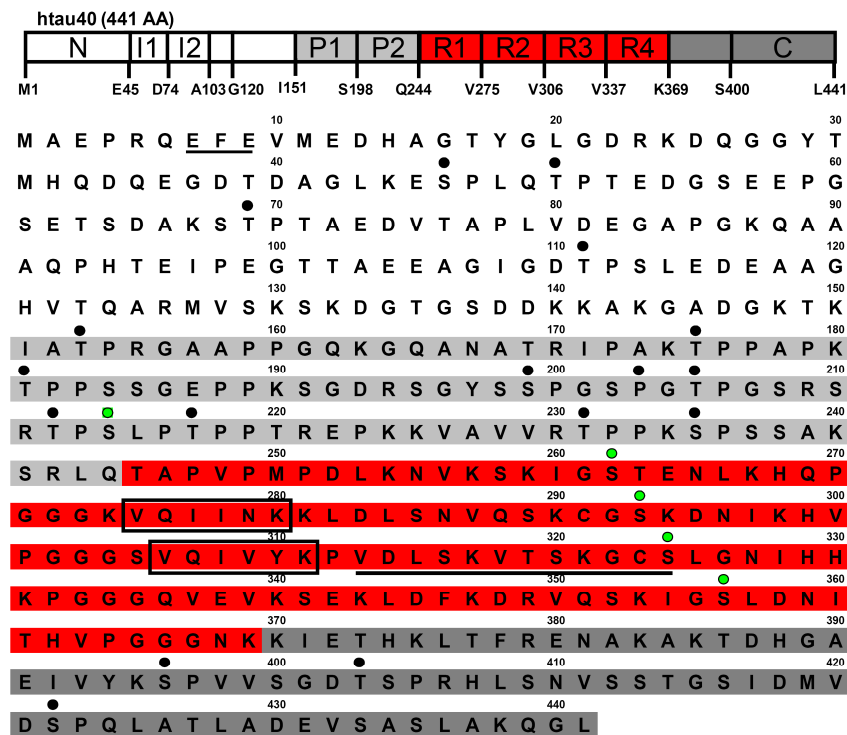
Figure 2.7: Primary structure of tau. Domains of htau40 and the corresponding sequences of amino acids are identically colored. SP/TP phosphorylation sites (●), non-proline directed sites (KXGS sites and S214) (○) are shown. Amino acid residues constituting the two hexapeptide motifs (PHF6* and PHF6) in R2 and R3 are boxed. Residues forming the discontinuous epitope recognized by the Alz-50 antibody are underlined (For tau sequences see Lee et al., 1988; Goedert et al., 1989).

of several stretches of positively charged amino acids present in the repeat domains and the flanking regions to microtubules. The residues [275]VQIINKKLDLS[285] strongly contribute to binding to the microtubules along with clusters of positively charged residues upstream of the PGGG motifs (Mukrasch et al., 2005; Mukrasch et al., 2007). In the flanking regions, the residues [225]KVAVVRT[231] and [240]KSRLQTAPV[248] (both in P2) and [370]KIETHKLTFEN[380] (in R') are not potential binding sites of microtubules (Mukrasch et al., 2007)

1.2.4.2 Tau conformation and specific conformational antibodies

In solution, Tau behaves as a "natively unfolded" or "intrinsically disordered" protein (Schweers et al., 1994). Tau adopts a "paperclip" conformation, whereby the N- and C-terminal domains approach each other and also the repeat domain (Jeganathan et al., 2006). Several observations suggest that tau cannot simply be a "random coil" in the strict sense.
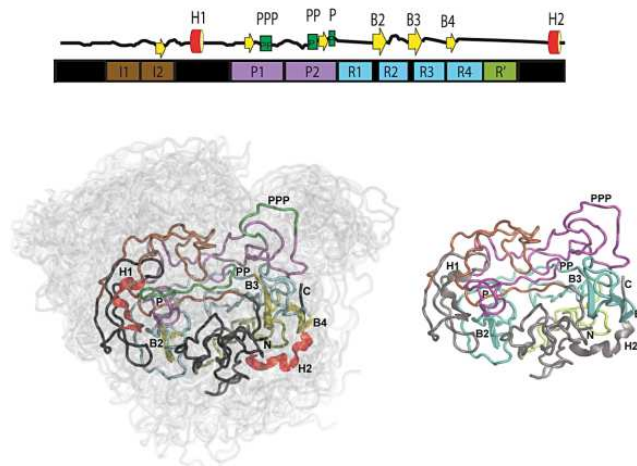
Figure 1.8: Native-state conformations of 441-residue tau in solution. Representation of the conformations of htau40 calculated from PRE data. Color coding follows the domain organization diagram shown above. Regions of transient α-helical structure (H1 [114-123] and H2 [428-437]) and ß-structure (B2 [336-345]) are shown in red and yellow, respectively. Polyproline II stretches (PPP [216-223] and PP [232-239]) are colored green. In the background an ensemble of 20 conformations is shown (reproduced from Mukrasch et al., 2009).

In addition, small angle x-ray scattering (SAXS) and Förster resonance energy transfer (FRET) were used to obtain insight into the structure of the tau protein (Mylonas et al., 2008; Jeganathan et al., 2006). These methods revealed that 441-residue tau is highly dynamic in solution with a distinct domain character and an intricate network of transient long-range contacts important for pathogenic aggregation. In Figure 1.8, the single-residue view provided by the NMR analysis reveals unique insights into the interaction of tau with microtubules (Mukrasch et al 2009).

Hyperphosphorylated tau (PHF-tau) is the major constituent of paired helical filaments (PHFs) from AD brains. This conclusion has been drawn based on the creation and characterization of monoclonal antibodies raised against PHFs, which can be classified into three categories: (a) those which recognize unmodified primary sequences of tau. (b) those which recognize phosphorylation-dependent epitopes on tau and (c) those which recognize conformation-dependent epitopes on tau. Of these antibodies, only the conformation-dependent antibodies appear to be capable of distinguishing normal tau from PHF-tau in solution. Phosphorylation of serine and threonine residues in proline-rich sequences induces a conformational change to a type II polyproline helix (Bielska et al., 2006).
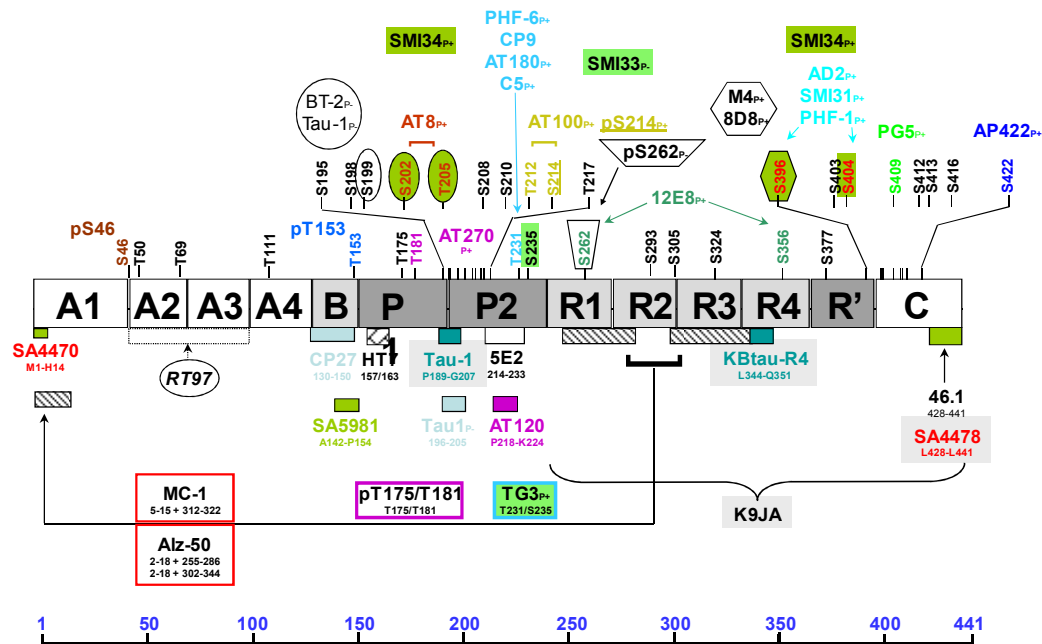
Figure 1.9: Overview of tau specific antibodies. Tau has very specific antibodies like 12E8 recognizing the repeat region only, or K9JA recognizing the repeat region plus C-terminus region. The conformational antibodies like MC1 and Alz-50 reside near the N-terminus (7-9) and in the third repeat (313-322) (Carmel et al., 1996; Jicha et al., 1997a; Jicha et al., 1997b), Tau-66 reactivity depends on the elements upstream of the repeat domain and residues in repeat R3 (Ghoshal et al., 2001), SM134 reacts to a folded state of tau wherein the repeat domain and one of the KSP motifs upstream or downstream from the repeats are required (Lichtenberg-Kraag et al., 1992), and antibody MN423 requires a truncation site downstream of the repeats (at Glu-391) and the residues within the repeat domain (reproduced from Skrabana et al., 2004).

Hints for special conformational states come from the reactivity of the antibodies such as Alz-50, MC1, Tau-66, MN423, and SM134 that have discontinuous epitopes on tau (listed in Table 1.2 and Fig. 1.9). Antibodies Alz-50 and MC1 recognize conformations of tau in brain tissue that occur at an early stage of AD. Their epitopes comprise residues near the N-terminus and in the third repeat and this conformation is called "pathological conformation of tau" as it precedes aggregation (Carmel et al., 1996; Jicha et al., 1997). Preliminary evidence from examination of the brains of patients in early stages of AD suggests that the Alz-50/MC1 conformational alteration of tau precede the appearance of PHFs further supporting this hypothesis. Further evidence for early conformational changes in tau come from studies with TG3, the epitope of which maps to phosphorylated Thr^{231} of recombinant tau. This antibody is only weakly reactive with a Thr^{231}/Ser^{235} di-phosphorylated synthetic peptide unless the peptide is conformationally altered (Jicha et al., 1997a). TG3 stains neuritic plaques, neuropil threads, and neurofibrillary tangles, but does not react with tau from human biopsy tissue (Vincent et al., 1996); therefore, exhibiting its high degree of specificity for AD pathology. TG3 also visualizes neurons susceptible to tangle-formation (Vincent et al., 1998), and thus seems to be a marker of early AD pathology.

Similarly, Tau-66 reactivity depends on the elements upstream of the repeat domain and residues in repeat R3 (Ghoshal et al., 2001), SM134 reacts to a folded state of tau wherein the repeat domain and one of the KSP motifs upstream or downstream from the repeats are required.

Antibody	Recognition sites	References
Alz50 and MC1	residues near the N-terminus (7-9) and in the third repeat (313-322)	Carmel et al., 1996; Jicha et al., 1997a; Jicha et al., 1997b
Tau-66	elements upstream of the repeat domain and residues in repeat R3	Ghoshal et al., 2001; Garcia-Sierra et al., 2003
MN423	a truncation site downstream of the repeats (at E391) and residues within the repeat domain	Skrabana et al., 2004
SMI34	repeat domain and one of the KSP motifs upstream or downstream from the repeats	Lichtenberg-Kraag et al., 1992

Table 1.2: Tau antibodies with discontinuous epitopes. They are often used in the analysis of an early stage of neurodegeneration.

1.2.4.3 Polymorphic structure of paired helical filaments

PHFs were identified as basic elements of neurofibrillary tangles (Kidd, 1963; Terry, 1963) and the subsequent isolation of PHFs from AD brain (Ihara et al., 1983; Wisniewski et al., 1984) enabled the analysis of the basic parameters of PHFs. It was shown that PHFs are ~ 8 nm x 20 nm in cross-section using negatively stained electron micrographs (Crowther and Wischik, 1985). Analysis of the protein compositions of PHFs revealed tau as the major component (Delacourte and Defossez, 1986; Kosik et al., 1986; Nukina and Ihara, 1986; Wood et al., 1986; Wischik et al., 1998b).

The assembly of PHFs *in vitro* was initially hampered by the high solubility of the protein. Assembly conditions were found in several steps by testing different tau constructs and optimizing assembly conditions including oxidation (Wille et al., 1992; Schweers et al., 1995; Barghorn and Mandelkow, 2002). Finally, aggregation of tau into PHFs *in vitro* was achieved by addition of polyanionic cofactors such as heparin (Goedert et al., 1996), RNA (Kampers et al., 1996) or arachidonic acid micelles (Wilson and Binder, 1997).

Tau fibrils reassembled *in vitro* can display a variable twist morphology between filaments assembled from different variants of tau proteins (e.g. different splicing variants), or even within a given filament. This has caused some concern whether the assembly products observed *in vitro* reflect those observed in AD brains. A plausible interpretation would be a slight variability in the contacts between subunits, which can give rise to differences in the overall fibril appearance. Another fundamental debate concerns the interpretation of the twisted appearance of the tau

fibrils alternative to the "paired helical" structure, and it has been proposed that tau fibrils could be considered as flat ribbons with a width of ~ 20-22 nm and a height of ~ 10-12 nm that twist around their longitudinal axis (Pollanen et al., 1997). The twisted appearance is variable as ~10% of tau fibrils found in AD brains show no twist and are therefore called "straight filaments" (Crowther and Wischik, 1985). In other diseases with tau pathology, the crossover repeat is ~160 nm (Ksiezak-Reading H et al., 1994). The apparent groove running down the longitudinal axis could resemble an artifact of staining, filling a depression in the fibril, rather than reflecting the division between two joining protofibrillar strands. The interpretation of PHFs as ribbon was mostly based on atomic force microscopy (AFM) and scanning tunneling microscopy (STM) (Pollanen et al., 1994; Moreno-Herrero et al., 2004) but was viewed with caution because of possible imaging artifacts (Allen et al., 1992). However, consistent with the "ribbon" interpretation, the ends of filaments or filament fragments usually show clean sharp edges. In contrast, fibrils consisting of two or more protofibrils would be expected to occasionally reveal protruding ends, reminiscent of the protofilament stubs protruding from microtubules (MTs). This is not observed in the case of tau fibrils. Further analysis showed that filaments from *in vitro* aggregation resembled filaments from AD brain such that the core of PHFs contain the repeat domains while the N- and C-terminal domains contribute to the "fuzzy coat" (Wischik et al., 1988a; von Bergen et al., 2006b). The core protein coincides roughly with the tau repeat domain of ~ 100-200 residues and accounts for only ~ 25-30% of the entire tau protein. The fuzzy coat should represent the major protein fraction in tau fibrils but so far has escaped the detection by microscopic methods. For example, fibrils assembled *in vitro* from full-length tau or from the repeat domain alone show only minor differences in diameters by negative stain EM (Barghorn et al., 2004). Similar results were obtained for tau proteins bound to MTs, that is the unstructured "projection domain", which does not bind to MTs and largely coincides with the termini in the "fuzzy coat", is nearly invisible on negatively stained or cryo-preserved unstained MTs (Santarella et al., 2004). All fibrils reveal structural polymorphism: "Thin twisted" and "thin smooth" fibrils resemble flat ribbons (cross-section ~10x15 nm) with diverse twist periodicities. In Fig. 1.10 "thick fibrils" show periodicities of ~65-70 nm and thicknesses of ~9-18 nm such as routinely reported for "paired helical filaments" (PHFs) but structurally resemble heavily twisted ribbons. Therefore, thin and thick fibrils assembled from different human tau isoforms challenge current structural models of PHFs. Furthermore, all tau fibrils reveal axial sub-periodicities of ~17-19 nm and, upon exposure to mechanical stress or hydrophobic surfaces, disassemble into uniform fragments that remain connected by thin thread-like structures (~2 nm) (Wegmann et al., 2010).
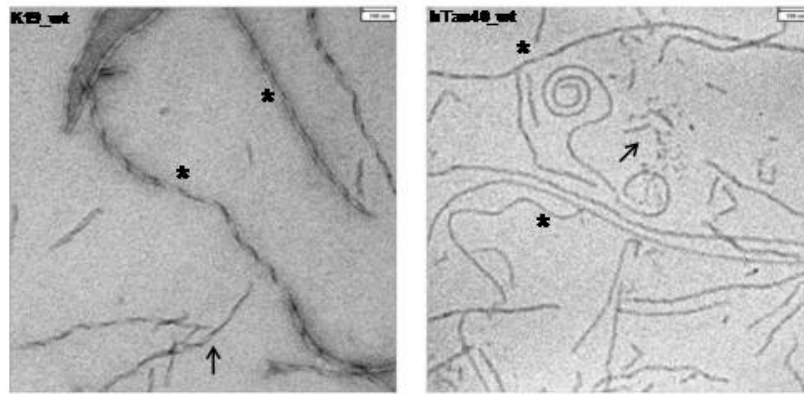
Figure 1.10: Variable tau fibril morphologies observed by EM. (A) EM image of K19wt fibrils with the typical appearance of paired helical filaments (PHFs). (B) Non selective EM images of hTau40wt fibril preparations show a heterogeneous mixture of fibril shapes and confirms the heterogeneity of fibril structures. Fibril morphologies differ in length, bending, internal twist, periodicity and thickness (* for thick fibrils and ↑ for thin fibrils, reproduced from Wegmann et al., 2010)

Hydrophobically induced disassembly is inhibited at enhanced electrolyte concentrations, indicating that the fragments resemble structural building blocks and the fibril integrity depends largely on hydrophobic and electrostatic interactions. Since full-length tau and repeat domain constructs assemble into fibrils of similar thickness, the "fuzzy coat" of tau protein termini surrounding the fibril axis is nearly invisible for AFM and EM, presumably due to its high flexibility (Wegmann et al., 2010).

1.3 Microtubule structure and function

Microtubules, often in concert with other cytoskeletal elements, perform a wide range of essential physiological functions. For example, due to their mechanical strength and stability, microtubules contribute to the maintenance of cell shape and provide scaffolding for intracellular transport. In addition, due to their ability to undergo rapid non-equilibrium dynamics, microtubules are also indispensable in cellular processes such as cell division, differentiation, and motility. Most likely, tubulin heterogeneity and differential MAP binding and function are the primary molecular mechanisms regulating microtubule cellular function (Kirschner et al., 1985; Mandelkow et al., 1988).

1.3.1 Tubulin isotype heterogeneity

Microtubules are long hollow ~25 nm wide cylindrical polymers primarily made up of tubulin αß heterodimers (Weisenberg et al., 1976; Luduena et al., 1977; reviewed in Desai and Mitchison, 1977). The α and ß tubulin monomers (~50 kD MW each) are approximately 50% identical at the amino acid level (Burns, 1991). In addition, α and ß tubulin exist as multiple isotypes as a result of both, extensive post-translational modifications (MacRae, 1997; Laferriere et al., 1997; reviewed in Lafenechere and Job, 2000) and the expression of multiple genes. Regulation of tubulin polymorphism may be one route by which microtubule properties are fine-tuned to play specific physiological roles (Bonnet et al., 2001). The genome of higher eukaryotes contains multiple (both expressed and pseudo) α and ß tubulin genes. Mammals possess six expressed genes for α-tubulin and seven expressed genes for ß- tubulin (Luduena, 1993). The mammalian ß isotopes generally differ (primarily in the carboxy terminus) more than the α isotopes. Indeed although encoded by two genes, α1 and α2 are identical at the amino acid level; differences between the two genes are located entirely in untranslated regions (Lewis et al., 1985). α and ß tubulin isotypes exhibit both tissue specific and developmentally regulated expression, particularly in the brain (Lewis et al., 1985; Hoffman and Cleveland, 1988; reviewed in Laferriere et al., 1997).

1.3.2 Macromolecular structure of tubulin dimers and microtubule polymers

The 3D structure of αß tubulin polymerized into zinc sheets, was solved at a resolution of 3.7 angstroms by Downing, Nogales and colleagues (Nogales et al., 1998, 1999) and has been used to model the 3D structure of microtubules. The α and ß tubulin subunits have virtually identical structures with dimensions of 4.6 x 4.0 x 6.5 nm (width, height and depth, respectively; Nogales et al., 1998). Each tubulin monomer has three structural domains, the N-terminal domain (aa1-205), an intermediate domain (aa206-381), and the C-terminal domain (aa382-453). The amino terminal domain forms a Rossmann fold (five alpha helices and six parallel beta strands). Three sequential alpha helices followed by a mixed beta sheet and two more helices and a "disordered" C-terminal tail. Functionally, the nucleotide binding domain sits at the base of the N-terminal domain (Mandelkow et al., 1985). The taxol-binding domain is located within the intermediate domain of ß tubulin, and the C-terminal domain has been shown to bind MAPs (Serrano et al., 1985; Rivas et al., 1988; Cross et al., 1991; Marya et al., 1994; Rao et al., 1994) and motor proteins (Hagiwara et al., 1994; Larcher et al., 1996).

The predominant arrangement of tubulin monomers in the microtubule polymers is the "B-lattice". In this arrangement lateral contacts between monomers in neighboring protofilaments

are made between homologous subunits (α-α, ß-ß) except the seam where heterogeneous subunits form contacts (Chretien and Wade, 1991; Song and Mandelkow, 1993). Laterally contacting monomers have a 10° pitch relative to monomers in the adjacent protofilaments and thereby form a 3-start helical path, i.e. one complete helical turn brings three monomers above the original protofilament starting point (Mandelkow et al., 1986; Song and Mandelkow, 1993; Kikkawa et al., 1994; reviewed in Mitchison and Desai, 1997). Although the microtubule lattice is conceptualized as helical, microtubules do not assemble by a classical helical polymerization reaction. Rather, microtubules grow as a sheet of protofilament that later close into tube.

In addition, microtubules are polar structures. Tubulin αß heterodimers orient, head-to-tail, to produce the non-covalently associated linear protofilaments. Subsequently, 13 (under most conditions) protofilaments interact laterally to form the hollow 25 nm diameter tube-like microtubule structure (Amos and Klug, 1974). One end of the microtubule, designated as the "minus" end, consists of α tubulin monomers, while the opposing or "plus" end, consists of ß tubulin monomers (Mitchison, 1993; Hirose et al., 1995; Fan et al., 1996). Functionally, there are differences in the polymerization at each of the two ends; the plus end (ß tubulin) being the faster growing end (Allen and Borisy, 1974). The functional polarity of the polymer ends contribute to the non-equilibrium dynamic behavior displayed by microtubules.

1.3.3 Microtubule assembly and dynamics

In solution, tubulin exists in a dynamic equilibrium between tubulin dimer and polymers; any tubulin present above a defined critical concentration of tubulin will form polymers (Mitchison and Kirschner, 1984a; reviewed in Desai and Mitchison, 1977; Hyman and Karsenti, 1998). The critical concentration and the nature of the polymer structure is influenced by a number of variables, such as the presence or absence of nucleating centers, the concentration of magnesium, calcium, zinc, GTP, MAPs or stabilizing compounds such as glycerol, DMSO or taxol etc (Mitchison and Kirschner, 1984a; Bre and Karsenti, 1990).

Microtubule assembly (Fig. 1.11) proceeds in two phases, nucleation and elongation. *In vivo*, γ tubulin (a third very minor species of tubulin; Oakley and Oakley, 1989), which is found solely in microtubule organizing centers (MTOC) (Mitchison and Kirschner, 1984b, McIntosh et al., 1985), participates in the nucleation of microtubule polymers (Zheng et al., 1995). MTOCs catalyze nucleation at tubulin concentrations below the concentration required for spontaneous assembly and also orient the microtubules so that the growing end is distal to the MTOC. *In vitro*, other nucleating centers such as axonemes or preformed microtubules (e.g. microtubule

'seeds') can serve the same function as MTOCs. In addition, MAPs are capable of nucleating *de-novo* tubulin polymerization in the absence of MTOCs (Bre and Karsenti, 1990).

The microtubule polymerization rate is controlled by the binding constant of GTP tubulin to the tubulin ends. However, experiments using GTP analogs indicate that GTP hydrolysis is only required for microtubule depolymerization but not for microtubule assembly (Penningroth and Kirschner, 1978; Mejiollano et al., 1990; Mandelkow et al., 1991;
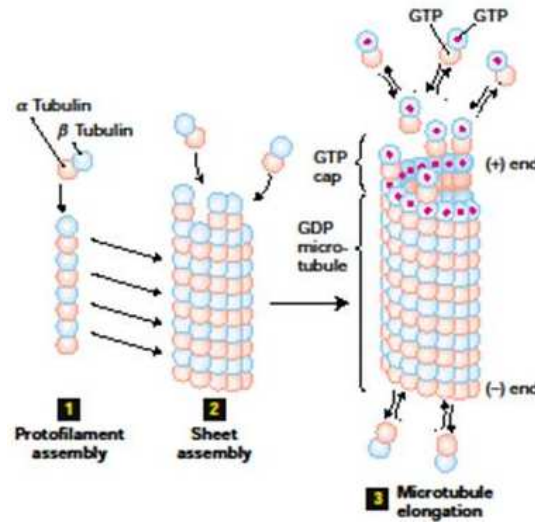
Figure 1.11: Stages in assembly of microtubules. Free αß-tubulin dimers associate longitudinally to form short protofilaments (1). These protofilaments are probably unstable and quickly associate laterally into more stable curved sheets (2). Eventually, a sheet wraps around into a microtubule with 13 protofilaments. The microtubule then grows by the addition of subunits to the end of protofilaments composing the microtubule wall (3). The free tubulin dimers have GTP (red dot) bound to the exchangeable nucleotide-binding site on the ß-tubulin monomer. After incorporation of a dimeric subunit into a microtubule, the GTP on the ß-tubulin (but not on the α-tubulin) is hydrolyzed to GDP. If the rate of polymerization is faster than the rate of GTP hydrolysis, then a cap of GTP-bound subunits is generated at the (+) end, although the bulk of ß-tubulin in a microtubule will contain GDP. The rate of polymerization is twice as fast at the (+) end as at the (-) end (Adopted from Molecular Cell Biology, fifth edition; Lodish et al., 2003).

Hyman et al., 1992). Both α and ß tubulin contain guanine nucleotide binding sites, but only GTP bound to ß tubulin (at the "exchangeable" or "E-site') is hydrolyzed to GDP (Weissenberg et al., 1976). At some point after microtubule polymerization GTP is hydrolyzed to GDP, which remains bound to β tubulin until depolymerization occurs, at which point GTP can be exchanged for GDP (Kirschner, 1978; Carlier,1989). In contrast, α tubulin binds to GTP in a non-exchangeable manner at the N-site (Spiegelman et al., 1977). The energy derived from the hydrolysis of GTP allows for two types of nonequilibrium polymerization dynamics observed, treadmilling (Margolis and Wilson, 1978; reviewed in Margolis and Wilson, 1998) and dynamic instability (Mitchison and Kirschner, 1984a; Horio and Hotani, 1986; reviewed in Desai and Mitchison, 1997). Although for any given set of conditions (tubulin concentration, buffer

conditions, etc.) the total polymer mass is constant, nevertheless a steady exchange of αβ heterodimers occurs at the microtubule ends. The microtubules under these conditions are said to be at "steady state". During steady state conditions due to the different rates of assembly at the two microtubule ends, there is a net addition of tubulin subunits at the plus ends of the microtubules. The physiological rates of treadmilling can vary widely in different cell types or within a single cell at different times during the cell cycle. For example, during metaphase and anaphase of mitosis, microtubules exhibit rapid subunit flux (Mitchison, 1989). Conversely the treadmilling rate of MAP-rich brain microtubules was found to be extremely slow (Margolis and Wilson, 1978), although rapid treadmilling is an intrinsic property of MAP-free brain microtubules (Panda et al., 1999). A second type of non-equilibrium behavior, dynamic instability, is due to differences in the rate of growth and disassembly of individual microtubules (Mitchison and Kirschner, 1984a; Walker et al., 1988; reviewed in Desai and Mitchison, 1997). Dynamic instability occurs because populations of microtubules exhibit a bulk steady state; the ends of individual microtubules randomly alternate between prolonged phases of polymerization and depolymerization (Mitchison and Kirschner, 1984a). Microtubules, therefore, assume two different functional and structural states, alternating between phases of growing and shortening (Walker et al., 1998). Transition events are referred to as catastrophe (switch from elongation to shortening) and rescue (transition from shortening to elongation). All changes in length over time can be described as the sum of four parameters: the elongation rate, the shortening rate, the catastrophe frequency, and the rescue frequency. Microtubules are significantly more dynamic at the plus end than at the minus end. In comparison to minus ends, plus ends exhibit greater changes in length over time due to higher rates of elongation, higher frequencies of catastrophe and a lower frequency of rescue (reviewed in Desai and Mitchison, 1997).

The rate of microtubule shortening is in the order of 2-3 times more rapid than the rate of elongation. In addition, although the elongation rate is dependent on the free tubulin concentration, the rate of shortening is independent of overall tubulin concentration. Another factor influencing the level of dynamic behavior is the presence of the structural microtubule associated proteins. Even at low molar ratios, tau (and the other structural MAPs) effectively stabilize microtubule dynamics, primarily by reducing the rate of shortening, although there can be a small positive effect on the rate of elongation, as well (Trinczek et al., 1995; Panda et al., 1995; Goode et al., 1997). The phase transitions in a population of microtubules may be uncorrelated so that the ensemble shows an apparent steady state. They can be synchronized, leading to oscillations of assembly and disassembly which can be observed by light scattering, X-ray scattering and EM (Mandelkow et al., 1988; Pirollet et al., 1987). Oscillations require GTP which is hydrolyzed during microtubule assembly. Depending on how GTP is supplied one can

distinguish two types of oscillations: the first is maintained by excess GTP in solution; it has typical periodicities of ~1-3 min. The second type of oscillation is achieved by a GTP regenerating system with low initial guanosine 5'-diphosphate (GDP) (Azhar et al., 1990); it has longer periodicities (~10 min; Pirollet, 1987).

Microtubules are the structural components within cells. Many cellular processes such as mitosis and vesicular transport mainly require the involvement of microtubules. Microtubules serve as the tracks for motor proteins which enables the intracellular transport of vesicles, organelles, and protein complexes (Hirokawa and Takemura, 2005; Mandelkow et al., 2007). During mitosis, microtubules function as strings attached to opposite ends of the cell and pull apart the aligned chromosomes. During these processes, microtubules are highly dynamic in terms of assembly and disassembly, which is modulated by microtubule-associated proteins (MAPs) that bind to the lattice surface of microtubules.

1.3 Aim of this study

The physiological role of protein tau is to stabilize microtubules; however, it aggregates into pathological paired helical filaments (PHFs) in AD. The well proven post-translational modification of tau is the increased phosphorylation (hyperphosphorylation) of tau at selected sites during AD. Several studies have linked the hyperphosphorylation of tau to its inability to bind microtubules as well as its proneness to efficient aggregation. Much of the attempts that used different experimental systems have lead to different hypothesis for the role of phosphorylation on tau aggregation (promoting vs. inhibiting) and microtubule binding ability (abolishing vs. conforming). Likewise, the effect of the site-specific pseudo-phosphorylation on the physiological function of tau (microtubule assembly) and the pathological aggregation of tau (PHF assembly) are still unknown.

The present study is to improve our understanding of the functional and physiological role of pseudo-phosphorylated and hyperphosphorylated tau. and to elucidate the conformation of tau in solution by various methods. Particular aims were:

(i) to study the effect of pseudo-phosphorylation upon aggregation propensity of tau (one of the pathological effects),

(ii) to study the effect of pseudo-phosphorylation upon microtubule assembly (one of the physiological role of tau in neurons,

(iii) to characterize the structural polymorphism of tau fibrils by using electron microscopy, and

(iv) to study the effect of temperature on the tau conformation in solution by various biophysical methods such as SAXS, CD and DLS.

2 Materials and Methods

2.1 Materials

2.1.1 Laboratory equipment

Analytical HPLC:

SMART-system with the following gel filtration columns:

Fast Desalting PC (3.2 mm x 100 mm)	Amersham Biosciences, Freiburg
Superose PC12 (3.2 mm x 300 mm)	Amersham Biosciences, Freiburg

Preparative FPLC:

Akta Explorer-system with the following gel filtration columns:

Superdex G200 HR 16/60 (120 ml)	Amersham Biosciences, Freiburg
Superdex G75 HR 16/60 (120 ml)	Amersham Biosciences, Freiburg

Akta Explorer-system with the following anion exchange columns:

SP Sepharose 16/10 (20 ml)	Amersham Biosciences, Freiburg

Spectrophotometers:

Kontron spectrophotometer	Kontron Instruments, Neufahrn
Tecan spectrophotometer	Labsystems, Frankfurt
Spex Fluromax spectrophotometer	Polytec, Waldbronn
Jasco J-810 CD spectrometer	Jasco, Gross-Umstadt

Centrifuges:

Eppendorf centrifuge type 5415C and 5402	Eppendorf, Hamburg
Table ultracentrifuge TL-100	Beckmann, München
Ulracentrifuge L8-70M	Beckmann, München

Miscellaneous:

Transmission electron microscope	CM-12 Phillips (Tecnai)
PCR machine	Eppendorf, Hamburg
Analytic balances type BP 310 S and PT 1200 Sartorius, Göttingen	
BTX electroporation system	Cole-Parmer Instrument, UK
Intelligent dark box II, Las-1000+	Fuji, Japan

2.1.2 Chemicals

Chemicals of highest quality were obtained from the following suppliers:

Sigma, Merck, Fluka, Serva, Gerbu, AppliChem, Amersham Pharmacia Biotech, New England Biolabs, Qiagen, Molecular Probes

2.1.3 Software

Vector NTI	Invitrogen, Karlsruhe
EMBOSS	http://emboss.sourceforge.net/

2.1.4 Molecular biology reagents

2.1.4.1 Kits, spin columns and reagents for DNA

Invisorb spin plasmid mini kit	Invitek, Berlin
Nucleospin gel extraction kit	Macherey-Nagel, Düren
Zero Blunt TOPO PCR cloning kit	Invitrogen, Karlsruhe
Agarose for DNA electrophoresis	Serva, Heidelberg
Effectene Transfection kit	Qiagen

2.1.4.2 Vectors and DNA standards

pNG2 (a derivative of pET-3a)	Merck-Novagen, Darmstadt
Small ladder	MBI Fermentas, St.Leon-Rot

2.1.4.3 Antibiotics and media

Ampicillin	Gerbu, Gaiberg
Carbenicillin	Applichem, Darmstadt
LB medium	Carl Roth GmBH, Karlsruhe
Hygromycin	Calbiochem

2.1.4.4 Bacterial strains

Cloning strains:

XL2-Blue and XL10-Gold	Stratagene, Netherlands
DH5α library efficiency	Invitrogen, Karlsruhe

Expression strain:

BL21 (DE3)	Invitrogen, Karlsruhe

2.1.4.5 Enzymes, substrates and nucleotides

All restriction endonucleases	New England Biolabs, Frankfurt
DNA ligase	New England Biolabs, Frankfurt

Pfu Ultra DNA polymerase	Stratagene, Netherlands
Pwo master mix	Roche diagnostic, Mahnheim
50X dNTPs master mix	Invitek, Berlin
MgCl$_2$	Merck-Novagen, Darmstadt
Taxol (Paclitaxol)	Sigma-Aldrich, Germany
Heparin	Sigma-Aldrich, Molecular Probes, Germany

2.1.5 Stock and working buffer solutions

PBS (1X): 1M solution of sodium di-hydrogen phosphate was slowly added to 1M di-sodium hydrogenphosphate solution with constant mixing on a magnetic stirrer until the pH reached 6.8

1X TAE: 40 mM Tris-acetate, 1mM EDTA (pH 8.0).

To make 50X TAE, 242 g Tris base, 57.1 g glacial acetic acid and 100 ml of 0.5 M EDTA (pH 8.0) were dissolved in water and adjusted to 1000 ml.

6X DNA loading buffer: 10 mM Tris-HCl (pH 7.6); 0.03 % bromophenol blue; 0.03 % xylene cyanol FF; 60 mM EDTA; 60 % glycerol.

TE Buffer: 10 mM Tris HCl pH 7.5; 1 mM EDTA.

1X SDS running buffer: 25 mM Tris base; 192 mM Glycine; 0.1% SDS.

To make 10X SDS running buffer (Laemmli buffer), 30.3 g Tris base, 144 g Glycine and 10 g SDS were dissolved and made up to 1000 ml with water.

4X SDS loading buffer: 200 mM Tris-HCl (pH 6.8), 400 mM DTT, 8 % SDS, 0.4 % Bromophenol blue, 50 % glycerol.

2.2 Methods
2.2.1 Molecular biology methods
2.2.1.1 Cultivation of *E.coli*
2.2.1.1.1 Culture medium

Lysogeny broth (LB) medium: 10 g Bacto-Tryptone, 5 g Bacto-yeast extract and 5 g NaCl in 1000 ml, sterilized by autoclaving and stored at 4°C (Bertanni G, 2004).

LB-agar plates: LB medium containing 1.5 % of agar was autoclaved and stored at 4°C. When needed, it was melted down in a microwave oven. After letting it to cool down to 55°C, an appropriate antibiotic was added and poured into petri plates with a diameter of 10 cm in the clean bench, allowed to solidify and stored at 4°C for further use.

SOC medium: 0.5 % Yeast extracts; 2 % Bacto-tryptone; 10 mM NaCl; 2.5 mM KCl; 10 mM MgSO₄; 10 mM MgCl₂; 20 mM Glucose.

2.2.1.1.2 Transformation of *E. coli* strains

E. coli cells competent for transformation were either purchased from commercial sources (see section 2.1.4.4) or prepared manually in the laboratory. The vector pNG2 in which all the tau constructs and mutants were created has ampicillin resistance.

Transformation by heat-shock method

XL2-Blue, XL10-Gold and DH5α cells were transformed with a plasmid of interest by the heat-shock method. For the transformation, 20-100 ng of DNA was added to 20-50 µl aliquots of competent cells and allowed to stand on ice for 30 minutes. Cells were then given heat shock at 42°C for 45 seconds and placed again on ice for 1-2 minutes. 200-300 µl of SOC medium were added to the cells and were incubated at 37°C with shaking for 1 hour. Finally, 100-200 µl of cells was plated on a LB agar plate containing ampicillin and were incubated overnight at 37°C.

Transformation by electroporation

E. coli - BL21-DE3 electrocompetent cells used for expression of the proteins were transformed by electroporation in which the electrocompetent cells and plasmid DNA were placed in a plastic cuvette containing electrodes and subjected to a short electric pulse of 2400 Volt/cm causing small pores in the membrane through which the DNA enters. For the transformation by electroporation, 0.5-1.0 ng of DNA was added to 20 µl of the electrocompetent cells and the mixture was transferred into a pre-chilled electroporation cuvette. The cuvette was placed in the electroporater (BTX electroporation system, Cole-Parmer Instrument, UK) and then electric pulse was applied. Precooled SOC medium was immediately added to the cells and was transferred to new sterile eppendorf tube. The cells were incubated at 37°C for 30 minutes with shaking and were plated on a LB agar plate containing ampicillin followed by overnight incubation of the plate at 37°C.

2.2.1.1.3 Inoculation and glycerol stocks of *E.coli*

A single colony of *E.coli* from LB agar plate was picked and inoculated into 5 ml LB medium containing ampicillin. This was incubated at 37°C with shaking to allow growth of *E.coli*. For long term storage, 0.7 ml of grown culture was gently mixed with 0.3 ml of sterile 100 % glycerol, shock frozen in liquid N₂ and stored at -80°C.

2.2.1.2 Mini preparation of plasmid DNA

Buffer P1	50 mM Tris/ HCL pH 8.0
	10 mM EDTA
	100 µg/ ml RNAse A
Buffer P2	0.2 M NaOH
	1% SDS
Buffer P3	3 M Potassium acetate pH 5.5
TE buffer	10 mM Tris, bring to pH 8.0 with HCl
	1 mM EDTA
PE buffer	10 mM Tris-HCl, bring to pH 7.5
	80% ethanol stored at room temperature

Briefly single *E.coli* colony was inoculated into 5 ml of LB medium containing 100 µg/ ml of antibiotic and grown overnight at 37°C in a shaker incubator. Cells were pelleted in a table-top centrifuge at 3,000 rpm for 5 min. Cell pellet was resuspended in 250 µl of P1 and 250 µl of P2 was added, mixed gently by inverting the tube 4-6 times. To this, 350 µl of P3 was added and gently mixed and centrifuged for 10 min at 13,000 rpm in a table-top eppendorf centrifuge. The supernatant was applied onto a QIA prep spin column and centrifuged for 1 min at 13,000 rpm. Flow through was discarded, the column was washed with 0.75 ml of buffer PE and centrifuged again for 1 min. Flow- through was discarded and the column was centrifuged for an additional 1 minute to remove any residual wash buffer. The column was placed in a clean eppendorf tube and 50 µl of TE buffer was added directly to the centre of the column. The column was let to stand for 1 min and plasmid DNA was eluted by centrifuging at 13,000 rpm for 1 min. the purified plasmid was stored at -20°C

2.2.1.3 Determination of DNA concentration and purity

The concentration and the degree of purity of the purified plasmid DNA was determined based on the Beer-Lambert law by measuring the absorbance at 260 nm and 280 nm:

$A_{260} = \varepsilon_{260}$ c l and A_{260} x 50 = µg/ml (when l = 1 cm) ………………. Equation 1

A_{260} is the absorbance at 260 nm, ε_{260} is the molar absorption coefficient, c is the molar concentration and l is the optical path length (usually 1 cm). For a protein-free and RNA-free solution of DNA the ratio of A_{260}/A_{280} should be 1.5-2.0. Any proteinaceous contamination present in the preparation would decrease the ratio to < 1.5 whereas RNA contamination would

increase the ratio to > 2.0. DNA preparations with A_{260}/A_{280} ratio of 1.5–2.0 were used for further analysis of concentration and purity of DNA.

2.2.1.4 Agarose gel electrophoresis of DNA

The size and purity of DNA was analyzed by agarose gel electrophoresis. For optimal resolution, the concentration of agarose was adapted to the size of the DNA of interest as listed in Table 2.1.

Agarose concentration (%)	DNA size (kb)
0.7	20-1
0.9	7-0.5
1.2	6-0.4
1.5	4-0.2
2.0	3-0.1

Table 2.1: Concentration of agarose used depending on DNA size. The table shows concentration of agarose to be used depending on the size of DNA to be analyzed (Sambrook and Maniatis, 1989).

The required amount of agarose was added to1X TAE buffer and dissolved completely by boiling the solution in a microwave oven. The agarose solution was poured into a casting tray containing sample comb and allowed to solidify. Then agarose gel was immersed in a chamber with TAE buffer and DNA samples prepared in gel loading buffer were loaded onto the gel. The electrophoresis was carried out at 100 V after the gel was stained in ethidium bromide (EtBr) bath (0.5 μg/ml). Binding of EtBr by intercalation of its ring system between the stacked base pairs of the DNA increases its fluorescent yield compared to that of the dye in free solution. During ultraviolet irradiation, DNA absorbs at 254 nm and transmits energy to the dye and the bound dye itself absorbs radiation at 302 nm, as well as 366 nm. As a result, the energy is reemitted at 590 nm in the reddish-orange region of the visible spectrum, which was used to visualize DNA under a UV transilluminator. The gel was photographed using a gel documentation system.

2.2.1.5 Site directed mutagenesis of DNA

Most of the mutations were created either using site-directed mutagenesis using the Quick Change site-directed mutagenesis kit (Stratagene, Netherlands) or using mega primer which is a short PCR product amplified with mutational primers.
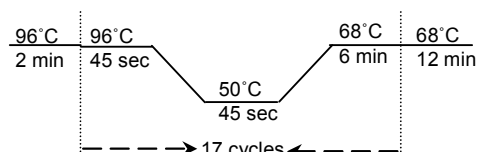
Site directed mutagenesis by complementary primers

The complementary primers, designed based on the template plasmid, carrying desired mutation were used to amplify the template plasmid using PCR.

The mixture of PCR reaction for site directed mutagenesis was as following:

10X *Pfu* ultra buffer	2.0 µl	PCR program used:
dsDNA template (25 ng/µl)	2.0 µl	
dNTPs (2.5 mM)	2.0 µl	
Forward primer (10 pmoles/µl)	1.0 µl	
Reverse primer (10 pmoles/µl)	1.0 µl	
Pfu ultra polymerase (2.5 U/µl)	0.5 µl	
H$_2$O to a final volume of	20 µl	

PCR program used:

```
96˚C    96˚C                              68˚C    68˚C
2 min   45 sec                            6 min   12 min
                         50˚C
                         45 sec
          - - - → 17 cycles ← - - -
```

In a PCR cycle, initial denaturation is done for few minutes at 96°C to unwind the plasmid DNA. The actual cycle involves continuous temperature shifts such that DNA is melted at higher temperature, primers are able to anneal to template at lower temperature and finally polymerase can exhibit its action at extension temperature. Annealing temperature depends on the primer content whereas the extension time varies with length of the template used.

Site directed mutagenesis by mega primer method

By this method, it was possible to introduce two or more mutations in a single PCR amplification of template by using initially created short PCR product with primers either one or both of them having desired mutations.

Generation of short fragment (mega primer)

PCR reaction mixture for the generation of short product was as following:

dsDNA template (25 ng/µl)	1.0 µl	PCR program used:
Forward primer	2.5 µl	
Reverse primer	2.5 µl	
H$_2$O to volume of	18.0 µl	
PWO master mix	25.0 µl	

PCR program used:

```
96˚C    96˚C                              68˚C    68˚C
2 min   45 sec                            1 min   5 min
                         50˚C
                         45 sec
          - - - → 27 cycles ← - - -
```
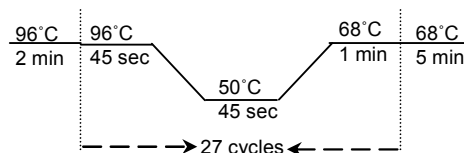
The short product (mega primer) obtained was gel purified and used for setting up long PCR.

Generation of long fragment by using mega primer

Since the mega primers created are usually between 50-300 nucleotides, annealing step in PCR cycle was not needed for next PCR for creating long product:

PCR reaction mixture as following:

Template (25 ng/μl)   2.0 μl   PCR program used:

dNTP (2.5mM)   2.0 μl

10X P*fu* ultra buffer   2.5 μl

Mega primer (100 ng/μl)   7.0 μl

Pfu ultra polymerase   0.2 μl

H$_2$O to volume of   25.0 μl

With all PCR for mutations, a negative control was set up with all the components without one of the primers. The amplifications were checked in 0.8 % agarose gel by loading 5 μl of PCR product.

DpnI digestion

The amplified PCR products were subjected to *DpnI* digestion resulting in the disruption of methylated template DNA (template) but not the amplified DNA which would carry mutation.

0.1-0.5 μl of *DpnI* was added directly to PCR products (both negative and positive controls) and incubated at 37°C for 2-3 hours. After the digestion, the digested 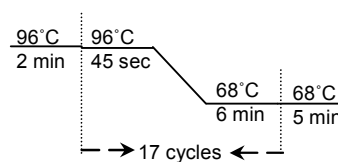products were again checked in 0.8 % agarose gel. Transformation of PCR products was done by heat shock method followed by plasmid preparation from few isolated colonies. The presence of mutation in the purified plasmid was confirmed by DNA sequencing.

2.2.1.6 DNA sequencing

The sequencing reactions were performed in 96 PCR machine using fluorescent dye labeling based on the Sanger method (Sanger et al., 1977)

Sequencing reaction mixture contained:

Terminator ready reaction mix   8 μl   The running cycles for sequencing in PCR:

DNA of interest (100 ng/μl)   5-7 μl

Primer (10 pmol/μl)   1 μl

H$_2$O to a final volume of   20 μl
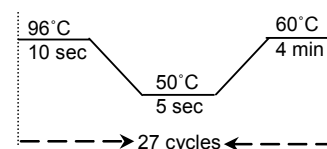
After PCR sequencing reaction, the DNA was pelleted by ethanol precipitation: To 20 μl of sequencing reaction, 16 μl of water and 64 μl of 95 % ethanol were added, mixed and centrifuged at 13000 rpm for 10 minutes at room temperature. The pellet from the centrifugation was washed with 250 μl of 70 % ethanol to remove any trace of salts by centrifugation at 13000 rpm for 10 minutes at room temperature. The pellet was then air dried at 90°C for 5 minutes, resuspended in 30 μl of HPLC-grade H$_2$O and was ready for sequencing.

The ABI PRISM 310 Genetic Analyzer (Applied Biosystems, Darmstadt) was used to sequence the DNA. The sequencing results were analyzed with the VectorNTI software (Invitrogen, Karlsruhe).

2.2.2 Biochemical and biophysical methods

2.2.2.1 SDS-PAGE

SDS-PAGE (sodium dodecyl sulfate polyacrylamide gel electrophoresis) was performed for the electrophoretic separation of the protein (Laemmli, 1970; Matsudaira and Burgess, 1978). By mixing the solution of proteins with SDS, the protein is denatured and gets a negative charge in proportion to its mass due to binding of SDS to the protein, yielding an approximately uniform mass to charge ratio. This enables the proteins to be separated strictly by their molecular weight. With the addition of SDS, proteins are briefly heated to 95°C in the presence of a reducing agent (DTT or β-BME) to promote denaturation. The denatured proteins are subsequently applied to one end of a layer of polyacrylamide gel submerged in a suitable buffer and an electric current is applied across the gel causing the negatively-charged proteins to migrate depending on their size. In SDS PAGE, the protein separation is performed using a discontinuous buffer system. In early stage of electrophoresis, an ion gradient is formed in the stacking gel that causes all of the proteins to focus into a single sharp band. A change of pH and the subsequent elimination of the ion gradient in the resolving gel causes the proteins to separate by the molecular size sieving.

A system with vertically oriented glass plates with 1 mm spacer in between was used for casting gels. The SDS-PAGE gels were cast as following: First the resolving gel (Table 2.2) poured between assembled glass plates and a layer of isopropanol was applied on it. After polymerization of the gel, the layer of isopropanol was removed. Then the stacking gel (Table 2.2) was put on top of the polymerized resolving gel and the combs were inserted.

Components	Separating gel		Stacking gel (4 %) (ml)
	10 % (ml)	17 % (ml)	
40 % Acrylamide/ Bis acrylamide (37.5:1)	15.00	25.60	5.40
Tris HCl (1.0 M, pH 8.8)	22.00	22.00	-
Tris HCl (0.25 M, pH 6.8)	-	-	27.00
10 % SDS	0.60	0.60	0.54
TEMED	0.12	0.12	0.108
10 % APS	0.065	0.065	0.065
H_2O	22.00	11.50	20.90

Table 2.2: Solutions for preparing SDS-PAGE gel. This table shows the compositions of solution used for making 10 % and 17 % SDS-PAGE gel.

To perform electrophoresis, the gel was placed in an electrophoresis chamber covered with 1X SDS-running buffer and combs were removed. The protein samples were mixed with Laemmli loading buffer and were denatured by heating at 95°C for 5 minutes. Then samples were loaded along with molecular weight marker proteins (Table 2.3) on to the wells and electrophoresis was performed at a constant current of 35 mA.

Protein name	Molecular weight (kDa)
β-Galactosidease	116.0
Bovine serum albumin	66.2
Lactate-dehydrogenase	45.0
Restriction endonuclease Bsp981	35.0
Lactoglobulin	18.0
Lysozyme	14.4

Table 2.3: Marker proteins for SDS-PAGE gel. The details of molecular weight marker proteins used for running the SDS gel are shown.

After the electrophoresis, the gel was transferred to the Coomassie staining solution (0.1 % Coomassie brilliant blue R-250, 45 % methanol and 9 % acetic acid) and stained for 20 minutes on an orbital shaking platform. To visualize protein bands on the gel, the gel was placed in the intensive destaining solution (50 % methanol, 10 % acetic acid) for 20 minutes and then in the normal destaining solution (5 % methanol, 7.5 % acetic acid).

2.2.2.2 Western blot (semi-dry)

Blotting buffer	75 mM Tris-Cl, 20% (v/v) methanol, pH 7.4
Phosphate-buffered saline (PBS)	140 mM NaCl, 2.7 mM KCl, 10 mM Na2HPO$_4$,
	1.8 mM KH$_2$HPO$_2$, pH 7.3
PBST	0.1% (v/v) Tween-20 in PBS
Blocking buffer	5% milk powder in PBST
Glycine stripping solution	0.2 M glycine pH 2.8, 0.5 M NaCl
SDS stripping solution	16 mM Tris-HCl pH 6.8, 2% SDS,
	0.1 M ß-mercaptoethanol

Six pieces of 3 mm Whatman paper and one piece of nitrocellulose membrane were cut to the size of the SDS gel. Gel and membrane were equilibrated for 5-15 min in methonal and blotting buffer. The blot was assembled without air bubbles.

For transfer, the current was set to 1 mA/ cm^2 gel size for 45-60 min. The membrane was then briefly washed with PBST and incubated in blocking buffer for one hour at room temperature or 37°C. Decoration with the primary antibody diluted in blocking buffer occurred overnight at 4°C. After three 10-20 min washes with PBST, the membrane was incubated with anti-mouse or

anti-rabbit secondary antibody diluted 1:2000 in blocking buffer, foe one hour at room temperature. The blot was washed three times 10-20 min with PBST and incubated with chemiluminescence substrate solution (ECL, Amersham Biosciences).

Stripping of nitrocellulose membranes

Removal of antibodies from a blot was done under mild conditions to reduce the background for incubation with another primary antibody, either from a different species or for a protein of clearly distinct size than in the first decoration. After washing the membrane in PBST, it was incubated 5-20 min in glycine stripping solution. The solution was neutralised with 1 M Tris-HCl pH 8.5, followed by several washes in PBST. If it was crucial to remove antibodies completely, the blot was incubated in SDS stripping solution for 30 min, tightly closed, on a wheel at 50°C, followed by several washes in PBST. Decoration of the membrane was done as described above, starting from the blocking step again.

2.2.2.2 Protein purification methods

2.2.2.2.1 Bacterial culture and harvesting

The cultivation of bacterial cells for the protein expression was done as following: either a single colony of the plasmid transformed into BL21-DE3 cells or from glycerol stocks was inoculated into 5 ml LB medium containing the ampicillin from LB agar plates and the culture was grown overnight at 37°C. 1 ml of this culture was used for inoculating 100 ml LB medium. This pre-culture was then used for inoculating a fresh 1 liter LB medium supplemented with ampicillin and grown at 37°C with shaking until the optical density at 600 nm (OD_{600}) reached 0.6. At this stage, 1 ml of this culture was collected and treated as uninduced control. The rest of the culture was induced with 0.5 mM IPTG and was let to grow at 37°C for 4-6 hours. The grown cells were then harvested by centrifugation at 8 krpm for 15 minutes (JLA rotor, Ultracentrifuge Coulter-Avanti J-26 XP, Beckmann) and resuspended in cell lysis buffer (20 mM Na-MES pH 6.8, 1 mM EGTA, 0.2 mM $MgCl_2$, 5 mM DTT, 1 mM PMSF, 10 µg/ml leupeptin, 2 mM benzamindin and 10 µg/ml pepstatin A).

2.2.2.2.2 Cell lysis and initial protein purification

The resuspended cells were subjected to mechanical cell disruption by high shear force using French press (A valve-type processor, SLM Instruments, UK). The cells were disrupted by forcing the cell suspension through a narrow valve under high pressure (20000-30000 psi or 140-210 MPa). The cell lysate was centrifuged at 40 krpm (Ti45 rotor, Ultracentrifuge Coulter-Optima LE-80K, Beckman) for 45 minutes at 4°C and the supernatant was collected. The further purification of tau was followed as described previously (Biernat et al., 1992). In brief, the

supernatant was added with NaCl to final concentration of 0.5 M and DTT to final concentration of 5 mM and was boiled at 95°C for 20 minutes. The sample after heating was again centrifuged at 40 krpm for 45 minutes at 4°C and the supernatant collected was dialyzed against suitable buffer required for further purification.

2.2.2.3.3 Purification by Chromatography

Further purification of tau was performed by fast performance liquid chromatography (FPLC) using Akta purifier and Akta explorer FPLC- devices (Amersham Biosciences, Freiburg).

2.2.2.3.3.1 Cation exchange chromatography

Ion exchange chromatography relies on charge-charge interactions between the proteins and the charges immobilized on the ion exchange resin. After the proteins are bound, elution of protein is carried out using a gradient of buffer, which steadily increases the ionic strength of the eluting solution. Alternatively, the pH of the elution buffer can be modified in order to give the protein or the matrix a charge at which they will not interact and proteins of interest elutes from the resin.

Since tau contains positive charges around pH 7.0, cationic exchangers were used and protein was eluted with a gradient of NaCl (varying ionic strength). The column used for cation exchange chromatography was SP-Sepharose 16/10 (Amersham Biosciences, Freiburg). After equilibration with 5 column volumes of the SP-Sepharose buffer A (20 mM Na-MES pH 6.8, 50 mM NaCl, 1 mM EGTA, 1 mM $MgSO_4$, 2 mM DTT, 0.1 mM PMSF), the dialyzed protein sample obtained either by heating or ammonium sulphate precipitation was loaded on the column using a super loop (Amersham Biosciences, Freiburg) and the column was washed with 5-7 column volumes of SP-Sepharose buffer A to remove unbound proteins.

The elution was carried out with a linear gradient of SP-Sepharose buffer B (20 mM Na-MES pH 6.8, 1 M NaCl, 1 mM EGTA, 1 mM $MgSO_4$, 2 mM DTT, 0.1 mM PMSF) in two steps: first from 0 to 60 % in 5-8 column volumes and then to 100 % in 1-2 column volumes. The eluted fractions were checked on SDS-PAGE and fractions containing the protein of interest were pooled together and concentrated using Amicon centrifugal filter devices (Millipore, UK).

2.2.2.3.3.2 Gel filtration chromatography

Gel filtration (or size exclusion) chromatography achieves separation of the analyses based on their differences in size and shape. The gel filtration column is tightly packed with porous polymer beads with different pore size. When the protein is made to pass through the beads using a single buffer solution, the larger molecules, which can not be accommodated into the pores of beads, elutes first and smaller molecules trapped into the pores elute later.

The concentrated protein solution from SP Sepharose column was injected onto pre-equilibrated gel filtration column (HiLoad 16/60 Superdex G200 or HiLoad Superdex G75, prep grade, Amersham Biosciences, Freiburg) using a 1 ml loop with an injection needle. Isocratic elution was performed with PBS buffer containing 1-2 mM DTT at a flow rate of 0.5 ml/min. The eluted fractions were analyzed on SDS-PAGE and pure protein fractions were used for further experiments.

2.2.2.3.3.3 Analytical size exclusion chromatography

Elution profiles of tau isoforms and constructs were obtained by size exclusion chromatography using a Superose PC12 column (Amersham Biosciences, Freiburg) connected to a SMART-HPLC system (Amersham Biosciences, Freiburg). A set of standard proteins and tau isoforms and constructs were subjected to isocratic elution in PBS or PBS containing 2 M GdnHCl with a flow rate of 20 µl/min and the elution was monitored by UV absorbance at 214, 256 and 280 nm. The elution volume of tau isoforms and constructs in the presence and absence of GdnHCl was then used to calculate the apparent Stokes radius of tau with reference to Stokes radii of standard proteins.

Determination of protein concentration:

For full length isoform of tau, a modified BCA method (BCA protein assay reagent, Sigma) was used to determine the concentrations of proteins. Protein sample (50 µl of 50-200 µg/µl) with mixed with 1 ml of reagent mixture (1 ml copper (II) sulfate (Sigma) 4% (w/v), 50 ml biocinchoninic acid solution (Sigma)), the mixture was incubated at 60°C for 30 minutes, and the absorption was measured at 562 nm in a spectrophotometer (Ultrospec 3000 pro and Ultrospec 3100 pro pharmachia Biotech). For the blank reference, H_2O was used instead of the protein solution.

For short tau constructs (K18 and K19), UV adsorption measurements at 214 nm were performed to determine the concentrations of proteins. Protein samples (50 µl of 50-200 µg/µl) were mixed with 95 µl of H_2O, transferred into a quartz microcuvette (1 mm path length, Hellima), and the absorption measured at 214 nm in the spectrophotometer (Ultrospec 3000 pro and Ultrospec 3100 pro pharmachia Biotech). For the zero reference the corresponding buffer of the protein solution was used. For both methods, the protein concentration was calculated from BSA (1 mg/ml, Sigma) standard curve, which was every time in parallel.

2.2.2.4 Cell Culture and transfection (N2a Tet-ON neuroblastoma cell line)

Inducible Tet-On, G418 resistant N2a cell lines were generated as described (Khlistunova et al., 2006). DNA fragments encoding the appropriate constructs of the full length (hTau40$_{wt}$,

hTau40$_{AT8*+AT100+PHF1}$, hTau40CΔ_{wt}, and hTau40C$\Delta_{AT8*+AT100+PHF1}$) were inserted into the bidirectional vector pBI-5 between ClaI and SalI restriction sites (pBI is an unpublished derivative of pBI-2).The constructs were used to express the full-length of hTau40 protein. Transient transfection of N2a Tet-On cells with full length Tau was done with Effectene transfection reagent (Qiagen, Germany). Tet-On inducible cells were cultured in Eagle's minimum essential medium supplemented with 10% fetal calf-serum, 2 mM glutamine, 0.1% nonessential amino acids and 600 µg/ml of G418. The expression of Tau constructs was induced by 1 µg/ml doxycycline.

2.2.2.5 Microtubule polymerization assay

The ability of tau and its mutants to promote microtubule assembly was monitored by UV light scattering at an angle of 90° and a wavelength of 350 nm in a quartz cuvette (path length-0.15 cm) in a Kontron spectrophotometer (Kontron Instruments, Germany) in the presence and absence of tau. A typical experiment was set as following: 5 µM tau was mixed with 30 µM tubulin dimer at 4°C in microtubule assembly buffer (100 mM Na-PIPES, pH
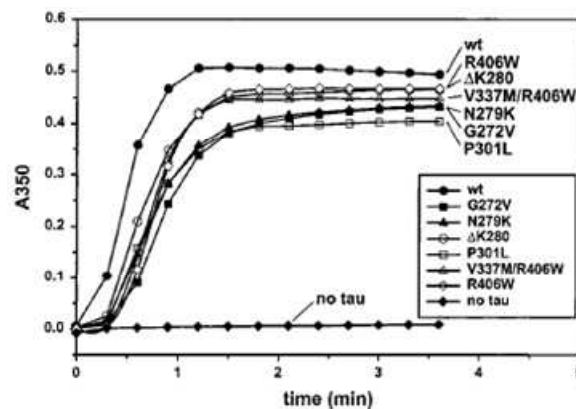
Figure 2.1: Microtubule assembly by tau mutants. Assembly of microtubules is observed by the optical density at 350 nm after a mixture of 30 µM tubulin and 5 µM tau at 4 °C was warmed to 37 °C. Tubulin alone is unable to polymerize because its concentration is below the critical concentration (bottom curve). Wild-type compared with the mutants of htau40 show a slightly increased ability to promote MT assembly. Figure reproduced from Barghorn et al., 2000.

6.9, 1 mM EGTA, 1 mM MgSO$_4$, 1 mM GTP, 1 mM DTT) in a final volume of 20 µl. The reaction was started by raising the temperature to 37°C. The control experiment was conducted without tau. Typical microtubule assembly curves stimulated by tau are shown in Figure 2.1.

2.2.2.5.1 Tau-induced microtubule binding

The reaction was started by raising the temperature to 37°C. For binding of tau to preassembled microtubules, tubulin assembly was performed in microtubule assembly buffer 100 mM Na-PIPES, pH 6.9, 1 mM EGTA, 1 mM MgSO$_4$, 1 mM GTP, 1 mM DTT. Tubulin (30 µM) was

incubated with 30 µM taxol (paclitaxel) at 37°C for 20-30 min to induce microtubule formation. The suspensions of the samples were fractionated by ultracentrifugation at 28,000 x g for 20 min. The stabilized microtubule solutions were then diluted to the desired concentration and titrated with different concentrations of tau to measure the interaction by cosediemention assay. The samples were fractionated by ultracentrifugation at 28,000 x g for 20 min. Supernants and pellets were analyzed by SDS-PAGE (10% polyacrylamide), and the percentages of tau protein in supernants (unbound) and pellets (microtubule-bound) were quantified by densitometry of the Coomassie Blue R-250-stained gels (AIDA IMAGE software).

2.2.2.6 Polymerization of tau *in vitro*

2.2.2.6.1 PHF assembly

Aggregation of tau protein was started by incubating soluble tau protein, typically in the concentration range of 50-500 µM and in the volume range of 20-100 µl, in the presence of the anionic cofactor heparin (MW ~ 3000 or ~ 6000 Da, Sigma, Munich) at 37°C with the protein to heparin ratio 4:1. For experiments of aggregation optimizing conditions, tau protein was taken either in various buffers and pH (of 20 mM concentration) or in a buffer (of 20 mM concentration) with incubation at various temperatures or in a buffer (of 20 mM concentration) containing increasing salt concentration. Aggregation reactions of tau constructs with 4 repeats were supplemented with 1 mM DTT and the typical incubation was ~ 3 days for tau constructs and ~ 5 days for full-length tau isoforms. The formation of aggregates was assayed by ThS fluorescence and the morphology of filaments was analyzed electron microscopy.

The pelleting of PHFs were done at 61 krpm (= 160000g) for 45 minutes at 4°C (TLA 100.3 rotor, TL-100 centrifuge, Beckmann). When needed, PHFs were resuspended with a buffer of choice and pelleted again by centrifugation to minimize the concentration of unpolymerized protein.

2.2.2.6.2 Thioflavin S (ThS) assay

PHF formation was monitored by ThS fluorescence assay (Friedhoff et al., 1998). It is well established that the binding and subsequent increase in ThS fluorescence is specific for the cross-ß-structure that is typical of amyloid fibers.

5 µl of PHF reaction mixture was mixed with 45 µl of 50 mM NH_4Ac containing 20 µM ThS and transferred into a 384-well plate (black microtiter 384 plate round well, ThermoLabsystems, Dreieich). After 15-30 minutes incubation to allow ThS to bind, fluorescence intensity was measured in a Tecan instrument (Ascent, Labsystems, Frankfurt). The experimental parameters were as follows: excitation wavelength = 440 nm, emission wavelength = 521 nm, excitation slit

width = 7.5 nm, emission slit width = 7.5 nm and the temperature = 25°C. Background fluorescence from ThS alone was subtracted when needed and the measurements were carried out in triplicates.

2.2.2.6.3 Light Scattering (90°)

Measurements were performed with a Spex Fluromax spectrophotometer (Polytec, Waldbronn, Germany), using 3x3 mm quartz microcuvettes from Hellma (Muhlheim, Germany) with 30 μl of sample volume at concentration of 25 μM. Experimental parameters were excitation and emission wavelength, 350 nm (90° scattering); scan range 320-400 nm: excitation slit width, 5 nm; emission slit width, 5 nm; integration time, 1 s; photomultiplier, 950 V. Each time three spectra were scanned and averaged. The protein samples were incubated at different time and temperatures (increasing temperature e.g. 10°C for 20 min, 50°C for 20 min, and 50°C for 120 min); the scattering of the buffer was subtracted. All experiments were measured twice. A positive control of strong scattering was obtained from fully aggregated PHFs, as confirmed by ThS fluorescence and electron microscopy.

2.2.2.6.4 ANS fluorescence measurement

Aggregation of tau was also monitored by ANS fluorescence. The increase of ANS fluorescence is observed when it binds to solvent exposed hydrophobic patches (Slavik, 1982). 5 μl of PHF reaction mixture was mixed with 45 μl of 50 mM sodium phosphate pH 7.0 containing 100 μM ANS and transferred into a 384-well plate (black micro titer 384 plate round well, ThermoLabsystems, Dreieich). The measurements were carried out at 25˚C in a TECAN spectrofluorimeter (Ascent, Labsystems, Frankfurt) using an excitation wavelength of 390 nm, an emission wavelength of 475 nm and spectral bandwidths of 7.5 and 7.5 nm for emission and excitation respectively. ANS fluorescence measurements in the presence of GdnHCl were carried out in the same conditions. The effect of GdnHCl on ANS fluorescence was eventually subtracted.

2.2.2.6.5 Transmission electron microscopy

Electron microscopy is an imaging technique in which a beam of electrons passes through a specimen and the transmitted beam is visualized on a photographic film or CCD camera. To enhance the structural details of a sample, staining with heavy metals such as osmium, lead or uranium can be used because the heavy atoms, having dense nuclei, scatter the electrons out of the optical path and hence areas where electrons are scattered appear dark on the screen or on a positive image.

The protein samples were diluted to 1-10 µM and placed on 600 mesh carbon coated copper grids for 45 seconds, washed twice with H_2O and negatively stained with 2 % uranyl acetate for 45 seconds. The specimens were examined with a Philips CM12 electron microscope at 100 kV and 80 kV. Images of PHFs were collected at magnification of 45000 either in the electron image films (SO-163, Eastman Kodak Co., 8.3 x 10.2 cm) and then developed, fixed and dried or captured with a CCD camera (TVIPS, Gauting, Germany) using EMMENU 4 software.

2.2.2.6.6 Sedimentation analysis

Samples of soluble Tau (concentration 20 µM in phosphate buffer pH 6.8) were incubated at different temperatures (10°C for 20 min, 50°C for 20 min, and 50°C for 120 min) and then the samples were collected centrifuged at 100000 x g for 30 min to generate a pellet fraction of Tau protein. After centrifugation, the samples were resuspended in buffer and SDS sample buffer was added to pellets and supernatants, followed by heating to 95°C for 10 min. The samples were run on SDS-PAGE gel containing 10% polyacrylamide gel, and the percentage of Tau protein in the supernatants and pellets were quantified by densitometry of the Coomassie Brilliant Blue R-250 stained gels using AIDA image analysis software.

2.2.2.7 Biochemical assay (Sarkosyl extraction)

For solubility assay, the cells were collected and pelleted down by centrifugation at 1000 X g for 5 min. The levels and solubility of Tau protein was determined by sarkosyl extraction (Greenberg et al., 1990). The cells were homogenized in 10 volumes (w/v) of buffer containing 10 mM Tris-HCl (pH 7.4), 0.8M NaCl, 1mM EGTA and 10% sucrose. The homogenate was spun for 20 min at 20000 X g, and the supernatant was retained. The pellets were re-homogenized in 5 volumes of homogenization buffer and re-centrifuged. Both supernatants were combined, brought to 1% N-laurylsarcosinate (w/v), and incubated for 1 hr at room temperature with shaking, followed by centrifugation at 100,000 X g for 1 hr. The sarkosyl-insoluble pellets were resuspended in 50 Mm Tris-HCl (pH 7.4), 0.5 ml/l g of starting material. The supernatant and sarkosyl insoluble pellet samples were analyzed by Western blotting. The amount of material loaded for supernatant and sarkosyl insoluble pellet represented about 0.5 and 15% of the total material present in the supernatant and pellet, respectively (the ratio between supernatant and Sarkosyl-in-soluble pellet was always 1:30). For quantification of Tau levels in each fraction, the Western blots were probed with pan-Tau antibody K9JA (DAKO, Glostrup, Denmark) and analyzed by densitometry (LAS 3000 and AIDA software, Raytest, Straubenhardt, Germany).

2.2.2.8 Circular dichroism spectroscopy

Circular dichroism (CD) spectroscopy measures differences in the absorption of left-handed polarized light versus right-handed polarized light which arise due to structural asymmetry. A typical CD spectrum contains both positive and negative signals. Information about the secondary structure of a protein can be obtained from the Far-UV spectral region
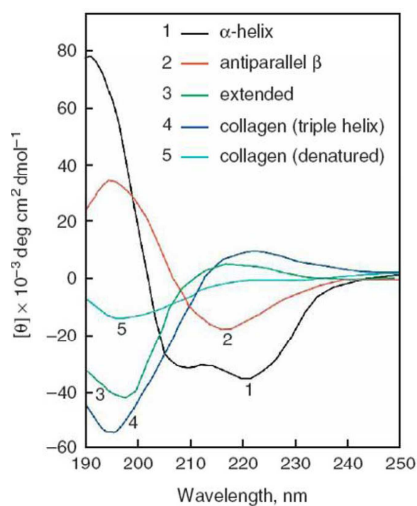
Figure 2.2: Reference CD spectra. Representative CD spectra of polypeptides and proteins are shown. (1) CD spectra of poly-L-lysine in the α-helical conformation (black), (2) in the antiparallel β-sheet (red) at pH 11.1, (3) extended conformation at pH 5.7 (green), (4) collagen in its native triple-helical (blue) and (5) collagen in denatured forms (cyan). Note that the extended conformation of poly-L-lysine is similar to the conformation of poly-L-proline II helix (Figure reproduced from Greenfield, 2006).

(190-250 nm). At this wavelength range, the chromophore is the peptide bond and the signal arises depending on whether it is located in a regular, folded environment. Secondary structures of protein, α-helix, ß-sheet, turn and random coil structures, each give rise to spectra with characteristic shape and magnitude (Fig. 2.2). The CD spectrum for a protein is in turn an average of the entire secondary structure populated in the protein.

All CD measurements were carried out with a Jasco J-810 CD spectrometer (Jasco, Groß-Umstadt) in a cuvette with a path length of 0.1 and 0.01 cm. The spectra were recorded at 20°C between 190-260 nm at a scanning speed of 100 nm/min with a bandwidth of 0.1 nm and a response time of 4 s. In each experiment, three spectra were summed and averaged.

3 Results

3.1. Proteins and phosphomimetic mutations

To assess the effect of phosphorylation on tau properties (aggregation vs. microtubule polymerizing ability), it would be ideal to have methods for site-specific phosphorylation of tau. However, phosphorylation of tau by any kinase generally results in heterogeneous reactions with a mixture of tau molecules phosphorylated at multiple sites to different extents. We therefore generated glu-mutants of tau where phosphorylatable serine or
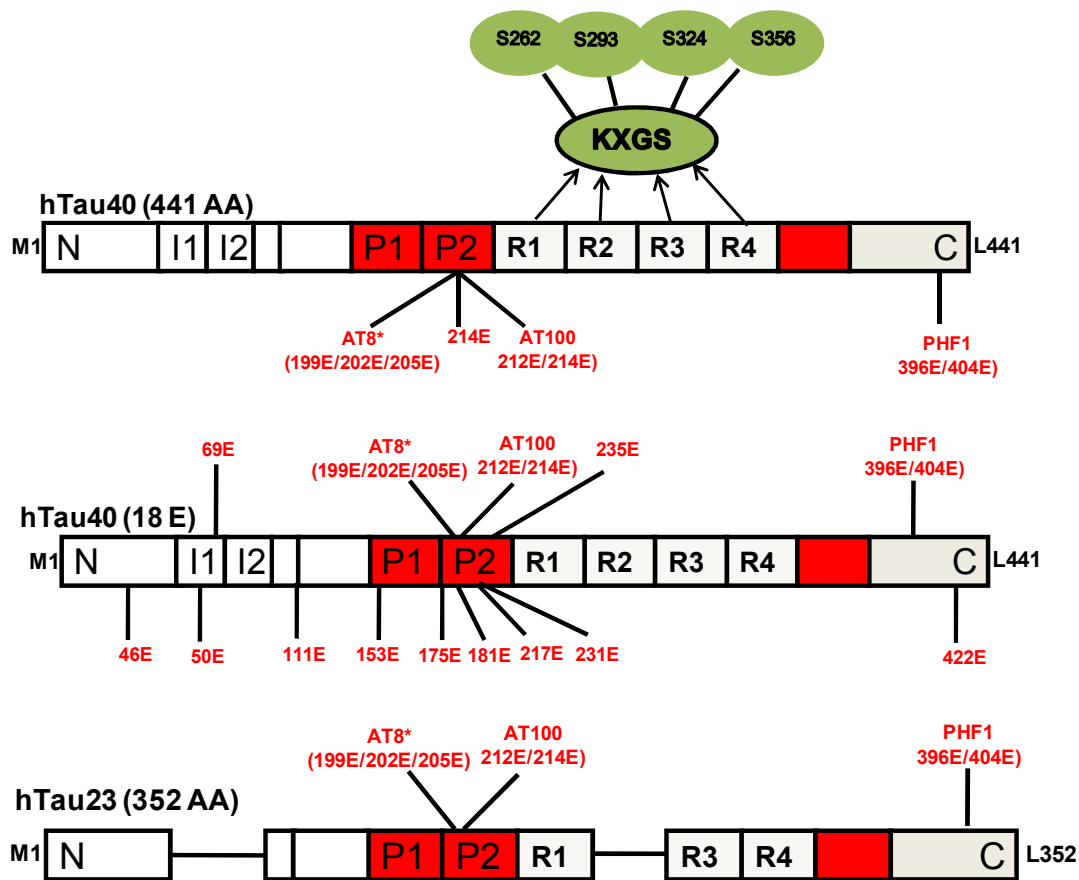
Figure 3.1: Pseudo-phosphorylated mutants of tau. The diagram shows the domain structure of htau40 (largest isoform in human CNS, 441 residues) and htau23 (smallest isoform in human CNS, 352 residues). The fetal isoform htau23 has a similar domain structure but lacks the N-terminal inserts I1, I2, and R2 in the repeat region. The repeat domain (R1-R4) together with flanking proline rich domains is important for binding to and assembling of microtubules. The repeat domains also contribute to the assembly into paired helical filaments (PHFs). All the positions of glu mutations to mimic the SP/TP phosphorylation (SP/TP to E) at sites recognized by Alzheimer specific antibodies such as AT8*, AT100 and PHF1 are shown. In addition, four pseudo-phosphorylation sites of KXGS motifs in the repeat domains of Tau (KXGS to KXGE) are also shown. The phosphorylation at KXGS motifs by non-proline directed kinases such as PKA, MARK, and SADK causes the detachment of tau from the microtubule surface and inhibits the aggregation into filaments.

threonine residues were replaced by glutamate, which is reasonable substitute for phosphorylation. Thus several tau mutants based on full-length isoforms of hTau40 and hTau23

were created bearing glutamate mutation at specific sites (Fig. 3.1), for example phosphorylated epitopes of antibodies AT8* (S199, S202, T205) (Biernat et al., 1992; Goedert et al., 1995) and AT100 (T212, S214) (Hoffmann et al., 1997; Zheng-Fischhöfer et al., 1998).

### 3.1.2 Aggregation propensity and microtubule assembly of hTau40214E

The functions of tau are regulated by phosphorylation. We were interested in the effect of phosphorylation on the global conformation of tau. In particular, we wanted to know whether phosphorylation could induce a state reminiscent of the pathological conformation seen by specific conformational antibodies. To mimic the phosphorylation *in vitro*, we used pseudo-phosphorylation mutants by substituting glu at the phosphorylatable residues. A series of tau mutants with single or multiple pseudo-phosphorylation sites was generated based on the full length isoform of hTau40 and hTau23. To analyze the effect of pseudo-phosphorylation at S214, we mutated S214 residue to glu and compared the mutant hTau40$_{214E}$ with the wild type, hTau40$_{wt}$, for aggregation and microtubule binding properties. Tau aggregation was followed by ThS fluorescence (Friedhoff et al., 1998).

The fluorescence intensity of ThS increases upon binding to cross ß-structure that is characteristic of protein aggregates and is taken as a measure of the formation of tau filaments (Friedhoff et al., 1998). As shown in (Fig. 3.2A) the ThS fluorescence signal indicates that the mutant hTau40$_{214E}$ aggregates much better than hTau40$_{wt}$ in the presence of heparin.

In order to confirm the increased aggregation propensity of the hTau40$_{214E}$ mutant by an independent method, a pelleting assay was used. Samples of the aggregation reaction were collected at regular intervals, pelleted by ultracentrifugation, and loaded on the SDS-PAGE. Better aggregation means higher protein amount in pellet and less protein in the supernatant fraction. Indeed, the increased amount of protein in the pellet fraction collected from the aggregation reaction of the mutant hTau40$_{214E}$ confirmed that this mutant aggregates more efficiently than hTau40$_{wt}$ in the presence of heparin (Fig. 3.2B and C, and the corresponding bar diagram showing only the pellet fraction, Fig. 3.2D). This is consistent with ThS measurements of the aggregation shown in (Fig.3.2A). Electron micrographs of the filaments formed from hTau40$_{S214E}$ show similar morphologies to that of hTau40$_{wt}$ (Fig. 3.2E and 3.2F).
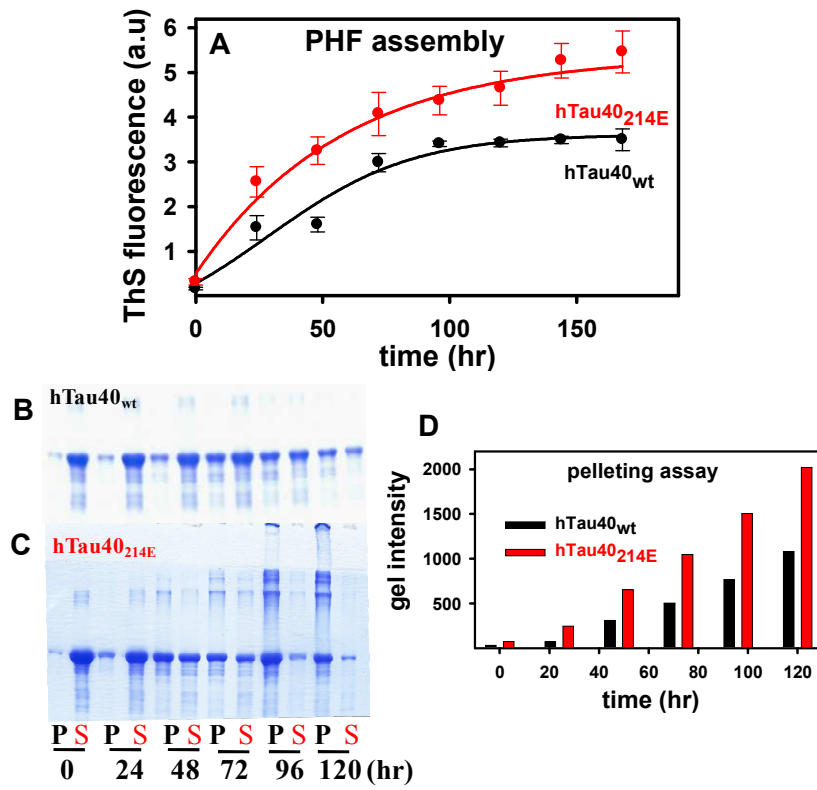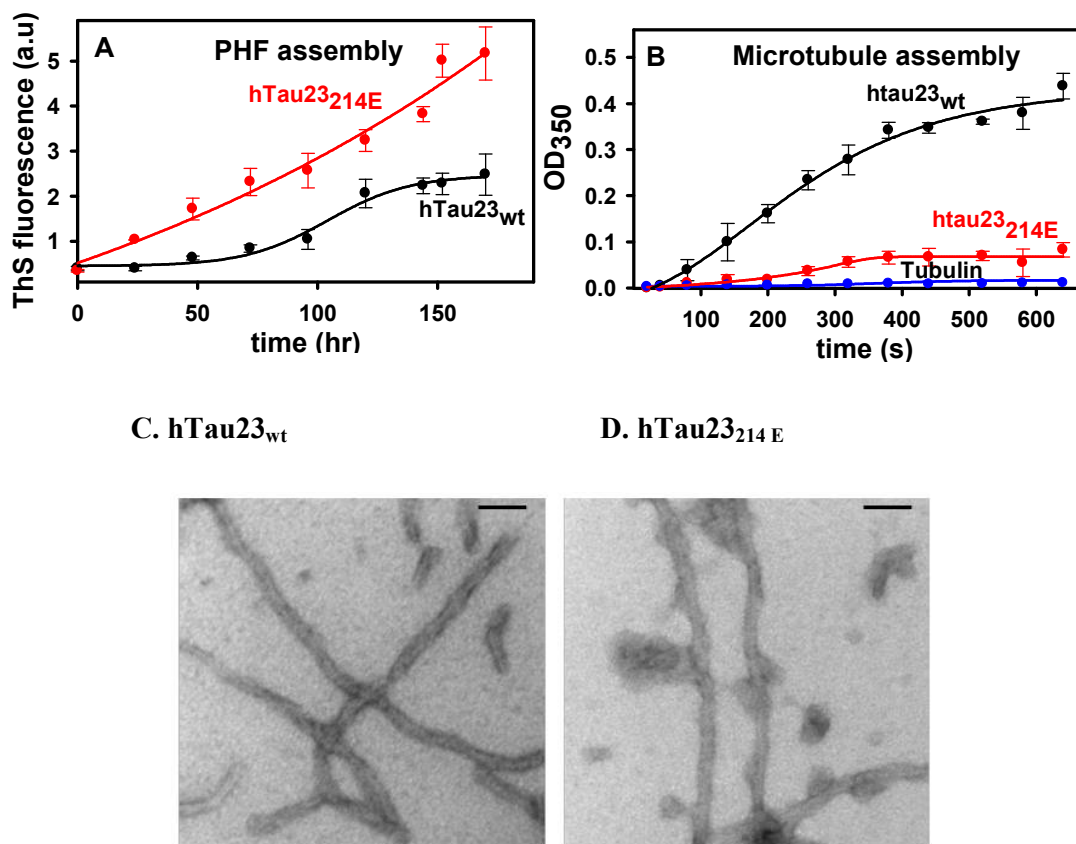
E. hTau40wt
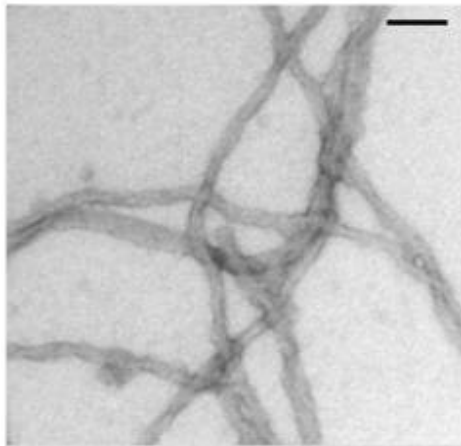
F. hTau40214 E
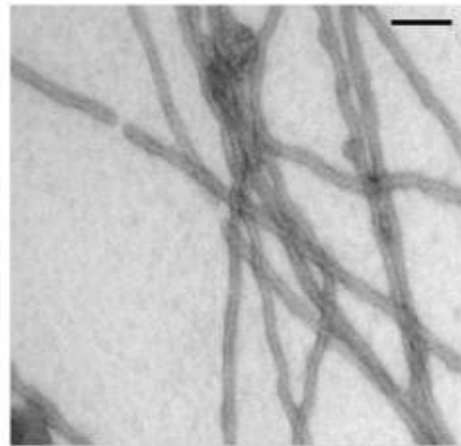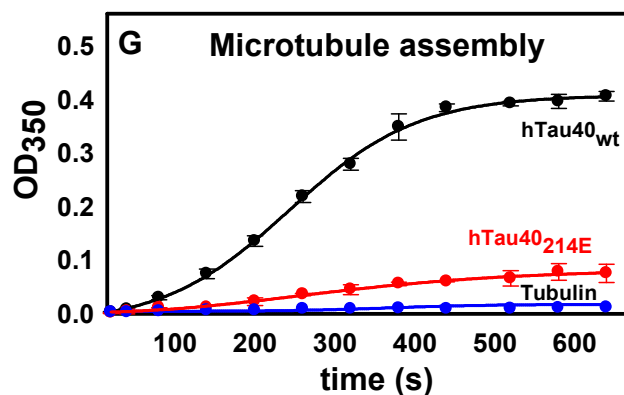
Figure 3.2: Aggregation propensity of hTau40 phospho-mimic mutant S214E . (A) Aggregation of hTau40$_{wt}$ and hTau40$_{214E}$ monitored by ThS fluorescence. The aggregation of wild-type and pseudo-phosphorylated tau was induced by taking 50 µM protein in 20 mM BES pH 7.4 buffer plus 25 mM NaCl in the presence of heparin 6000 (molar ratio of tau:heparin = 4:1) and incubation at 37°C. The aggregation reaction of hTau40 which contains two natural cysteines is supplemented with DTT. The extent of aggregation was then measured by ThS fluorescence at different time intervals. Note that the pseudo-phosphorylated hTau40$_{214E}$ (red line) reaches a higher level of ThS fluorescence intensity compared with hTau40$_{wt}$ (black line) indicating that the substitution of glu at 214 enhances the aggregation efficiency of tau. (B) Pelleting assay of hTau40$_{wt}$ aggregation and (C) Pelleting assay of hTau40$_{214E}$ aggregation. The aggregation reaction samples at given time intervals were centrifuged at 100,000xg for 30 minutes to collect the pellet (= filaments) .The pellet fractions were then loaded on the SDS-PAGE gel, and the corresponding amounts quantified by densitometry were plotted as a bar diagram. Note that tau isoform with S214E mutation aggregates more efficiently compared with wild-type Tau, indicating a higher amount of protein in the pellet as shown by the SDS-PAGE gel (B and C) and the corresponding bar diagram showing only the pellet fraction (D). This is consistent with ThS measurements of the aggregation shown in (A). (E and F) Electron micrographs of filaments formed from hTau40$_{wt}$ and hTau40$_{214E}$ in the presence of heparin. Both filaments are similar in morphology, scale bar correspond to 70 nm. (G) Microtubule polymerization ability of hTau40$_{wt}$ and hTau40$_{214E.}$ Note that tau mutant bearing the single point mutation at S214E strongly suppresses MT polymerization (red line) whereas wild-type tau shows normal ability of assembling microtubules (black line). The bottom curve (blue line) shows there is no assembly of tubulin alone without tau.

To check the effect of glu mutation at 214 on the physiological function of tau, the microtubule polymerizing ability of this mutant was compared with unmodified tau. The tau was mixed with tubulin dimer at 4°C and assembly was started by raising the temperature to 37°C. Fig. 3.2G shows that wild-type tau assembled microtubules normally, as indicated by increasing light scattering at 350 nm. However, the microtubule polymerizing ability of hTau40$_{214E}$ is completely lost as the light scattering of this reaction is almost equal to that of tubulin alone which remains unpolymerized over the reaction time. The inability of tau carrying glu at 214 to induce microtubule polymerization reflects the observation that the phosphorylation of tau at S214 can detach tau from the microtubule surface.

3.1.3 Aggregation propensity and microtubule assembly of hTau23 214E

Another series of tau mutants based on the full length, three repeat isoform of hTau23 was generated with certain pseudo-phosphorylation sites, alone or in combination. We were

interested to know whether the number of repeats has any impact on the aggregation and tau-microtubule interaction of S214E mutant tau.

Figure 3.3: Aggregation propensity of the hTau23 phospho-mimic mutant S214E. (A) Aggregation of hTau23$_{wt}$ and hTau23$_{214E}$ monitored by ThS fluorescence. The aggregation of wild-type and pseudo-phosphorylated tau was induced by taking 50 µM protein in 20 mM BES pH 7.4 buffer plus 25 mM NaCl in the presence of heparin 6000 (molar ratio of Tau:heparin = 4:1) and incubation at 37°C. The extent of aggregation was measured by ThS fluorescence at different time intervals. Note that the pseudo-phosphorylated hTau23$_{214E}$ (red line) reaches a higher level of ThS fluorescence intensity compared with hTau23$_{wt}$ (black line) indicating that the substitution of glu at 214 enhances the aggregation efficiency of tau. (B) Microtubule polymerization ability of hTau23$_{wt}$ and hTau23$_{214E.}$ The ability of tau mutants to assemble microtubule was assessed by light scattering at 350nm in the presence and absence of tau. Note that tau mutant bearing the single point mutation at S214E strongly suppresses MT polymerization (red line) whereas wild-type tau shows normal ability of assembling microtubules (black line). The bottom curve (blue line) shows there is no assembly of tubulin alone without tau. C and D Electron micrographs of filaments formed from hTau23$_{wt}$ and hTau23$_{214E}$ in the presence of heparin. Both filaments are similar in morphology. Scale bars correspond to 70 nm.

The hTau40wt (with four repeats) can bind strongly to microtubules, whereas the hTau23wt (shortest isoform) has only three repeats and binds weakly to microtubules, which results in a lower stabilization of microtubules (Gustke et al., 1994; Ackmann et al., 2000). A similar increase of aggregation propensity and reduction of microtubule polymerizing ability was observed for the S214E mutant of hTau23 (Fig. 3.3). Electron micrographs of the filaments formed from hTau23$_{214E}$ show similar morphologies to that of hTau23$_{wt}$ (Fig. 3.3C and 3.3D) in the presence of heparin.

3.1.4 Aggregation propensity and microtubule assembly of pseudo-phosphorylation at single arm epitope

The choice of phosphorylation sites were based on the epitopes of antibodies that are characteristically elevated in Alzheimer's disease (Fig. 3.1). For example, the triple mutation S199E + S202E + T205E generates pseudo-phosphorylation at the epitope recognized by antibody AT8. For brevity, we will refer to this mutant as the "AT8*" mutant. Phosphorylation at Ser^{202} and Thr^{205} suffices for the reaction with antibody AT8, but Ser^{199} is usually also phosphorylated in brain tissue and can be detected by the antibody, hence we chose the triple mutation and denote it as AT8*. Similarly, the "AT100" mutant contains mutations T212E + S214E, and the "PHF1" mutant contains S396E + S404E. Phosphorylation at these sites generates the epitopes for antibodies AT100 and PHF1.

We first describe the effects of "single arm" pseudo-phosphorylation, either upstream of the repeat domain (sites AT8*, AT100) or downstream (PHF1). The phosphorylation at S202 and T205 recognized by antibody AT8 appears to be an early event in the progression of AD, prior to the formation of tau pre-tangles (Braak et al., 1994). Figure 3.4A shows the aggregation propensity of $hTau40_{AT8*}$. The intensity of the aggregation of the mutant $hTau40_{AT8*}$ is similar to that of $hTau40_{wt}$. Note that pseudo-phosphorylation at the AT8* site has no effect on tau aggregation in the presence of heparin and is similar to the aggregation of $hTau40_{wt}$. This indicates that the phosphorylation recognized by epitope of AT8* does not directly contribute to enhance the aggregation propensity. By contrast, pseudo-phosphorylation at the AT8* site significantly reduced the microtubule polymerizing ability of tau, according to light scattering at 350 nm (Fig. 3.4B). This points out that the phosphorylation recognized by the epitope of AT8* may still contribute to the toxic function of tau by reducing microtubule assembly ability, albeit showing no effect on the aggregation.

To check the effect of pseudo-phosphorylation at the AT100 epitope, another "single arm" epitope, residues T212 + S214 were mutated to glu residues ($hTau40_{212E+214E}$ = $hTau40_{AT100}$). The aggregation extent of this mutant measured by ThS fluorescence is similar to that of $hTau40_{wt}$ in the presence of heparin (Fig. 3.4C). This indicates that pseudo-phosphorylation at the AT100 epitope exhibits no effect on aggregation. Phosphorylation of tau at T212 + S214 is carried out by two kinases, GSK3β and PKA, in a sequential manner and recognized by monoclonal antibody AT100 (Zheng-Fischhöfer et al., 1998). On the other hand, the microtubule polymerizing ability of $hTau40_{AT100}$ (Fig. 3.4D) is significantly
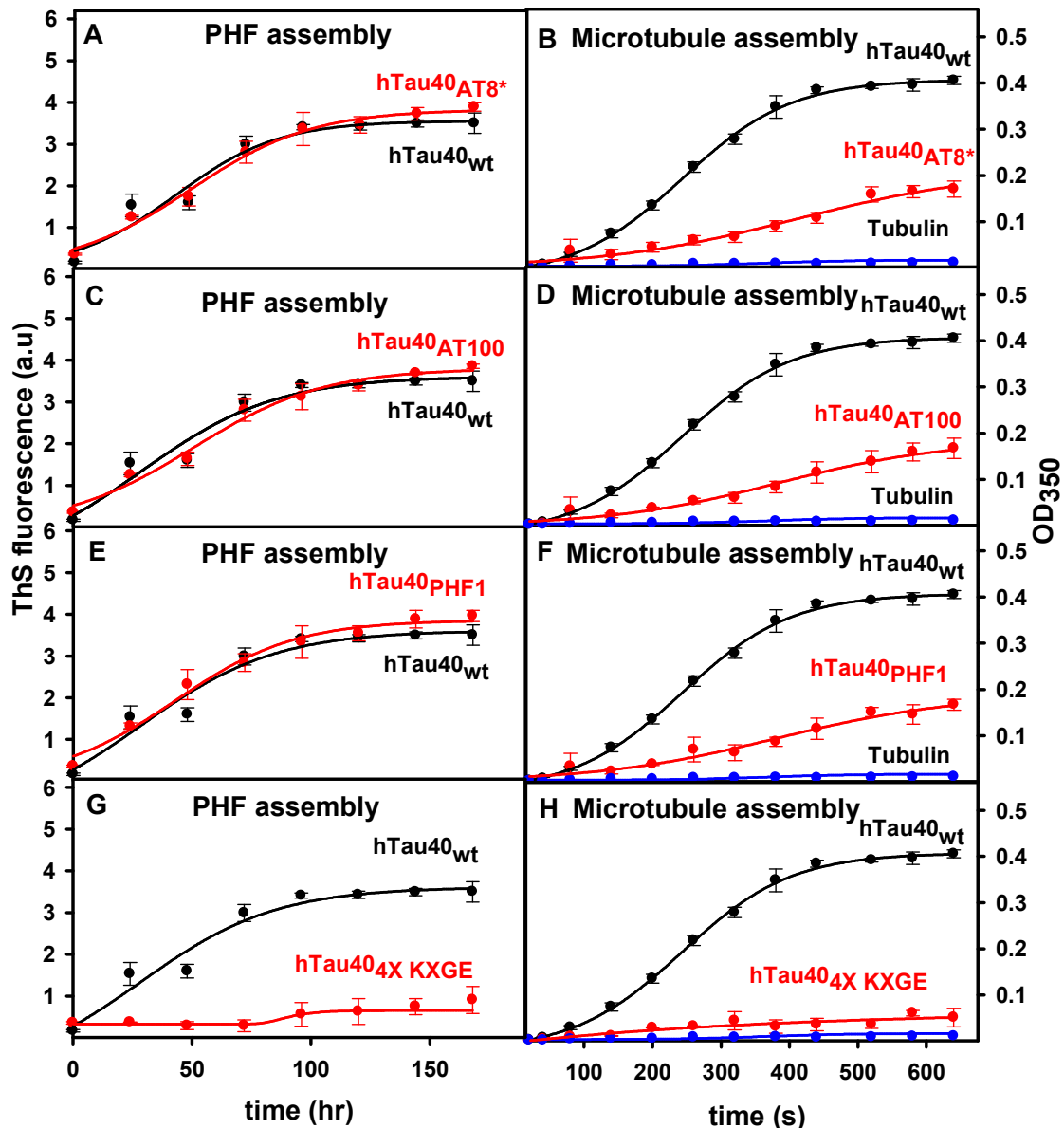
Figure 3.4: Aggregation propensity and microtubule assembly of 'single arm' phospho-mimic mutants of hTau40. (A) Aggregation of hTau40$_{AT8*}$ ascertained by ThS fluorescence. The aggregation of wild-type and pseudo-phosphorylated tau was induced by taking 50 µM protein in 20 mM BES pH 7.4 buffer plus 25 mM NaCl in the presence of heparin 6000 (molar ratio of tau:heparin = 4:1) and incubation at 37°C. The aggregation reaction of hTau40 which contains two natural cysteines is supplemented with DTT. The extent of aggregation was then measured by ThS fluorescence at different time intervals. Note that the pseudo-phosphorylated AT8* mutant (199E+202E+205E) reaches a similar level of aggregation as hTau40 wild-type. (B) Microtubule polymerization ability of hTau40$_{AT8*}$. The tau mutant bearing the single AT8*epitope exhibits reduced microtubule polymerization compared to the wild-type. (C) and (D) Aggregation and microtubule assembly of hTau40$_{AT100}$. The AT100 mutant pseudo-phosphorylated at 212E+214E attains a similar level of aggregation as the hTau40 wild-type, but the level of microtubule assembly is reduced. (E) and (F) Aggregation and microtubule assembly of hTau40$_{PHF1}$. The PHF1 mutant pseudo-phosphorylated at 396E+404E also reaches a level of aggregation similar to that of the hTau40 wild-type and also shows reduced microtubule assembly (G) Aggregation of hTau40$_{4xKXGE}$ monitored by ThS fluorescence. The aggregation of hTau40 mutant carrying glu mutations to mimic the phosphorylation at four KXGS motifs in the repeat domains (262E+293E+324E+356E) was assessed in the presence of heparin. Note that the pseudo-phosphorylation at KXGS motifs abrogates the aggregation propensity compared to the hTau40wt. (H) Microtubule polymerizing ability of hTau40$_{wt}$ and hTau40$_{4xKXGE}$. Note that the tau mutant bearing at KXGS motifs strongly suppresses MT polymerization (redline) whereas wild-type tau shows normal

ability of assembling microtubules (black line). The bottom line curve (blue line) shows that there is no
assembly of tubulin alone without tau.

less than hTau40$_{wt}$ but not completely abolished as in the case of hTau40$_{214E}$ (see Fig. 3.2G).
This indicates that the additional pseudo-phosphorylation at T212 can less reduced microtubule
assembly than compared to the effect of a single pseudo-phosphorylation at S214 that shows
complete reduction in microtubule assembling ability.

The antibody PHF1 recognizes phosphorylation of tau at S396 and S404 in the arm downstream
of the repeats. To analyze the effect of pseudo-phosphorylation at the PHF1 epitope, a hTau40
mutant was created bearing glu mutants at S396 and S404 (hTau40$_{PHF1}$). The aggregation
behavior of the mutant hTau40$_{PHF1}$ is similar to that of hTau40$_{wt}$ in the presence of heparin as
indicated by ThS fluorescence signal (Fig. 3.4E), indicating that pseudo-phosphorylation at
PHF1 does not affect the aggregation very much. Though earlier reports have shown that the
phosphorylation at S396+S404 increases the tau polymerization in the presence of arachidonic
acid (Abraha et al., 2000). This may be due to the variation in the experimental conditions and
constructs used in this study. On the other hand, (Fig. 3.4F) the microtubule polymerizing ability
of hTau40$_{PHF1}$ is significantly decreased compared with that of hTau40$_{wt}$ (Fig. 3.4F). These
results show that pseudo-phosphorylation at the flanking domains (AT8*, AT100, and PHF1) do
not exert any effect on the aggregation rather they show a moderate effect on the microtubule
polymerizing ability.

3.1.5 Aggregation propensity and microtubule assembly of KXGS motifs

Within the tau protein, there are 30 different sites that are modified post-translationally by
phosphorylation. The phosphorylation at the KXGS motifs in the repeat domains of tau by non-
proline directed kinases such as MARK, PKA, and SADK is shown to reduce tau binding to
microtubules (Brandt et al., 1994; Drewes et al., 1997; Illenberger et al., 1998; Zheng-Fischhofer
et al., 1998). In order to check this effect *in vitro*, we created a hTau40 mutant bearing glu
mutation at S262, S293, S325, and S356 (hTau40$_{4xKXGE}$). The aggregation of hTau40$_{4xKXGE}$ is
completely attenuated in the presence of heparin as the ThS fluorescence signal was very low
over the reaction time (Fig. 3.4 G). We observed that pseudo-phosphorylation at KXGS motifs is
structurally unfavorable for the packing of tau molecules into filaments. Note that the pseudo-
phosphorylation at the four KXGS motifs abrogates the aggregation capacity of tau in the
presence of heparin. This is consistent with the earlier studies showing that phosphorylation at
the KXGS motifs protects tau against aggregation (Schneider et al., 1999).

On the other hand, the analysis of the microtubule polymerizing ability (Fig. 3.4H) of
hTau40$_{4xKXGE}$ showed that the pseudo-phosphorylation at the four KXGS motifs completely

abolishes the microtubule polymerizing ability of tau. This is again in consistency with the earlier studies showing that the phosphorylation at KXGS motifs detaches tau from microtubules (Drewes et al., 1997). The aggregation and microtubule assembly property of pseudo-phosphorylated tau at KXGS motifs completely reflects the *in vivo* observation (Biernat et al., 1999). These result show that pseudo-phosphorylation can emulate the effect of real phosphorylation at KXGS motifs (Biernat et al., 1993 and Drewes et al., 1995).

3.1.6 Aggregation propensity and microtubule assembly of combined pseudo-phosphorylation at certain epitopes

We next asked whether the aggregation and microtubule polymerization of tau is affected by a combination of pseudo-phosphorylated epitopes. In other words, we combined a pseudo-phosphorylation (*e.g.* 214E, 4X KXGE) with epitope specific sites (*e.g.* AT8*, AT100, and
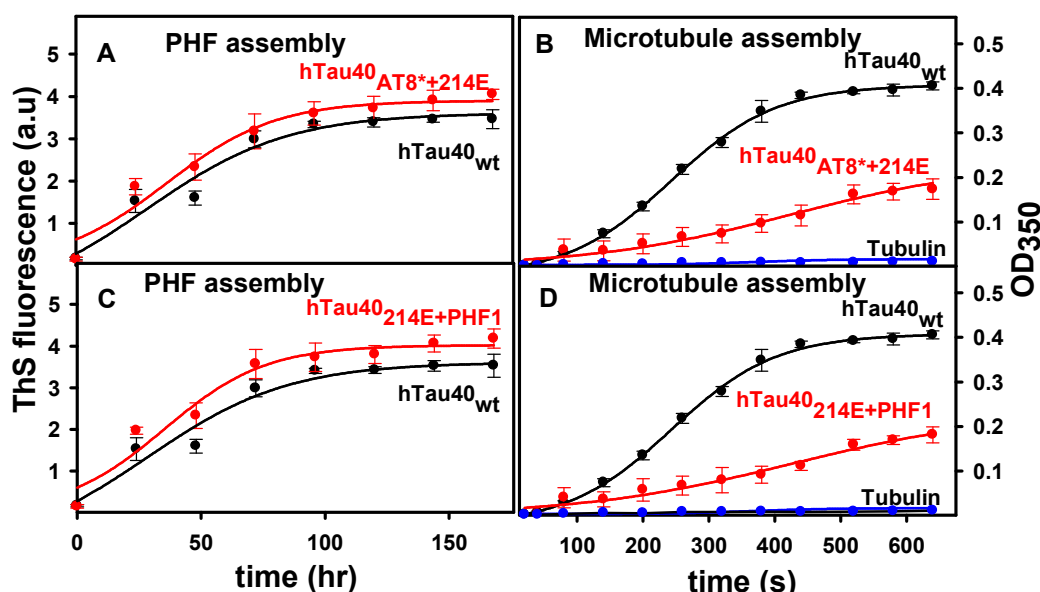
Figure 3.5: Aggregation propensity and microtubule assembly of 'double' or 'double arm' phospho-mimic mutants of hTau40. (A) and (B) Aggregation and microtubule assembly of hTau40$_{AT8*+214E}$. The aggregation of wild-type and pseudo-phosphorylated tau was induced by taking 50 μM protein in 20 mM BES pH 7.4 buffer plus 25 mM NaCl in the presence of heparin 6000 (molar ratio of tau:heparin = 4:1) and incubation at 37°C. The aggregation reaction of hTau40 which contains two natural cysteines is supplemented with DTT. The extent of aggregation was then measured by ThS fluorescence at different time intervals. Note that the pseudo-phosphorylated hTau40$_{AT8*+214E}$ (red line) reaches the same level of ThS fluorescence intensity compared with hTau40$_{wt}$ (black line) indicating that the substitution of glu at AT8*+214E has no effect on the aggregation. On the other hand, hTau40$_{AT8*+214E}$ shows a significant reduction in the microtubule polymerizing ability. (C) and (D) Aggregation and microtubule assembly of hTau40$_{214E+PHF1}$. Note that the pseudo-phosphorylated hTau40$_{214E+PHF1E}$ (red line) reaches only slightly increased levels of ThS fluorescence intensity compared with hTau40$_{wt}$ (black line) indicating that the substitution of glu at AT8*+214E has no effect on the aggregation. On the other hand, hTau40$_{214E+PHF1E}$ shows a significant reduction in the microtubule polymerizing ability.

PHF1) and also created combinations of epitope-specific pseudo-phosphorylation (*e.g.* AT8*+PHF1 and AT100+PHF1). We created a mutant based on hTau40 with glu mutations mimicking AT8* epitope plus mutation of 214 (hTau40$_{AT8*+214E}$) and tested its aggregation and microtubule assembly properties. The ThS fluorescence signal from the aggregation reaction of this mutant is almost similar to that of wild-type hTau40 (Fig. 3.5A), indicating that combination of pseudo-phosphorylation at 214 and AT8* site does not affect the aggregation to a large extent. However, this mutant showed a substantial reduction in polymerization of microtubules (Fig. 3.5B). This result indicates that the effect of 214 alone (see Fig. 3.2G) is reversed by additional mutation in the flanking domains.
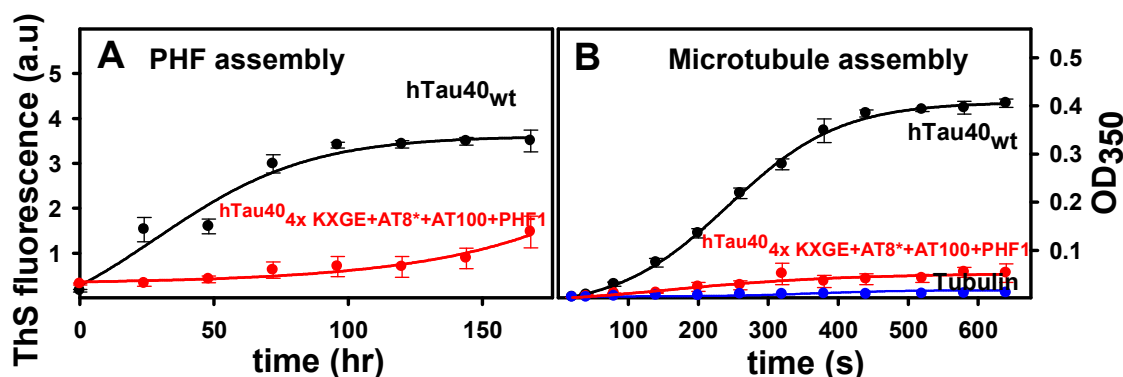
Figure 3.6: Aggregation propensity and microtubule assembly of hTau40 mutants mimicking phosphorylation in the repeat domain and in the flanking regions. (A) Aggregation of htau40$_{AT8*+AT100+PHF1+4xKXGE}$ monitored by ThS fluorescence. The aggregation of wild-type and pseudo-phosphorylated tau was induced by taking 50 µM protein in 20 mM BES pH 7.4 buffer plus 25 mM NaCl in the presence of heparin 6000 (molar ratio of tau:heparin = 4:1) and incubation at 37°C. The aggregation reaction of hTau40 which contains two natural cysteines is supplemented with DTT. The extent of aggregation was then measured by ThS fluorescence at different time intervals. Note that the pseudo-phosphorylation at KXGS motifs with flanking regions, hTau40$_{AT8*+AT100+PHF+4xKXGE}$ (red line) abrogates the aggregation propensity compared to the hTau40$_{wt}$ (black line). (B) Microtubule polymerization ability of htau40$_{AT8*+AT100+PHF1+4xKXGE}$. Note that the tau mutant bearing the mutations at all 4four KXGE motifs and at the flaking regions (AT8*+AT100+PHF1) strongly suppresses MT polymerization (red line) whereas wild-type tau shows normal ability of assembling microtubules (black line). The bottom curve (blue line) shows there is no assembly of tubulin without tau.

We then created mutants that carry pseudo-phosphorylation at flanking domains upstream and downstream to the repeat domains and investigated the change in the aggregation and microtubule polymerizing properties. The mutant based on hTau40 with a combination of glu mutations at S214 and the PHF1 site (396E+404E) showed no significant differences in the aggregation efficiency to that of wild-type hTau40 (Fig. 3.5C). On the hand this mutant, hTau40$_{214E+PHF1}$, shows a significant decrease in the ability to promote microtubule polymerization. This again confirms that the effect of 214E is reversed by additional mutations in the flanking domains (Fig. 3.5D).

Hence, we asked whether the inhibitory effect of pseudo-phosphorylation at KXGS motifs could be rescued by flanking pseudo-phosphorylation. To analyze that, we created a hTau40 mutant with the combination of pseudo-phosphorylation at epitopes AT8*, AT100, PHF1, and the four KXGS motifs, $hTau40_{AT8*+AT100+PHF1+4xKXGE}$. The aggregation of this mutant followed by ThS fluorescence showed that this mutant did not aggregate (Fig. 3.6A). This indicates the inability of the flanking pseudo-phosphorylation to counteract that in KXGS motifs. This indicates that 4xKXGE (see fig. 3.4 G) pseudo-phosphorylation exhibits a strong inhibitory effect on the aggregation even in the presence of the additional flanking mutations at AT8*+AT100+PHF1 (which by itself increase aggregation significantly, Fig. 3.9A). At the same time, this mutant $hTau40_{AT8*+AT100+PHF1+4xKXGE}$ showed complete reduction in the ability to polymerize microtubules (Fig. 3.6 B). This again proves the strong inhibitory effect of the phosphorylation at KXGS motifs. This clearly indicates that glu mutation at KXGS motifs can not be overridden by the flanking pseudo-phosphorylation at AT8*+AT100+PHF1 (which by itself show no effect on the microtubule polymerizing ability of tau, Fig. 3.10).

3.1.7 Aggregation propensity and microtubule assembly of 'double' or 'double arm' pseudo-phosphomemitic mutants of the fetal isoform of hTau23

We next asked whether the aggregation and microtubule polymerization of tau is affected by a combination of pseudo-phosphorylated epitopes on the level of three repeat hTau23. We first describe the effect of double epitope or double arm combination (double arm denotes two epitopes mutated to glutamic acid) of glu mutations at the AT8* + AT100, AT8* + PHF1, and AT8* + AT100 + PHF1 sites. Pseudo-phosphorylation mutant $hTau23_{AT8*+AT100}$ aggregates much better than $hTau23_{wt}$, indicated by the extent of ThS fluorescence intensity (Fig. 3.7A). This result suggests that the combination of AT8* + AT100 has only a moderate effect on enhancing aggregation in the presence of heparin. In addition, this mutant also exhibits a reduced capacity to promote microtubule polymerization (Fig. 3.7B).

We then created mutants that carry pseudo-phosphorylation at the flanking domains upstream and downstream of the repeat domains and investigated the change in the aggregation and microtubule polymerizing properties. In Fig. 3.7B, the double arm pseudo-phosphorylation based on $hTau23_{AT8*+PHF1}$ does increase the aggregation extent measured by ThS fluorescence. This result clearly indicates that the double arm pseudo-phosphorylation mutant $hTau23_{AT8*+PHF1}$ somewhat increases the aggregation propensity. On the other hand this mutant $hTau23_{AT8*+PHF1}$ also showed a significant reduction in the microtubule polymerization compared to hTau23wt (Fig. 3.7D).
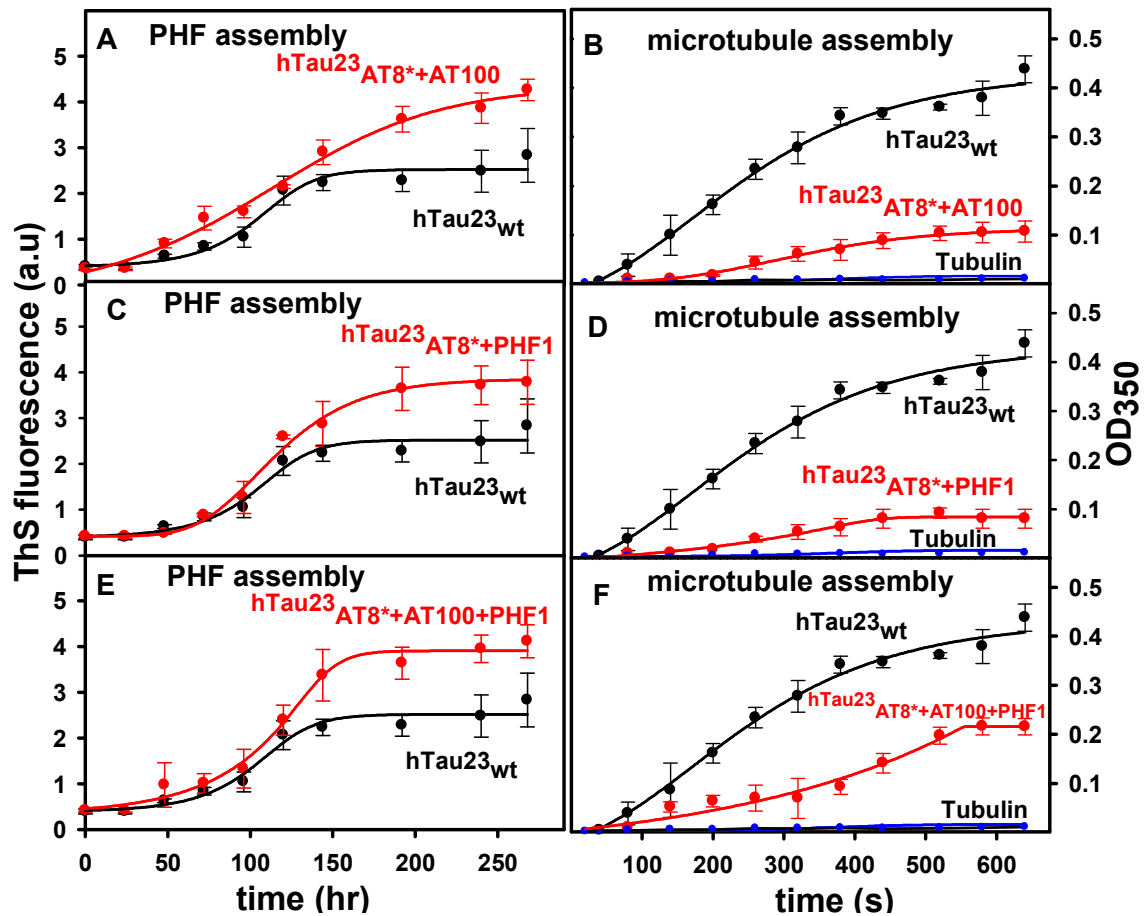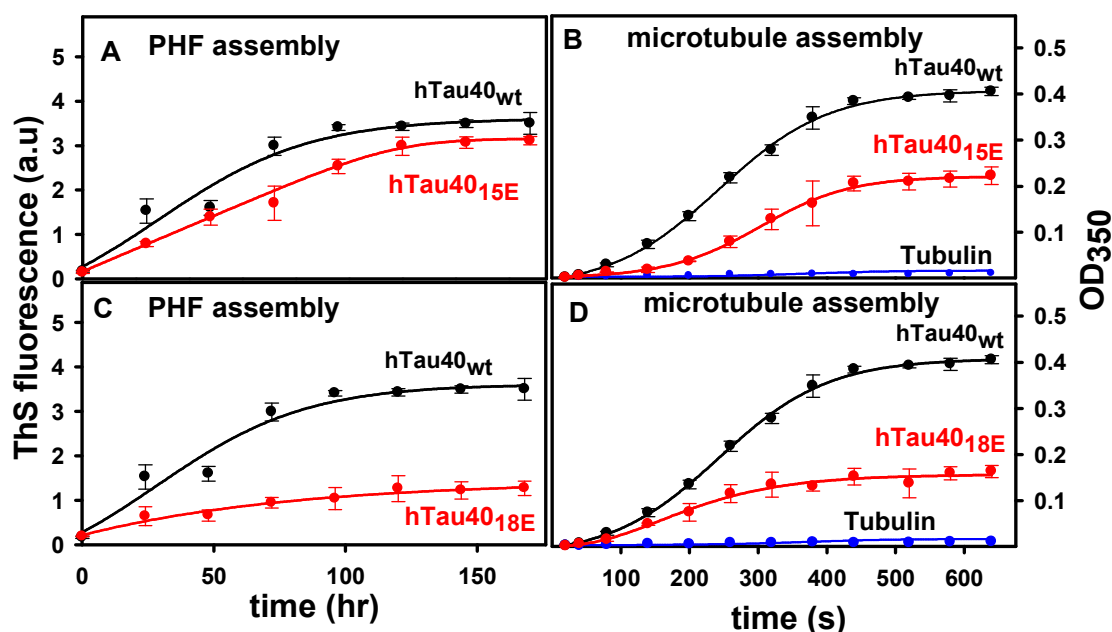
Figure 3.7: Aggregation propensity and microtubule assembly of 'double arm' phospho-mimic mutants of the fetal isoform hTau23. (A) and (B) Aggregation and microtubule assembly of hTau23$_{AT8*+AT100}$. The aggregation of wild-type and pseudo-phosphorylated tau was induced by taking 50 µM protein in 20 mM BES pH 7.4 buffer plus 25 mM NaCl in the presence of heparin 6000 (molar ratio of Tau:heparin = 4:1) and incubation at 37°C. The extent of aggregation was measured by ThS fluorescence at different time intervals. Note that the pseudo-phosphorylated hTau23$_{AT8*+AT100}$ (red line) reaches a higher level of ThS fluorescence intensity compared with hTau23$_{wt}$ (black line) indicating that the substitution of glu at AT8*+AT100 enhances the aggregation efficiency of tau. (C) and (D) Aggregation and microtubule assembly of hTau23$_{AT8*+PHF1}$. The double arm pseudo-phosphorylation based on hTau23 (hTau23$_{AT8*+PHF1}$) does increase the aggregation extent, measured by Th S fluorescence. (E) and (F) Aggregation and microtubule assembly of hTau23$_{AT8*+AT100+PHF1}$. The double arm pseudo-phosphorylation based on hTau23 (hTau23$_{AT8*+AT100+PHF1}$) does increase the aggregation extent, measured by Th S fluorescence, and also reduced the microtubule polymerization. The bottom curve (blue line) shows there is no assembly of tubulin without tau.

We then created a triple epitope mutant based on hTau23 that has a combination of pseudo-phosphorylations at the epitopes AT8* + AT100 + PHF1 (that is: S199, S202, T205, T212, S214, S396, and S404 were mutated to glu). The aggregation behavior of hTau23$_{AT8*+AT100+PHF1}$ was analyzed by ThS fluorescence. The double arm pseudo-phosphorylation at triple epitopes AT8* + AT100 + PHF1 increases the aggregation extent (Fig. 3.7E) and is similar to hTau40$_{AT8*+AT100+PHF1}$ (see Fig. 3.9A). On the other hand, the pseudo-phosphorylation of hTau23$_{AT8*+AT100+PHF1}$ induced a substantial reduction in its ability to promote microtubule polymerization (Fig. 3.7F).

3.1.8 Aggregation propensity and microtubule assembly of multiple pseudo-phosphorylation of tau

We finally investigated the effect of hyperphosphorylation by mimicking SP/TP phosphorylation at 15 and 18 sites that are known to be hyperphosphorylated in tau of AD brain. The insertion of glu mutations at 15 SP/TP sites includes positions: T111, T153, T175, T181, S199, S202, S205, T212, S214, T217, T231, S235, S396, S404, and S422. This mutant is denoted as $hTau40_{SP/TP}$ $_{(15E)}$. The aggregation of the mutant $hTau40_{SP/TP\ (15E)}$ is very similar to that of $hTau40_{wt}$ in the presence of heparin (Fig. 3.8A), indicating that the pseudo-

Figure 3.8: Aggregation propensity and microtubule assembly of hyper-phosphorylated tau: (A) Aggregation of $hTau40_{SP/TP\ (15E)}$ monitored by ThS fluorescence. The pseudo-phosphorylation at (T111, T153, T175, T181, S199, S202, S205, T212, S214, T217, T231, S235, S396, S404, and S422) was created to mimic hyperphosphorylation of tau at SP/TP motifs found in Alzheimer disease. The aggregation of wild-type and pseudo-phosphorylated tau was induced by taking 50 µM protein in 20 mM BES pH 7.4 buffer plus 25 mM NaCl in the presence of heparin 6000 (molar ratio of tau:heparin = 4:1) and incubation at 37°C. The aggregation reaction of hTau40 which contains two natural cysteines is supplemented with DTT. The extent of aggregation was then measured by ThS fluorescence at different time intervals. Note that the pseudo-phosphorylated $hTau40_{15E}$ (red line) slightly reduced the level of ThS fluorescence intensity compared with $hTau40_{wt}$ (black line) indicating that the substitution of glu at 15E has little effect on the aggregation. (B) Microtubule polymerization ability of $hTau40_{SP/TP\ (15E)}$. The hTau40 mutant pseudo-phosphorylated at 15 SP/TP motifs shows a significantly reduced ability to promote microtubule assembly. This indicates that the hyperphosphorylation of tau impairs the microtubule polymerization ability of tau. (C) Aggregation of $hTau40_{SP/TP\ (18E)}$ monitored by ThS fluorescence. The hTau40 mutant pseudo-phosphorylated at 18SP/TP motifs (including 3 additional sites in the N-terminal inserts domain, S46E, T50E, and T69E plus 15 sites mentioned above) show very little aggregation ability in the presence of heparin compared with $hTau40_{wt}$. (D) Microtubule polymerization ability of $hTau40_{SP/TP\ (18E)}$. Note that this mutant further reduced microtubule assembly.

phosphorylation at 15 SP/TP sites does not seem to have a strong effect on the aggregation efficiency. This result clearly indicates that the hyper (pseudo-) phosphorylation does not seem to drive tau into aggregation efficiently. However, this mutant did show a slightly reduced ability to polymerize microtubules (Fig. 3.8B). The pseudo-phosphorylation at 18 SP/TP sites includes 3 additional sites within the N-terminal inserts (S46, T50, and T69 plus the 15 sites mentioned above) and is denoted hTau40$_{SP/TP\ (18E)}$. The mutant hTau40$_{SP/TP\ (18E)}$ showed surprisingly a high reduction in aggregation in the presence of heparin compared with wild-type hTau40, measured by ThS fluorescence intensity (Fig. 3.8C). This indicates that multiple pseudo-phosphorylations can further dampen the aggregation efficiency of tau in the presence of heparin.

Similarly, the microtubule polymerization ability of hTau40$_{SP/TP\ (18E)}$ was further reduced (Fig. 3.8D). This clearly indicates that hTau40 bearing the pseudo-phosphorylation at 18 SP/TP motifs also shows a significantly reduced ability to promote microtubule assembly and is similar to that of hTau40$_{SP/TP\ (15E)}$.

3.2 Proline directed pseudo-phosphorylation at AT8*, AT100, and PHF1 sites

Tau in solution adopts preferred long range interactions between the repeat domain and the C-terminus and between the N-and C-terminus (paperclip conformation) as measured by FRET. In solution, the C-terminal domain of tau is unexpectedly close (19-23 Å) to the repeat domain and therefore causes a pronounced FRET signal, whereas the N-terminal domain (residue 17) is not within the FRET range of the repeat domain, but close to the C-terminal tail whereby it causes FRET (21-24 Å) (Jeganathan et al., 2006). The paperclip conformation becomes tighter or looser, depending on the pseudo-phosphorylation state. In particular pseudo-phosphorylation at the epitope of the diagnostic antibody AT8* (S199E + S202E + T205E) moves the N-terminal domain away from the C-terminal domain. Pseudo-phosphorylation at the PHF1 epitope (S396E + S404E) moves the C-terminal domain away from the repeat domain. In both cases the paperclip conformation is opened up. By contrast, the combination of AT8* and PHF1 sites leads to compaction of the paperclip, such that the N-terminus approaches the repeat domain. The compaction becomes even stronger by combining pseudo-phosphorylated AT8*, AT100, and PHF1 epitopes. The phosphorylation at critical sites upstream or downstream of the repeats indeed modifies the global conformation of tau, so that the paperclip structure is either opened or tightened. In the later case the N-terminal domain approaches the repeat domain, which is reminiscent of the conformation recognized by conformation-dependent antibodies Alz-50 and MC1 (Jeganathan et al., 2008).

3.2.1 Aggregation propensity and microtubule assembly properties of pseudo-phosphorylation mutant at AT8*, AT100, and PHF1 epitopes

Since the functions of tau are regulated by phosphorylation we were interested whether this would affect the global conformation. In particular, we wanted to know whether phosphorylation could induce a state reminiscent of the pathological conformation seen by antibodies. To mimic the phosphorylation *in vitro*, we used pseudo-phosphorylation mutants by substituting glu at the phosphorylatable residues. The choice of phosphorylation sites was based on the epitopes of antibodies that are characteristically elevated in AD. To check whether the conformation of tau is affected by a combination of pseudo-phosphorylated epitopes, we tested the combination of glu mutations at the AT8*, AT100, and PHF1 epitopes with the "triple epitope" mutant hTau40$_{AT8*+AT100+PHF1}$. The aggregation behavior and microtubule assembly properties of hTau40$_{AT8*+AT100+PHF1}$ was reported in our recent study (Jeganathan et al., 2008). Based on the FRET analysis of tau mutants carrying pseudo-phosphorylation for these epitopes, we reasoned that a tight compaction of global folding due
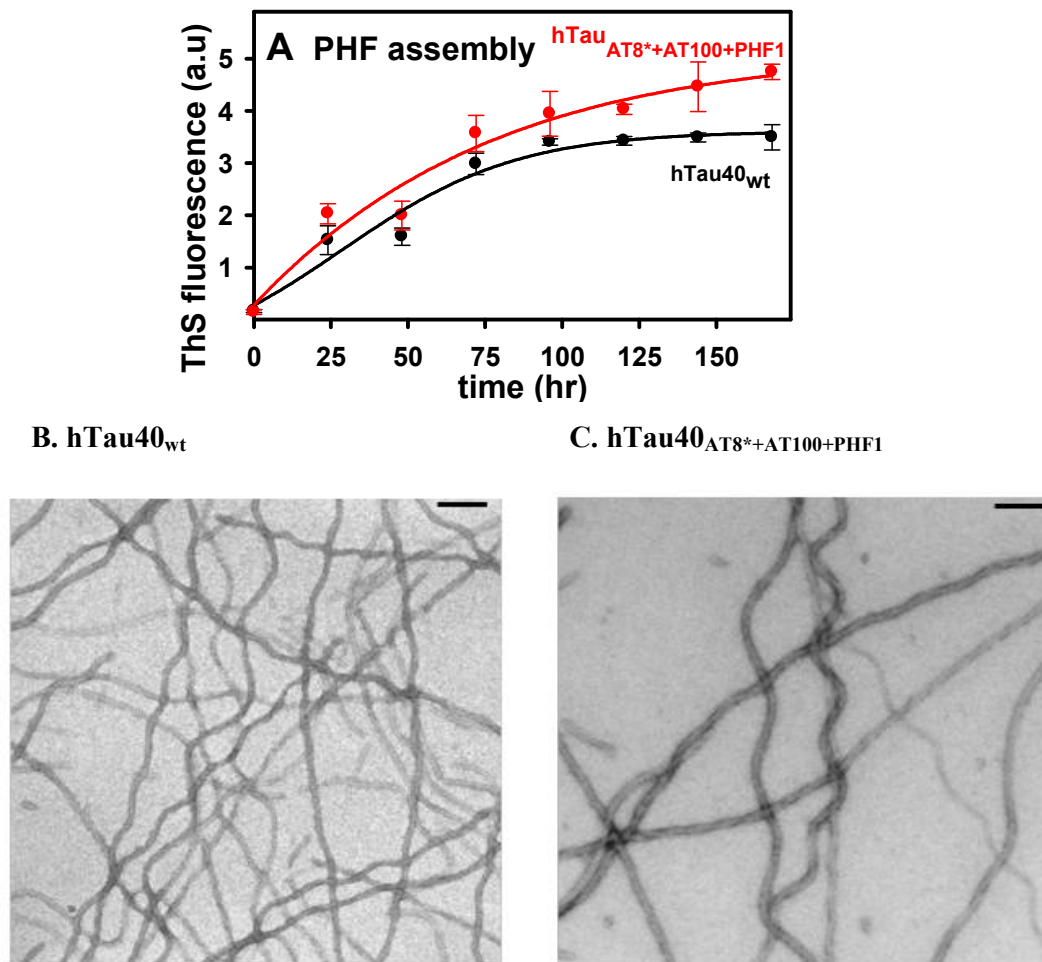
Figure 3.9: Aggregation propensity of phosphomimetic mutant hTau40_{AT8*+AT100+PHF1}: (A) Aggregation of hTau40_{AT8*+AT100+PHF1} monitored by ThS fluorescence. Aggregation was induced from 50 µM protein in 20 mM BES pH 7.4 plus 25 mM NaCl buffer with addition of heparin 6000 (molar ratio of Tau: heparin = 4:1) and DTT. The pseudo-phosphorylated protein reaches a higher level of ThS fluorescence than hTau40wt. (B) Electron micrographs of the filaments formed from hTau40_{wt} and hTau40_{AT8*+AT100+PHF1} in the presence of heparin. Scale bars indicate 100 nm.

to the pseudo-phosphorylation at the epitopes of AT8*+AT100+PHF1 may cause a moderate but significant increase in the aggregation of this mutant in the presence of heparin (Fig. 3.9A). However, the microtubule polymerizing ability of hTau40_{AT8*+AT100+PHF1} showed no marked difference in microtubule assembly (Fig. 3.10). To relate the global conformation changes of tau induced by pseudo-phosphorylation to the functions of tau we tested the propensity to aggregation, the ability to promote microtubule polymerization, and the reaction with antibodies MC1 and Alz-50 which are characteristic of pathological conformations of tau in AD. These properties were compared for wild-type tau and the triple pseudo-phosphorylation mutant hTau40_{AT8*+AT100+PHF1}. In the aggregation kinetics, hTau40_{AT8*+AT100+PHF1} showed a moderate but significant increase of ThS fluorescence intensity compared to hTau40_{wt} (Fig 3.9A).

This result suggests that the compaction due to the pseudo-phosphorylation at both arms (AT8* + AT100 + PHF1) raises the tendency for aggregation (beyond the effect of polyanions alone).

Both hTau40$_{wt}$ and hTau40$_{AT8*+AT100+PHF1E}$ form fibrils of similar morphology in presence of heparin.
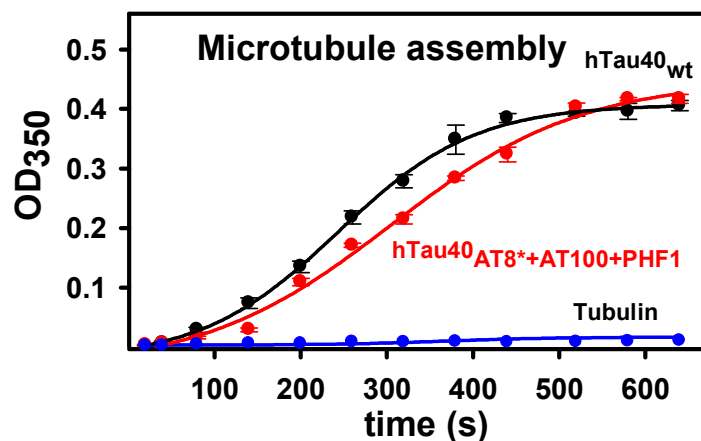


Figure 3.10: Microtubule assembly of phosphomimetic mutant hTau40$_{AT8*+AT100+PHF1}$: Microtubule polymerization in the presence of hTau40$_{wt}$ and hTau40$_{AT8*+AT100+PHF1}$. Both proteins reach similar final levels, but the pseudo-phosphorylated protein shows a somewhat longer lag time. The bottom curve (blue line) shows that there is no assembly of tubulin without tau.

In contrast, the microtubule polymerizing ability of hTau40$_{AT8*+AT100+PHF1}$ showed no difference in final level and only a small retardation on assembly rate was observed (Fig. 3.10). This is consistent with the notion that the AD-like phosphorylation in the flanking domains has no or only a small effect on tau-microtubule interactions.

3.2.2 Pseudophosphorylation at AT8 and PHF1 epitopes induces compaction and generates a pathological (Alz-50 and MC1) conformation

The cleavage of the C-terminal tail by caspases is believed to favor tau aggregation (Gamblin et al., 2003). The deletion of the C-terminal tail allows the N-terminal domain to approach the repeats (similar to the compaction by double arm phosphorylation at AT8* + AT100 + PHF1, Jeganathan et al., 2008). We created a tau mutant lacking amino acids 422-441 (hTauΔCT), and then we tested the reactivity of the mutant hTauΔCT with antibodies MC1 and Alz-50 (Fig. 3.11 A and C). There was a clear increase in signal for the triple-site mutant (AT8* + AT100 + PHF1) hTau40/N-R$_{AT8*+AT100+PHF1}$. Remarkably, the increase became very pronounced with the C-terminal truncated mutant of hTau40ΔCT/N-R$_{AT8*+AT100+PHF1,}$ compared with the unphosphorylated protein hTau40ΔCT/N-R. Both these observations suggest that the compaction of the molecule observed by FRET resembles the "pathological conformation" detected by the MC1 and Alz-50 antibodies. The bar diagrams shows the blot intensities for MC1 and Alz-50. The most exciting aspect of the results is the relationship between Alzheimer-like phosphorylation (at AT8*, AT100, and PHF1) epitopes, the compaction of the paperclip
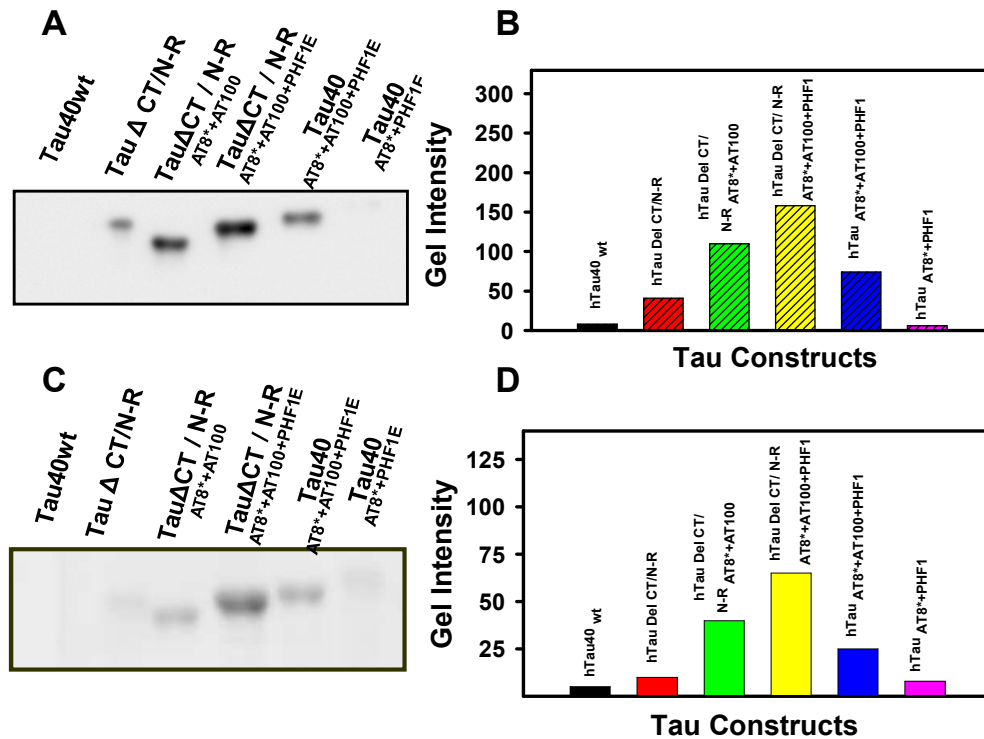
Figure 3.11: MC1 and Alz-50 reactivity of phosphomimic mutants of tau: (A and C) Western blots showing reactivity of MC1and Alz-50 (conformational antibodies whose discontinuous epitope comprises residues from the N-terminal and repeat domain, detecting the folding of the protein) with phosphomimic mutants of tau. Note that double arm pseudo-phosphorylation causes an increased MC1 and Alz-50 reactivity. (B and D) shows the quantification of blots for MC1 and Alz-50.

conformation and the reactivity of tau with antibodies that report on the pathological conformation of tau in early stages of AD, such as MC1, Alz-50, and others. This reaction is best observed in brain tissue and has been difficult to reproduce with tau *in vitro*. However, the fact that the most compact conformations are the ones showing the highest reactivity with MC1 and Alz-50 (Fig. 3.11 A and C) argues that the compaction of the paper clip conformation reflects the pathological state. The increase in MC1 and Alz-50 reactivity becomes more pronounced when the C-terminal tail is absent, which argues that this tail normally opposes close approach between the N-terminus and the repeats (consistent with the paperclip model).

3.2.3 Aggregation propensity of hTau$_{40AT8*+AT100+PHF1}$ and C-terminus deletion mutants expressed in neuroblastoma cell2 (N2a)

The phosphorylation abnormality in tau from patients with AD appears to be an increased stoichiometry and a decreased turnover of phosphate incorporated at selected sites.

To test the ability of the pseudo-phosphorylated mutant hTau40$_{AT8*+AT100+PHF1}$, we transiently transfected this mutant or hTau40$_{wt}$ as a control into the inducible neuroblastoma cell line N2a,

and the constructs were expressed by addition of doxycyclin. The presence of tau aggregates was tested by sarkosyl extraction of the cells and analysis of soluble and insoluble components.

The resulting proteins were separated by SDS-gel electrophoresis and blotted with tau specific antibody K9JA. Figure 3.12A illustrates that after three days of protein expression the control protein hTau40 remains mostly in soluble fraction. The expression of hTau40$_{AT8*+AT100+PHF1}$ leads to noticeable accumulation of material in the sarkosyl-insoluble pellet representing tau aggregation. 0.5% of aggregated hTau40$_{AT8*+AT100+PHF1}$ compared to hTau40$_{wt}$ confirms moderate increase in the aggregation. This result is in complete agreement with the *in vitro* result shown above (Fig.3.9A).
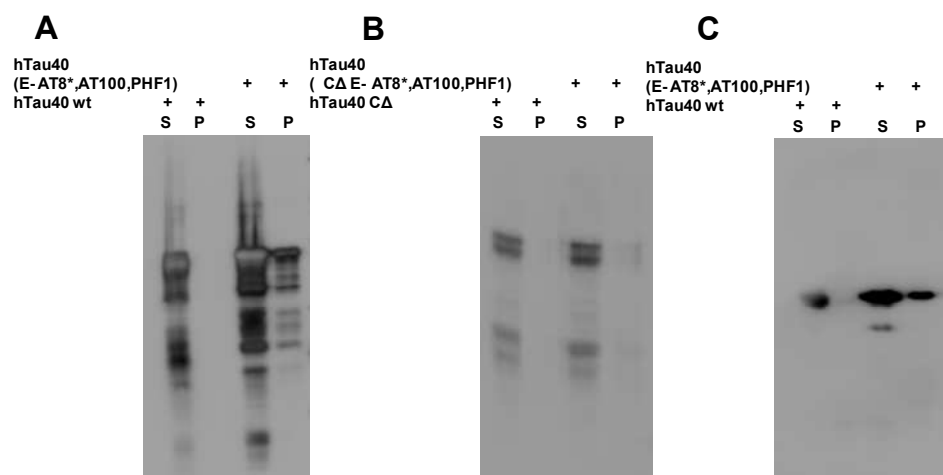
Figure 3.12: Aggregation propensity of pseudo-phosphorylation mutants expressed in N2a cells: (A) Aggregation propensity of hTau40$_{wt}$ and hTau40$_{AT8*+AT100+PHF1}$ (pseudo-phosphorylated at three epitopes) in full length in neuroblastoma N2a cell line; blot analysis with K9JA (independent of phosphorylation). (B) Aggregation propensity of hTau40ΔCT421 and hTau40 ΔCT421$_{AT8*+AT100+PHF1}$ (pseudo-phosphorylated at three epitopes) in hTau40 truncated at D421 in neuroblastoma N2a cell line; blot analysis with K9JA (independent of phosphorylation). (C) The blot with MC1 conformational antibody performed on soluble and insoluble protein fractions on the level of hTau40$_{wt}$ and hTau40$_{AT8*+AT100+PHF1}$ molecules. The analysis shows stronger signal coming from soluble and insoluble fractions of E-mutated hTau40$_{AT8*+AT100+PHF1}$. In the case of hTau40$_{wt}$ only a weak MC1 signal in the soluble fraction was observed.

In the N2a cells we have to do with endogenous phosphorylation of hTau40$_{wt}$ resulting in a combination of E-mutated hTau40$_{AT8*+AT100+PHF1}$ epitopes with some additional phospho-sites. Figure 3.12B illustrates soluble and insoluble protein fractions on the level of hTau40 molecules truncated at D421 (hTau40ΔCT421$_{wt}$ and hTau40ΔCT421$_{AT8*+AT100+PHF1}$). In both cases the proteins were nearly entirely soluble. Some traces of insoluble material are visible in the case of hTau40ΔCT421 and hTau40ΔCT421$_{AT8*+AT100+PHF1}$. The mutant of hTau40ΔCT421$_{AT8*+AT100+PHF1}$ molecule aggregated much more efficiently than hTau40ΔCT421$_{wt}$. Figure 3.12C shows the blot analysis with MC1 conformational antibody performed on soluble and insoluble protein fractions on the level of hTau40$_{wt}$ and

hTau40$_{AT8*+AT100+PHF1}$ molecules. The analysis shows stronger signal coming from soluble and insoluble fractions of E-mutated hTau40$_{AT8*+AT100+PHF1}$. In the case of hTau40$_{wt}$ we observed only a weak MC1 signal in soluble fraction, exclusively.

This result is accompanied by a strong increase in the reaction with conformation-dependent antibodies Alz-50 and MC1. There was a clear increase in signal for the triple-site mutant Tau/N-R$_{AT8*+AT100+PHF1}$. Remarkably, the increase in Alz-50 and MC1 reactivity becomes more pronounced when the C-terminal truncated version of the protein TauΔCT/N-R$_{AT8*+AT100+PHF1}$, compared with the unphosphorylated protein TauΔCT/N-R (Fig. 3.11A and B). Both these observations suggest that the compaction of the molecule observed by FRET resembles the "pathological conformation" detected by Alz-50 and MC1 antibodies (Jeganathan et al., 2008). The data provide a framework for the global folding of tau dependent on proline-directed phosphorylation in the domains flanking the repeats and the consequences for pathological properties of tau.

3.3 Polymorphic assembly of human tau fibrils

The fibrils of tau in AD brains are commonly termed "paired helical filaments" (PHFs) because of their appearance in EM (Kidd, M. 1963). PHF formation is thought to be similar to the aggregation of other amyloidogenic proteins. Two protofibrils seem to be wound around one another exposing a crossover repeat of ~80 nm, a maximal width of ~22 nm and a narrow waist of ~12 nm (Crowther, 1991; Wegmann et al., 2010). Tau fibrils found in AD brains show no twist and are therefore called "straight filaments". In other diseases with tau pathology, the crossover repeat is ~160 nm (Ksiezak-Reading et al., 1994). Besides, tau fibrils reassembled *in vitro* can display a variable twist between filaments assembled from different variants of tau proteins (*e.g.* different splicing variants) or even within a given filament. This has caused some concern whether the assembly products observed *in vitro* reflect those observed in AD brains. Considering all these open questions and the importance of aggregated tau as a potential target for therapy of AD and related tauopathies, we initiated a study of tau isoforms and tau domains by EM (electron microscopy) and AFM (high resolution atomic force microscopy). For this analysis, PHFs derived from hTau40, hTau40K18ΔK280, hTau23, K19, K18, and K18ΔK280 were used. The mutation ΔK280 occurs in FTDP-17 and causes an increased tendency to form PHFs (Goedert et al., 1999; Barghorn et al., 2000). The AFM topography was done in collaboration with Susanne Wegmann and Daniel Müller, ETHZ, Basel, Switzerland.

3.3.1 Tau proteins assemble into polymorphous fibrils

In this work we characterize the structure of fibrils assembled in *vitro* from various Tau isoforms and constructs with different domain compositions. PHF assembly was initiated by the polyanionic cofactor heparin, which helps to overcome the kinetic nucleation barrier and reproduces tau fibrils with *bona fide* PHF-like structures (Goedert et al., 1996; Perez et al., 1996). The longest isoform in the human central nervous system (CNS), hTau40, contains a repeat domain of four repeats (R1 to R4) and consists of 441 amino acids (aa). The three repeat isoform hTau23 lacks R2 and is 352 aa long. The deletion mutation ΔK280, which has been discovered in Tau related dementia FTDP-17 (van Swieten et al., 2007), significantly enhances the speed of tau aggregation into fibrils (Barghorn et al., 2000). Constructs containing only the repeat domains of full-length hTau40, hTau23, hTau40$_{ΔK280}$ and short constructs named K18 (130 aa), K19 (99 aa), and K18$_{ΔK280}$ (129 aa) were used.
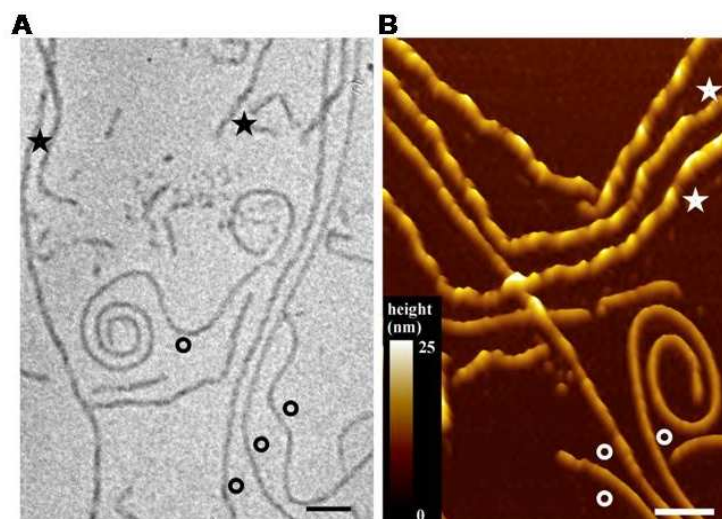
Figure 3.13 Fibril assembly of hTau40wt: (A) Non-selective EM images of hTau40 fibril preparations show a heterogeneous mixture of fibril shapes. (B) AFM topographs of the same fibril preparation confirm the heterogeneity of fibril structures but reveal details with superior contrast. Fibril morphologies differ in length, bending, internal twist, periodicity, and thickness (★ for thick fibrils, bright yellow on color scale, and O for thin fibrils, brown on the color scale). This structural heterogeneity was largely independent of the tau isoform and construct from which the fibrils self-assembled (Figure 3.14). Notably, while the fibril thickness in EM images is given by the apparent width of the structure, it is reflected by the fibril height in AFM topographs. AFM topographs were recorded in imaging buffer (10 mM Tris-HCl, pH 7.4, 50 mM KCl) and exhibit a full color range that corresponds to vertical scale of 25 nm as indicated by the color scale bar. Length scale bars in A and B correspond to 100 nm. (Reproduced from Wegmann et al., 2010).

Although considerably shorter, the repeat domain forms fibrils similar to the full-length proteins but are more prone to aggregation; presumably they are lacking the N- and C- terminal domains that protect the core against unfavorable interactions (Binder et al., 2005; Friedhoff et al., 1998). Randomly picked micrographs of all *in vitro* preparations showed a variable degree of polymorphic fibril appearances in both EM and AFM (Fig. 3.13A and B). Compared to EM images, AFM topographs provided a superior contrast. The fibrils had different lengths and their morphology varied in bending, periodicity, twisting, thickness, and substructure. This heterogeneity among fibrils was independent of the tau isoform from which they assembled (Fig. 3.13, Fig. 3.14, and Fig. 3.15).

To check whether this polymorphism depends on sample preparation, we imaged all fibrils of the different tau isoforms in their native state (Fig. 3.13, Fig. 3.14, and Fig. 3.15) and in the tau fibrils fixed state, in which the fibrils were crosslinked before or after adsorption to the microscopy slide using 0.5% glutaraldehyde (Fig. 3.16). In all cases, the tau fibrils imaged in buffer solution showed the same structural diversity. Thus, we conclude that the fibril polymorphism reflects an inherent property of tau. In the following, we characterized the tau fibril morphologies in more detail. The heterogeneity was independent of the tau isoform from which the fibrils self-assembled Fig. 3.15.
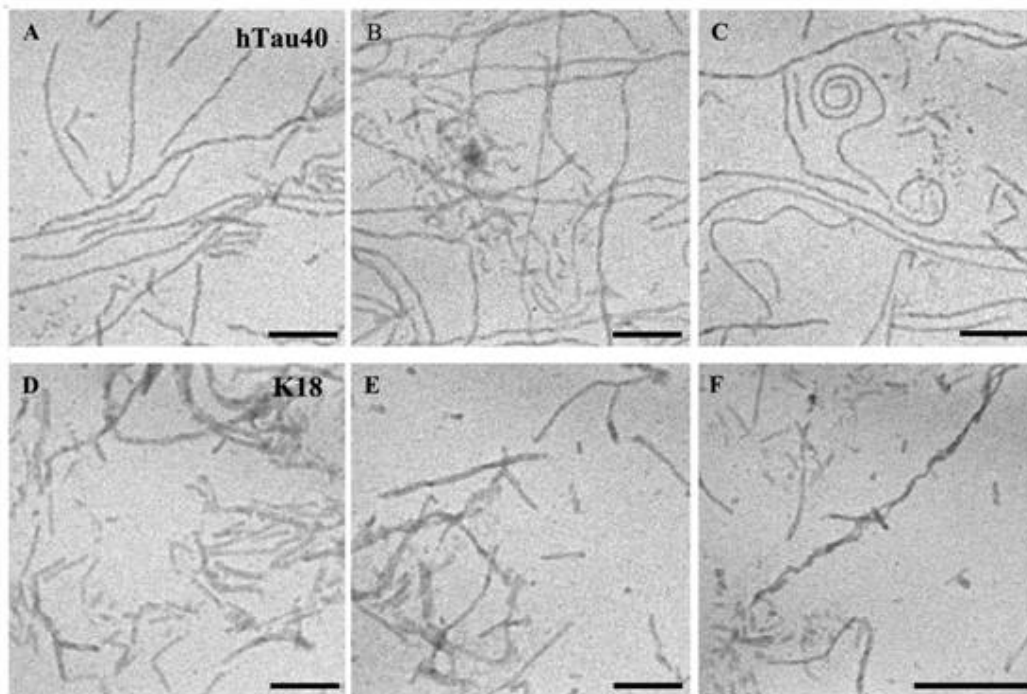
Figure 3.14: Variable tau fibril morphologies observed by EM. EM pictures of hTau40 (A, B and C) and of K18 (D, E and F), scale bars correspond to 200 nm. The fibril preparations show heterogenous morphologies. (Reproduced from Wegmann et al., 2010).

A. K19$_{wt}$ **B. K19$_{wt}$**
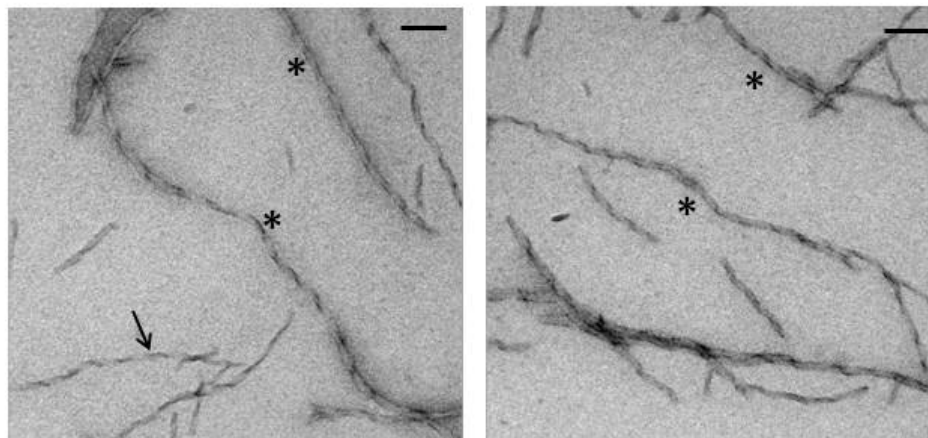
Figure 3.15: K19wt fibril morphologies observed by EM. EM pictures of K19 wt (A-B), scale bars correspond to 100 nm. The fibril preparations show heterogenous morphologies. * denotes thick fibrils and ↓ denotes thin fibrils.

hTau40_{wt}
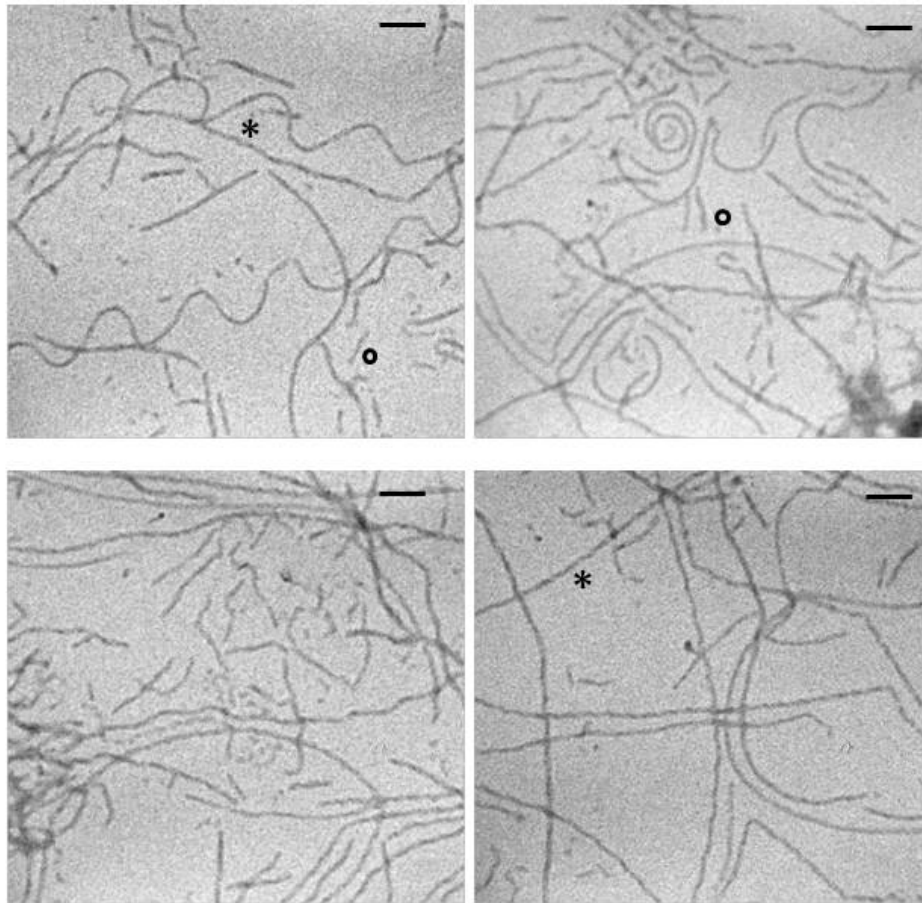
Figure 3.16 Fibril assembly of hTau40 fixed with 0.5% glutaraldehyde: Non-selective EM images of hTau40wt fibril preparations show a heterogeneous mixture. Fibrils were fixed with 0.5% glutaraldehyde. The structural heterogeneity was largely independent of the tau isoforms and constructs from which the fibrils self-assembled. Notably, the fibril thickness in EM images is given by the apparent width of the structure. Scale bars correspond to 100 nm (Fig. 3.13). Fibril morphologies differ in length, bending, internal twist, periodicity, and thickness (⋆ for thick fibrils and O for thin fibrils).

3.4 Temperature-dependent changes in tau conformation

Tau in solution behaves like a random coil, as judged by electron microscopy, x-ray diffraction, circular dichorism, FTIR, fluorescence spectroscopy, and other methods (Garcia et al., 2001). Structural investigations of tau are largely hampered by the unfolded nature of this protein. The lack of structure in natively unfolded proteins is hypothesized to be due to their low content of hydrophobicity and a high net charge near physiological pH (Uversky et al., 2001). Natively unfolded proteins are thought to adopt different conformations in solution. In this study, we have therefore investigated the determinants of the unfolded nature of soluble tau in solution under different temperature conditions (Shkumatov et al., 2011) by using various biophysical methods (CD, DLS, and SAXS). The SAXS measurements were done at beam line X33, in collaboration with Alexander Shkoumatov and Dimitri Svergun, EMBL, Hamburg.

3.4.1 Effect of temperature on tau conformation in solution by small-angle x-ray scattering (SAXS) analysis

The full-length tau (hTau40$_{wt}$), its pseudo-phosphorylation mutant (hTau40$_{AT8*+AT100+PHF1}$), the shortest isoform of tau (hTau23$_{wt}$), and the repeat domain (K19$_{wt}$) were measured by small-angle x-ray scattering (SAXS). No major changes were observed between the wild type protein and the pseudo-phosphorylation mutant. To investigate the effect of temperature on the overall dimensions of the constructs, we first carried out SAXS measurements at 50°C under equilibrium conditions. The samples were placed in the sample changer tray at 10°C and slowly (~30 min) warmed up to 50°C. Then the samples were injected into the measuring cell, which was also kept at 50°C. The radii of gyration (Rg) values for all constructs are summarized in Table 3.1

Rg distributions of the longer constructs were close to those expected for random coils, whereas the shorter constructs appeared more extended than random coils, in agreement with the results reported by Mylonas et al., 2008.

Surprisingly, different results were obtained under non-equilibrium temperature conditions, when the samples were kept in the tray at one temperature and then transferred to the measurement cell tempered to either higher or lower temperature. Two cases were explored, "quick heating" (sample tray at 10°C, measurement cell at 50°C) and "fast cooling" (sample tray at 50°C, measurement cell at 10°C). For each measurement, the measuring cell filled with the sample was held for half a minute prior to exposure in order to ensure that the desired temperature is reached (cell volume ~25µl). The experiments under non-equilibrium conditions

(quick heating / fast cooling) showed that long tau constructs adopt a more compact and folded conformation as judged by Rg (Table 3.1).

Radii of Gyration						
construct **(no. of aa)**	**_Rg_ (nm) at different temperature conditions.** **Temperature in sample holder/measurement cell, °C/°C**					
	10→10	**50→50**	**10→50**	**50→10**	**10→50** **(1 day)**	**50→10** **(1 day)**
hTau40wt (441)	6.6±0.3	6.5±0.3	5.5±0.3	5.6±0.3	6.3±0.3	6.1±0.3
hTau40$_{AT8*+AT100+PHF}$	6.6±0.3	6.7±0.3	5.9±0.3	-	-	-
hTau23 (352)	5.9±0.2	5.9±0.2	5.9±0.2	5.9±0.2	-	-
K19 (98)	3.5±0.2	3.5±0.2	3.5±0.2	3.7±0.2	-	-

Table 3.1 Radii of gyration for hTau40wt and other constructs (data reproduced from Shkumatov et al., 2011).

Several independent SAXS measurements with samples from different batches were performed to verify the observed unusual effect. They reproducibly revealed the compaction of the full length tau upon quick heating and fast cooling. The latter effect was measurable also after minutes and even hours of the incubation of the protein at 10°C, indicating that the compaction has a memory effect. We performed additional measurements on incubated hTau40$_{wt}$, which revealed that the compact state is preserved for at least 3 hours of incubation, but after 24 hours the protein is nearly reverted back to the native state. The pseudo-phosphorylated tau construct (hTau40$_{AT8*+AT100+PHF1}$) showed a tendency to aggregate over time and could thus not be measured under similar conditions.

3.4.2 Effect of temperature on tau in solution by circular dichroism (CD) spectroscopy

In order to further confirm the obtained results, we employed other techniques providing information about the structure in solution. Our CD experiments did not show the memory effect when different temperature protocols were employed. Thus, the small angle x-ray scattering results reveal a global property, whereas CD measures averaged local properties. To test if elevated temperature could cause a structural transition, the secondary structure of the soluble tau was determined by CD at various temperatures (5, 25, 45, 65, and 95°C). Upon stepwise elevation of temperature, the CD spectra of hTau40$_{wt}$ underwent a shift: the negative peak at 200 nm became less pronounced and the value at 217 nm became more negative with an isosbestic point around 210 nm (Fig. 3.17). By varying the time of incubation and the protocol of temperature shifts we found that the CD spectrum depends essentially on the temperature, but

not on the memory effect. Note that proteins or peptides containing a large fraction of polyproline helix II (PPII) show a similar temperature dependent CD which can be explained by a gradual change from a conformation rich in PPII to extended conformations (Sanchez-Puig et al., 2005; Eker et al., 2003). Thus, the "memory effect" seen by SAXS appears to be specific for the global changes in the protein seen by X-rays, not for the average local structure seen by CD.
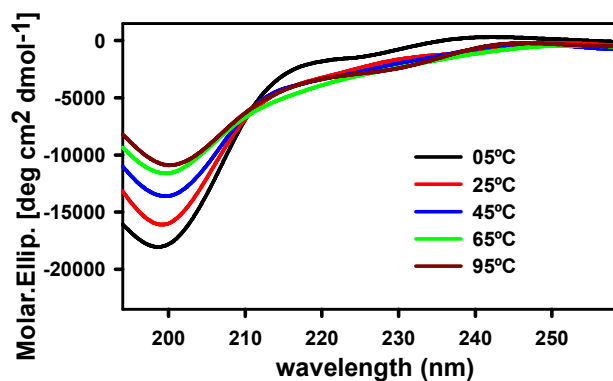
Figure 3.17: CD spectra of temperature dependence of tau: CD spectra of tau at different temperatures: Note that the negative peak at 200 nm becomes filled in as the temperature rises. Very similar traces are obtained by different protocols of varying the temperature and time of incubation, indicating the presence, but not the extent of local conformational changes (reproduced from Shkumatov et al., 2011).

3.4.3 Temperature effect of tau in solution by light scattering and sedimentation analysis

To measure the effect of temperature on the aggregation of hTau40wt by light scattering at 90°, we kept the samples at 10°C for 20 min, 50°C for 20 min, and 50°C for 120 min and measured at room temperature. Figure 3.18 confirms that the temperature was not inducing any aggregation. The results obtained with light scattering clearly suggest that there was no aggregation at the various temperatures. The positive control of fully aggregated PHFs was confirmed by ThS fluorescence and electron microscopy. The hTau40wt protein samples were kept at 10°C for 20 min, 50°C for 20 min, and 50°C for 120 min, and after incubation all the samples were collected, pelleted by ultracentrifugation, and pellets and supernatants were analyzed by SDS gel electrophoresis (Fig. 3.19 A and B). The results confirmed that aggregation in the tau solutions was negligible. This suggests that the memory effect revealed by X-ray scattering is due solely to changes in temperature.
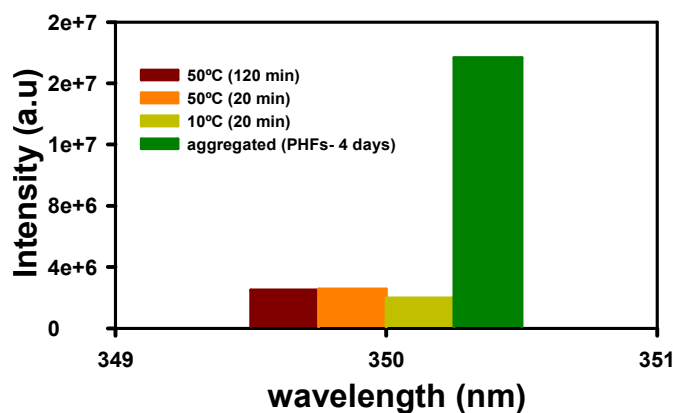
Figure 3.18: Light scattering of tau after thermal treatment: Light scattering intensities (90°, 350 nm) of soluble tau and aggregated PHS (green bar). Samples of soluble tau protein (concentration 25 µM, phosphate buffer pH 6.8) were incubated at various temperatures and time periods, 10°C for 20 min, 50°C for 20 and 120 min. Note that there was no increase in scattering intensity from the samples of the soluble Tau, indicating that there was no measurable aggregation during the course of the experiment. As a control, aggregated PHFs (concentration 25 µM of tau) show high scattering intensity (reproduced from Shkumatov et al., 2011).
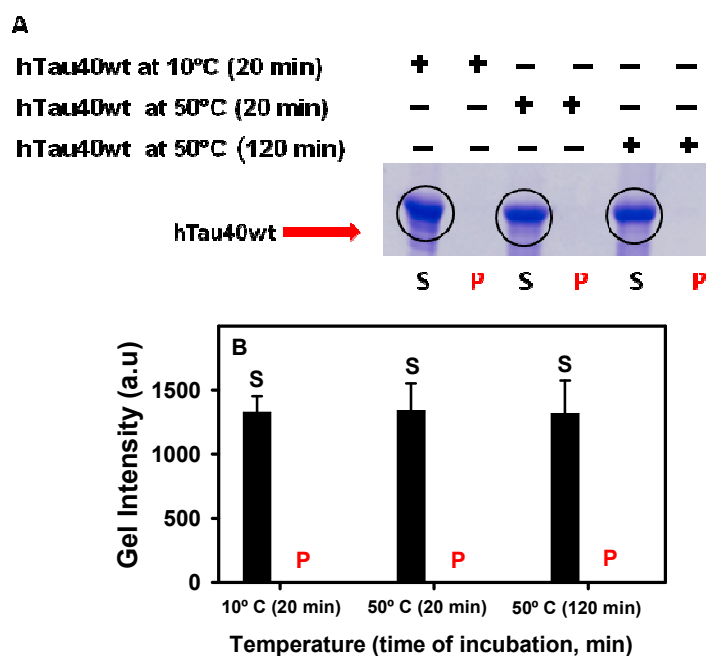
Figure 3.19: Effect of thermal treatment of tau by sedimentation analysis: (A) Coomassie blue (R-250) stained SDS-PAGE illustrating the sedimentation of soluble tau at different temperatures and incubation periods. S and P represent supernatant and pellet. Note that there is no detectable aggregated protein in the pellet. (B) Quantification of the samples from A (reproduced from Shkumatov et al., 2011).

3.4.4 Dynamic light scattering measurements of hTau40wt by different temperatures

To obtain independent information on the temperature dependence of the apparent size of tau, DLS measurements were performed. The hydrodynamic radius R_h of hTau40wt at 10°C was 5.6 nm (Fig. 3.20 A), and this value did not change upon slow heating to 50°C. However, when

hTau40wt was quickly heated up to 50°C for 20 min incubated and measured, the R_h dropped to 5.3 nm (Fig 3.20 B).

This compaction was in line with the SAXS results under non-equilibrium temperature conditions, although the decrease of the R_h was smaller than that of the R_g values from SAXS. It is interesting to note that the ratio of R_g/R_h depends on the flexibility of the macromolecule. For a rigid structure, R_g is close to R_h (R_g/R_h ranging form ~1.1 for anisometric polymers to ~0.8 for a solid sphere). For flexible system Rg may significantly exceed R_h, such that R_g/R_h reaches 1.5 for a random coil (Rubinstein et al., 2003). Our results therefore indicate that quickly heated or fast cooled tau becomes not only more compact, but also less flexible than the native protein. The memory effect is observed with full-length tau
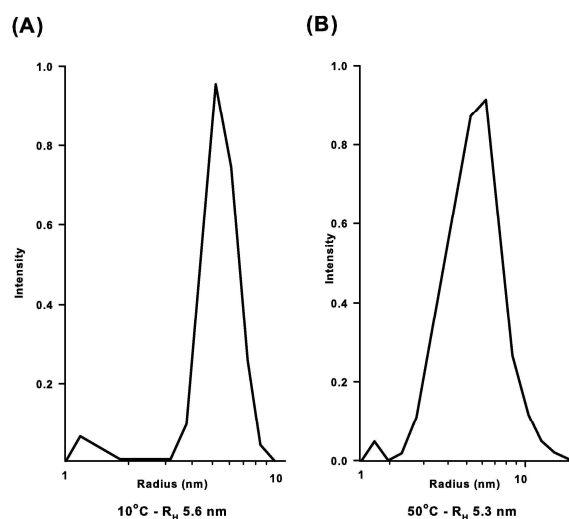
Figure 3.20: Dynamic light scattering measurements for hTau40wt at different temperatures: Comparison of R_H values obtained at different temperatures: (A) 10°C for 20 min (R_H 5.6 nm) and (B) 50°C for 120 min (R_H 5.3 nm). Note that with increasing temperature (50°C for 120 min), R_H becomes smaller. This indicates that the protein is somewhat more compact at higher temperature (reproduced from Shkumatov et al., 2011).

but not with the repeat domain alone, suggesting that interplay between domains in the whole protein might be responsible for the effect. One possible explanation could be the interplay between the acidic N-terminal domain (which varies among the tau isoforms due to alternative splicing) and the basic repeat domain (which also differs between isoforms).

4 Discussion

Microtubule-associated protein tau is an interesting protein from three perspectives:

1. Tau is the major component of neurofibrillary tangles (NFT), a characteristic pathological hallmark of Alzheimer's disease (AD).

2. The mechanisms by which tau stabilizes microtubules in healthy neurons, or conversely, forms insoluble aggregates in diseased cells is the focus of intense investigation. Tau is necessary for neurite outgrowth and maintenance, and suppression of tau synthesis causes retraction and decay of neurites reminiscent of the decay in AD (Hanemaaijer et al., 1991; Kosik et al., 1994). On the other hand tau serves as regulator of intracellular traffic in neurons and in particular affects kinesin-dependent transport along with microtubules (Ebneth et al., 1998). These observations provide the justification for studying the molecular and cell biological functions of tau protein

3. Tau belongs to the growing class of natively unfolded proteins or intrinsically disordered proteins (IDPs), which can display novel features in protein chemistry.

3.5 Effect of phosphorylation on PHF aggregation

In AD, tau is more highly phosphorylated than normal adult tau (~8 vs ~2 Pi/molecule; Ksiezak-Reading et al., 1992). It has been proposed that a high degree of phosphorylation promotes PHF formation (Bancher et al., 1991). The AD like phosphorylation is particularly evident on SP/TP motifs in the domains flanking the repeats. These are phosphorylated by proline-directed kinases (*e.g.* MAP kinase, GSK3ß, cdk5) and are recognized by several antibodies which are therefore useful as diagnostic reagents (Friedhoff et al., 1999). In addition, AD tau shows enhanced phosphorylation at sites targeted by other kinases, for example S262 in the first repeat (phosphorylated most efficiently by MARK, but also by PKA) or S214 (a target of PKA). The origin of the enhanced phosphorylation is a matter of debate. However, it could be due to an over-activity of kinases or an underactivity of phosphatases (Matsuo et al., 1994). In either case the initial cause could be a misregulation of some signal cascade, possibly triggered by a toxic challenge, which affects the interplay between cellular kinases and phosphatases. The balance of kinases and phosphatases could be perturbed in neurons, causing an elevated phosphorylation of tau. This would then lead to the dissociation of tau from microtubules so that microtubules become destabilized, axonal traffic would become impaired, and axons decay. The hyperphosphorylated tau could in turn aggregate into paired helical filaments. The basic assumption of the hypothesis is therefore the phosphorylation of tau would promote paired helical filaments.

There are several consequences of phosphorylation of tau:

1) If tau was to be released from microtubules by "abnormal" phosphorylation during neurodegeneration, it should be phosphorylated at sites that decrease the affinity of tau to microtubule binding. The best sites are S262 or S214 (targets of MARK or PKA) because both have a pronounced effect on tau's affinity to microtubules (Drewes et al., 1998).

2) The "abnormal" phosphorylation of tau in degenerating neurons promotes tau's aggregation into PHFs.

3) Specifically, the abnormal phosphorylation of tau preferentially promotes the interaction between the repeat domains because they form the backbone of PHF assembly *in vivo* and *in vitro.*

4) Since most sites considered to be diagnostic for "abnormal" phosphorylation are in SP or TP motifs in the domains flanking the repeats, proline-directed phosphorylation should promote PHF assembly. This is also not observed since the SP or TP motifs have a weak influence, on both tau-microtubule interactions and PHF assembly.

From a structural point of view, the effect of tau phosphorylation is very difficult to address because the structure of tau is not known, and because tau is a highly flexible molecule capable of adopting many conformations (Schweers et al., 1994). From a kinetic point of view we know that the assembly of monomeric tau into PHFs passes through several stages (Schneider et al., 1999),

1) dimerization *(e.g.* involving oxidation of Cys^{322}),

2) interactions with polyanions (presumably resulting in some conformational change),

3) aggregation of dimers into filaments.

We can therefore distinguish the phosphorylation sites with strong effects or weak effects.

1) The "strong inhibitory" sites include the KXGS motifs and neighboring residues in the repeats (notably S262, S320, S324, S356) and S214 in the N-terminal flanking region. We believe that pseudo-phosphorylation at KXGS motifs is structurally unfavorable for the packing of tau into filaments. Note that the pseudo-phosphorylation at all four KXGS motifs completely abrogates the aggregation capacity (Fig. 3.4G) of tau in the presence of heparin. This is consistent with the earlier studies showing that phosphorylation at KXGS motifs protects tau against aggregation (Schneider et al., 1999).

2) The effect of pseudo-phosphorylation at KXGS motif could be rescued by flanking pseudo-phosphorylation (Fig. 3.6A). This result indicates the inability of the flanking pseudo-phosphorylation to counteract that in KXGS motifs.

3) The "strong" site S214 does not perturb the initial dimerization and therefore must affect a later step in PHF assembly (Schneider et al., 1999). These findings are clearly contrary to mutation at 214 which had higher aggregation propensity. From the current observation in Fig 3.2A, the mutation S214E promotes tau into PHFs in the case of hTau23 as well (Fig. 3.3A).

On the other hand the "strong" sites in the KXGS motifs of the repeats clearly inhibit the dimerization of tau. This finding agrees with the current observation in Fig 3.4G. Note that MARK phosphorylates the KXGS motifs of the repeat domains much more efficiently than PKA, especially S262 (Drewes et al., 1995; Scott et al., 1993). The repeat domain forms the core of the PHF (Wischik et al., 1988; Novak et al., 1993) and therefore one may expect that the phosphorylation of this domain has an influence on PHF assembly as observed. However, it is not obvious why a more distant residue such as S214 should have such a large influence, especially when considering the disordered and flexible nature of tau (Schweers et al., 1994). A possible explanation is that tau adopts a conformation by which the N-terminal flanking domain is folded over the repeat domain, putting S214 in a position where its phosphorylation can block the addition of further subunits to PHFs (Schneider et al., 1999). Supporting evidence for possible folded conformations of tau comes from the reactivity of tau antibodies (*e.g.*, SMI-34, Alz-50, TG-3; Lichtenberg et al., 1992; Carmel et al., 1996; Jicha et al., 1997) or related studies (Goode et al., 1997), and this may explain why S214 forms part of an Alzheimer specific epitope (antibody AT-100, Zheng-Fischhöfer et al., 1998; Hoffmann et al., 1997).

The extensive phosphorylation of SP or TP motifs has been taken as evidence that this type of phosphorylation promotes PHF assembly. On the contrary, results by Schneider et al., 1999, argue that these sites have a weak inhibitory effect on PHF assembly. They can be phosphorylated either before or after assembly, and their high content of phosphorylation in AD tau could merely reflect the altered balance of kinases and phosphatases in degenerating neurons (Trojanowski et al., 1995).

4.1.1 A single epitope phosphorylation site does not influence the aggregation

Phosphorylation at single epitopes (either AT8*, AT100, or PHF1) does not influence the aggregation of hTau40. The choice of testing these phosphorylation sites was based on the epitopes of antibodies that are characteristically elevated in Alzheimer disease (Fig.3.1). For example, the triple mutation S199E + S202E + T205E generates pseudo-phosphorylation at the epitope recognized by antibody AT8 (Biernat et al., 1992; Otvos et al., 1994; Goedert et al., 1995). The phosphorylation at S202 + T205 recognized by antibody AT8 appears to be an early event in the progression of AD, prior to the formation of tau pre-tangles (Braak et al., 1994). Tau

pseudo-phosphorylated at Ser^{202} + Thr^{205} by S/T to E mutations suffices for the reaction with antibody AT8, but Ser^{199} is usually also phosphorylated in brain tissue and can be detected by the antibody; hence we chose the triple mutation and denoted it as AT8*. The phosphorylation of tau at T212 + S214 is carried out by two kinases, GSK3β and PKA, in a sequential manner and recognized by monoclonal antibody AT100 (Zheng-Fischhofer et al., 1998). Tau modified at single epitopes AT8* or AT100 (Fig. 3.4A and C) does not affect the aggregation. The 'PHF1 mutant' pseudo-phosphorylated at S396E + S404E generates the epitope for antibody PHF1 (Greenberg et al., 1992; Otvos et al., 1994). Phosphorylation at S396 + S404 is shown to preserve the protective effect of pseudo-phosphorylation against the aggregation of tau (Abraha et al., 2000) (Fig. 3.4E). This is in contrast to an earlier report that the aggregation of $hTau40_{PHF1}$ mutant in the presence of arachidonic acid is increased (Abraha et al., 2000). It may be due to the variations in the experimental conditions and constructs used in this study. The combination of pseudo-phosphorylation at certain epitopes has moderate effects on aggregation rate in the level of $hTau40_{AT8*+214E}$, $hTau40_{214E+\ PHF1}$ (Fig. 3.5A and C), as well as $hTau23_{AT8*+AT100}$ and $hTau23_{AT8*+PHF1}$ (Fig. 3.7 A and C).

4.1.2 Hyperphosphorylation protects tau against assembly into PHFs

Hyperphosphorylation of tau protein is a pathological hallmark of AD and other tauopathies; however, its functional implications are unclear. In particular, it is not known whether the hyperphosphorylated state of tau is a cause or a consequence of the events which occur during the development of tau pathology such as the formation of insoluble tau aggregates and neuronal degeneration. Many sites which become phosphorylated in PHF-tau were identified, and the data strongly suggest that hyperphosphorylation of tau involves a concerted and sequential action of several kinases. It has been reported that substitutions of individual serines for negatively charged amino acids mimics structural and functional consequences of phosphorylation at many sites (Schneider et al., 1999; Leger et al., 1997). We followed this up in more detail and changed 15 serine/ threonine residues to glutamate to create a PHF tau-like hyperphosphorylation state. This strategy enabled us to analyze a defined state of tau for structural and functional consequences and to determine functional interference between normal tau and PHF-like tau protein. Our current findings clearly indicate that multiple pseudo-phosphorylation of tau does not enhance its aggregation tendency (Fig. 3.8A). We further included three additional pseudo-phosphorylation sites in the N-terminal insert domains (S46, T50, and T69) in addition to the 15 sites mentioned above. This indicates that multiple pseudo-phosphorylation can further dampen the aggregation efficiency of tau (Fig. 3.8C). This is contrary to the popular view that hyperphosphorylation of tau enhances the aggregation into PHFs.

4.1.3 Effect of phosphorylation on microtubule assembly

The interaction of tau and other MAPs with microtubules is regulated by phosphorylation, and this in turn affects the structure and dynamics of the microtubule cytoskeleton. In particular, tau becomes highly phosphorylated in the neurofibrillary pathology of Alzheimer's disease and hence loses its binding capacity to microtubules (Yoshida and Ihara, 1993).

In addition, AD tau shows enhanced phosphorylation at sites targeted by other kinases, for example, S262 in the first repeat (phosphorylated most efficiently by MARK, but also by PKA) or S214 (a target of PKA). S214 can be rapidly and selectively phosphorylated *in vitro* by PKA. Phosphorylation at this residue strongly decreases the tau-microtubule interaction *in vitro*, suppresses microtubule assembly, and may be a key factor in the observed detachment of tau from microtubules during mitosis (Illenberger et al., 1998). The microtubule polymerizing ability of hTau40$_{214E}$ is completely lost as the light scattering (Fig. 3.2G) of this reaction is almost equal to that of the tubulin alone which remains unpolymerized over the reaction time. The inability of tau carrying glu at 214 to support microtubule assembly reflects the observation that the phosphorylation of tau at S214 can detach Tau from microtubule surface (Brandt et al., 1994; Illenberger et al., 1998; Zheng-Fischhöfer et al., 1998). The same results are obtained with hTau23$_{214E}$ as well (Fig. 3.3B). The NMR analysis also shows that the region of tau responsible for binding to microtubules extends mainly from ~210 to 380 aa (Mukrasch et al., 2007; Sillen et al., 2007) and is therefore consistent with an important role of tau phosphorylation at S214. The phosphorylation at S202 + T205 recognized by antibody AT8 appears to be an early event in the progression of AD, prior to the formation of tau pre-tangles (Braak et al., 1994). The pseudo-phosphorylation at the AT8* site significantly reduces the microtubule polymerizing ability of tau (Fig. 3.4B). This indicates that the phosphorylation at the AT8* epitope may still contribute to the toxic function of tau by reducing microtubule assembly ability. The phosphorylation of tau at T212 + S214 is carried out by two kinases, GSK3β and PKA, in a sequential manner and recognized by monoclonal antibody AT100 (Zheng-Fischhöfer et al., 1998). The microtubule polymerizing ability of hTau40$_{AT100}$ (Fig. 3.4D) is significantly less than hTau40$_{wt}$ but not completely abolished as in the case of hTau40$_{214E}$ (see Fig. 3.2G). This indicates that the additional pseudo-phosphorylation at T212+S214 assembles microtubule (Fig. 3.4D) much better than the effect of a single pseudo-phosphorylation at S214 that shows complete reduction in microtubule assembling ability. The phosphorylation of tau at AT100 epitope has been shown to reduce microtubule binding both *in vitro* and *in vivo* (Brandt et al., 1994; Illenberger et al., 1998; Zheng-Fischhöfer et al., 1998). The microtubule polymerizing ability of hTau40$_{PHF1}$ is significantly decreased compared to hTau40$_{wt}$ (Fig. 3.4F). These results show that pseudo-

phosphorylation at the flanking domains (AT8*, AT100, and PHF1) have a moderate effect on the microtubule polymerizing ability.

S.no	Constructs	Glu mutations	Aggregation (ThS)	Microtubule assembly
1	htau40wt		+++	+++
2	htau40$_{214E}$	214	+++++	− − −
3	htau40$_{4xKXGE}$	262, 293, 305, 356	− − −	− − −
4	htau40$_{AT8*+AT100+PHF1}$	202, 205, 212, 214, 396, 404	+++++	+++
5	htau40$_{AT8*+AT100+PHF1 +4x KXGE}$	262, 293, 305,356, 202, 205, 212, 214,396,404	− − −	− − −
6	htau40$_{AT100}$	212, 214	+++	+
7	htau40$_{AT8*}$	202, 205	+++	+
8	htau40$_{PHF1}$	396, 404	+++	+
9	htau40$_{214E+AT8*}$	214, 202, 205	+++	+
10	htau40$_{214E+PHF1*}$	214, 396, 404	+++	+
11	htau40$_{15E}$	111, 153, 175, 181, 199, 202, 205, 212, 214, 217, 231, 235, 396, 404, 422	++	+
12	htau40$_{18E}$	46, 50, 69, 111, 153, 175, 181, 199, 202, 205, 212, 214, 217, 231, 235, 396, 404, 422	++	+
13	htau23wt		+++	+++
14	htau23$_{214E}$	214	++++	−
15	htau23$_{AT8*+AT100}$	202, 205, 212, 214	++++	+
16	htau23$_{AT100}$	212, 214	+++	+
17	htau23$_{AT8*+PHF1}$	202, 205, 396, 404	++++	+
18	htau23$_{AT8*+AT100+PHF1}$	202, 205, 212, 214, 396, 404	++++	++

   4.1 In ThS monitored aggregation +++ indicates control aggregation of hTau40wt and hTau23wt: +++++ increased stimulatory aggregation; ++ reduced aggregation; − − − strongly inhibitory aggregation. Microtubule assembly rate: +++ indicates control of microtubule assembly for hTau40wt and hTau23wt; ++ reduced microtubule assembly; − inhibitory microtubule assembly; − − completely detached tau from microtubules (strong inhibitory effect on microtubule assembly).

The phosphorylation at the KXGS motifs in the repeat domains of tau by non-proline directed kinases such as MARK, PKA, and SADK is shown to reduced tau binding to microtubules (Brandt et al., 1994; Drewes et al., 1997; Illenberger et al., 1998; Zheng-Fischhöfer et al., 1998). The mutant hTau40$_{4XKXGE}$ showed that pseudo-phosphorylation at the site of 4X KXGS motifs (Fig. 3.4G) completely abolishes the microtubule polymerizing ability of tau. This is again consistent with the earlier studies where it is shown that phosphorylation at KXGS motifs detaches tau from microtubules (Biernat et al., 1993; Drewes et al., 1997). At the same time, hTau40$_{AT8*+AT100+PHF1+4X\ KXGE}$ showed complete reduction in the ability to polymerize microtubules (Fig. 3.6 B). This again proves the strong effect of phosphorylation at the KXGS

motifs. This indicates that glu mutation at KXGS motifs can not be overridden by the flanking pseudo-phosphorylation at AT8*+AT100+PHF1 (which by itself shows no effect on the microtubule polymerizing ability of tau, Fig. 3.10). The 214E+AT8* mutant showed a substantial reduction in the polymerizing property of microtubules (Fig. 3.5B). This result indicates that the effect of 214E alone (see Fig. 3.2G) is reversed by additional mutation in the flanking domains. On the other hand, $hTau40_{214E+PHF1}$ show a significant decrease in the ability to promote microtubule polymerization. This again confirms that the effect of 214E is by itself reversed by additional mutation in the flanking domains (Fig. 3.5D). The proline-directed protein kinases have received a great deal of attention because phospho-epitopes at SP/TP sites are recognized by antibodies that preferentially detect tau in brain tissue from patients with tauopathies. Phosphorylation at the SP/TP disease-associated sites plays a key role in microtubule assembly *in vitro*. The microtubule polymerization ability of $hTau40_{SP/TP\ (15E)}$ and $hTau40_{SP/TP\ (18E)}$ was further reduced (Fig. 3.8B and D). This clearly indicates that hTau40 bearing the pseudo-phosphorylation at 18 SP/TP motifs also shows a significantly reduced ability to promote microtubule assembly and is similar to that of $hTau40_{SP/TP\ (15E)}$. This clearly suggests that pseudo-phosphorylation at different sites (flanking regions, repeats and) reduced its affinity to microtubules, thus leading to the aggregation and formation of paired helical filaments. These results provide insight into the pathogenesis of tau protein and contribute to a better understanding of the molecular processes in Alzheimer's disease.

4.2 Pathologic conformation of tau influenced by pseudo-phosphorylation

To relate the global conformational change of tau induced by pseudo-phosphorylation to the functions of tau we tested the propensity for aggregation, the ability to promote microtubule polymerization, and the reaction with MC1 and Alz-50 which is characteristic of a pathological conformation of tau in AD. These properties were compared for wild-type tau and the triple pseudo-phosphorylated mutant $hTau40_{AT8*+AT100+PHF1}$, which shows the tightest compaction of the paperclip conformation (Jeganathan et al., 2008). In the aggregation assay, $hTau40_{AT8*+AT100+PHF1}$ shows a moderate but significant increase of ThS fluorescence compared to $hTau40_{wt}$ (Fig. 3.9A). This suggests that the compaction due to the pseudo-phosphorylation at both arms (AT8*+AT100+PHF1) raises the tendency for aggregation (beyond the effect of polyanions alone; Fig. 3.9A). In contrast, the microtubule polymerizing ability of $hTau40_{AT8*+AT100+PHF1}$ showed no difference in final extent and only a small retardation on assembly rate was observed. This is consistent with the notion that the AD-like phosphorylation in the flaking domains has no or only a small effect on tau microtubule interactions (Leger et al., 1997; Biernat et al., 1993; Cho et al., 2003; Jeganathan et al., 2008).

Perhaps the most provocative aspect of the results is the relationship between Alzheimer-like phosphorylation epitopes (AT8*, AT100, and PHF1) and the compaction of the paperclip conformation. The reactivity of AT8*, AT100, and PHF1 tau with antibodies that report on the pathological conformation of tau in early stages of AD, such as MC1, Alz-50, and other conformational antibodies. This reaction is best observed in brain tissue and has been difficult to reproduce with tau *in vitro.* However, the fact that the most compact conformations are also the ones showing the highest reactivity with MC1 and Alz-50 (Fig.3.11A-D), argues that the compaction of paperclip conformations reflects the pathological state (Jeganathan et al., 2008). The increase in MC1 and Alz-50 reactivity becomes more pronounced when the C-terminal tail is absent, which argues that this tail normally opposes a close approach between N-terminus and the repeats (consistent with the paperclip model; Jeganathan et al., 2006). As a caveat, we note that antibody Alz-50 shows only a very weak reaction, both for wild-type soluble tau and phospho-mimic mutants, albeit the epitope comprises similar residues of tau as antibody MC1 (Jicha et al., 1997). In the case of neurons, we speculate that multiple phosphorylation plus stabilization by other interactions may lead to the enhanced visibility of the pathological conformation seen in brain tissue.

Whether or not this conformation promotes aggregation directly or by some other intermediate states (*e.g.* oligomers of tau) remains open at present. From a structural perspective, the folding of the N- and C-domains over the repeat domain would be expected to protect against aggregation, and indeed tau forms aggregates more readily when the non-repeat domains are cleaved off (Binder et al., 2005; von Bergen et al., 2000; Wille et al., 1992; Kampers et al., 1999; Berry et al., 2003). This is reminiscent of other amyloid aggregation processes that are enabled only when the protective surroundings are removed, *e.g.* by cleavage or unfolding (Dobson et al., 1999; Uversky et al, 2007). Contrary of these principles, we found that the compact pseudo-phosphorylated conformation forms aggregates somewhat more readily, whereas microtubule interaction shows little change. Both these observations suggest that the compaction of the molecule observed by FRET resembles the "pathological conformation" detected by the MC1 and Alz-50 antibody (Jeganathan et al., 2008). A possible explanation is that the compactions of the paperclip takes place such that the amyloid-forming hexapeptide motifs in the repeat domain become exposed, which would then promote further aggregation. These issues must await further structural analysis, for example by environmental sensitive tags.

4.3 Polymorphic assembly of human tau fibrils

4.3.1 Tau fibrils are polymorphic but show common properties

All fibrils assembled from tau isoforms and constructs investigated in this work showed the above mentioned features, suggesting that the assembly of tau into differently shaped fibrils may follow common mechanisms.

To generate different fibril structures, different assembly mechanisms may coexist for the same tau protein. Because different tau isoforms and constructs form a similar polymorphic set of fibril structures that contain ß-stacked tau repeat domains (Berriman et al., 2003; Goux et al., 2004; Skraban et al., 2006), it may be speculated that all tau protein assemblies share common structural similarities. (i) Thick and thin fibrils exposed ~17-19 nm periodicities. The protein mass per fibril length obtained from STEM measurements on purified unstained fibrils (von Bergen et al., 2006) suggested an average density of ~3.5 molecules per nanometer for native full length hTau40wt and ~4.5 molec./nm in the K19 fibrils. Accordingly, an ~17 nm subunit would consist of 17 nm x 3.5 molec./nm = 60 hTau40 molecules and 17 nm x 4.5 molec./nm = 77 K19 molecules. Such dimensions of a subunit seem reasonable when compared with oligomers of other amyloid-forming proteins like Aß (~40 molecules Aß; Orte et al., 2008) or other prion protein (14-28 molecules PrP[sc]; Silveria et al., 2005). (ii) All thin and thick fibrils showed the same minimal height (thickness) of ~9-11 nm. (iii) All fibrils could disassemble into smaller fragments that remained connected by a thread-like structure. (iv) Hydrophobic interactions seem to play a major role for the integrity of the fibrils, regardless of the given tau isoform and the presence of the N- and C-termini. (v) Electrostatic interactions could be tuned to compensate destabilizing hydrophobic interactions.

4.3.2 Thin and thick tau fibrils and twisted ribbons

One critical parameter to distinguish fibrils of different morphological classes is to measure their height in AFM topographs. It could be that thick fibrils represent PHFs. Two alternative PHF models have been discussed in the literature.

- One model assumes a single flat ribbon structure with an internal twist around the fibril axis (Wischik et al., 1988; Crowther RA, 1990; Ruben et al., 2005).

- The other model suggests two protofibrils twisted around each other; hence the name "paired helical filaments" (Kidd M, 1936; Pollanen et al., 1994; Pollanen et al., 1997).

Thick fibrils showed height corrugations ranging from ~11 to 19 nm (hTau40) and from ~10 to 16 nm for (K19). The mean thin fibril height was ~11 nm for hTau40and ~9 nm for K19. Thus, thick and thin fibrils show the same minimum height of ~9-11 nm. The thin fibrils clearly suggest that tau assembles into flat ribbons. Apparently, these tau ribbons can be corrugated, and

in some cases we have observed the transition of a smooth thin ribbon into corrugated thin ribbon. However, such a thin ribbon, if twisted around its longitudinal axis, could easily form a thick twisted fibril. Thus, the polymorphic tau fibrils would expose the same basic architecture of a ribbon providing a consistent explanation of the observed structures. Small differences in the interactions between the tau subunits may induce changes in their packaging and lead either to flat, slightly corrugated, or twisted tau ribbons or fibrils (Wegmann et al., 2010).

4.4 Compaction form of tau in solution

The structural information of tau protein in solution has been difficult to obtain as it lacks defined structure which also precludes a crystallographic analysis. Spectroscopic evidences (CD, FTIR, intrinsic fluorescence and other biophysical methods), solution X-ray scattering and hydrodynamic evidence highlight the "natively unfolded" nature of tau, characterized by a lack of secondary structure, Gaussian coil-type character with persistence length around 2 nm and unusually large volume (Barghorn et al., 2004; Li et al., 2002; Schweers et al., 1994; von Bergen et al., 2000). Electron microscopy revealed that tau can be visualized as a rather extended rod-like form (Wille et al., 1992). When bound to microtubules, tau tends to align along the protofilament ridges but retains much of its disordered state (Al-Bassam et al., 2002; Santarella et al., 2004). NMR spectroscopy confirms the paucity of secondary structure, but in addition highlights certain sequence motifs in the repeat domain with an enhanced propensity for β-structure which are known to play a role in the abnormal aggregation into PHFs (Goux et al., 2004; Mukrasch et al., 2005; von Bergen et al., 2000).

The temperature-dependent CD spectra of tau suggest a small and gradual change that can be explained by a transition between two states, indicated by the isosbestic point at 210 nm. With increasing temperature, tau isoforms and constructs showed a spectral shift with a decrease of intensity at 200 nm and an increase of intensity at 217 nm indicating a structural transition with an isosbestic point at ~210 nm (Jeganathan et al., 2008; Shkumatov et al., 2011). The temperature-dependent CD spectra of tau did not show major shift from 200 nm as expected for a structural transition from random coil (~200 nm) to α-helix or ß-structure (~217 nm). This temperature-dependent CD of tau is similar to that of the polyproline II helix (PPII) for which the spectral change upon temperature rise is attributed to the transition to more disorder or flat ß-structure (Makarov et al., 1992; Eker et al., 2003; Rath et al., 2005). PPII is a left handed helix with three residues per turn and the rise per residue is ~3.1Å. The mean residue ellipticity (MRE) of PPII observed by CD ranges from -60000 (collagen and poly-L-lysine) to -20000 deg cm^2 dmol^{-1} (model peptides) (Eker et al., 2003; Rath et al., 2005; Greenfield, 2006). In the case of tau, the MRE is ~ -16000 deg cm^2 dmol^{-1} which falls within the range of -20000 to -5000 deg

cm^2 dmol^{-1} that is observed for the denatured and natively unfolded proteins (Uversky et al., 2001; Barghorn et al., 2004; Greenfield et al., 2006; Jeganathan et al., 2008; Kjaergaard et al., 2010; Shkumatov et al., 2011). Also shown by NMR, tau constructs contain very little PPII conformation but contain stretches of amino acids with a tendency for ß-structure (Mukrasch et al., 2005; Mukrasch et al., 2007). Based on this, it is reasonable to assume that the nascent ß-structure elements are strengthened at high temperatures probably by increase of hydrophobic interactions. However, the 200/217 nm ratio of the spectra as a function of temperature suggest that structure induction may be a transient one and can not be propagated in cooperative fashion pointing to lack of significant amount of hydrophobic amino acids. A similar pattern of spectral change upon temperature elevation was observed for α-synuclein and interpreted as the formation of a partially folded intermediate due to the increase of hydrophobic interactions (Uversky et al., 2001). Securin is unstructured in solution, and also belongs to the family of natively unfolded proteins. In the case of securin it was suggested that presence of a small amount of a polyproline helix II (PPII) might be the reason for such behavior (Sanchez-Puig et al., 2005).

The polypeptide chain of tau has been shown to remain mostly natively disordered, loose and flexible under different conditions (Mukrasch et al., 2009; Jeganathan et al., 2006). This structural plasticity is necessary for the unique functional repertoire of IDPs, which is complementary to the catalytic activates of ordered proteins (Uversky et al., 2009). Changes occurring under different conditions have been reported for tau (Mukrasch et al., 2009). There is some global folding (hairpin model, whereby N- and C-terminal domains approach the repeat domain), which could affect Rg. It is noteworthy that the hairpin model also shows compaction in some conditions (as determined by FRET), for example after hyperphosphorylation at several sites, consistent with the reaction of antibodies MC1 or Alz-50, which are characteristic of incipient Alzheimer disease (Jeganathan et al., 2008). It is therefore clear that the unfolded nature of tau protein allows it to adopt either more extended or compact conformations. It is intriguing to speculate that the compaction and memory effect observed after rapid heating/cooling may be related to the compaction observed (Fig. 4.2). The memory effect is observed with full-length tau, but not with the repeat domain alone, suggesting that the interplay between domains in the whole protein might be responsible for the effect. We performed additional measurements on incubated hTau40wt, which revealed that the compact state is preserved for at least 3 hour of incubation, but after 24 hour, the protein is nearly reverted back to the native state (Fig 4.1). One possible explanation could be the interplay between the acidic N-terminal domain (which varies among the tau isoforms due to alternative splicing) and the

basic repeat domain (which also differs between the isoforms). This possibility will be addressed in future studies.
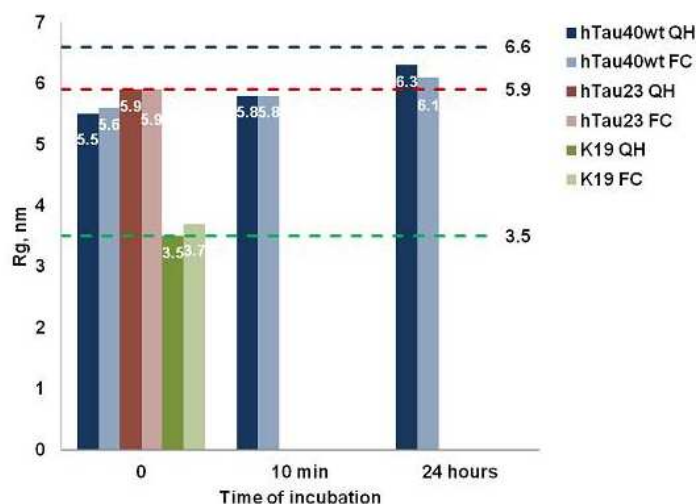
Figure 4.1: Time course of the radius of gyration hTau40wt measured by SAXS. Changes in radius of gyration for different tau samples over time. The dashed lines represent R_g (nm) values for the tau constructs (dark blue – hTau40wt, red – hTau23, green – K19) measured at 10°C. Blue columns represent hTau40wt under non-equilibrium (dark blue - Quick Heating; light blue - Fast Cooling) conditions measured before and after incubation. The R_g values of the samples incubated after temperature jump for 24 hours is similar to that of the wild type. Red columns represent annealed and quenched forms of hTau23 (dark red – Quick Heating, light red – Fast Cooling). Green columns represent annealed and quenched forms of K19 (green – Quick Heating; light green – Fast Cooling). The short constructs (hTau23 and K19), as opposed to the full length ones, do not change their overall size under non-equilibrium temperature conditions (reproduced from Shkumatov et al., 2011).
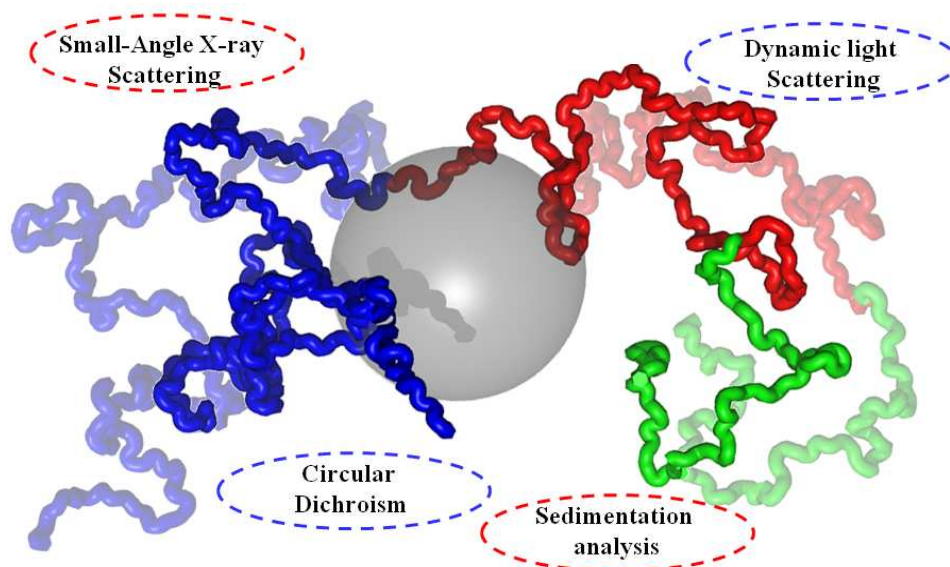
Figure 4.2: Hypothetical model of tau conformation in solution by different methods: Hypothetical model of Tau conformation before (pale colors) and after compaction induced by a temperature jump (bold colors). The N-terminus (residues 1-243) is colored in blue, the repeat domain (residues 244-368) in red, and the C-terminus (residues 369-441) in green. The extent of compaction is enlarged for better visibility. The gray sphere represents the Stokes radius of a well-folded protein (α-amylase) of the same chain length as hTau40 (Mylonas et al., 2007), illustrating that tau occupies a larger volume in space, both in the normal and compacted states.

The potential of SAXS is illustrated in the present work revealing an unusual effect of compaction of the intrinsically unfolded tau protein under non-equilibrium temperature conditions. An analogous compaction has also been observed as a result of post-translational modifications of tau and is reminiscent of tau conformations during incipient Alzheimer disease, as seen by conformation-dependent antibodies (Jeganathan et al., 2008; Jicha et al., 1997).

5 Summary

Tau is one of the microtubule associated proteins which can bind and stabilize microtubules. It is classified as a natively unfolded protein. It has a very low content of secondary structural elements. Tau aggregates into insoluble fibers called paired helical filaments in Alzheimer's disease. The residual folding and intramolecular interactions within tau are largely unknown, and the factors contributing to the formation and stability of PHFs and different morphologies of PHFs are not well understood. The results of the present studies are aimed at better understanding of the effect of phosphorylation on the aggregation propensity and tau-microtubule interaction. The effect of phosphorylation sites in the KXGS motifs within the repeats and in the SP/TP motifs of the flanking regions were studied. We also studied tau fibril polymorphism by Electron Microscopy and Atomic Force Microscopy. We further studied tau in solution by increasing temperature using different biophysical methods (CD spectroscopy, static and dynamic light scattering and small angle x-ray scattering). These observations could form a basis for elucidating the molecular and physiological role of phosphorylation at the repeat domains and in the flanking regions. The results are summarized as follows:

(i) The pseudo-phosphorylation of KXGE motifs within the repeat domains of tau has a strong negative effect on both the tau-microtubule interaction and the aggregation into paired helical filaments. KXGE mutants on the basis of three repeat domain and four repeat domain constructs show a low tendency to aggregate and form amorphous aggregates instead of PHFs. Pseudo-phosphorylation in the SP/TP motifs in the N- and C-terminal domains of the flanking regions has only a moderate effect, both on the tau-microtubule interaction and on the aggregation into paired helical filaments. Overall, the results show that the physiological tau-microtubule interaction and the pathological tau-tau interaction similarly can be influenced by phosphorylation.

(ii) The combined pseudo-phosphorylation of AT8* and PHF1 sites leads to compaction of the paperclip conformation, such that the N-terminus approaches the repeat domain. When the C-terminus tail is cleaved from tau, the compaction becomes even stronger by combining pseudo-phosphorylated AT8*, AT100, and PHF1 epitopes. This is accompanied by a strong increase in the reaction with conformation-dependent antibodies MC1 and Alz-50, suggesting the generation of a pathological conformation characteristic of tau in AD. Furthermore, the compact paperclip conformation enhances the aggregation propensity to paired helical filaments but has little effect on microtubule interactions.

(iii) High resolution atomic force and electron microscopy were employed to study fibrils assembled from different human tau isoforms and domains. All fibrils reveal structural polymorphism: the "thin twisted" and "thin smooth" fibrils resemble flat ribbons (cross-section ~10 x 15 nm) with diverse twist periodicities. "Thick fibrils" show periodicities of ~65-70 nm and thicknesses of ~9-18 nm as routinely reported for "paired helical filaments" but structurally resemble heavily twisted ribbons. Therefore, thin and thick fibrils assembled from different human tau isoforms challenge current structural models of paired helical filaments. The full-length tau and repeat domain constructs assemble into fibrils of similar thickness, the "fuzzy coat" of tau protein termini surrounding the fibril axis is nearly invisible for atomic force microscopy and electron microscopy, presumably because of its high flexibility.

(iv) The unfolded nature of tau protein allows it to adopt either more extended or compact conformations. It is intriguing to speculate that the compaction and memory effect observed after rapid heating/cooling may be related to the compaction observed upon hyperphosphorylation, characteristic of incipient neuronal degeneration in AD. The "memory effect" is observed with full-length tau, but not with the repeat domain alone, suggesting that the interplay between domains in the whole protein might be responsible for the effect. One possible explanation could be the interplay between the acidic N-terminal domain (which varies among the tau isoforms due to alternative splicing) and the basic repeat domain (which also differs between the isoforms).

6 References

Ackmann, M., Wiech, H., and Mandelkow, E. (2000). Nonsaturable binding indicates clustering of tau on the microtubule surface in a paired helical filament-like conformation. The Journal of biological chemistry *275*, 30335-30343.

Abraha, A., Ghoshal, N., Gamblin, T.C., Cryns, V., Berry, R.W., Kuret, J., and Binder, L.I. (2000). C-terminal inhibition of tau assembly in vitro and in Alzheimer's disease. J Cell Sci *113 Pt 21*, 3737-3745.

Alonso, A., Zaidi, T., Novak, M., Grundke-Iqbal, I., and Iqbal, K. (2001). Hyperphosphorylation induces self-assembly of tau into tangles of paired helical filaments/straight filaments. Proc Natl Acad Sci U S A *98*, 6923-6928.

Al-Bassam, J., Ozer, R.S., Safer, D., Halpain, S., and Milligan, R.A. (2002). MAP2 and tau bind longitudinally along the outer ridges of microtubule protofilaments. J Cell Biol *157*, 1187-1196.

Allen, MJ, Hud, NV, Balooch, M, Tench, RJ, Siekhaus, WJ and Balhorn, R. (1992) Tip-radius-induced artifacts in AFM images of protamine-complexed DNA fibers. *Ultramicroscopy*, 42-44 (Pt B), 1095-1100.

Allen, C., and Borisy, G.G. (1974). Structural polarity and directional growth of microtubules of Chlamydomonas flagella. J Mol Biol *90*, 381-402.

Andreadis, A. (2005). Tau gene alternative splicing: expression patterns, regulation and modulation of function in normal brain and neurodegenerative diseases. Biochimica et biophysica acta *1739*, 91-103.

Andronesi, OC, von Bergen, M, Biernat, J, Seidel, K, Griesinger, C, Mandelkow, E and Baldus, M. (2008) Characterization of Alzheimer's-like paired helical filaments from the core domain of tau protein using solid-state NMR spectroscopy. *J Am Chem Soc*, 130, 5922-5928.

Amos, L., and Klug, A. (1974). Arrangement of subunits in flagellar microtubules. J Cell Sci *14*, 523-549.

Avila, J. (2006). Tau phosphorylation and aggregation in Alzheimer's disease pathology. FEBS letters *580*, 2922-2927.

Augustinack, J.C., Schneider, A., Mandelkow, E.M., and Hyman, B.T. (2002). Specific tau phosphorylation sites correlate with severity of neuronal cytopathology in Alzheimer's disease. Acta Neuropathol (Berl) *103*, 26-35.

Azhar, S., and Murphy, D.B. (1990). Structural plugs at microtubule ends may regulate polymer dynamics in vitro. Cell Motil Cytoskeleton *15*, 156-161.

Baldwin, R.L. (1986). Temperature dependence of the hydrophobic interaction in protein folding. Proceedings of the National Academy of Sciences of the United States of America *83*, 8069-8072.

Barghorn, S., Zheng-Fischhofer, Q., Ackmann, M., Biernat, J., von Bergen, M., Mandelkow, E.M., and Mandelkow, E. (2000). Structure, microtubule interactions, and paired helical filament aggregation by tau mutants of frontotemporal dementias. Biochemistry *39*, 11714-11721.

Barghorn, S., and Mandelkow, E. (2002). Toward a unified scheme for the aggregation of tau into Alzheimer paired helical filaments. Biochemistry *41*, 14885-14896.

Barghorn, S., Davies, P., and Mandelkow, E. (2004). Tau paired helical filaments from Alzheimer's disease brain and assembled in vitro are based on beta-structure in the core domain. Biochemistry *43*, 1694-1703.

Baron, U., Freundlieb, S., Gossen, M., and Bujard, H. (1995). Co-regulation of two gene activities by tetracycline via a bidirectional promoter. Nucleic Acids Res *23*, 3605-3606.

Barre, P., and Eliezer, D. (2006). Folding of the repeat domain of tau upon binding to lipid surfaces. Journal of molecular biology *362*, 312-326.

Baumann, K., Mandelkow, E.M., Biernat, J., Piwnica-Worms, H., and Mandelkow, E. (1993). Abnormal Alzheimer-like phosphorylation of tau-protein by cyclin-dependent kinases cdk2 and cdk5. FEBS letters *336*, 417-424.

Berriman, J., Serpell, L.C., Oberg, K.A., Fink, A.L., Goedert, M., and Crowther, R.A. (2003). Tau filaments from human brain and from in vitro assembly of recombinant protein show cross-beta structure. Proceedings of the National Academy of Sciences of the United States of America *100*, 9034-9038.

Biernat, J., Mandelkow, E.M., Schröter, C., Lichtenberg-Kraag, B., Steiner, B., Berling, B., Meyer, H.E., Mercken, M., Vandermeeren, A., Goedert, M.*, et al.* (1992). The switch of tau protein to an Alzheimer-like state includes the phosphorylation of two serine-proline motifs upstream of the microtubule binding region. EMBO J *11*, 1593-1597.

Biernat, J., and Mandelkow, E.M. (1999). The development of cell processes induced by tau protein requires phosphorylation of serine 262 and 356 in the repeat domain and is inhibited by phosphorylation in the proline-rich domains. Mol Biol Cell *10*, 727-740.

Binder, L.I., Guillozet-Bongaarts, A.L., Garcia-Sierra, F., and Berry, R.W. (2005). Tau, tangles, and Alzheimer's disease. Biochimica et biophysica acta *1739*, 216-223.

Bonnet, C., Boucher, D., Lazereg, S., Pedrotti, B., Islam, K., Denoulet, P., and Larcher, J.C. (2001). Differential binding regulation of microtubule-associated proteins MAP1A, MAP1B, and MAP2 by tubulin polyglutamylation. J Biol Chem *276*, 12839-12848.

Braak, H., and Braak, E. (1995). Staging of Alzheimer's disease-related neurofibrillary changes. Neurobiol Aging *16*, 271-278; discussion 278-284.

Brandt, R., Lee, G., Teplow, D.B., Shalloway, D., and Abdel-Ghany, M. (1994). Differential effect of phosphorylation and substrate modulation on tau's ability to promote microtubule growth and nucleation. The Journal of biological chemistry *269*, 11776-11782.

Brandt, R., Leger, J., and Lee, G. (1995). Interaction of tau with the neural plasma membrane mediated by tau's amino-terminal projection domain. J Cell Biol *131*, 1327-1340.

Bre, M.H., and Karsenti, E. (1990). Effects of brain microtubule-associated proteins on microtubule dynamics and the nucleating activity of centrosomes. Cell Motil Cytoskeleton *15*, 88-98.

Bright, JN, Woolf, TB and Hoh, JH. (2001) Predicting properties of intrinsically unstructured proteins. *Prog Biophys Mol Biol*, 76, 131-173.

Butner, K.A., and Kirschner, M.W. (1991). Tau protein binds to microtubules through a flexible array of distributed weak sites. J Cell Biol *115*, 717-730.

Burns, R.G. (1991). Alpha-, beta-, and gamma-tubulins: sequence comparisons and structural constraints. Cell Motil Cytoskeleton *20*, 181-189.

Caceres, A., Mautino, J., and Kosik, K.S. (1992). Suppression of MAP2 in cultured cerebellar macroneurons inhibits minor neurite formation. Neuron *9*, 607-618.

Carlson, S.W., Branden, M., Voss, K., Sun, Q., Rankin, C.A., and Gamblin, T.C. (2007). A complex mechanism for inducer mediated tau polymerization. Biochemistry *46*, 8838-8849.

Carmel, G., Mager, E.M., Binder, L.I., and Kuret, J. (1996). The structural basis of monoclonal-antibody Alz50s selectivity for Alzheimer's-disease pathology. Journal of Biological Chemistry *271*, 32789-32795.

Chen, J., Kanai, Y., Cowan, N.J., and Hirokawa, N. (1992). Projection domains of MAP2 and tau determine spacings between microtubules in dendrites and axons. Nature *360*, 674-677.

Chiti, F., Taddei, N., Baroni, F., Capanni, C., Stefani, M., Ramponi, G., and Dobson, C.M. (2002). Kinetic partitioning of protein folding and aggregation. Nat Struct Biol *9*, 137-143.

Chiti, F., and Dobson, C.M. (2006). Protein misfolding, functional amyloid, and human disease. Annual review of biochemistry *75*, 333-366.

Chretien, D., and Wade, R.H. (1991). New data on the microtubule surface lattice. Biol Cell *71*, 161-174.

Cleveland, D.W., Hwo, S.Y., and Kirschner, M.W. (1977). Physical and chemical properties of purified tau factor and the role of tau in microtubule assembly. Journal of molecular biology *116*, 227-247.

Crowther, R.A., and Wischik, C.M. (1985). Image reconstruction of the Alzheimer paired helical filament. Embo J *4*, 3661-3665.

Crowther, R.A. (1991). Straight and paired helical filaments in Alzheimer disease have a common structural unit. Proceedings of the National Academy of Sciences of the United States of America *88*, 2288-2292.

Cross, D., Dominguez, J., Maccioni, R.B., and Avila, J. (1991). MAP-1 and MAP-2 binding sites at the C-terminus of beta-tubulin. Studies with synthetic tubulin peptides. Biochemistry *30*, 4362-4366.

Cummings, J.L. (2004). Alzheimer's disease. The New England journal of medicine *351*, 56-67.

D'Souza, I., Poorkaj, P., Hong, M., Nochlin, D., Lee, V.M., Bird, T.D., and Schellenberg, G.D. (1999). Missense and silent tau gene mutations cause frontotemporal dementia with parkinsonism-chromosome 17 type, by affecting multiple alternative RNA splicing regulatory elements. Proceedings of the National Academy of Sciences of the United States of America *96*, 5598-5603.

Daggett, V., and Fersht, A. (2003a). The present view of the mechanism of protein folding. Nature reviews *4*, 497-502.

Daggett, V., and Fersht, A.R. (2003b). Is there a unifying mechanism for protein folding? Trends in biochemical sciences *28*, 18-25.

Delacourte, A., and Defossez, A. (1986). Alzheimer's disease: Tau proteins, the promoting factors of microtubule assembly, are major components of paired helical filaments. J Neurol Sci *76*, 173-186.

Desai, A., and Mitchison, T.J. (1997). Microtubule polymerization dynamics. Annu Rev Cell Dev Biol *13*, 83-117.

Derkinderen, P., Scales, T.M., Hanger, D.P., Leung, K.Y., Byers, H.L., Ward, M.A., Lenz, C., Price, C., Bird, I.N., Perera, T.*, et al.* (2005). Tyrosine 394 is phosphorylated in Alzheimer's paired helical filament tau and in fetal tau with c-Abl as the candidate tyrosine kinase. J Neurosci *25*, 6584-6593.

Ding, H., Matthews, T.A., and Johnson, G.V. (2006). Site-specific phosphorylation and caspase cleavage differentially impact tau-microtubule interactions and tau aggregation. J Biol Chem *281*, 19107-19114.

Drewes, G., Lichtenberg-Kraag, B., Doring, F., Mandelkow, E.M., Biernat, J., Goris, J., Doree, M., and Mandelkow, E. (1992). Mitogen activated protein (MAP) kinase transforms tau protein into an Alzheimer-like state. Embo J *11*, 2131-2138.

Drewes, G., Ebneth, A., Preuss, U., Mandelkow, E.M., and Mandelkow, E. (1997). MARK, a novel family of protein kinases that phosphorylate microtubule-associated proteins and trigger microtubule disruption. Cell *89*, 297-308.

Drewes, G., Ebneth, A., and Mandelkow, E.M. (1998). MAPs, MARKs and microtubule dynamics. Trends Biochem Sci *23*, 307-311.

Drubin, D.G., and Kirschner, M.W. (1986). Tau protein function in living cells. J Cell Biol *103*, 2739-2746.

Ebneth, A., Godemann, R., Stamer, K., Illenberger, S., Trinczek, B., and Mandelkow, E. (1998). Overexpression of tau protein inhibits kinesin-dependent trafficking of vesicles, mitochondria, and endoplasmic reticulum: implications for Alzheimer's disease. J Cell Biol *143*, 777-794.

Ebneth, A., Drewes, G., Mandelkow, E.M., and Mandelkow, E. (1999). Phosphorylation of MAP2c and MAP4 by MARK kinases leads to the destabilization of microtubules in cells. Cell Motil Cytoskeleton *44*, 209-224.

Eidenmuller, J., Fath, T., Hellwig, A., Reed, J., Sontag, E., and Brandt, R. (2000). Structural and functional implications of tau hyperphosphorylation: information from phosphorylation-mimicking mutated tau proteins. Biochemistry *39*, 13166-13175.

Eidenmuller, J., Fath, T., Maas, T., Pool, M., Sontag, E., and Brandt, R. (2001). Phosphorylation-mimicking glutamate clusters in the proline-rich region are sufficient to simulate the functional deficiencies of hyperphosphorylated tau protein. Biochem J *357*, 759-767.

Eftink, M.R. (1991). Fluorescence techniques for studying protein structure. Methods Biochem Anal *35*, 127-205.

Eker, F., Griebenow, K., and Schweitzer-Stenner, R. (2003). Stable conformations of tripeptides in aqueous solution studied by UV circular dichroism spectroscopy. Journal of the American Chemical Society *125*, 8178-8185.

Elcock, A.H. (1998). The stability of salt bridges at high temperatures: implications for hyperthermophilic proteins. Journal of molecular biology *284*, 489-502.

Esposito, G., Viglino, P., Novak, M., and Cattaneo, A. (2000). The solution structure of the C-terminal segment of tau protein. J Pept Sci *6*, 550-559.

Esmaeli-Azad, B., McCarty, J.H., and Feinstein, S.C. (1994). Sense and antisense transfection analysis of tau function: tau influences net microtubule assembly, neurite outgrowth and neuritic stability. J Cell Sci *107 (Pt 4)*, 869-879.

Fan, J., Griffiths, A.D., Lockhart, A., Cross, R.A., and Amos, L.A. (1996). Microtubule minus ends can be labelled with a phage display antibody specific to alpha-tubulin. J Mol Biol *259*, 325-330.

Fath, T., Eidenmuller, J., and Brandt, R. (2002). Tau-mediated cytotoxicity in a pseudohyperphosphorylation model of Alzheimer's disease. J Neurosci *22*, 9733-9741.

Fellous, A., Francon, J., Lennon, A.M., and Nunez, J. (1977). Microtubule assembly in vitro. Purification of assembly-promoting factors. Eur J Biochem *78*, 167-174.

Fernandez-Escamilla, A.M., Rousseau, F., Schymkowitz, J., and Serrano, L. (2004). Prediction of sequence-dependent and mutational effects on the aggregation of peptides and proteins. Nat Biotechnol *22*, 1302-1306.

Ferri, C.P., Prince, M., Brayne, C., Brodaty, H., Fratiglioni, L., Ganguli, M., Hall, K., Hasegawa, K., Hendrie, H., Huang, Y.*, et al.* (2005). Global prevalence of dementia: a Delphi consensus study. Lancet *366*, 2112-2117.

Fitzkee, N.C., and Rose, G.D. (2004). Reassessing random-coil statistics in unfolded proteins. Proceedings of the National Academy of Sciences of the United States of America *101*, 12497-12502.

Friedhoff, P., Schneider, A., Mandelkow, E.M., and Mandelkow, E. (1998). Rapid assembly of Alzheimer-like paired helical filaments from microtubule-associated protein tau monitored by fluorescence in solution. Biochemistry *37*, 10223-10230.

Gamblin, T.C., Berry, R.W., and Binder, L.I. (2003a). Modeling tau polymerization in vitro: a review and synthesis. Biochemistry *42*, 15009-15017.

Gamblin, T.C., Chen, F., Zambrano, A., Abraha, A., Lagalwar, S., Guillozet, A.L., Lu, M., Fu, Y., Garcia-Sierra, F., LaPointe, N.*, et al.* (2003b). Caspase cleavage of tau: linking amyloid and neurofibrillary tangles in Alzheimer's disease. Proceedings of the National Academy of Sciences of the United States of America *100*, 10032-10037.

Garcia-Sierra, F., Ghoshal, N., Quinn, B., Berry, R.W., and Binder, L.I. (2003). Conformational changes and truncation of tau protein during tangle evolution in Alzheimer's disease. J Alzheimers Dis *5*, 65-77.

Garcia, M.L., and Cleveland, D.W. (2001). Going new places using an old MAP: tau, microtubules and human neurodegenerative disease. Curr Opin Cell Biol *13*, 41-48.

Gasteiger E., Hoogland C., Gattiker A., Duvaud S., Wilkins M.R., Appel R.D., and A, B. (2005). Protein Identification and Analysis Tools on the ExPASy Server. John M Walker (ed): The Proteomics Protocols Handbook, Humana Press, 571-607.

Ghoshal, N., Garcia-Sierra, F., Fu, Y., Beckett, L.A., Mufson, E.J., Kuret, J., Berry, R.W., and Binder, L.I. (2001). Tau-66: evidence for a novel tau conformation in Alzheimer's disease. J Neurochem *77*, 1372-1385.

Goedert, M., Spillantini, M.G., Potier, M.C., Ulrich, J., and Crowther, R.A. (1989). Cloning and sequencing of the cDNA encoding an isoform of microtubule-associated protein tau containing four tandem repeats: differential expression of tau protein mRNAs in human brain. Embo J *8*, 393-399.

Goedert, M., Jakes, R., and Vanmechelen, E. (1995). Monoclonal antibody AT8 recognises tau protein phosphorylated at both serine 202 and threonine 205. Neurosci Lett *189*, 167-169.

Goedert, M. (1996). Tau protein and the neurofibrillary pathology of Alzheimer's disease. Ann N Y Acad Sci *777*, 121-131.

Goedert, M., Jakes, R., Spillantini, M.G., Hasegawa, M., Smith, M.J., and Crowther, R.A. (1996). Assembly of microtubule-associated protein tau into Alzheimer-like filaments induced by sulphated glycosaminoglycans. Nature *383*, 550-553.

Goedert, M., Jakes, R., and Crowther, R.A. (1999). Effects of frontotemporal dementia FTDP-17 mutations on heparin-induced assembly of tau filaments. FEBS letters *450*, 306-311.

Gong, C.X., Liu, F., Wu, G., Rossie, S., Wegiel, J., Li, L., Grundke-Iqbal, I., and Iqbal, K. (2004). Dephosphorylation of microtubule-associated protein tau by protein phosphatase 5. J Neurochem *88*, 298-310.

Gong, C.X., Liu, F., Grundke-Iqbal, I., and Iqbal, K. (2005). Post-translational modifications of tau protein in Alzheimer's disease. J Neural Transm *112*, 813-838.

Goode, B.L., Denis, P.E., Panda, D., Radeke, M.J., Miller, H.P., Wilson, L., and Feinstein, S.C. (1997). Functional interactions between the proline-rich and repeat regions of tau enhance microtubule binding and assembly. Mol Biol Cell *8*, 353-365.

Goode, B.L., and Feinstein, S.C. (1994). Identification of a novel microtubule binding and assembly domain in the developmentally regulated inter-repeat region of tau. J Cell Biol *124*, 769-782.

Gong, C.X., Liu, F., Grundke-Iqbal, I., and Iqbal, K. (2005). Post-translational modifications of tau protein in Alzheimer's disease. J Neural Transm *112*, 813-838.

Gordon-Weeks, P.R., Mansfield, S.G., Alberto, C., Johnstone, M., and Moya, F. (1993). A phosphorylation epitope on MAP 1B that is transiently expressed in growing axons in the developing rat nervous system. Eur J Neurosci *5*, 1302-1311.

Goux, W.J., Kopplin, L., Nguyen, A.D., Leak, K., Rutkofsky, M., Shanmuganandam, V.D., Sharma, D., Inouye, H., and Kirschner, D.A. (2004). The formation of straight and twisted filaments from short tau peptides. The Journal of biological chemistry *279*, 26868-26875.

Gray, JJ. (2004) The interaction of proteins with solid surfaces. *Curr Opin Struct Biol*, 14, 110-115.

Greenberg, S.G., Davies, P., Schein, J.D., and Binder, L.I. (1992). Hydrofluoric acid-treated tau PHF proteins display the same biochemical properties as normal tau. J Biol Chem *267*, 564-569.

Greenfield, N., and Fasman, G.D. (1969). Computed circular dichroism spectra for the evaluation of protein conformation. Biochemistry *8*, 4108-4116.

Greenfield, N.J. (2006). Using circular dichroism spectra to estimate protein secondary structure. Nature protocols *1*, 2876-2890.

Gustke, N., Steiner, B., Mandelkow, E.M., Biernat, J., Meyer, H.E., Goedert, M., and Mandelkow, E. (1992). The Alzheimer-like phosphorylation of tau protein reduces microtubule binding and involves Ser-Pro and Thr-Pro motifs. FEBS letters *307*, 199-205.

Gustke, N., Trinczek, B., Biernat, J., Mandelkow, E.M., and Mandelkow, E. (1994). Domains of tau protein and interactions with microtubules. Biochemistry *33*, 9511-9522.

Hagiwara, H., Yorifuji, H., Sato-Yoshitake, R., and Hirokawa, N. (1994). Competition between motor molecules (kinesin and cytoplasmic dynein) and fibrous microtubule-associated proteins in binding to microtubules. J Biol Chem *269*, 3581-3589.

Hardy, J., and Selkoe, D.J. (2002). The amyloid hypothesis of Alzheimer's disease: progress and problems on the road to therapeutics. Science *297*, 353-356.

Haase, C., Stieler, J.T., Arendt, T., and Holzer, M. (2004). Pseudophosphorylation of tau protein alters its ability for self-aggregation. J Neurochem 88, 1509-1520.

Haass C, Selkoe DJ. Soluble protein oligomers in neurodegeneration: lessons from the Alzheimer's amyloid beta-peptide. Nat Rev Mol Cell Biol 2007;8(2):101-112.

Hasegawa, M., Smith, M.J., and Goedert, M. (1998). Tau proteins with FTDP-17 mutations have a reduced ability to promote microtubule assembly. FEBS letters *437*, 207-210.

Heins, S., Song, Y.H., Wille, H., Mandelkow, E., and Mandelkow, E.M. (1991). Effect of MAP2, MAP2c, and tau on kinesin-dependent microtubule motility. J Cell Sci Suppl *14*, 121-124.

Hiraoka, S., Yao, T.M., Minoura, K., Tomoo, K., Sumida, M., Taniguchi, T., and Ishida, T. (2004). Conformational transition state is responsible for assembly of microtubule-binding domain of tau protein. Biochem Biophys Res Commun *315*, 659-663.

Hirokawa, N. (1993). Axonal transport and the cytoskeleton. Current opinion in neurobiology *3*, 724-731.

Hirokawa, N. (1994). Microtubule organization and dynamics dependent on microtubule-associated proteins. Curr Opin Cell Biol *6*, 74-81.

Hirokawa, N., and Takemura, R. (2005). Molecular motors and mechanisms of directional transport in neurons. Nat Rev Neurosci *6*, 201-214.

Hirose, K., Fan, J., and Amos, L.A. (1995). Re-examination of the polarity of microtubules and sheets decorated with kinesin motor domain. J Mol Biol *251*, 329-333.

Hoffman, P.N., and Cleveland, D.W. (1988). Neurofilament and tubulin expression recapitulates the developmental program during axonal regeneration: induction of a specific beta-tubulin isotype. Proc Natl Acad Sci U S A *85*, 4530-4533.

Hoffmann, R., Lee, V.M., Leight, S., Varga, I., and Otvos, L., Jr. (1997). Unique Alzheimer's disease paired helical filament specific epitopes involve double phosphorylation at specific sites. Biochemistry *36*, 8114-8124.

Hong, M., Zhukareva, V., Vogelsberg-Ragaglia, V., Wszolek, Z., Reed, L., Miller, B.I., Geschwind, D.H., Bird, T.D., McKeel, D., Goate, A.*, et al.* (1998). Mutation-specific functional impairments in distinct tau isoforms of hereditary FTDP-17. Science (New York, NY *282*, 1914-1917.

Horiguchi, T., Uryu, K., Giasson, B.I., Ischiropoulos, H., LightFoot, R., Bellmann, C., Richter-Landsberg, C., Lee, V.M., and Trojanowski, J.Q. (2003). Nitration of tau protein is linked to neurodegeneration in tauopathies. Am J Pathol *163*, 1021-1031.

Hutton, M., Lendon, C.L., Rizzu, P., Baker, M., Froelich, S., Houlden, H., Pickering-Brown, S., Chakraverty, S., Isaacs, A., Grover, A.*, et al.* (1998). Association of missense and 5'-splice-site mutations in tau with the inherited dementia FTDP-17. Nature *393*, 702-705.

Hutton, M. (2001). Missense and splice site mutations in tau associated with FTDP-17: multiple pathogenic mechanisms. Neurology *56*, S21-25.

Hyman, A., and Karsenti, E. (1998). The role of nucleation in patterning microtubule networks. J Cell Sci *111 (Pt 15)*, 2077-2083.

Hyman, A.A., Salser, S., Drechsel, D.N., Unwin, N., and Mitchison, T.J. (1992). Role of GTP hydrolysis in microtubule dynamics: information from a slowly hydrolyzable analogue, GMPCPP. Mol Biol Cell *3*, 1155-1167.

Ihara, Y., Abraham, C., and Selkoe, D.J. (1983). Antibodies to paired helical filaments in Alzheimer's disease do not recognize normal brain proteins. Nature *304*, 727-730.

Illenberger, S., Drewes, G., Trinczek, B., Biernat, J., Meyer, H.E., Olmsted, J.B., Mandelkow, E.M., and Mandelkow, E. (1996). Phosphorylation of Microtubule Associated Proteins MAP2 and MAP4 by the Protein Kinase p110[mark]: Phosphorylation Sites and Regulation of Microtubule Dynamics. J Biol Chem *271*, 10834-10843.

Illenberger, S., Zheng-Fischhofer, Q., Preuss, U., Stamer, K., Baumann, K., Trinczek, B., Biernat, J., Godemann, R., Mandelkow, E.M., and Mandelkow, E. (1998). The endogenous and cell cycle-dependent phosphorylation of tau protein in living cells: implications for Alzheimer's disease. Mol Biol Cell *9*, 1495-1512.

Ishiguro, K., Shiratsuchi, A., Sato, S., Omori, A., Arioka, M., Kobayashi, S., Uchida, T., and Imahori, K. (1993). Glycogen synthase kinase 3 beta is identical to tau protein kinase I generating several epitopes of paired helical filaments. FEBS letters *325*, 167-172.

Jeganathan, S., von Bergen, M., Brutlach, H., Steinhoff, H.J., and Mandelkow, E. (2006). Global hairpin folding of tau in solution. Biochemistry *45*, 2283-2293.

Jeganathan, S., Hascher, A., Chinnathambi, S., Biernat, J., Mandelkow, E.M., and Mandelkow, E. (2008). Proline-directed Pseudo-phosphorylation at AT8 and PHF1 Epitopes Induces a Compaction of the Paperclip Folding of Tau and Generates a Pathological (MC-1) Conformation. J Biol Chem *283*, 32066-32076.

Jeganathan, S, von Bergen, M, Mandelkow, EM and Mandelkow, E. (2008) The natively unfolded character of tau and its aggregation to Alzheimer-like paired helical filaments. *Biochemistry*, 47, 10526-10539.

Jicha, G.A., Bowser, R., Kazam, I.G., and Davies, P. (1997a). Alz-50 and MC-1, a new monoclonal antibody raised to paired helical filaments, recognize conformational epitopes on recombinant tau. J Neurosci Res *48*, 128-132.

Jicha, G.A., Lane, E., Vincent, I., Otvos, L., Jr., Hoffmann, R., and Davies, P. (1997b). A conformation- and phosphorylation-dependent antibody recognizing the paired helical filaments of Alzheimer's disease. J Neurochem *69*, 2087-2095.

Johnson, G.V., and Stoothoff, W.H. (2004). Tau phosphorylation in neuronal cell function and dysfunction. J Cell Sci *117*, 5721-5729.

Kampers, T., Friedhoff, P., Biernat, J., Mandelkow, E.M., and Mandelkow, E. (1996). RNA stimulates aggregation of microtubule-associated protein tau into Alzheimer-like paired helical filaments. FEBS letters *399*, 344-349.

Kaylor, J., Bodner, N., Edridge, S., Yamin, G., Hong, D.P., and Fink, A.L. (2005). Characterization of oligomeric intermediates in alpha-synuclein fibrillation: FRET studies of Y125W/Y133F/Y136F alpha-synuclein. J Mol Biol *353*, 357-372.

Kidd, M. (1963). Paired helical filaments in electron microscopy of Alzheimer's disease. Nature (Lond) *197*, 192-193.

Kikkawa, M., Ishikawa, T., Nakata, T., Wakabayashi, T., and Hirokawa, N. (1994). Direct visualization of the microtubule lattice seam both in vitro and in vivo. J Cell Biol *127*, 1965-1971.

Kirchner, K., and Mandelkow, E.M. (1985). Tubulin domains responsible for assembly of dimers and protofilaments. EMBO J *4*, 2397-2402.

Kirschner, M.W. (1978). Microtubule assembly and nucleation. Int Rev Cytol *54*, 1-71.

Kirschner, D.A., Abraham, C., and Selkoe, D.J. (1986). X-ray diffraction from intraneuronal paired helical filaments and extraneuronal amyloid fibers in Alzheimer disease indicates cross-beta conformation. Proceedings of the National Academy of Sciences of the United States of America *83*, 503-507.

Kim, Y., Ho, S.O., Gassman, N.R., Korlann, Y., Landorf, E.V., Collart, F.R., and Weiss, S. (2008). Efficient site-specific labeling of proteins via cysteines. Bioconjug Chem *19*, 786-791.

Kishi, M., Pan, Y.A., Crump, J.G., and Sanes, J.R. (2005). Mammalian SAD kinases are required for neuronal polarization. Science (New York, NY *307*, 929-932.

Khlistunova, I., Biernat, J., Wang, Y., Pickhardt, M., von Bergen, M., Gazova, Z., Mandelkow, E., and Mandelkow, E.M. (2006).

Inducible expression of Tau repeat domain in cell models of tauopathy: aggregation is toxic to cells but can be reversed by inhibitor drugs. J Biol Chem *281*, 1205-1214.

Kjaergaard M, Norholm AB, Hendus-Altenburger R, Pedersen SF, Poulsen FM, Kragelund BB. Temperature-dependent structural changes in intrinsically disordered proteins: formation of alpha-helices or loss of polyproline II? Protein Sci 2010;19(8):1555-1564.

Kosik, K.S., Joachim, C.L., and Selkoe, D.J. (1986). Microtubule-associated protein tau (tau) is a major antigenic component of paired helical filaments in Alzheimer disease. Proceedings of the National Academy of Sciences of the United States of America *83*, 4044-4048.

Kosik, K.S., and McConlogue, L. (1994). Microtubule-associated protein function: lessons from expression in Spodoptera frugiperda cells. Cell Motil Cytoskeleton *28*, 195-198.

Kyte, J., and Doolittle, R.F. (1982). A simple method for displaying the hydropathic character of a protein. Journal of molecular biology *157*, 105-132.

Laemmli, U.K. (1970). Cleavage of structural proteins during the assembly of the head of bacteriophage T4. Nature *227*, 680-685.

Laferriere, N.B., MacRae, T.H., and Brown, D.L. (1997). Tubulin synthesis and assembly in differentiating neurons. Biochem Cell Biol *75*, 103-117.

Larcher, J.C., Boucher, D., Lazereg, S., Gros, F., and Denoulet, P. (1996). Interaction of kinesin motor domains with alpha- and beta-tubulin subunits at a tau-independent binding site. Regulation by polyglutamylation. J Biol Chem *271*, 22117-22124.

Lee, G., Cowan, N., and Kirschner, M. (1988). The primary structure and heterogeneity of tau protein from mouse brain. Science (New York, NY *239*, 285-288.

Lee, G., Newman, S.T., Gard, D.L., Band, H., and Panchamoorthy, G. (1998). Tau interacts with src-family non-receptor tyrosine kinases. J Cell Sci *111 (Pt 21)*, 3167-3177.

Lee, G. (2005). Tau and src family tyrosine kinases. Biochimica et biophysica acta *1739*, 323-330.

Lee, V.M., Goedert, M., and Trojanowski, J.Q. (2001). Neurodegenerative tauopathies. Annual review of neuroscience *24*, 1121-1159.

Lee, V.M., and Trojanowski, J.Q. (2006). Mechanisms of Parkinson's disease linked to pathological alpha-synuclein: new targets for drug discovery. Neuron *52*, 33-38.

Lewis, S.A., Lee, M.G., and Cowan, N.J. (1985). Five mouse tubulin isotypes and their regulated expression during development. J Cell Biol *101*, 852-861.

Li, G., Levitus, M., Bustamante, C., and Widom, J. (2005). Rapid spontaneous accessibility of nucleosomal DNA. Nature structural & molecular biology *12*, 46-53.

Li, L., von Bergen, M., Mandelkow, E.M., and Mandelkow, E. (2002). Structure, stability, and aggregation of paired helical filaments from tau protein and FTDP-17 mutants probed by tryptophan scanning mutagenesis. The Journal of biological chemistry *277*, 41390-41400.

Li, W., and Lee, V.M. (2006). Characterization of Two VQIXXK Motifs for Tau Fibrillization in Vitro. Biochemistry *45*, 15692-15701.

Lichtenberg-Kraag, B., Mandelkow, E.M., Biernat, J., Steiner, B., Schroter, C., Gustke, N., Meyer, H.E., and Mandelkow, E. (1992). Phosphorylation-dependent epitopes of neurofilament antibodies on tau protein and relationship with Alzheimer tau. Proceedings of the National Academy of Sciences of the United States of America *89*, 5384-5388.

Litersky, J.M., and Johnson, G.V. (1995). Phosphorylation of tau in situ: inhibition of calcium-dependent proteolysis. J Neurochem *65*, 903-911.

Litman, P., Barg, J., and Ginzburg, I. (1994). Microtubules are involved in the localization of tau mRNA in primary neuronal cell cultures. Neuron *13*, 1463-1474.

Lu, Q., Soria, J.P., and Wood, J.G. (1993). p44mpk MAP kinase induces Alzheimer type alterations in tau function and in primary hippocampal neurons. J Neurosci Res *35*, 439-444.

Luduena, R.F. (1993). Are tubulin isotypes functionally significant. Mol Biol Cell *4*, 445-457.

Makarov, A.A., Lobachov, V.M., Adzhubei, I.A., and Esipova, N.G. (1992). Natural polypeptides in left-handed helical conformation. A circular dichroism study of the linker histones' C-terminal fragments and beta-endorphin. FEBS letters *306*, 63-65.

Mandelkow, EM, Mandelkow, E and Milligan, RA. (1991) Microtubule dynamics and microtubule caps: a time-resolved cryo-electron microscopy study. *J Cell Biol*, 114, 977-991.

Mandelkow, E., Song, Y.H., Schweers, O., Marx, A., and Mandelkow, E.M. (1995). On the structure of microtubules, tau, and paired helical filaments. Neurobiol Aging *16*, 347-354.

Mandelkow, E., von Bergen, M., Biernat, J., and Mandelkow, E.M. (2007). Structural principles of tau and the paired helical filaments of Alzheimer's disease. Brain pathology (Zurich, Switzerland) *17*, 83-90.

Mandelkow, E.M., and Mandelkow, E. (1998). Tau in Alzheimer's disease. Trends Cell Biol *8*, 425-427.

Mandelkow, E., and Bordas, J. (1986). Time-resolved X-ray scattering of microtubule assembly using synchrotron radiation. Methods Enzymol *134*, 657-676.

Mandelkow, E., and Mandelkow, E.M. (1986). Quick-frozen microtubules studied by cryoelectron microscopy and image processing. Ann N Y Acad Sci *483*, 13-23.

Mandelkow, E., Mandelkow, E.M., and Bordas, J. (1986a). Microtubule assembly and disassembly studied by synchrotron X-ray scattering and cryoelectron microscopy. Ann N Y Acad Sci *466*, 650-655.

Mandelkow, E.M., Drewes, G., Biernat, J., Gustke, N., Van Lint, J., Vandenheede, J.R., and Mandelkow, E. (1992). Glycogen synthase kinase-3 and the Alzheimer-like state of microtubule-associated protein tau. FEBS Lett *314*, 315-321.

Mandelkow, E.M., Herrmann, M., and Ruhl, U. (1986b). Tubulin domain structure studied by limited proteolysis and antibody labeling. Ann N Y Acad Sci *466*, 645-649.

Mandelkow, E.M., and Mandelkow, E. (1992). Microtubule oscillations. Cell Motil Cytoskeleton *22*, 235-244.

Mandelkow, E.M., and Mandelkow, E. (1998). Tau in Alzheimer's disease. Trends Cell Biol *8*, 425-427.

Mandelkow, E.M., Mandelkow, E., and Milligan, R.A. (1991). Microtubule dynamics and microtubule caps: a time-resolved cryo-electron microscopy study. J Cell Biol *114*, 977-991.

Mandelkow, E.M., Rapp, R., and Mandelkow, E. (1986c). Microtubule structure studied by quick freezing: cryo-electron microscopy and freeze fracture. J Microsc *141*, 361-373.

Mandelkow, E.M., Schultheiss, R., Rapp, R., Muller, M., and Mandelkow, E. (1986d). On the surface lattice of microtubules: helix starts, protofilament number, seam, and handedness. J Cell Biol *102*, 1067-1073.

Mandelkow, E.M., Schweers, O., Drewes, G., Biernat, J., Gustke, N., Trinczek, B., and Mandelkow, E. (1996). Structure, microtubule interactions, and phosphorylation of tau protein. Ann N Y Acad Sci *777*, 96-106.

Margolis, R.L., and Wilson, L. (1978). Opposite end assembly and disassembly of microtubules at steady state in vitro. Cell *13*, 1-8.

Margolis, R.L., and Wilson, L. (1998). Microtubule tread milling: what goes around comes around. Bioassays *20*, 830-836.

Margolis, R.L., Wilson, L., and Keifer, B.I. (1978). Mitotic mechanism based on intrinsic microtubule behavior. Nature *272*, 450-452.

Margittai, M., and Langen, R. (2004). Template-assisted filament growth by parallel stacking of tau. Proceedings of the National Academy of Sciences of the United States of America *101*, 10278-10283.

Margittai, M., and Langen, R. (2006). Side Chain-dependent Stacking Modulates Tau Filament Structure. The Journal of biological chemistry *281*, 37820-37827.

Marx, A., Pless, J., Mandelkow, E.M., and Mandelkow, E. (2000). On the rigidity of the cytoskeleton: are MAPs cross linkers or spacers of microtubules? Cell Mol Biol (Noisy-le-grand) *46*, 949-965.

Marya, P.K., Syed, Z., Fraylich, P.E., and Eagles, P.A. (1994). Kinesin and tau bind to distinct sites on microtubules. J Cell Sci *107 (Pt 1)*, 339-344.

Matsudaira, P.T., and Burgess, D.R. (1978). SDS microslab linear gradient polyacrylamide gel electrophoresis. Anal Biochem *87*, 386-396.

Matsumoto, S., and Hammes, G.G. (1975). Fluorescence energy transfer between ligand binding sites on aspartate transcarbamylase. Biochemistry *14*, 214-224.

Minoura, K., Tomoo, K., Ishida, T., Hasegawa, H., Sasaki, M., and Taniguchi, T. (2002). Amphipathic helical behavior of the third repeat fragment in the tau microtubule-binding domain, studied by (1)H NMR spectroscopy. Biochem Biophys Res Commun *294*, 210-214.

MacRae, T.H. (1997). Tubulin post-translational modifications--enzymes and their mechanisms of action. Eur J Biochem *244*, 265-278.

McIntosh, J.R., Roos, U.P., Neighbors, B., and McDonald, K.L. (1985). Architecture of the microtubule component of mitotic spindles from Dictyostelium discoideum. J Cell Sci *75*, 93-129.

Mitchison, T., and Kirschner, M. (1984a). Dynamic instability of microtubule growth. Nature *312*, 237-242.

Mitchison, T., and Kirschner, M. (1984b). Microtubule assembly nucleated by isolated centrosomes. Nature *312*, 232-237.

Mitchison, T.J. (1989). Polewards microtubule flux in the mitotic spindle: evidence from photoactivation of fluorescence. J Cell Biol *109*, 637-652.

Mitchison, T.J. (1993). Localization of an exchangeable GTP binding site at the plus end of microtubules. Science *261*, 1044-1047.

Moreno-Herrero, F, Seidel, R, Johnson, SM, Fire, A and Dekker, NH. (2006) Structural analysis of hyperperiodic DNA from *Caenorhabditis elegans*. *Nucleic Acids Res*, 34, 3057-3066.

Mukrasch, M.D., Biernat, J., von Bergen, M., Griesinger, C., Mandelkow, E., and Zweckstetter, M. (2005). Sites of TAU important for aggregation populate beta-structure and bind to microtubules and polyanions. J Biol Chem.

Mukrasch, M.D., von Bergen, M., Biernat, J., Fischer, D., Griesinger, C., Mandelkow, E., and Zweckstetter, M. (2007). The 'Jaws' of the Tau-microtubule interaction. The J Bio Chem.

Mukrasch, MD,, Bibow, S., Korukottu, J., Jeganathan, S., Biernat, J., Griesinger, C., Mandelkow, E., Zweckstetter, M. Structural polymorphism of 441-residue tau at single residue resolution. PLoS Biol 2009; 7(2):e34.

Mukhopadhyay, R and Hoh, JH. (2001) AFM force measurements on microtubule-associated proteins: the projection domain exerts a long-range repulsive force. *FEBS Lett*, 505, 374-378.

Necula, M., Chirita, C.N., and Kuret, J. (2005). Cyanine dye N744 inhibits tau fibrillization by blocking filament extension: implications for the treatment of tauopathic neurodegenerative diseases. Biochemistry *44*, 10227-10237.

Necula, M., and Kuret, J. (2004). Pseudophosphorylation and glycation of tau protein enhance but do not trigger fibrillization in vitro. J Biol Chem *279*, 49694-49703.

Necula, M., and Kuret, J. (2005). Site-specific pseudophosphorylation modulates the rate of tau filament dissociation. FEBS Lett *579*, 1453-1457.

Nogales, E, Wolf, SG and Downing, KH. (1998) Structure of the alpha beta tubulin dimer by electron crystallography. *Nature*, 391, 199-203.

Nogales, E., Whittaker, M., Milligan, R.A., and Downing, K.H. (1999). High-resolution model of the microtubule. Cell *96*, 79-88.

Nogales, E., Wolf, S.G., Khan, I.A., Luduena, R.F., and Downing, K.H. (1995). Structure of tubulin at 6.5 A and location of the taxol-binding site. Nature *375*, 424-427.

Novak, M., Kabat, J., and Wischik, C.M. (1993). Molecular characterization of the minimal protease resistant tau-unit of the Alzheimer's-disease paired helical filament. EMBO J *12*, 365-370.

Nozaki, Y., and Tanford, C. (1970). The solubility of amino acids, diglycine, and triglycine in aqueous guanidine hydrochloride solutions. The Journal of biological chemistry *245*, 1648-1652.

Nukina, N., and Ihara, Y. (1986). One of the antigenic determinants of paired helical filaments is related to tau protein. J Biochem (Tokyo) *99*, 1541-1544.

Oakley, C.E., and Oakley, B.R. (1989). Identification of gamma-tubulin, a new member of the tubulin superfamily encoded by mipA gene of Aspergillus nidulans. Nature *338*, 662-664.

Orte, A, Birkett, NR, Clarke, RW, Devlin, GL, Dobson, CM and Klenerman, D. (2008) Direct characterization of amyloidogenic oligomers by single-molecule fluorescence. *Proc Natl Acad Sci U S A*, 105, 14424-14429.

Otvos, L., Jr., Feiner, L., Lang, E., Szendrei, G.I., Goedert, M., and Lee, V.M. (1994). Monoclonal antibody PHF-1 recognizes tau protein phosphorylated at serine residues 396 and 404. J Neurosci Res *39*, 669-673.

Panda, D., Goode, B.L., Feinstein, S.C., and Wilson, L. (1995). Kinetic stabilization of microtubule dynamics at steady state by tau and microtubule-binding domains of tau. Biochemistry *34*, 11117-11127.

Pawar, A.P., Dubay, K.F., Zurdo, J., Chiti, F., Vendruscolo, M., and Dobson, C.M. (2005). Prediction of "aggregation-prone" and "aggregation-susceptible" regions in proteins associated with neurodegenerative diseases. J Mol Biol *350*, 379-392.

Pirollet, F., Job, D., Margolis, R.L., and Garel, J.R. (1987). An oscillatory mode for microtubule assembly. EMBO J *6*, 3247-3252.

Pollanen, MS, Markiewicz, P and Goh, MC. (1997) Paired helical filaments are twisted ribbons composed of two parallel and aligned components: image reconstruction and modeling of filament structure using atomic force microscopy. *J Neuropathol Exp Neurol*, 56, 79-85.

Poorkaj, P., Bird, T.D., Wijsman, E., Nemens, E., Garruto, R.M., Anderson, L., Andreadis, A., Wiederholt, W.C., Raskind, M., and Schellenberg, G.D. (1998). Tau is a candidate gene for chromosome 17 frontotemporal dementia. Ann Neurol *43*, 815-825.

Rankin, C.A., Sun, Q., and Gamblin, T.C. (2005). Pseudo-phosphorylation of tau at Ser202 and Thr205 affects tau filament formation. Brain Res Mol Brain Res *138*, 84-93.

Rao, S., Krauss, N.E., Heerding, J.M., Swindell, C.S., Ringel, I., Orr, G.A., and Horwitz, S.B. (1994). 3'-(p-azidobenzamido) taxol photolabels the N-terminal 31 amino acids of beta-tubulin. J Biol Chem *269*, 3132-3134.

Rath, A., Davidson, A.R., and Deber, C.M. (2005). The structure of "unstructured" regions in peptides and proteins: role of the polyproline II helix in protein folding and recognition. Biopolymers *80*, 179-185.

Reynolds, M.R., Berry, R.W., and Binder, L.I. (2005). Site-specific nitration and oxidative dityrosine bridging of the tau protein by peroxynitrite: implications for Alzheimer's disease. Biochemistry *44*, 1690-1700.

Rice, P., Longden, I., and Bleasby, A. (2000). EMBOSS: the European Molecular Biology Open Software Suite. Trends Genet *16*, 276-277.

Rissman, R.A., Poon, W.W., Blurton-Jones, M., Oddo, S., Torp, R., Vitek, M.P., LaFerla, F.M., Rohn, T.T., and Cotman, C.W. (2004). Caspase-cleavage of tau is an early event in Alzheimer disease tangle pathology. J Clin Invest *114*, 121-130.

Rivas, C.I., Vera, J.C., and Maccioni, R.B. (1988). Anti-idiotypic antibodies that react with microtubule-associated proteins are present in the sera of rabbits immunized with synthetic peptides from tubulin's regulatory domain. Proc Natl Acad Sci U S A *85*, 6092-6096.

Rivetti, C and Codeluppi, S. (2001). Accurate length determination of DNA molecules visualized by atomic force microscopy: evidence for a partial B- to A-form transition on mica. *Ultramicroscopy*, 87, 55-66.

Ruben, G.C., Novak, M., Edwards, P.C., and Iqbal, K. (2005). Alzheimer paired helical filaments (PHFs) studied by high-resolution TEM: what can vertical Pt-C replication tell us about the organization of the pronase-digested PHF core? Microsc Res Tech *67*, 196-209.

Sambrook, J., and Maniatis, T. (1989). Gel Electrophoresis of DNA. Molecular Cloning: A Laboratory Manual *Second Edition*, 6.5.

Sanchez-Puig, N., Veprintsev, D.B., and Fersht, A.R. (2005). Human full-length Securin is a natively unfolded protein. Protein Sci *14*, 1410-1418.

Sanger, F., Nicklen, S., and Coulson, A.R. (1977). DNA sequencing with chain-terminating inhibitors. Proceedings of the National Academy of Sciences of the United States of America *74*, 5463-5467.

Santarella, R.A., Skiniotis, G., Goldie, K.N., Tittmann, P., Gross, H., Mandelkow, E.M., Mandelkow, E., and Hoenger, A. (2004). Surface-decoration of microtubules by human tau. Journal of molecular biology *339*, 539-553.

Schneider, A., Biernat, J., von Bergen, M., Mandelkow, E., and Mandelkow, E.M. (1999). Phosphorylation that detaches tau protein from microtubules (Ser262, Ser214) also protects it against aggregation into Alzheimer paired helical filaments. Biochemistry *38*, 3549-3558.

Schuler, B., Lipman, E.A., and Eaton, W.A. (2002). Probing the free-energy surface for protein folding with single-molecule fluorescence spectroscopy. Nature *419*, 743-747.

Schweers, O., Schonbrunn-Hanebeck, E., Marx, A., and Mandelkow, E. (1994). Structural studies of tau protein and Alzheimer paired helical filaments show no evidence for beta-structure. The Journal of biological chemistry *269*, 24290-24297.

Schweers, O., Mandelkow, E.M., Biernat, J., and Mandelkow, E. (1995). Oxidation of cysteine-322 in the repeat domain of microtubule-associated protein tau controls the in vitro assembly of paired helical filaments. Proceedings of the National Academy of Sciences of the United States of America *92*, 8463-8467.

Seitz, A., Kojima, H., Oiwa, K., Mandelkow, E.M., Song, Y.H., and Mandelkow, E. (2002). Single-molecule investigation of the interference between kinesin, tau and MAP2c. Embo J *21*, 4896-4905.

Serrano, L., Avila, J., and Maccioni, R.B. (1984). Controlled proteolysis of tubulin by subtilisin: localization of the site for MAP2 interaction. Biochemistry *23*, 4675-4681.

Serrano, L., Montejo de Garcini, E., Hernandez, M.A., and Avila, J. (1985). Localization of the tubulin binding site for tau protein. Eur J Biochem *153*, 595-600.

Silveira, JR, Raymond, GJ, Hughson, AG, Race, RE, Sim, VL, Hayes, SF and Caughey, B. (2005) The most infectious prion protein particles. *Nature*, 437, 257-261.

Shkumatov, A.V., Chinnathambi, S., Mandelkow, E., and Svergun, D.I. (2011). Structural memory of natively unfolded tau protein detected by small-angle X-ray scattering. Proteins *79*, 2122-2131.

Sillen, A., Barbier, P., Landrieu, I., Lefebvre, S., Wieruszeski, J.M., Leroy, A., Peyrot, V., and Lippens, G. (2007). NMR Investigation of the Interaction between the Neuronal Protein Tau and the Microtubules. Biochemistry *46*, 3055-3064.

Skrabana, R., Kontsek, P., Mederlyova, A., Iqbal, K., and Novak, M. (2004). Folding of Alzheimer's core PHF subunit revealed by monoclonal antibody 423. FEBS letters *568*, 178-182.

Slavik, J. (1982). Anilinonaphthalene sulfonate as a probe of membrane composition and function. Biochimica et biophysica acta *694*, 1-25.

Sontag, E., Nunbhakdi-Craig, V., Lee, G., Brandt, R., Kamibayashi, C., Kuret, J., White, C.L., 3rd, Mumby, M.C., and Bloom, G.S. (1999). Molecular interactions among protein phosphatase 2A, tau, and microtubules. Implications for the regulation of tau phosphorylation and the development of tauopathies. The Journal of biological chemistry *274*, 25490-25498.

Song, Y.H., Heins, S., Mandelkow, E., and Mandelkow, E.M. (1991). Aluminum fluoride, microtubule stability, and kinesin rigor. J Cell Sci Suppl *14*, 147-150.

Sontag, E., Nunbhakdi-Craig, V., Lee, G., Bloom, G.S., and Mumby, M.C. (1996). Regulation of the phosphorylation state and microtubule-binding activity of Tau by protein phosphatase 2A. Neuron *17*, 1201-1207.

Spillantini, M.G., Murrell, J.R., Goedert, M., Farlow, M.R., Klug, A., and Ghetti, B. (1998). Mutation in the tau gene in familial multiple system tauopathy with presenile dementia. Proceedings of the National Academy of Sciences of the United States of America *95*, 7737-7741.

Steinhoff, H.J. (1990). Residual motion of hemoglobin-bound spin labels and protein dynamics: viscosity dependence of the rotational correlation times. Eur Biophys J *18*, 57-62.

Steinhoff, H.J. (2002). Methods for study of protein dynamics and protein-protein interaction in protein-ubiquitination by electron paramagnetic resonance spectroscopy. Front Biosci *7*, c97-110.

Steinhilb, M.L., Dias-Santagata, D., Mulkearns, E.E., Shulman, J.M., Biernat, J., Mandelkow, E.M., and Feany, M.B. (2007). S/P and T/P phosphorylation is critical for tau neurotoxicity in Drosophila. J Neurosci Res.

Terry, R.D. (1963). The Fine Structure of Neurofibrillary Tangles in Alzheimer's Disease. J Neuropathol Exp Neurol *22*, 629-642.

Thies, E., and Mandelkow, E.M. (2007). Missorting of tau in neurons causes degeneration of synapses that can be rescued by the kinase MARK2/Par-1. J Neurosci *27*, 2896-2907.

Tian, Q., and Wang, J. (2002). Role of serine/threonine protein phosphatase in Alzheimer's disease. Neurosignals *11*, 262-269.

Timasheff, S.N. (2002). Thermodynamic binding and site occupancy in the light of the Schellman exchange concept. Biophysical chemistry *101-102*, 99-111.

Trinczek, B., Biernat, J., Baumann, K., Mandelkow, E.M., and Mandelkow, E. (1995). Domains of tau protein, differential phosphorylation, and dynamic instability of microtubules. Mol Biol Cell *6*, 1887-1902.

Trojanowski, J.Q., and Lee, V.M. (1995). Phosphorylation of paired helical filament tau in Alzheimer's disease neurofibrillary lesions: focusing on phosphatases. Faseb J *9*, 1570-1576.

Uversky, V.N., Gillespie, J.R., and Fink, A.L. (2000). Why are "natively unfolded" proteins unstructured under physiologic conditions? Proteins *41*, 415-427.

Uversky, V.N., Li, J., and Fink, A.L. (2001). Evidence for a partially folded intermediate in alpha-synuclein fibril formation. The Journal of biological chemistry *276*, 10737-10744.

Uversky, V.N. (2002a). What does it mean to be natively unfolded? Eur J Biochem *269*, 2-12.

Uversky, V.N. (2002b). Natively unfolded proteins: a point where biology waits for physics. Protein Sci *11*, 739-756.

Uversky VN. Intrinsically Disordered Proteins and Their Environment: Effects of Strong Denaturants, Temperature, pH, Counter Ions, Membranes, Binding Partners, Osmolytes, and Macromolecular Crowding. Protein J 2009;28(7-8):305-325.

van Swieten, J., and Spillantini, M.G. (2007). Hereditary frontotemporal dementia caused by Tau gene mutations. Brain pathology (Zurich, Switzerland) *17*, 63-73.

van Swieten, JC, Bronner, IF, Azmani, A, Severijnen, LA, Kamphorst, W, Ravid, R, Rizzu, P, Willemsen, R and Heutink, P. (2007) The DeltaK280 mutation in MAP tau favors exon 10 skipping in vivo. *J Neuropathol Exp Neurol*, 66, 17-25.

von Bergen, M., Friedhoff, P., Biernat, J., Heberle, J., Mandelkow, E.M., and Mandelkow, E. (2000). Assembly of tau protein into Alzheimer paired helical filaments depends on a local sequence motif ((306)VQIVYK(311)) forming beta structure. Proceedings of the National Academy of Sciences of the United States of America *97*, 5129-5134.

von Bergen, M., Barghorn, S., Li, L., Marx, A., Biernat, J., Mandelkow, E.M., and Mandelkow, E. (2001). Mutations of tau protein in frontotemporal dementia promote aggregation of paired helical filaments by enhancing local beta-structure. The Journal of biological chemistry *276*, 48165-48174.

von Bergen, M., Barghorn, S., Biernat, J., Mandelkow, E.M., and Mandelkow, E. (2005). Tau aggregation is driven by a transition from random coil to beta sheet structure. Biochimica et biophysica acta *1739*, 158-166.

von Bergen, M., Barghorn, S., Jeganathan, S., Mandelkow, E.M., and Mandelkow, E. (2006a). Spectroscopic approaches to the conformation of tau protein in solution and in paired helical filaments. Neurodegener Dis *3*, 197-206.

von Bergen, M., Barghorn, S., Muller, S.A., Pickhardt, M., Biernat, J., Mandelkow, E.M., Davies, P., Aebi, U., and Mandelkow, E. (2006b). The core of tau-paired helical filaments studied by scanning transmission electron microscopy and limited proteolysis. Biochemistry *45*, 6446-6457.

Walker, R.A., O'Brien, E.T., Pryer, N.K., Soboeiro, M.F., Voter, W.A., Erickson, H.P., and Salmon, E.D. (1988). Dynamic instability of individual microtubules analyzed by video light microscopy: rate constants and transition frequencies. J Cell Biol *107*, 1437-1448.

Weingarten, M.D., Lockwood, A.H., Hwo, S.Y., and Kirschner, M.W. (1975). A protein factor essential for microtubule assembly. Proceedings of the National Academy of Sciences of the United States of America *72*, 1858-1862.

Weisenberg, R.C., Deery, W.J., and Dickinson, P.J. (1976). Tubulin-nucleotide interactions during the polymerization and depolymerization of microtubules. Biochemistry *15*, 4248-4254.

Wilhelmsen, K.C., Lynch, T., Pavlou, E., Higgins, M., and Nygaard, T.G. (1994). Localization of disinhibition-dementia-parkinsonism-amyotrophy complex to 17q21-22. Am J Hum Genet *55*, 1159-1165.

Wille, H., Drewes, G., Biernat, J., Mandelkow, E.M., and Mandelkow, E. (1992). Alzheimer-like paired helical filaments and antiparallel dimers formed from microtubule-associated protein tau in vitro. J Cell Biol *118*, 573-584.

Williamson, R., Scales, T., Clark, B.R., Gibb, G., Reynolds, C.H., Kellie, S., Bird, I.N., Varndell, I.M., Sheppard, P.W., Everall, I.*, et al.* (2002). Rapid tyrosine phosphorylation of neuronal proteins including tau and focal adhesion kinase in response to amyloid-beta peptide exposure: involvement of Src family protein kinases. J Neurosci *22*, 10-20.

Wilson, D.M., and Binder, L.I. (1995). Polymerization of microtubule-associated protein tau under near-physiological conditions. The Journal of biological chemistry *270*, 24306-24314.

Wilson, D.M., and Binder, L.I. (1997). Free fatty acids stimulate the polymerization of tau and amyloid beta peptides. In vitro evidence for a common effector of pathogenesis in Alzheimer's disease. Am J Pathol *150*, 2181-2195.

Wischik, C.M., Novak, M., Edwards, P.C., Klug, A., Tichelaar, W., and Crowther, R.A. (1988a). Structural characterization of the core of the paired helical filament of Alzheimer disease. Proceedings of the National Academy of Sciences of the United States of America *85*, 4884-4888.

Wischik, C.M., Novak, M., Thogersen, H.C., Edwards, P.C., Runswick, M.J., Jakes, R., Walker, J.E., Milstein, C., Roth, M., and Klug, A. (1988b). Isolation of a fragment of tau derived from the core of the paired helical filament of Alzheimer disease. Proceedings of the National Academy of Sciences of the United States of America *85*, 4506-4510.

Wisniewski, H.M., Merz, P.A., and Iqbal, K. (1984). Ultrastructure of paired helical filaments of Alzheimer's neurofibrillary tangle. J Neuropathol Exp Neurol *43*, 643-656.

Wood, J.G., Mirra, S.S., Pollock, N.J., and Binder, L.I. (1986). Neurofibrillary tangles of Alzheimer disease share antigenic determinants with the axonal microtubule-associated protein

tau (tau). Proceedings of the National Academy of Sciences of the United States of America *83*, 4040-4043.

Woody, R.W., Clark, D.C., Roberts, G.C., Martin, S.R., and Bayley, P.M. (1983). Molecular flexibility in microtubule proteins: proton nuclear magnetic resonance characterization. Biochemistry *22*, 2186-2192.

Wu, P., and Brand, L. (1994). Conformational flexibility in a staphylococcal nuclease mutant K45C from time-resolved resonance energy transfer measurements. Biochemistry *33*, 10457-10462.

Wurth, C., Guimard, N.K., and Hecht, M.H. (2002). Mutations that reduce aggregation of the Alzheimer's Abeta42 peptide: an unbiased search for the sequence determinants of Abeta amyloidogenesis. Journal of molecular biology *319*, 1279-1290.

Yoshida, H., Crowther, R.A., and Goedert, M. (2002). Functional effects of tau gene mutations deltaN296 and N296H. J Neurochem *80*, 548-551.

Zingsheim, H.P., Herzog, W., and Weber, K. (1979). Differences in surface morphology of microtubules reconstituted from pure brain tubulin using two different microtubule-associated proteins: the high molecular weight MAP 2 proteins and tau proteins. Eur J Cell Biol *19*, 175-183.

Zheng-Fischhofer, Q., Biernat, J., Mandelkow, E.M., Illenberger, S., Godemann, R., and Mandelkow, E. (1998). Sequential phosphorylation of Tau by glycogen synthase kinase-3beta and protein kinase A at Thr212 and Ser214 generates the Alzheimer-specific epitope of antibody AT100 and requires a paired-helical-filament-like conformation. Eur J Biochem *252*, 542-552.

7 Appendix

A.1. Abbreviations

(v/v)	Volume per volume
(w/v)	Weight per volume
~	Approximately
Å	Angstrom (0.1 nm)
AD	Alzheimer's disease
ANS	8-anilino-1-naphthalene sulfonic acid
AFM	Atomic force microscopy
AUC	Analytical ultracentrifugation
A ß	amyloid ß-peptide
BES	N, N-bis (2-hydoxyethyl)-2-aminoethanosulfonic acid
Bis Tris	Bis-(2-Hydroxylmethyl)-amino (hydroxymethyl)-methane
BSA	Bovine serum albumin
CCD	Charge coupled device
CD	Circular dichroism
DMF	N, N-dimethyl formamide
Dmax	Maximum particle diameter
DLS	Dynamic light scattering
DTT	Dithiothreitol
EDTA	Ethylendiaminetetraacetate
EGTA	Ethylenglycol-bis-(2-aminoethylether)-N, N, N', N'-tetra acetic acid
EM	Electron microscope
EOM	Ensemble optimization method
FPLC	Fast performance liquid chromatography
FRET	Fluorescence resonance energy transfer
FTDP-17	Frontotemporal dementia and parkinsonism linked to Chromosome-17
FTIR	Fourier transform infrared
GdnHCl	Guanidine hydrochloride
H_2O	Water
HCl	Hydrochloric acid
HEPES	N-2-Hydroxyethyl-piperazine-N-2-ethanesulfonic acid
HPLC	High pressure liquid chromatography
IPTG	Isopropyl-D-β-galactopyranoside

IDP	Intrinsically disordered protein
k Da	Kilo Dalton
Krpm	1000 revolutions per minute
LB	Lysogeny broth (Luria-Bertani)
MAPs	Microtubule-associated proteins
MARK	MAP/microtubule affinity regulating kinase
MES	2-(N-morpholino) ethanesulfonic acid
$MgCl_2$	Magnesium chloride
$MgSO_4$	Magnesium sulphate
MOPS	2-(N-morpholino) propanesulfonic acid
MT	Microtubules
MTOC	Microtubule organizing centre
MRE	Mean residue ellipticity
NaAc	Sodium acetate
NaCl	Sodium chloride
NaP	Sodium phosphate
NFT	Neurofibrillary tangles
NH_4Ac	Ammonium Acetate
NMR	Nuclear magnetic resonance spectroscopy
PAGE	Polyacrylamide gel electrophoresis
PBS	Phosphate buffered saline
PCR	Polymerization chain reaction
PHFs	Paired helical filaments
pI	Isoelectric point
PIPES	Piperazine-N, N'- bis- (2-ethanesulfonic) acid
PKA	Protein kinase A
PMSF	Phenylmethylsulfonylfluoride
PPII	Polyproline II helix
Rg	Radius of gyration
Rh	Hydrodynamic radius
SDS	Sodium dodecyl sulfate
STEM	Scanning transmission electron microscopy
SAXS	Small-angle X-ray scattering
SAS	Small-angle Scattering
TE	Tris-EDTA

ThS   Thioflavin S

Tris   Tris-(Hydroxylmethyl)-aminomethane

A.2. List of figures

A.3. Oligonucleotides

S46A S50A.for	cgctggcctgaaagaagctcccctgcaggcccccactgaggacgg
S46A S50A.rev	ccgtcctcagtgggggcctgcaggggagcttctttcaggccagcg
S69A.for	cctctgatgctaagagcgtctcaacagcggaagatgtgac
S69A.rev	gtcacatcttccgctgttggagcgctcttagcatcagagg
S214A AP17x.for	gctcgcgcgctccggcccttccagctccacccac
S214A AP17x.rev	gtgggtggagctggaagggccggagcgcgcgagc
S214E AP17x.for	gctcgcgcgctccggagcttccagctccacccac
S214E AP17x.rev	gtgggtggagctggaagctccggagcgcgcgagc
D421 Ct.for	catcgatggatcctgatcagtctaccaatgtcgatgctgccggtgg
D421 Ct.rev	ccaccggcagcatcgcattggtagactgatcaggatccatcgatg
D421A del Ct.for	ggcggccgctcagtctaccatgtcgatgctgccggtgg
D418 del Ct.for	ggcggccgctcagtcgatgctgccggtggaggagaca

| hT40 mlu I Nt.for | aacgcgtatggctgagccccgcca |
| hT40 Not I Ct.for | ggcggccgcggatcctgatcacaaaccctgct |

A.4. Properties associated with standard amino acids

Amino acid	Abbreviated names		pKa of side chain	Hydropathy index[¥]
Nonpolar, aliphatic side chains				
Glycine	Gly	G		-0.4
Alanine	Ala	A		1.8
Valine	Val	V		4.2
Leucine	Leu	L		3.8
Isoleucine	Ile	I		4.5
Methionine	Met	M		1.9
Aromatic side chains				
Phenylalanine	Phe	F		2.8
Tyrosine	Tyr	Y	10.07	-1.3
Tyrptophan	Trp	W		-0.9
Polar, uncharged side chains				
Serine	Ser	S		-0.8
Proline	Pro	P		1.6
Threonine	Thr	T		-0.7
Cysteine	Cys	C		2.5
Asparagine	Asn	N	8.18	-3.5
Glutamine	Gln	Q		-3.5
Positively charged side chains				
Lysine	Lys	K	10.53	-3.9
Histidine	His	H	6.00	-3.2
Arginine	Arg	R	12.48	-4.5
Negatively charged side chains				
Aspartate	Asp	D	3.65	-3.5
Glutamate	Glu	E	4.25	-3.5

¥ - A scale combining hydrophobicity and hydrophilicity of side chains that used to measure the tendency of an amino acid to seek an aqueous environment (negative values) or a hydrophobic environment (positive values) (Kyte and Doolittle, 1982).

8 Acknowledgement

Structural memory of natively unfolded tau protein detected by small-angle X-ray scattering

Alexander V. Shkumatov,[1]# Subashchandrabose Chinnathambi,[2,3]#
Eckhard Mandelkow,[2,3]* and Dmitri I. Svergun[1]*

[1] European Molecular Biology Laboratory, Hamburg Outstation c/o DESY, Notkestrasse 85, 22603 Hamburg, Germany

[2] Max-Planck-Unit for Structural Molecular Biology c/o DESY, Notkestrasse 85, 22607 Hamburg, Germany

[3] DZNE, German Center for Neurodegenerative Diseases, c/o CAESAR, 53175 Bonn, Germany

ABSTRACT

Small-angle X-ray scattering (SAXS) is a universal low-resolution method to study size and shape of globular proteins in solution but recent developments facilitate the quantitative characterization of the structure and structural transitions of metastable systems like partially or completely unfolded proteins. We present here a study of temperature induced transitions in tau, a natively unfolded protein involved in Alzheimer's disease. Previous studies on full length tau and several disease-related mutants provided information about the residual structure in different domains revealing a specific role and extended conformations of the so-called repeat domains, which are considered to be responsible for the formation of amyloid-like fibrils ("paired helical filaments"). Here, we employ SAXS to investigate the temperature dependent properties of tau. Slow heating/cooling of the full length protein from 10°C to 50°C did not lead to detectable changes in the overall size. Surprisingly, quick heating/cooling caused tau to adopt a significantly more compact conformation, which was stable over up to 3 h and represents a structural "memory" effect. This compaction is not observed for the shorter tau constructs containing largely the repeat domains. The structural and functional implications of the observed unusual behavior of tau under nonequilibrium conditions are discussed.

INTRODUCTION

Small-angle X-ray scattering (SAXS) is a fundamental method for structure analysis of materials, including biological macromolecules in solution.[1] SAXS can probe structure on a broad range of macromolecular sizes under near native conditions.[2] This method allows one not only to study the low resolution structure but also to analyze structural changes in response to variation of external conditions (pH, temperature, light, ligands, cofactors, denaturants, etc.). In a SAXS experiment, the macromolecular solution is exposed to a collimated beam of X-ray photons, and the intensity of elastic scattering is recorded as a function of the scattering angle. Dilute aqueous solutions of proteins, nucleic acids, or other macromolecules give rise to an isotropic scattering intensity, which depends on the modulus of the momentum transfer s ($s = 4\pi\sin(\theta)/\lambda$, where 2θ is the angle between the incident and scattered beam):

$$I(s) = < I(s) >_{\Omega} = < A(s)A*(s) >_{\Omega} \qquad (1)$$

where the scattering amplitude $A(s)$ is a Fourier transformation of the particle electron density, and the scattering intensity is averaged over all orientations (Ω). Following subtraction of the solvent scattering, the background corrected intensity $I(s)$ is proportional to the scattering of a single particle averaged over all orientations.[2]

Several overall parameters can be obtained directly from the scattering curves of macromolecular solutions enabling fast sample characterization. These parameters include the molecular mass (MM), radius of gyration (R_g), maximum particle diameter (D_{max}), and the hydrated particle volume (V_p).[2] Further, computational approaches to retrieve low resolution three-dimensional (3D) structural models of proteins and complexes, either *ab initio* or by rigid body modeling, are well established and widely used in structural biology.[3–5]

Importantly, unlike most other structural methods, SAXS is applicable to flexible and metastable systems. One can characterize equilibrium and nonequilibrium mixtures and monitor kinetic processes such as (dis)assembly[6] and (un)folding.[7] In particular, SAXS can be employed to quantitatively characterize the overall structure and structural transitions of partially or completely unfolded proteins, including intrinsically disordered proteins (IDPs), an interesting and important class of metastable objects.

Characterization of IDPs using SAXS

The scattering profile measured from a solution of a metastable system (e.g., a flexible system such as an IDP) reflects an average of the large number of conformations that the protein adopts in solution. Traditionally, Kratky plots ($I(s) \cdot s^2$ as a function of s) have been used to identify disordered states and distinguish them from globular ones.[7] The scattering intensity of a globular protein behaves approximately as $1/s^4$, yielding a bell-shaped Kratky plot with a well-defined maximum. Conversely, an ideal Gaussian chain has a $1/s^2$ dependence of $I(s)$, forming a plateau at large s values. For unfolded proteins, the Kratky plot also presents a plateau instead of the maximum observed for the globular proteins, and the plateau is followed by a monotonic increase at larger s.

When studying IDPs, SAXS patterns are normally analyzed in combination with other experimental techniques and bioinformatics tools to identify unstructured regions. Circular dichroism (CD), nuclear magnetic resonance (NMR), fluorescence spectroscopy, and hydrodynamic techniques such as size exclusion chromatography, analytical ultracentrifugation (AUC), or dynamic light scattering (DLS) have been used in combination with SAXS to identify proteins as IDPs.[8–10]

IDPs are often involved in signaling processes and must change their global properties upon environmental modifications within the cell to bind to, or detach from, their natural partners. SAXS is a suitable tool to rapidly monitor structural changes in proteins upon such environmental modifications. The changes, associated with varying pH,[11] ionic strength,[12] temperature,[13,14] presence of specific ions,[14] phosphorylation,[14] or additives,[15] must induce global size variation in IDPs to be monitored by SAXS. These global alterations are reflected again in the apparent R_g, D_{max}, and the appearance of the Kratky plots.

CD combined with NMR studies of natively unfolded proteins have identified structural changes upon heating that result from the disordering of α-helices and polyproline II (PPII) structure, the combined effect of which is to promote (local or global) compaction.[13] The interpretation of the changes observed by CD spectroscopy is ambiguous. This is caused by the low resolution of this technique and the fact that structural changes in different segments may have spectroscopic contributions that cancel each other's signal. Specifically, folding of α-helices and unfolding of PPII structures give rise to a similar change in the CD spectrum.[13] Recently, temperature-induced structural changes in IDPs have been reexamined using three different proteins: ACTR, NHE1, and Spd1.[13] From a combined analysis using CD spectroscopy, SAXS, NMR chemical shift, and peptide mimics, the bulk of the observed change in ellipticity with temperature is suggested to be due to a redistribution of the statistical coil ensemble, where PPII-like conformations are lost with increasing temperature. The transiently formed α-helices, however, lose helical structures at increased temperatures.[13]

Recent novel data analysis methods make it possible to describe the flexibility of IDP ensembles in solution based on SAXS data.[16] Bernado *et al.*[17] proposed an approach allowing for the coexistence of different protein conformations contributing to the average experimental scattering pattern. In the first step, this ensemble optimization method (EOM) generates a pool of random models seeking to cover the protein conformational space. A theoretical scattering curve is then calculated for each model. In the second step, a genetic algorithm selects subsets of protein models. Here, a chromosome is the ensemble of structures and the individual structural models are the genes. Cycles of mutations and crossings among the different "chromosomes" help to explore a variety of combinations. The average experimental scattering is calculated for each subset and fitted to the experimental SAXS data to yield the discrepancy,

$$\chi^2 = \frac{1}{N-1} \sum_j \left[\frac{I_{exp}(S_j) - cI_{calc}(S_j)}{\sigma(S_j)} \right]^2$$

where N is the number of experimental points, c is a scaling factor, $I_{exp}(s_j)$ and $I_{calc}(s_j)$ are the experimentally determined and ensemble averaged calculated intensities, respectively, and $\sigma(s_j)$ is the experimental error at the momentum transfer S_j. This goodness of fit guides the genetic algorithm by allowing only the ensembles with the best scores to proliferate to the next generation.

This strategy provides a distribution of the size properties of disordered proteins in solution. Therefore, the traditional single value averaged R_g description of a flexible

state can be replaced by a more precise picture that is the density of accessible R_g values. As a consequence, small populations of nascent structural elements, or the presence of transient interactions between remote regions of the chain can be easily identified. The localization of these structural features can be addressed though the simultaneous analysis of profiles measured for different fragments of the protein of interest. The EOM approach has become very popular in the studies of metastable systems such as multidomain proteins with flexible linkers and IDPs, and a number of successful applications have already been reported by different groups.[13,18,19] In this article, EOM is employed to study the influence of temperature on the conformations of tau protein.

Tau structure studied by SAXS and NMR

Alzheimer's disease is the most common form of dementia among elderly people.[20] Histological findings in patient brains include amyloid plaques and neurofibrillary tangles, composed of β-amyloid and tau protein, respectively. The neurofibrillary tangles are formed from β-sheet rich "Paired Helical Filaments" (PHFs) which in turn are aggregates of hyperphosphorylated tau protein.[21–24] Physiologically, tau is a microtubule-associated protein[25,26] occurring mainly in the axons of neurons, where it stabilizes microtubules. In the human Central Nervous System, it is found in six alternatively spliced isoforms ranging from 352 to 441 residues depending on the presence or absence of exons 2, 3, and 10.[27,28] In fetal brain, the smallest isoform (ht23-lacking exons 2, 3, and 10) is the predominant one, whereas in adult brain, all isoforms can be found in roughly equal amounts.[29] Tau contains four semiconserved sequences of 31 or 32 residues, so-called "repeats." The second repeat corresponds to exon 10 and may be absent in some of the isoforms. The repeat domain is essential both for the binding to microtubules as well as for the aggregation of tau into PHFs.[29] The domain structure of the full length tau is schematically illustrated in Figure 1.

Overall, tau has a very low content of secondary structure as shown by sequence analysis (very high content of polar residues) and CD experiments.[29,31] In vitro tau aggregation can be induced efficiently only by incubation with polyanions (e.g., heparin[28]). Moreover, phosphorylation negatively regulates both tau-microtubule as well as tau-tau interactions, with some of the sites being responsible for both.[22] Interestingly, in Alzheimer's disease PHFs tau is hyperphosphorylated, a process that is poorly understood.

Structural investigations of tau are largely hampered by the unfolded nature of this protein. However, recent studies attempted to gain insights into the 3D structure of tau.[29,32] Mylonas et al.[29] studied the structures of various forms and deletion mutants of tau by SAXS. From radii of gyration, Kratky plots, and the data fitting with the EOM, it was clearly shown that all constructs
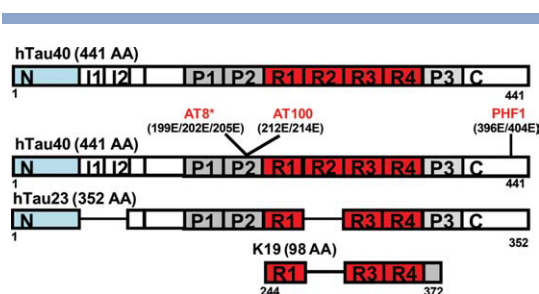
Figure 1

Studied tau constructs and their domain composition. Bar diagram showing the domains of tau (full length isoform hTau40wt, 441 residues, hTau40$_{AT8*+AT100+PHF1}$, hTau23wt, and K19wt). To mimic the phosphorylation *in vitro,* pseudophosphorylation mutants with Glu substituted at the phosphorylable residues were used.[30] Tau domains are broadly divided into the N-terminal "projection domain" (amino acids M1-Y197) and C-terminal "assembly domain" (amino acids Y198-L441). The C-terminal assembly domain includes three or four pseudorepeats (~ 31 residues each, R1–R4), which together with their proline-rich flanking regions (P1 and P2) constitute the microtubule binding region. Repeat R2 and the two near N-terminal inserts (I1 and I2) may be absent due to alternative splicing. The N-terminal 120 residues have an overall acidic character, the rest of the molecule has a basic character. [Color figure can be viewed in the online issue, which is available at wileyonlinelibrary.com.]

were unfolded, but structural differences were detected between the sequence domains. It was found that the repeat domain, which is considered the core constituent of the PHFs, is more extended than the terminal parts. Moreover, aggregation-promoting mutations have little effect on the overall shape of the protein in solution, even though they cause some rearrangements of the domains as seen by FRET.[31,33] These results favor a paper-clip model of tau structure[31] and provide a clearer picture of the overall domain structure of tau and the contributions of different domains and phosphorylation states to the dynamic behavior of tau. Mukrasch et al.[32] analyzed the structural polymorphism of full length tau at high resolution using NMR. A novel methodology revealed that 441-residue tau is highly dynamic in solution with a distinct domain character and an intricate network of transient long-range contacts important for pathogenic aggregation. Basically, the structural model of tau showed it in a much more compact form than previously expected from the EM images.[27] However, the molecule is still loosely packed, highly flexible, and exchanges between a large number of conformations, consistent with large average values of the hydrodynamic radius.

MATERIALS AND METHODS

Protein preparation

The constructs of tau displayed in Figure 1 were prepared as described previously.[34] Briefly, the tau isoforms were obtained using PCR amplification and subcloned into expression vector pNG2 [a derivative of pET-3a

(Merck-Novagen, Darmstadt, Germany)]. Recombinant proteins were expressed in the *Escherichia coli* BL21 (DE3) strain (Merck-Novagen). The expressed protein was purified from bacterial extracts by making use of the heat stability of the tau protein and by FPLC SP-Sepharose (GE Healthcare, Freiburg, Germany). The cell pellet was resuspended in the boiling extraction buffer [50 mM MES, 500 mM NaCl, 1 mM MgSO$_4$, 1 mM EGTA, and 5 mM DTT (pH 6.8)] complemented with a protease inhibitor cocktail. The cells were disrupted with a French pressure cell and subsequently boiled for 20 min. The soluble extract was isolated by centrifugation, and the supernatant was dialyzed against two changes of cation exchange chromatography buffer A [50 mM MES, 50 mM NaCl, 1 mM MgSo$_4$, 1 mM EGTA, 2 mM DTT, and 0.1 mM PMSF (pH 6.8)] and loaded on a FPLC SP-Sepharose column. The proteins were eluted with a linear gradient of cation exchange chromatography buffer B (20 mM MES, 1 M NaCl, 1 mM MgSO$_4$, 1 mM EGTA, 2 mM DTT, and 0.1 mM PMSF (pH 6.8)]. The purity of proteins was ascertained by SDS-PAGE. Where necessary, breakdown products were removed by using the additional gel filtration column Superdex G75 or G200 with PBS buffer [137 mM NaCl, 3 mM KCl, 10 mM Na$_2$HPO$_4$, 2 mM KH$_2$PO$_4$ (pH 7.4)]. Before SAXS data collection, the protein samples were prepared by concentration on an Amicon Ultra-15 device (Millipore, Bedford, MA) and the protein concentrations were determined by absorbance at 214 nm and the reflective index measurements.

CD Spectroscopy

Measurements were carried out with a Jasco J-810 CD spectrometer (Jasco, Gross-Umstadt, Germany) in a cuvette with a path length of 0.1 cm. The parameters were scanning speed, 100 nm/min; bandwidth, 0.1 nm; response time, 4 s; measurement temperature, 10°C. The CD spectra were normalized for concentration at 214 nm using BSA as standard. In each experiment, three spectra were summed and averaged. The proteins were measured at 5°C, 25°C, 45°C, 65°C, and 95°C.

Light scattering

Measurements were performed with a Spex Fluromax spectrophotometer (Polytec, Waldbronn, Germany), using 3 × 3 mm quartz microcuvettes from Hellma (Muhlheim, Germany) with 30 μL sample volume at a concentration of 25 μM. Experimental parameters were excitation and emission wavelength, 350 nm (90° scattering); scan range, 320–400 nm; excitation slit width, 5 nm; emission slit width, 5 nm; intergration time, 1 s; photomultiplier voltage, 950 V. Each time, three spectra were scanned and averaged. The protein samples were incubated at different time and temperatures (increasing temperature e.g., 10°C for 20 min, 50°C for 20 min, and 50°C for 120 min); the

scattering of the buffer was subtracted. All samples were measured twice. A positive control of strong scattering was obtained from fully aggregated PHFs, as confirmed by ThS fluorescence and electron microscopy.

Sedimentation analysis

Samples of soluble tau (concentration 20 μM in phosphate buffer pH 6.8) were incubated at different temperatures (10°C for 20 min, 50°C for 20 min, and 50°C for 120 min) and then centrifuged at 100,000g for 30 min to generate a pellet fraction of tau protein. After the centrifugation, the samples were resuspened in buffer, SDS sample buffer was added to pellets and supernatants, followed by heating to 95°C for 10 min. The samples were run on SDS-PAGE gels containing 10% polyacrylamide gel, and the percentages of tau protein in the supernatants and pellets were quantified by densitometry of the Coomassie Blue R-250-stained gels using AIDA image analysis software.

Dynamic light scattering

DLS experiments were carried out using the Spectro-scatterer 201 (RiNA GmbH, Berlin, Germany) with a He-Ne laser providing light of 690 nm wavelength and an output power in the range of 10–50 Mw. Samples of soluble tau (concentration 100 μM in phosphate buffer pH 6.8) were incubated at different times and temperatures (increasing temperature e.g., 10°C for 20 min and 50°C for 120 min). The samples (30 μL) were placed in a quartz cuvette and measured at a constant temperature of 20°C using an autopilot function accumulating 20 measurements per sample. The corresponding molecular masses were calculated by standard procedures.

SAXS

Small angle X-ray scattering (SAXS) data were collected in several experimental sessions on the EMBL X33 beamline of the storage ring DORIS III (DESY, Hamburg). X33 uses a fixed wavelength of 1.5 Å and is equipped with a photon counting Pilatus 1 M pixel detector (67 × 420 mm^2). Samples were exposed using 60-μL volumes loaded into a vacuum cell with polycarbonate or mica windows. A standard data collection time of 2 min was used for all samples split into eight 15-s time frames to detect and discard possible radiation damage effects. The data were averaged after normalization to the intensity of the transmitted beam and the scattering of the buffer was subtracted using PRIMUS.[35]

All measurements were performed using the automated SAXS sample changer,[36] where the samples are kept in a temperature-controlled sample tray and injected into the independently temperature-controlled measuring cell. During the nonequilibrium temperature experiments, the measurement cell was tempered to 50 and 10°C, whereas the temperature in the sample holder was
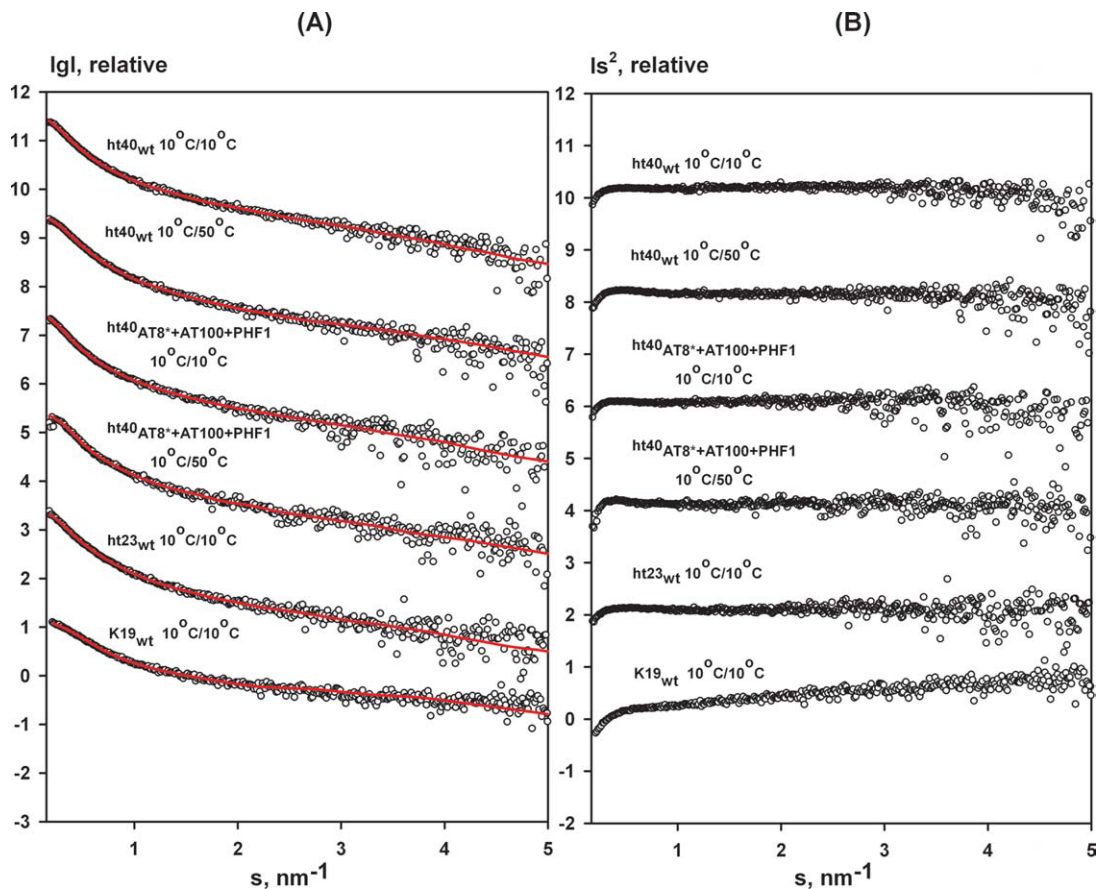
Figure 2

SAXS measurements on tau constructs. (**A**) Experimental SAXS data (o) with corresponding ensemble fit (—) for full-length constructs (hTau40wt, hTau40$_{AT8*+AT100+PHF1}$) are shown at equilibrium (10°C/10°C) and nonequilibrium temperature conditions (10°C/50°C). Experimental data for short constructs (hTau23, K19) are shown at equilibrium temperature condition (10°C/10°C). Plots display the logarithm of the scattering intensity as a function of momentum transfer s = 4πsin(θ)/λ, where 2θ is the scattering angle and λ is the X-ray wavelength. (**B**) Kratky plots corresponding to data in panel A. Experimental SAXS profiles were appropriately displaced along the logarithmic axis for better visualization and overlaid with corresponding ensemble fits. [Color figure can be viewed in the online issue, which is available at wileyonlinelibrary.com.]

set to 10 and 50°C, respectively. At equilibrium temperature conditions, the measurement cell and sample tray were held at the same temperature. The full length hTau40wt and hTau40$_{AT8*+AT100+PHF1}$ were measured at concentrations ranging from 2 to 10 mg/mL; the short constructs K19 and hTau23 in the range 2 to 20 mg/mL.

The data were processed using standard procedures by PRIMUS.[35] The forward scattering $I(0)$ and the radii of gyration R_g were evaluated using the Guinier approximation[37] assuming that at very small angles ($s < 1.3/R_g$) the intensity is represented as $I(s) = I(0)\exp(-(sR_g)2/3)$. For longer constructs, the indirect transform package GNOM[38] was used to compute the R_g.

RESULTS AND DISCUSSION

The full length tau (hTau40wt), its phosphorylation mutant (hTau40$_{AT8*+AT100+PHF1}$) and the two deletion mutants hTau23 and K19 were measured by SAXS and

the scattering patterns are displayed in Figure 2. The R_g values at 10°C agree with those reported by Mylonas et al.,[29] and the Kratky plots (Fig. 2, right panel) indicate that all constructs are unfolded. No major changes were observed between the wild type protein and the phosphorylation mutant. To investigate the effect of temperature on the overall dimensions of the constructs, we first carried out SAXS measurements at 50°C under equilibrium conditions. The samples were placed in the sample changer tray at 10°C and slowly (~ 30 min) warmed up to 50°C. Then the samples were injected into the measuring cell, which was also kept at 50°C. The R_g values for all constructs summarized in Table I reveal no significant changes compared with the equilibrium data collected at 10°C (see also typical scattering data for hTau40wt in Supporting Information Fig. 1). To quantitatively characterize the ensemble properties of these constructs under equilibrium conditions, EOM was applied to all measured data sets. The EOM analysis allowed us

Table I
Radii of Gyration

Construct (no. of aa)	Rg (nm) at different temperature conditions. Temperature in sample holder/ measurement cell, °C/°C			
	10/10	50/50	10/50	50/10
hTau40wt (441)	6.6 ± 0.3	6.5 ± 0.3	5.5 ± 0.3	5.6 ± 0.3
hTau40$_{AT8* + AT100 + PHF1}$ (441)	6.6 ± 0.3	6.7 ± 0.3	5.9 ± 0.3	-
hTau23 (352)	5.9 ± 0.2	5.9 ± 0.2	5.9 ± 0.2	5.9 ± 0.2
K19 (98)	3.5 ± 0.2	3.5 ± 0.2	3.5 ± 0.2	3.7 ± 0.2

to neatly fit the experimental data from all constructs (Fig. 2, left panel) and the obtained results depicted in Figure 3 demonstrate that no major differences are observed between the 10°C and 50°C samples. Both the average sizes and the widths of the R_g distributions in the selected ensembles were only marginally affected by temperature, and all the differences were within the experimental errors. The distributions of the longer constructs were close to those of the random pools, whereas

the shorter constructs appeared more extended than the random coils, in agreement with the results reported by Mylonas et al.[29]

Surprisingly, different results were obtained under nonequilibrium temperature conditions, when the samples were kept in the tray at one temperature and then transferred to the measurement cell tempered to either higher or lower temperature. Two cases were explored, "quick heating" (sample tray at 10°C, measurement cell at 50°C) and "fast cooling" (sample tray at 50°C, measurement cell at 10°C). Each time when the measuring cell was filled the sample was held for half a minute prior to exposure to ensure that the desired temperature is reached (cell volume $\sim$ 25 µL). The experiments under nonequilibrium conditions (quick heating/cooling) showed that long tau constructs adopt a more compact and folded conformation, as judged by R_g (Table I) and the Kratky plots (Fig. 2, right panel). Also the ensembles selected by the EOM displayed the distributions shifted to smaller R_g values compared with equilibrium tempera-
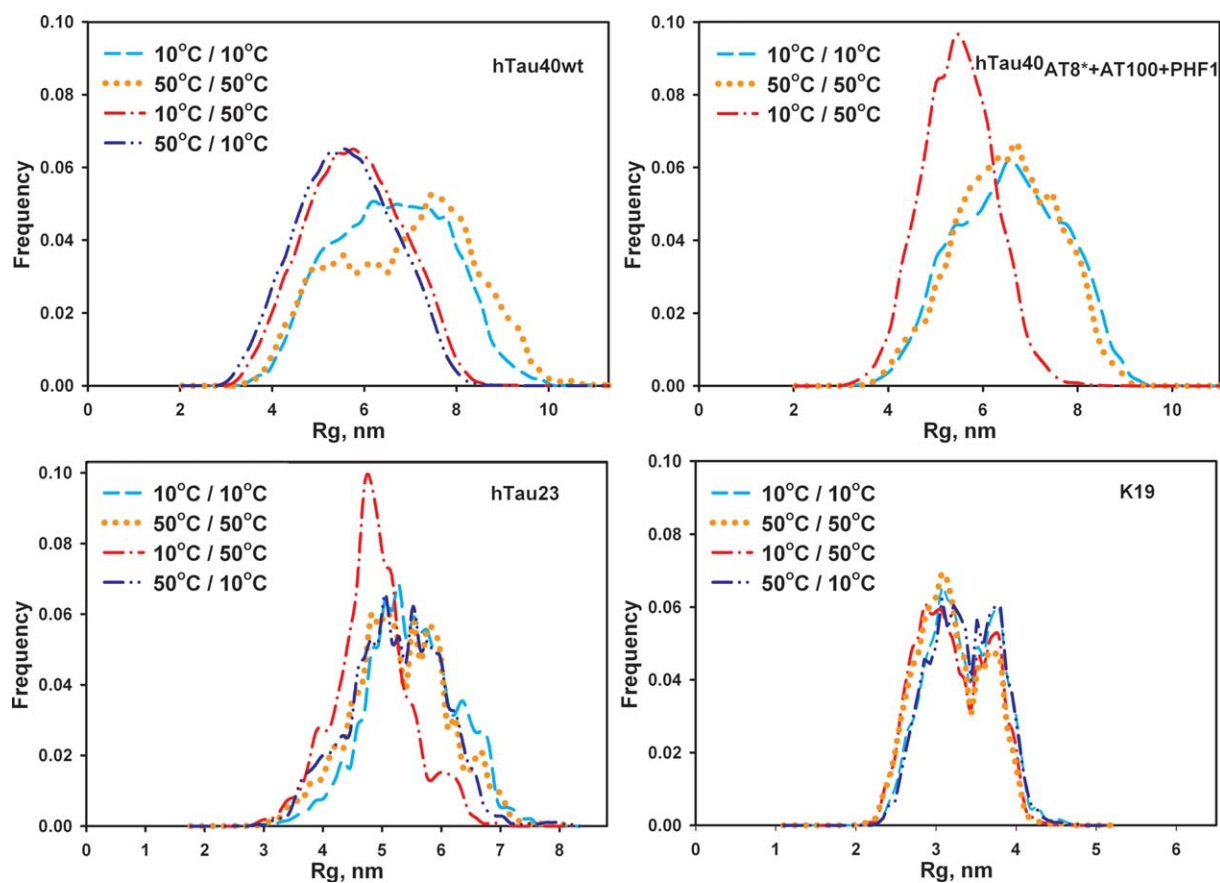
Figure 3
Temperature-jump induced changes in the ensemble dimensions studied by SAXS. Ensemble optimization analysis of the SAXS profile measured for full-length (hTau40wt, hTau40$_{AT8*+AT100+PHF1}$) and short (hTau23, K19) tau constructs at equilibrium (10°C/10°C, 50°C/50°C) and nonequilibrium temperature conditions (10°C/50°C, 50°C/10°C). Radius of gyration distributions ensembles under equilibrium conditions: 10°C/10°C (– –), 50°C/50°C (···) and nonequilibrium conditions: 10°C/50°C (– ·–), 50°C/10°C (– ·· –). [Color figure can be viewed in the online issue, which is available at wileyonlinelibrary.com.]
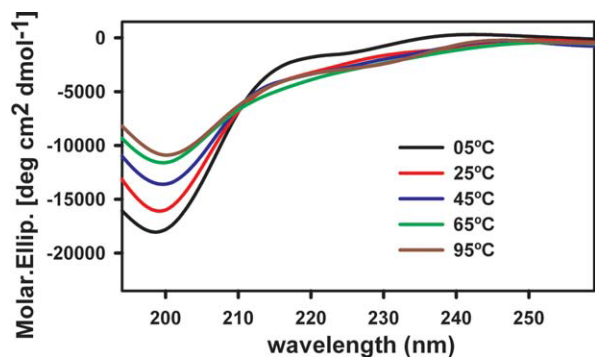
Figure 4

CD spectra of tau and temperature dependence. CD spectra of tau at different temperatures: 5°C, 25°C, 45°C, 65°C, and 95°C. Note that the negative peak at 200 nm becomes filled in as the temperature rises. Very similar traces are obtained by different protocols of varying the temperature change and time of incubation, indicating the presence, but not the extent of local conformational changes. [Color figure can be viewed in the online issue, which is available at wileyonlinelibrary.com.]

ture conditions (Fig. 3). At the same time, the short constructs demonstrated a behavior similar to the equilibrium temperature conditions, i.e., no dependence on the temperature history (Table I and Fig. 3).

Several independent experimental SAXS sessions with samples from different batches were performed to verify the observed unusual effect. They reproducibly revealed the compaction of the full length tau upon quick heating and fast cooling. The latter effect was measurable also after minutes and even hours of incubation of the protein at 10°C, indicating that the compaction has a memory effect. We performed additional measurement on incubated hTau40wt, which revealed that the compact state is preserved for at least 3 h of incubation, but after 24 h, the protein is nearly reverted back to the native state (Supporting Information Figs. 1 and 2). The pseudophosphorylated tau construct showed a tendency to aggregate over time and could thus not be measured under similar conditions.

To further confirm the obtained results, we employed other techniques providing information about the structure in solution. Our CD experiments did not show the memory effect when different temperature protocols were employed. Thus, the X-ray results reveal a global property, whereas CD measures average local properties. To test if elevated temperature could cause a structural transition, the secondary structure of soluble tau was determined by CD at various temperatures (5, 25, 45, 65, and 95°C). Upon stepwise elevation of temperature, the CD spectra of hTau40wt underwent a shift: the negative peak at 200 nm became less pronounced and the value at 217 nm became more negative with an isosbestic point around 210 nm (Fig. 4), also see [39]. By varying the time of incubation and the protocol of temperature shifts, we found that the CD spectrum depends essentially on the

temperature only, but not on the history. Thus, the "memory effect" seen by SAXS appears to be specific for the global changes in the protein seen by X-rays, not for the average local structure seen by CD.

To test the aggregation kinetics of hTau40wt measured by light scattering at 90° with increasing temperature, we kept the samples at 10°C for 20 min, 50°C for 20 min, and 50°C for 120 min and measured at room temperature. Figure 5(A) confirms that temperature was not inducing any aggregation. The results obtained from the light scattering clearly suggest that there was no aggrega-
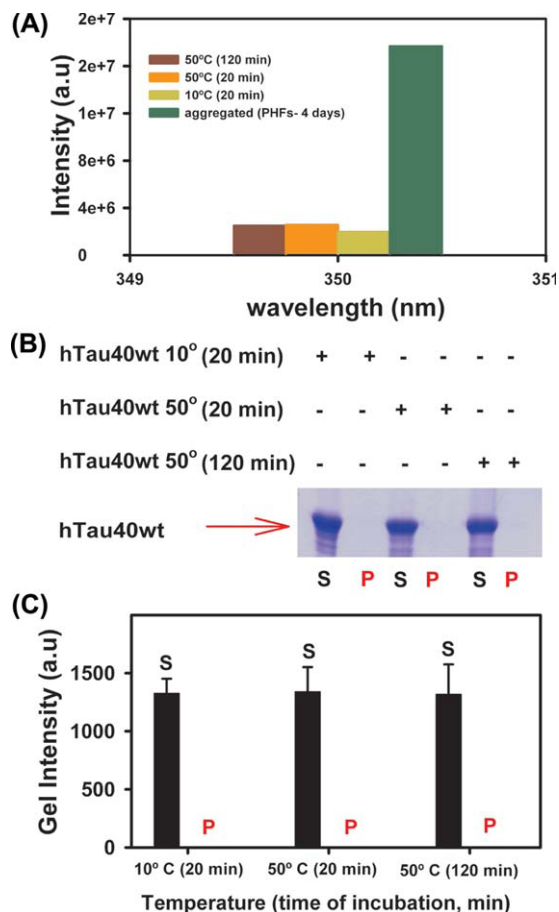
Figure 5

Light scattering and sedimentation analysis of tau. (**A**) Light scattering (90°, 350 nm) of soluble tau. Samples of soluble tau protein (concentration 25 μM, phosphate buffer pH 6.8) were incubated at various temperatures and time periods, 10°C for 20 min, 50°C for 20 min, 50°C for 120 min. Note that there was no increase in scattering intensity from the samples of soluble tau, indicating that there was no measurable aggregation during the duration of the experiment. As a control, aggregated PHFs (concentration 25 μM of tau) show a high scattering intensity. (**B**) Coomassie blue (R-250) stained with SDS-PAGE (sodium dodecyl sulfate-polyacrylamide gel) illustrating the sedimentation analysis of soluble tau at different temperatures and incubation periods. S and P represent supernatant and pellet. Note that there is no detectable aggregated protein in the pellet. (**C**) Quantification of (B). [Color figure can be viewed in the online issue, which is available at wileyonlinelibrary.com.]
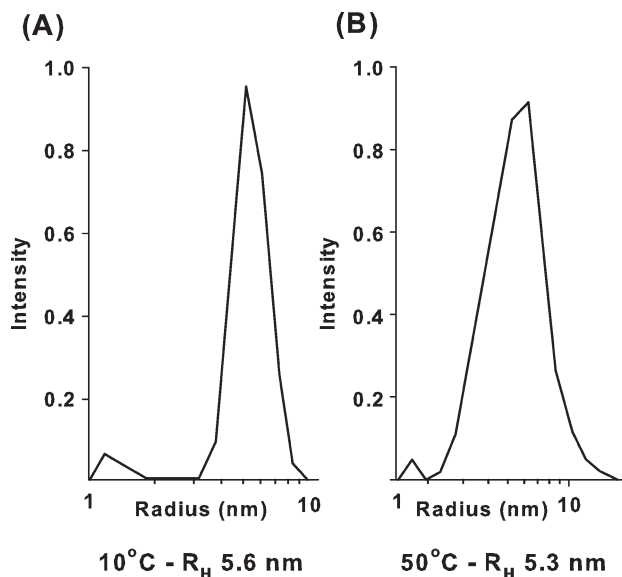
Figure 6

DLS measurement for hTau40wt at different temperatures. (**A**) Example of determination of R_H by DLS (10°C for 20 min (R_H 5.6 nm). (**B**) Comparison of R_H values obtained at different temperatures, e.g., 10°C for 20 min (R_H 5.6 nm) and 50°C for 120 min (R_H 5.3 nm). Note that at increasing temperature (50°C for 120 min), R_H becomes smaller. This indicates that the protein is somewhat more compact at higher temperature.

tion at various temperatures. The positive control of fully aggregated PHFs was confirmed by ThS fluorescence and electron microscopy. The same sets of samples were incubated, and after reaction all the samples were collected, pelleted by ultracentrifugation, and pellets and supernatants were analyzed by SDS gel electrophoresis [Fig. 5(B,C)]. The results confirmed that aggregation in the tau solutions was negligible. This suggests that the memory effect revealed by X-ray scattering is due solely to changes in temperature.

To obtain independent information on the temperature dependence of the apparent size of tau, DLS measurements were performed. The hydrodynamic radius R_h of hTau40wt at 10°C was 5.6 nm [Fig. 6(a)], and this value did not change upon slow heating to 50°C (data not shown). However, when hTau40wt was quickly heated to 50°C, incubated and measured, the R_h dropped to 5.3 nm [Fig. 6(b)]. This compaction was in line with the SAXS results under nonequilibrium temperature conditions, although the decrease of the R_h was smaller than that of the R_g values from SAXS. It is interesting to note here that the ratio of R_g/R_h depends on the flexibility of the macromolecule. For rigid structures, R_g is close to R_h (R_g/R_h ranging from ~ 1.1 for anisometric polymers to ~ 0.8 for a solid sphere). For flexible systems R_g may significantly exceed R_h, such that R_g/R_h reaches 1.5 for a random coil.[40] Our results therefore indicate that the

quenched tau becomes not only more compact, but, expectedly, also less flexible than the native protein.

The polypeptide chain of tau has been shown to remain mostly natively disordered, loose, and flexible under different conditions.[31,32] This structural plasticity is necessary for the unique functional repertoire of IDPs, which is complementary to the catalytic activities of ordered proteins.[41] Changes occurring under different conditions have been reported for tau.[32] There is some global folding (hairpin model, whereby N- and C-terminal domains approach the repeat domain), which could affect R_g. It is noteworthy that the hairpin model also shows compaction in some conditions (as determined by FRET), for example after hyperphosphorylation at several sites, consistent with the reaction with antibodies MC1 or Alz50, that are characteristic of incipient Alzheimer disease.[33] It is therefore clear that the unfolded nature of tau protein allows it to adopt either more extended or compact conformations. It is intriguing to speculate that the compaction and memory effect observed after rapid heating/cooling may be related to the compaction observed upon hyperphosphorylation, characteristic of incipient neuronal degeneration in AD. The memory effect is observed with full-length tau but not with the repeat domain alone, suggesting that the interplay between different domains in the whole protein might be responsible for the effect. One possible explanation could be the interplay between the acidic N-terminal domain (which varies among the tau isoforms due to alternative splicing) and the basic repeat domain (which also differs between isoforms). These issues will be addressed in future studies.

CONCLUSION

IDPs are important representatives of metastable proteins, which are difficult to study by high resolution X-ray crystallography due to their inherent flexibility. SAXS is one of the most important methods allowing for quantitative structural descriptions of such objects. The possibility of modeling the SAXS data in terms of ensembles of conformations opens new perspectives in the study of unstructured and partially folded proteins. SAXS is easily applicable under changing conditions like temperature, pH, salinity etc., and even under nonequilibrium conditions, as demonstrated in the present manuscript. The structural information that can be derived from SAS data applying the EOM strategy can be complemented by information collected with other structural techniques. Especially promising here is the combination with NMR that has been traditionally applied to the study of unfolded and partially folded proteins, but the techniques like CD, DLS, calorimetry also deliver important additional information. The potential of SAXS employed together with other methods is illustrated in the present

work revealing an unusual effect of compaction of the intrinsically unfolded tau protein under nonequilibrium temperature conditions. An analogous compaction has also been observed as a result of post-translational modifications of tau and is reminiscent of tau conformations during incipient Alzheimer disease, as seen by conformation-dependent antibodies.[30,33]

ACKNOWLEDGMENTS

REFERENCES

1. Feigin LA, Svergun DI. Structure analysis by small-angle x-ray and neutron scattering. New York: Plenum Press; 1987. xiii, 335 p.

2. Mertens HD, Svergun DI. Structural characterization of proteins and complexes using small-angle X-ray solution scattering. J Struct Biol 2010;172:128–141.

3. Svergun DI, Koch MHJ. Advances in structure analysis using small-angle scattering in solution. Curr Opin Struct Biol 2002;12:654–660.

4. Petoukhov MV, Konarev PV, Kikhney AG, Svergun DI. ATSAS 2.1—towards automated and web-supported small-angle scattering data analysis. J Appl Cryst 2007;40:s223–s228.

5. Putnam CD, Hammel M, Hura GL, Tainer JA. X-ray solution scattering (SAXS) combined with crystallography and computation: defining accurate macromolecular structures, conformations and assemblies in solution. Quart Rev Biophys 2007;40:191–285.

6. Akiyama S, Nohara A, Ito K, Maeda Y. Assembly and disassembly dynamics of the cyanobacterial periodosome. Mol Cell 2008;29:703–716.

7. Doniach S. Changes in biomolecular conformation seen by small angle X-ray scattering. Chem Rev 2001;101:1763–1778.

8. Gast K, Damaschun H, Eckert K, Schulze-Forster K, Maurer HR, Muller-Frohne M, Zirwer D, Czarnecki J, Damaschun G. Prothymosin alpha: a biologically active protein with random coil conformation. Biochemistry 1995;34:13211–13218.

9. Paz A, Zeev-Ben-Mordehai T, Lundqvist M, Sherman E, Mylonas E, Weiner L, Haran G, Svergun DI, Mulder FA, Sussman JL, Silman I. Biophysical characterization of the unstructured cytoplasmic domain of the human neuronal adhesion protein neuroligin 3. Biophys J 2008;95:1928–1944.

10. Gazi AD, Bastaki M, Charova SN, Gkougkoulia EA, Kapellios EA, Panopoulos NJ, Kokkinidis M. Evidence for a coiled-coil interaction mode of disordered proteins from bacterial type III secretion systems. J Biol Chem 2008;283:34062–34068.

11. Konno T, Tanaka N, Kataoka M, Takano E, Maki M. A circular dichroism study of preferential hydration and alcohol effects on a denatured protein, pig calpastatin domain I. Biochim Biophys Acta 1997;1342:73–82.

12. Munishkina LA, Fink AL, Uversky VN. Conformational prerequisites for formation of amyloid fibrils from histones. J Mol Biol 2004;342:1305–1324.

13. Kjaergaard M, Norholm AB, Hendus-Altenburger R, Pedersen SF, Poulsen FM, Kragelund BB. Temperature-dependent structural changes in intrinsically disordered proteins: formation of alpha-helices or loss of polyproline II? Protein Sci 2010;19:1555–1564.

14. He G, Ramachandran A, Dahl T, George S, Schultz D, Cookson D, Veis A, George A. Phosphorylation of phosphophoryn is crucial for its function as a mediator of biomineralization. J Biol Chem 2005;280:33109–33114.

15. Hong DP, Fink AL, Uversky VN. Structural characteristics of alpha-synuclein oligomers stabilized by the flavonoid baicalein. J Mol Biol 2008;383:214–223.

16. Bernado P, Svergun DI. New perspectives in small-angle scattering to study unstructured states of proteins. In: O'Doherty CB, Byrne AC, editors. Protein misfolding. Nova Publishers, New York, 2008.

17. Bernado P, Mylonas E, Petoukhov MV, Blackledge M, Svergun DI. Structural characterization of flexible proteins using small-angle X-ray scattering. J Am Chem Soc 2007;129:5656–5664.

18. Petoukhov MV, Vicente JB, Crowley PB, Carrondo MA, Teixeira M, Svergun DI. Quaternary structure of flavorubredoxin as revealed by synchrotron radiation small-angle X-ray scattering. Structure 2008;16:1428–1436.

19. Bernado P, Modig K, Grela P, Svergun DI, Tchorzewski M, Pons M, Akke M. Structure and Dynamics of Ribosomal Protein L12: An Ensemble Model Based on SAXS and NMR Relaxation. Biophys J 2010;98:2374–2382.

20. Haass C, Selkoe DJ. Soluble protein oligomers in neurodegeneration: lessons from the Alzheimer's amyloid beta-peptide. Nat Rev Mol Cell Biol 2007;8:101–112.

21. von Bergen M, Friedhoff P, Biernat J, Heberle J, Mandelkow EM, Mandelkow E. Assembly of tau protein into Alzheimer paired helical filaments depends on a local sequence motif ((306)VQI-VYK(311)) forming beta structure. Proc Natl Acad Sci USA 2000;97:5129–5134.

22. Margittai M, Langen R. Template-assisted filament growth by parallel stacking of tau. Proc Natl Acad Sci USA 2004;101:10278–10283.

23. Binder LI, Guillozet-Bongaarts AL, Garcia-Sierra F, Berry RW. Tau, tangles, and Alzheimer's disease. Biochim Biophys Acta 2005;1739:216–223.

24. Mandelkow E, von Bergen M, Biernat J, Mandelkow EM. Structural principles of tau and the paired helical filaments of Alzheimer's disease. Brain Pathol 2007;17:83–90.

25. Drubin DG, Kirschner MW. Tau protein function in living cells. J Cell Biol 1986;103(6 Pt 2):2739–2746.

26. Butner KA, Kirschner MW. Tau protein binds to microtubules through a flexible array of distributed weak sites. J Cell Biol 1991;115:717–730.

27. Wille H, Mandelkow EM, Mandelkow E. The juvenile microtubule-associated protein MAP2c is a rod-like molecule that forms antiparallel dimers. J Biol Chem 1992;267:10737–10742.

28. Goedert M, Jakes R, Spillantini MG, Hasegawa M, Smith MJ, Crowther RA. Assembly of microtubule-associated protein tau into Alzheimer-like filaments induced by sulphated glycosaminoglycans. Nature 1996;383:550–553.

29. Mylonas E, Hascher A, Bernado P, Blackledge M, Mandelkow E, Svergun DI. Domain conformation of tau protein studied by solution small-angle X-ray scattering. Biochemistry 2008;47:10345–10353.

30. Jicha GA, Bowser R, Kazam IG, Davies P. Alz-50 and MC-1, a new monoclonal antibody raised to paired helical filaments, recognize conformational epitopes on recombinant tau. J Neurosci Res 1997;48:128–132.

31. Jeganathan S, von Bergen M, Brutlach H, Steinhoff HJ, Mandelkow E. Global hairpin folding of tau in solution. Biochemistry 2006;45:2283–2293.

32. Mukrasch MD, Bibow S, Korukottu J, Jeganathan S, Biernat J, Griesinger C, Mandelkow E, Zweckstetter M. Structural polymorphism of 441-residue tau at single residue resolution. PLoS Biol 2009;7:e34.

33. Jeganathan S, Hascher A, Chinnathambi S, Biernat J, Mandelkow EM, Mandelkow E. Proline-directed pseudo-phosphorylation at AT8 and PHF1 epitopes induces a compaction of the paperclip folding of Tau and generates a pathological (MC-1) conformation. J Biol Chem 2008;283:32066–32076.

34. Barghorn S, Mandelkow E. Toward a unified scheme for the aggregation of tau into Alzheimer paired helical filaments. Biochemistry 2002;41:14885–14896.

35. Konarev PV, Volkov VV, Sokolova AV, Koch MHJ, Svergun DI. PRIMUS - a Windows-PC based system for small-angle scattering data analysis. J Appl Crystallogr 2003;36:1277–1282.

36. Round AR, Franke D, Moritz S, Huchler R, Fritsche M, Malthan D, Klaering R, Svergun DI, Roessle M. Automated sample-changing robot for solution scattering experiments at the EMBL Hamburg SAXS station X33. J Appl Crystallogr 2008;10:913–917.

37. Guinier A. La diffraction des rayons X aux tres petits angles; application a l'etude de phenomenes ultramicroscopiques. Ann Phys (Paris) 1939;12:161–237.

38. Svergun DI. Determination of the regularization parameter in indirect-transform methods using perceptual criteria. J Appl Crystallogr 1992;25:495–503.

39. Jeganathan S, von Bergen M, et al. The natively unfolded character of tau and its aggregation to Alzheimer-like paired helical filaments. Biochemistry 2008;47:10526–10539.

40. Rubinstein M, Colby RH. Polymer physics. New York: Oxford University Press; 2003.

41. Uversky VN. Intrinsically disordered proteins and their environment: effects of strong denaturants, temperature, pH, counter ions, membranes, binding partners, osmolytes, and macromolecular crowding. Protein J 2009;28:305–325.

Communications

The Dynamic Structure of Filamentous Tau**

Stefan Bibow, Marco D. Mukrasch, Subashchandrabose Chinnathambi, Jacek Biernat,
Christian Griesinger, Eckhard Mandelkow, and Markus Zweckstetter*

Filaments of the protein tau are a characteristic occurrence in Alzheimer disease and many other neurodegenerative disorders[1–3] and the distribution of tau filaments correlates well with the loss of neurons and cognitive functions in Alzheimer disease.[4] Filament formation of tau filaments is based on structural transitions from random coil to β-structure, to give the paired helical filaments (PHFs) which share common characteristics of amyloid fibrils.[5–6]

Protease digestion and solvent-accessibility studies demonstrated that the "core" of PHFs is mainly built from repeat sequences in the C-terminal half of the tau protein.[7] The PHF core is surrounded by a "fuzzy coat", of more than 200 residues that come from the N-terminal half of the protein as well as the C-terminus (Figure 1a).[7,8] Electron paramagnetic resonance and nuclear magnetic resonance (NMR) suggested that residues within the fuzzy coat are highly flexible.[9,10] Biochemical studies have shown that the fuzzy coat is important for tau aggregation as well as neurotoxicity.[11–13] Herein we characterized the dynamic structure of PHFs formed by 441-residue tau (htau40), the longest isoform of tau present in the human central nervous system (Figure 1a), at single-residue level using NMR spectroscopy.

We aggregated ^{15}N-labeled htau40 into insoluble filaments. NMR diffusion experiments[14] demonstrated that the observed NMR signals arises from aggregated tau protein with a molecular mass of more than 1 MDa (Figure 1b). In a two-dimensional heteronuclear single quantum coherence (HSQC) spectrum employing high-resolution magic-angle spinning (HR-MAS) (see Figure S1 in the Supporting Infor-

mation),[15] we observed about 260 signals (Figure 1c and Figure S2 and S3 in the Supporting Information). Sequence-specific resonance assignment of 244 of these signals (BMRB accession number: 17920; see Figure S2 in the Supporting Information) identified most of the residues in the N-terminal domain up to Thr212 and at the C-terminus starting at Val399.[6,10] No signals were detected for residues between Thr212 and Val399, suggesting that residues in the central domain are too immobile to be detected by liquid-state NMR spectroscopy in agreement with previous studies.[10] Comparison with monomeric htau40 revealed that the NMR resonances of many residues were strongly reduced in filamentous htau40 (Figure 1d,e). Most strikingly, the sections His121–Lys130 and Met1–Gly37 that are separated from the fibril core by 170 residues or more, showed changes in position and intensity of NMR signals (Figure 1e and Figure S2c in the Supporting Information). The presence of chemical exchange in these regions was further supported by ^{15}N spin relaxation measurements (Figure 1f and Supporting Figure S3). In agreement with chemical exchange, additional peaks were observed in close proximity to several of these residues (Figure 1f and Figure S4 in the Supporting Information). The additional signals could not be connected in triple-resonance experiments or using exchange spectroscopy because of low signal-to-noise and signal overlap. Therefore, we assigned the additional peaks to the residue for which the assigned cross-peak of the major peak set had the greatest similarity in chemical shifts and paramagnetic relaxation enhancement (see Figure S5 in the Supporting Information). This procedure indicates that the additional peaks arise from residues at the N- and C-terminus. No peak doubling was observed at the N- and C-terminus in monomeric tau (see Figure S4 in the Supporting Information), highlighting the specificity of the multiple conformations in PHF tau.

We revealed the identity of the PHF-specific conformations through measurements of paramagnetic relaxation enhancements (PREs),[17] in which nitroxide spin labels are attached to cysteine residues at various positions in the PHF tau. The resulting broadening of amide resonances caused by enhanced relaxations rate through the paramagnetic nitroxide label, is quantified through the intensity ratios in the paramagnetic and diamagnetic states (Figure 2). The PRE effect scales as the inverse sixth power of the distance between the unpaired electron of the nitroxide unit and the NMR spin, providing a powerful probe of distances. ^{15}N spin relaxation times (Figure 1f) indicate that the fuzzy coat of PHFs is highly dynamic on a broad scale suggesting that the correlation time of the electron—amide proton internuclear vector is comparable to that of small water soluble proteins. Initially, we measured PRE broadening for PHFs with a

[*] S. Bibow, Dr. M. D. Mukrasch, Prof. Dr. C. Griesinger, Prof. Dr. M. Zweckstetter
Department of NMR-based Structural Biology, Max Planck Institute for Biophysical Chemistry
Am Fassberg 11, 37077 Göttingen (Germany)
E-mail: mzwecks@gwdg.de

S. Chinnathambi, Dr. J. Biernat, Prof. Dr. E. Mandelkow
Max Planck Unit for Structural Molecular Biology
c/o DESY, Notkestrasse 85, 22607 Hamburg (Germany)
and
DZNE, German Center for Neurodegenerative Diseases, and CAESAR, Ludwig-Erhard-Allee 2, 53175 Bonn (Germany)

Supporting information for this article is available on the WWW under http://dx.doi.org/10.1002/anie.201105493.
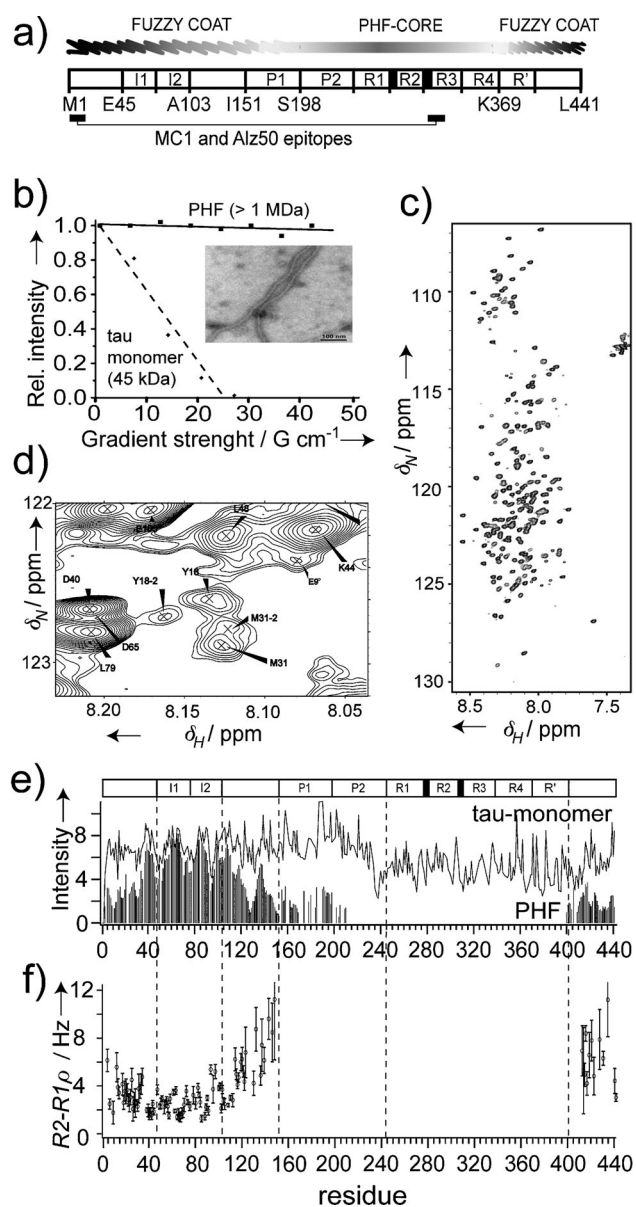
Figure 1. NMR spectroscopy of the dynamics in filamentous tau.
a) Schematic representation of 441-residue tau with the inserts I1 and I2 that are removed by alternative splicing, the proline-rich regions P1 and P2, and the pseudo-repeats R1–R4. Top: Proposed regions for the fuzzy coat and the fibrillar core. Below: Location of the epitopes (residues 1–18 and 313–322) of the monoclonal antibodies Alz50 and MC1. b) NMR diffusion experiments for monomeric tau (dashed line) and PHF tau (solid line) with an electron micrograph from PHFs used in this study. c) 2D [^{1}H,^{15}N]-HSQC spectrum of PHF tau. d) Selected region of the HSQC of PHF tau demonstrating the presence of multiple conformations for Tyr18 and Met31. e) Comparison of absolute signal intensities of PHF tau (bars) and monomeric tau (line). f) Relaxation rates illustrating significant motions in the μs–ms timescale for the N-terminus of filamentous tau.

nitroxide attached to position 15 (Figure 2 a–c); 40 residues at the N-terminus were broadened with PRE intensity ratios below 0.6. In addition, NMR spectroscopy revealed that Ala119–Asp133, the proline-rich region (Ile151–Thr212) and the C-terminal fuzzy coat (Val399–Ala429) are in transient contact with the N-terminus of PHF tau. The similarity of the

PRE intensity ratio profile (Figure 2b) with the pattern of NMR signal intensities of PHF tau (Figure 1e) suggests that the PHF-specific conformations are caused by formation of transient long-range interactions. The global folding of the fuzzy coat of PHFs was further supported by paramagnetic effects observed for a nitroxide radical at position 125 (Figure 2 d, e, f). Control experiments prove that the observed paramagnetic effects are mostly of intramolecular nature (see Figure S6 in the Supporting Information).

To directly probe the interaction between the fibril core and the fuzzy coat, we attached the nitroxide spin label to the native cysteine Cys322 of filamentous tau (Figure 2g–i). Attachment of the nitroxide label to Cys322 caused signal broadening in residue stretches close to Gln124, a region that transiently populates helical conformations (see Figure S7 in the Supporting Information), Ala152 and Asn167–Thr212, as well as Ser409-Ala426 at the C-terminus. Thus, residues in the projection domain and at the C-terminus contact the PHF-core residue Cys322 consistent with partial protection of the C-terminus to proteolysis in PHF tau.[18] The strongest effect, however, was observed for the first 30 residues at the N-terminus using either the major or the minor peak set observed for the N-terminal residues (Figure 2h and Figure S5c in the Supporting Information). Taken together NMR spectroscopy revealed a network of long-range interactions between conserved regions of filamentous tau.

To obtain insight into the mechanism of formation of long-range interactions in PHF tau, we performed NMR measurements of PHF tau at high ionic strength and of a mutant version of PHF tau in which Phe8 and Val10 were replaced by serine. Mutation of Phe8 and Val10, two hydrophobic residues at the N-terminus of tau, did not affect chemical exchange broadening in PHF tau (Figure 3a). In contrast, at high ionic strength the intensity profile of PHF tau was very similar to the profile observed for monomeric tau (Figure 3b). Only in regions neighboring the fibril core, that is residues 170–212 and 399–441, the intensity in the fuzzy coat remained low, most likely due to restricted motion inferred by the nearby fibril core. The strong impact of ionic strength demonstrates that electrostatic interactions are important for formation of the network of intramolecular long-range interactions in PHF tau.

For improved Alzheimer disease diagnosis antibodies were developed that detect changes in the conformation of tau.[19–21] The monoclonal antibodies Alz50 and MC1 recognize conformational changes in the tau protein that appear before the assembly of PHFs and are then also found in PHF, but are not present in normal brain.[20,22] The specificity of Alz50 and MC1 for pathological tau is due to a unique conformation of tau in the disease state and requires two discontinuous epitopes that are separated by about 300 residues and are located at the N-terminus (residues 1–18) and in the repeat region (residues 313–322).[20,22,23] Our paramagnetic NMR measurements demonstrated that the two discontinuous epitopes are in transient contact and are part of a network of long-range interactions that links the fuzzy coat with the PHF core (Figure 2). Comparison with NMR measurements in monomeric tau (Figure 3c and Figure S8 in the Supporting Information) showed that the paramagnetic
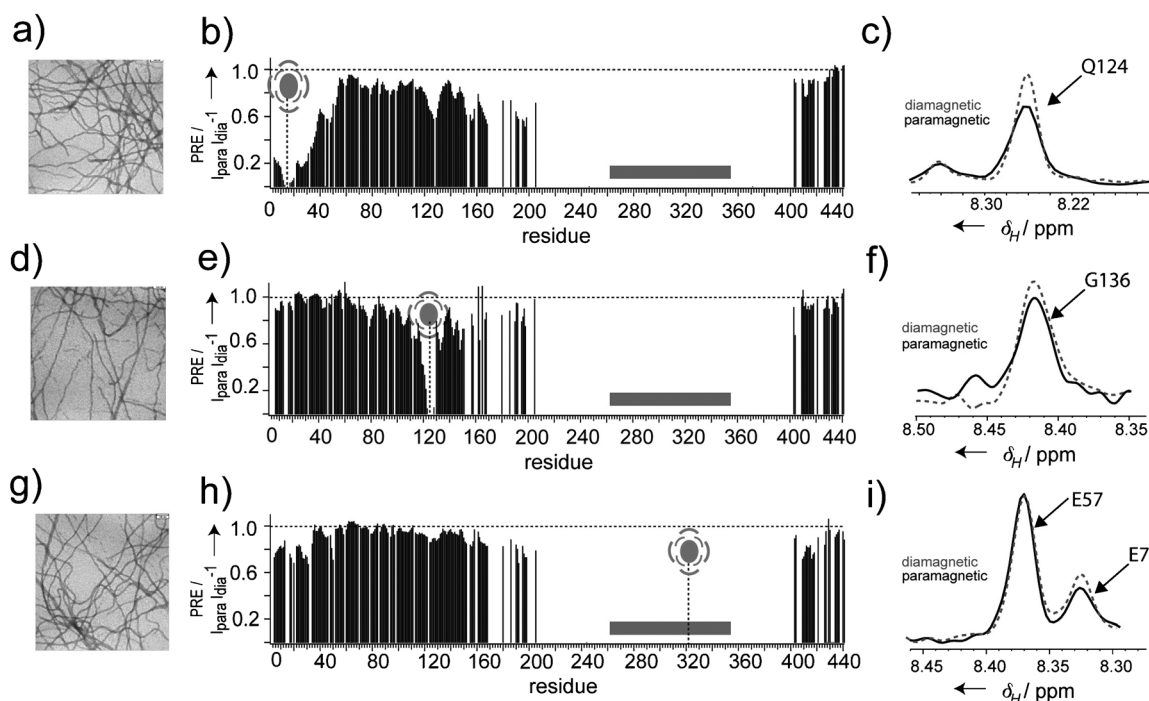
Figure 2. Transient long-range contacts in filamentous tau. a)–c) Paramagnetic NMR of PHFs with the nitroxide label attached at position 15. a) Electron micrograph, b) PRE profiles of amide protons, and c) selected region from [^{1}H,^{15}N]-HSQC in the paramagnetic (black) and diamagnetic state (gray dashed line). Intensity ratios were averaged over a three-residue window. Decreases in peak intensity ratios that occur far from the site of spin-labeling (more than 10 residues) are indicative of long-range contacts (<25 Å) between the spin-label and distant areas of sequence. The location of the fibril core identified by solid-state NMR spectroscopy is shown as a gray bar. d)–f) Paramagnetic NMR of PHFs with the nitroxide label attached at position 125. g)–i) Paramagnetic NMR of PHFs with the nitroxide label attached at the native Cys322.

effects induced at the N-terminus became stronger in PHF tau demonstrating that the interaction between the two discontinuous epitopes of the monoclonal Alz50 and MC1 antibodies is tightened in PHF tau. In addition, PHF-specific long-range contacts were observed between the proline-rich domain, the region next to Met127 and the N- and C-terminus. The network of long-range contacts involving several regions in filamentous tau explains the requirement of residues 155–244 and 305–314 for recognition by the conformation-specific antibody Tau66,[24] as well as the attenuation of Alz50 and MC1 antibody reactivity upon deletion of residues 46–241.[25] In addition, the observed long-range contacts are mostly intramolecular despite the high local concentration of tau in PHFs, in agreement with failed attempts at creating the Alz50 and MC1 epitopes intermolecularly by combining complementary NH$_2$- and COOH-terminal deletion mutants with an epitop.[20,22]

There is increasing evidence that soluble oligomeric tau species, rather than filamentous tau, may be the critical toxic moiety underlying neurodegeneration.[26] Biochemical studies using recombinant tau have demonstrated a clear selectivity of Alz50 and MC1 for PHF tau: the interaction of Alz50 with PHF-tau is nearly two orders of magnitude greater in affinity than its interaction with recombinant monomeric tau.[25] However, MC1 and Alz50 also bind to a non-filamentous, soluble pool of abnormal tau that is able to self-assemble into PHFs in a concentration-dependent manner,[27] suggesting that both PHFs and soluble oligomers of tau are recognized

by Alz50 and MC1. Our study reveals that the two epitopes of the Alz50 and MC1 antibody are already weakly in contact in monomeric tau, but the interaction is tightened during aggregation (Figure 3c) providing a potential mechanism for the recognition of both oligomeric and PHF tau.

In summary, our study demonstrates that the core structure of tau filaments interacts with otherwise unstructured segments within the protein (Figure 4). It rationalizes the conformation-specific antibodies of tau and highlights the heterogeneity within aggregate structures.

Experimental Section

Recombinant preparation of tau: Expression, purification, and isotope labeling of wild-type and mutant htau40 were performed as described previously.[28] NMR samples contained ^{15}N- or ^{13}C/^{15}N-labeled protein in 95% H$_2$O/5% D$_2$O and 50 mM phosphate buffer, pH 6.8.

Spin labeling of tau: Spin labeling of tau was performed as described previously[28]. To probe for intermolecular contacts, a 1:1 mixture of ^{14}N C15A291/G322-htau40 and ^{15}N-labeled A291/G322-htau40 was prepared. The nitroxide spin label MTSL was attached to ^{14}N-labeled C15A291/G322-htau40 prior to mixing and aggregation.

Formation of paired helical filaments: PHFs of wild-type and mutant htau40 were formed by mixing ^{13}C/^{15}N or ^{15}N-labeled protein (ca. 1.5 mM) with heparin 5000 (heparin:tau 1:4) and incubation at 37°C for 4 days. The reaction was then pelleted at 160 000 g for 40 min. The protein supernatant was complemented again with heparin and incubated for another 4 days. To remove any residual monomeric tau as well as the aggregation inducer heparin, PHF
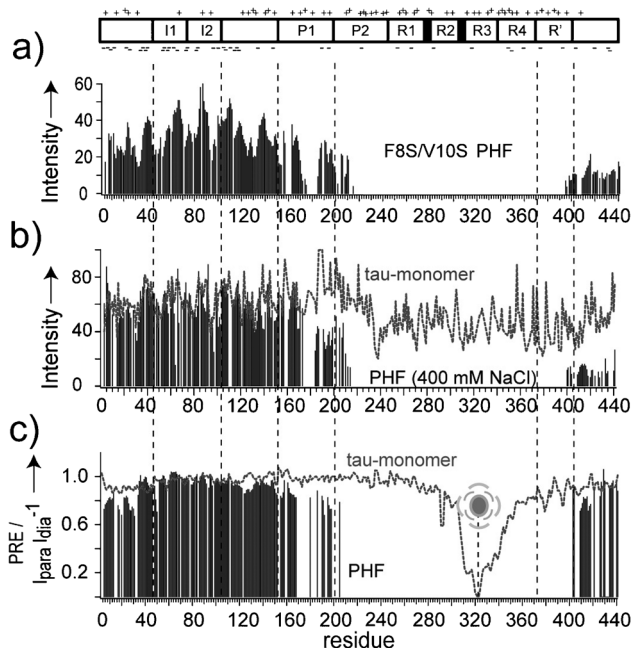
Figure 3. Ionic-strength dependence of transient interactions in filamentous tau. a) NMR signal intensities observed in a 2D [^{1}H,^{15}N]-HSQC of mutant PHF tau, in which Phe8 and Val10 were replaced by serine. b) Comparison of absolute NMR signal intensities in PHF tau at increased ionic strength (400 mM NaCl; bars) and in monomeric tau (gray dashed line). c) Comparison of the PRE intensity profile of monomeric tau (gray dashed line) and PHF tau (bars), when a nitroxide spin label was attached to the native Cys322. At the N-terminus, PRE intensity ratios are lower in PHF tau than in monomeric tau revealing a tightening of long-range contacts. Top: The domain organization of htau40 and the location of negative and positive charges.
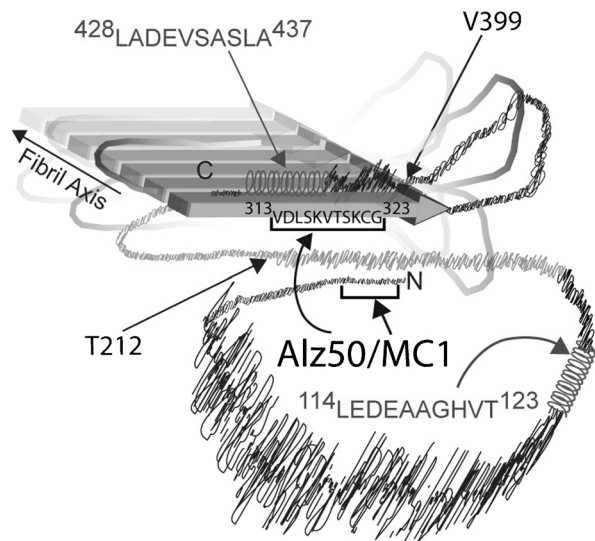
Figure 4. Model of the network of long-range interactions specific for PHF tau. Regions of transient helical structure are indicated. The gray bars with arrow heads represent the fibrillar core identified by solid-state NMR spectroscopy. Higher NMR signal intensities in the fuzzy coat are indicated by an increasing width of the protein chain. Spatial proximity between different parts of the chain indicates tertiary contacts that were revealed by paramagnetic NMR experiments. The two discontinuous epitopes of the conformation-specific antibodies Alz50 and MC1, residues 1–18 and 313–322, are labeled.

pellets were ultracentrifuged, the pellets were washed with fresh buffer not containing heparin and centrifuged again (40000 rpm, 4 °C, 40 min). The steps were repeated at least 3 times prior to the NMR measurements. 1D NMR spectra demonstrated that no residual heparin was left (see Figure S1 in the Supporting Information).

NMR spectroscopy: NMR experiments were conducted on a 900 MHz spectrometer (Bruker) at 278 K. NMR samples contained 40–80 mg of htau40 fibrils in a volume of 60 μL. A 3D constant-time HNCA experiment was recorded with a HR-MAS spinning frequency of 6 kHz, 2048 × 68 × 88 points (^{1}H × ^{13}C × ^{15}N) and 50 scans, resulting in a total experimental time of 4 days and 3 h. PRE effects were measured from the peak intensity ratios between two 2D ^{15}N–^{1}H HSQC NMR spectra of PHF tau, which was tagged with a nitroxide spin label, before and after addition of 4 mM DTT (dithio threitol) heated to 42 °C for 30 min before measurement.

Full Methods are available in the Supporting Information.

[1] C. Ballatore, V. M. Lee, J. Q. Trojanowski, *Nat. Rev. Neurosci.* **2007**, *8*, 663–672.
[2] C. Haass, D. J. Selkoe, *Nat. Rev. Mol. Cell Biol.* **2007**, *8*, 101–112.
[3] S. A. Small, K. Duff, *Neuron* **2008**, *60*, 534–542.
[4] H. Braak, E. Braak, *Acta Neuropathol.* **1991**, *82*, 239–259.
[5] J. Berriman, L. C. Serpell, K. A. Oberg, A. L. Fink, M. Goedert, R. A. Crowther, *Proc. Natl. Acad. Sci. USA* **2003**, *100*, 9034–9038.
[6] O. C. Andronesi, M. von Bergen, J. Biernat, K. Seidel, C. Griesinger, E. Mandelkow, M. Baldus, *J. Am. Chem. Soc.* **2008**, *130*, 5922–5928.
[7] C. M. Wischik, M. Novak, P. C. Edwards, A. Klug, W. Tichelaar, R. A. Crowther, *Proc. Natl. Acad. Sci. USA* **1988**, *85*, 4884–4888.
[8] T. A. Schoenfeld, R. A. Obar, *Int. Rev. Cytol.* **1994**, *151*, 67–137.
[9] M. Margittai, R. Langen, *Proc. Natl. Acad. Sci. USA* **2004**, *101*, 10278–10283.
[10] A. Sillen, J. M. Wieruszeski, A. Leroy, A. B. Younes, I. Landrieu, G. Lippens, *J. Am. Chem. Soc.* **2005**, *127*, 10138–10139.
[11] Y. Wang, S. Garg, E. M. Mandelkow, E. Mandelkow, *Biochem. Soc. Trans.* **2010**, *38*, 955–961.
[12] N. E. LaPointe, G. Morfini, G. Pigino, I. N. Gaisina, A. P. Kozikowski, L. I. Binder, S. T. Brady, *J. Neurosci. Res.* **2009**, *87*, 440–451.
[13] P. M. Horowitz, N. LaPointe, A. L. Guillozet-Bongaarts, R. W. Berry, L. I. Binder, *Biochemistry* **2006**, *45*, 12859–12866.
[14] E. O. Stejskal, J. E. Tanner, *J. Chem. Phys.* **1965**, *42*, 288–292.
[15] A. N. Garroway, *J. Magn. Reson.* **1982**, *49*, 168–171.
[16] A. Sillen, J.-M. Wieruszeski, A. Leroy, A. B. Younes, I. Landrieu, G. Lippens, *J. Am. Chem. Soc.* **2005**, *127*, 10138–10139.
[17] J. R. Gillespie, D. Shortle, *J. Mol. Biol.* **1997**, *268*, 170–184.
[18] M. von Bergen, S. Barghorn, S. A. Muller, M. Pickhardt, J. Biernat, E. M. Mandelkow, P. Davies, U. Aebi, E. Mandelkow, *Biochemistry* **2006**, *45*, 6446–6457.
[19] E. M. Sigurdsson, *Curr. Alzheimer Res.* **2009**, *6*, 446–450.
[20] G. A. Jicha, R. Bowser, I. G. Kazam, P. Davies, *J. Neurosci. Res.* **1997**, *48*, 128–132.
[21] M. Mercken, M. Vandermeeren, U. Lubke, J. Six, J. Boons, A. Van de Voorde, J. J. Martin, J. Gheuens, *Acta Neuropathol.* **1992**, *84*, 265–272.
[22] G. Carmel, E. M. Mager, L. I. Binder, J. Kuret, *J. Biol. Chem.* **1996**, *271*, 32789–32795.

[23] G. A. Jicha, B. Berenfeld, P. Davies, *J. Neurosci. Res.* **1999**, *55*, 713–723.

[24] N. Ghoshal, F. Garcia-Sierra, Y. Fu, L. A. Beckett, E. J. Mufson, J. Kuret, R. W. Berry, L. I. Binder, *J. Neurochem.* **2001**, *77*, 1372–1385.

[25] G. A. Jicha, R. Bowser, I. G. Kazam, P. Davies, *J. Neurosci. Res.* **1997**, *48*, 128–132.

[26] A. de Calignon, L. M. Fox, R. Pitstick, G. A. Carlson, B. J. Bacskai, T. L. Spires-Jones, B. T. Hyman, *Nature* **2010**, *464*, 1201–1204.

[27] C. L. Weaver, M. Espinoza, Y. Kress, P. Davies, *Neurobiol. Aging* **2000**, *21*, 719–727.

[28] M. D. Mukrasch, S. Bibow, J. Korukottu, S. Jeganathan, J. Biernat, C. Griesinger, E. Mandelkow, M. Zweckstetter, *PLoS Biol.* **2009**, *7*, e34.

Human Tau Isoforms Assemble into Ribbon-like Fibrils That Display Polymorphic Structure and Stability*⒮

Susanne Wegmann[‡1], **Yu Jin Jung**[§1], **Subashchandrabose Chinnathambi**[¶], **Eva-Maria Mandelkow**[¶],
Eckhard Mandelkow[¶2], and **Daniel J. Muller**[‡3]

From the ‡Department of Biosystems Science and Engineering, ETH Zürich, CH-4058 Basel, Switzerland, the §Biotechnology Center, University of Technology, 01307 Dresden, Germany, and the ¶Max-Planck-Unit for Structural Molecular Biology, c/o DESY, 22607 Hamburg, Germany and the German Center for Neurodegenerative Diseases, c/o CAESAR, 53175 Bonn, Germany

Fibrous aggregates of Tau protein are characteristic features of Alzheimer disease. We applied high resolution atomic force and EM microscopy to study fibrils assembled from different human Tau isoforms and domains. All fibrils reveal structural polymorphism; the "thin twisted" and "thin smooth" fibrils resemble flat ribbons (cross-section ∼10 × 15 nm) with diverse twist periodicities. "Thick fibrils" show periodicities of ∼65–70 nm and thicknesses of ∼9–18 nm such as routinely reported for "paired helical filaments" but structurally resemble heavily twisted ribbons. Therefore, thin and thick fibrils assembled from different human Tau isoforms challenge current structural models of paired helical filaments. Furthermore, all Tau fibrils reveal axial subperiodicities of ∼17–19 nm and, upon exposure to mechanical stress or hydrophobic surfaces, disassemble into uniform fragments that remain connected by thin thread-like structures (∼2 nm). This hydrophobically induced disassembly is inhibited at enhanced electrolyte concentrations, indicating that the fragments resemble structural building blocks and the fibril integrity depends largely on hydrophobic and electrostatic interactions. Because full-length Tau and repeat domain constructs assemble into fibrils of similar thickness, the "fuzzy coat" of Tau protein termini surrounding the fibril axis is nearly invisible for atomic force microscopy and EM, presumably because of its high flexibility.

Abnormal protein aggregation is a hallmark of a variety of human diseases, especially those appearing at advanced age. Alzheimer disease (AD)[4] is the leading cause of dementia in the elderly population and is characterized by two types of protein aggregates. Extracellular amyloid aggregates mainly consist of

the Aβ protein, whereas intracellular neurofibrillary tangles consist mainly of fibrils from Tau, a microtubule-binding protein (1, 2). In both cases, the self-assembly of the proteins can be achieved *in vitro* from recombinant proteins, and mechanisms of these pathological reactions are under intense investigation (3–7). It is hoped that the inhibition of pathological fibrous aggregates or their precursors would reduce the toxic effects on neurons (8). To achieve this goal, knowledge on the building principles of such aggregates would be invaluable. Some progress along this road has been made for the fibrils of the Aβ peptide (40–42 residues). The embedded proteins have a high content of β-strands that fold in a U-shaped manner and stack to form pairs of parallel β-sheets (9). By contrast, Tau is 10 times larger (up to 441 residues, depending on the isoform (Fig. 1)) and largely disordered. Details on the folding and subunit interactions in the aggregated state are mostly unknown; however, β-structure formation is important as well (10–12).

The fibrils of Tau in AD brains are commonly termed "paired helical filaments" (PHFs) because of their appearance in EM (13). Two protofibrils seem to be wound around one another exposing a crossover repeat of ∼80 nm, a maximal width of ∼22 nm, and a narrow waist of ∼12 nm (see Fig. 3 in Ref. 14). The twisted appearance is variable as follows: ∼10% of Tau fibrils found in AD brains show no twist and are therefore called "straight filaments." In other diseases with Tau pathology, the crossover repeat is ∼160 nm (15). Likewise, Tau fibrils reassembled *in vitro* can display a variable twist between filaments assembled from different variants of Tau proteins (*e.g.* different splicing variants) or even within a given filament. This has caused some concern whether the assembly products observed *in vitro* reflect those observed in AD brains. A plausible interpretation would be a slight variability in the contacts between subunits, which then can give rise to differences in the overall fibril appearance.

Another fundamental debate concerns the interpretation of the twisted appearance of the Tau fibrils. As an alternative to the "paired helical" structure, it has been proposed that Tau fibrils could be considered as flat ribbons with a width of ∼22 nm and a height of ∼12 nm that twist around their longitudinal axis (16). The apparent groove running down the longitudinal axis could resemble an artifact of staining filling a depression in the fibril, rather than reflecting the division between two joining protofibrillar strands. The interpretation of PHFs as ribbons was mostly based on atomic force microscopy (AFM) and scanning tunneling microscopy (17, 18), but it was viewed with cau-

tion because of possible imaging artifacts (19). However, consistent with the "ribbon" interpretation, the ends of filaments or filament fragments usually show clean sharp edges. In contrast, fibrils consisting of two or more protofibrils would be expected to occasionally reveal protruding ends, reminiscent of the protofilament stubs protruding from microtubules (MTs). This is not observed in the case of Tau fibrils. In this study, we therefore use mostly the term "Tau fibrils" rather than PHFs or ribbons to avoid a bias in interpretation.

A further enigmatic aspect of Tau fibrils is the nature of the "fuzzy coat," which can be digested from the "PHF core" (20). The core protein coincides roughly with the Tau repeat domain of ~100–120 residues and accounts for only ~25–30% of the entire Tau protein. Thus, the fuzzy coat should represent the major protein fraction in Tau fibrils, but so far it has escaped detection by microscopic methods. For example, fibrils assembled *in vitro* from full-length Tau or from the repeat domain alone show only minor differences in diameter by negative stain EM (21). Similar results were obtained for Tau proteins bound to MTs, and the unstructured "projection domain," which does not bind to MTs. This domain that largely coincides with the Tau termini in the fuzzy coat, is nearly invisible on negatively stained or cryo-preserved unstained MTs (22).

Considering these open questions and the importance of aggregated Tau as a potential target for therapy of AD and related Tauopathies, we initiated a study of Tau isoforms and Tau domains by state-of-the-art AFM. Although AFM cannot provide the spatial resolution of EM, it provides topographs of biological specimens in buffer solution at an exceptional signal-to-noise ratio and a resolution approaching ~1 nm (23). Thus, AFM allows single biological macromolecules to be observed in molecular detail. In addition, AFM allows manipulating single proteins to characterize their inter- and intramolecular interactions (24, 25). We applied high resolution AFM to reveal detailed structural information of Tau fibrils assembled from six different Tau isoforms and repeat unit constructs. These experiments were conducted in buffer solution at room temperature to guarantee the native integrity of the Tau fibrils. Instead of the commonly reported uniform PHF population, we found that all Tau proteins self-assembled into fibrils that showed populations of variable apparent thickness and twist. Upon mechanical stress as well as exposure to hydrophobic surfaces, the fibrils disassembled into their oligomeric building blocks of ~15 nm length, which were connected by thin (height ~2 nm) thread-like stretches. We further demonstrate that hydrophobic and electrostatic interactions play a major role in stabilizing Tau fibrils.

EXPERIMENTAL PROCEDURES

Chemicals and Proteins—Heparin (average molecular mass of 6000 Da), guanidine hydrochloride, and ThS were purchased from Sigma. Full-length human Tau isoforms hTau40, hTau23, hTauΔK280, and Tau constructs K18, K19, and K18ΔK280 (Fig. 1*A*) were expressed in *Escherichia coli* and purified by heat treatment and FPLC Mono S chromatography (Amersham Biosciences) as described previously (21). The purity of the proteins was analyzed by SDS-PAGE, and the protein concentrations were determined by absorbance at 214 nm.

PHF Assembly—Aggregation was induced by incubating soluble Tau or Tau constructs typically in the range of 50 μM in volumes of 20 μl at 37 °C in 20 mM BES, pH 7.4, plus 25 mM NaCl buffer with the anionic cofactor heparin 6000 (molar ratio of Tau to heparin = 4:1) for incubation times of ~3 days for short constructs (K18, K19, and K18ΔK280) or ~6–7 days for full-length proteins (hTau40, hTau23, and hTauΔK280). The formation of aggregates was monitored by ThS fluorescence and electron microscopy.

ThS Fluorescence—5 μl of 50 μM assembly reactions were diluted to 50 μl with NH_4Ac, pH 7, containing 20 μM ThS. Then ThS fluorescence was measured in a Tecan spectrofluorimeter (Crailsheim, Germany) with an excitation wavelength of 440 nm and an emission wavelength of 521 nm (slit width 7.5 nm each) in a 384-well plate (black microtiter 384 plate round well; ThermoLabsystems, Dreieich, Germany). Measurements were carried out at 25 °C, and the background fluorescence was subtracted when needed.

Electron Microscopy—Protein solutions were diluted to 1–10 μM and placed on 600 mesh carbon-coated copper grids for 45 s, washed twice with H_2O, and negatively stained with 2% uranyl acetate for 45 s. The samples were examined with Philips CM12 electron microscope at 100 kV.

AFM Sample Immobilization on Mica and HOPG—The Tau sample was diluted in PBS or in adsorption buffer (10 mM Tris-HCl, pH 7.4, 50 mM KCl) to a final concentration of 1–2 μM. A drop (~20 μl) of the Tau solution was placed onto freshly cleaved mica or highly ordered pyrolytic graphite (HOPG) to allow adsorption of the sample for ~15 min. Excess protein was removed by rinsing the sample with imaging buffer (10 mM Tris-HCl, pH 7.4, 50 mM KCl). To characterize the influence of ions on the Tau fibril morphology, the imaging buffer (10 mM Tris-HCl, pH 7.4) had varying electrolyte concentrations (0, 10, 50, 166, and 300 mM KCl or 50 mM NaCl). Low pH imaging was done using adsorption and imaging in buffer (10 mM acetate, 10 mM KCl) adjusted to pH 5. For high pH imaging, adsorption and imaging of Tau fibrils were done in 10 mM Tris, 150 mM KCl adjusted to pH 9. When mentioned, HOPG was coated by poly-L-lysine, L-glutamate, or L-threonine (Sigma) using adsorption buffer containing 0.1% of the respective amino acid. To cross-link fibrils adsorbed to mica, they were first adsorbed to mica, then incubated for 30–60 s in adsorption buffer containing 0.5% glutaraldehyde, and subsequently washed several times with imaging buffer. Cross-linking of Tau fibrils in solution prior to surface deposition was achieved by adding 0.5% glutaraldehyde for 15–30 s to the fibril solution containing 1–2 μM Tau protein.

AFM Imaging and Data Analysis—AFM imaging was performed in oscillation mode using a Nanoscope III (Di-Veeco, Santa Barbara, CA) and Si_3N_4 cantilevers (NPS series, Di-Veeco) exhibiting spring constants of ~0.32 N/m at resonance frequencies in buffer of 8.5 to 10 kHz. To achieve minimal imaging forces between AFM stylus and sample, the drive amplitude was set between 0.5 and 1.0 V, and the amplitude set point was adjusted manually to compensate for the thermal drift of the AFM. Mean bending angles of Tau fibrils were determined semi-automatically by employing a DNA tracing routine in LabVIEW (National Instruments) (26). The persis-
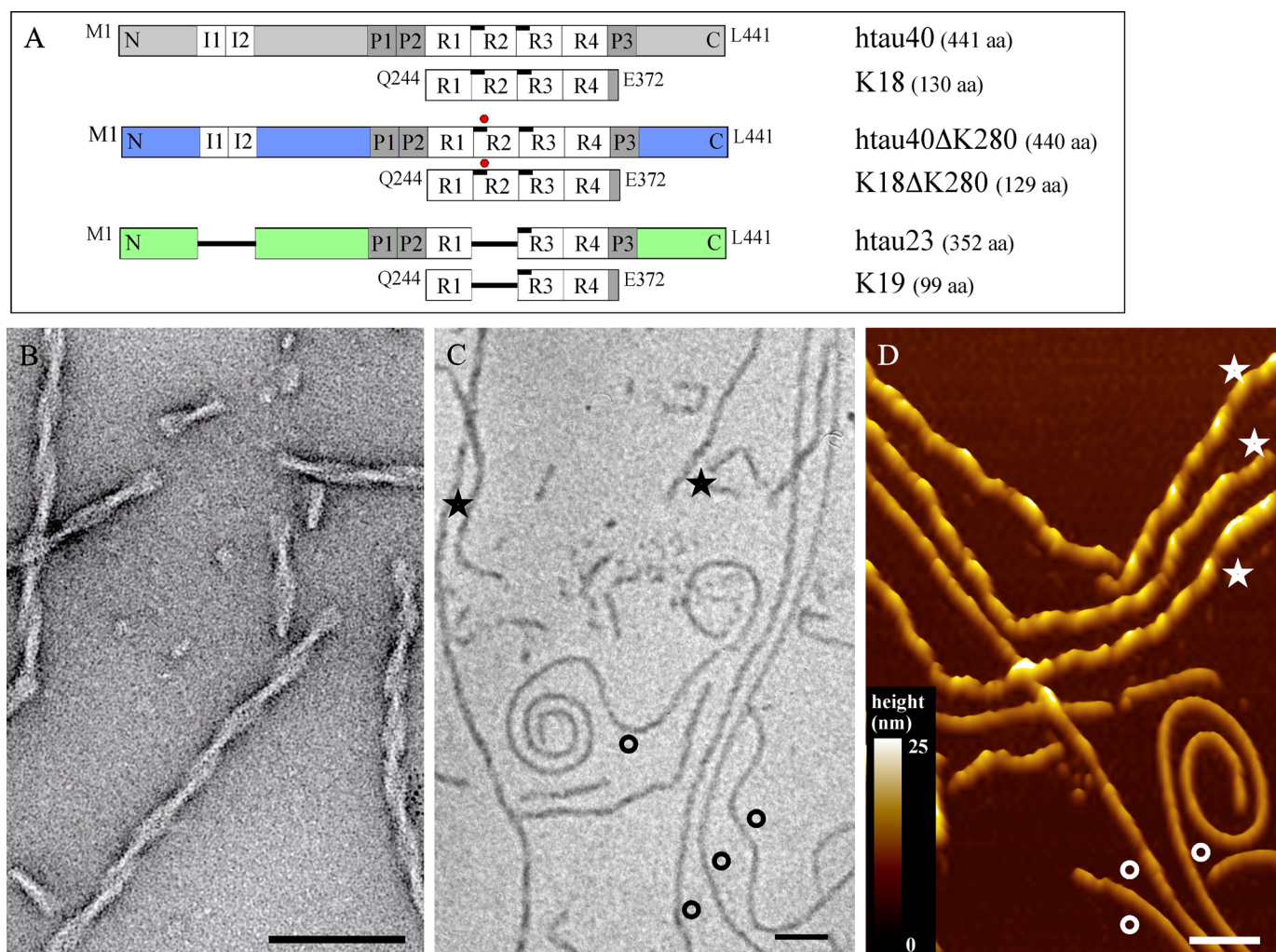
FIGURE 1. **Survey of Tau isoforms, constructs, and fibril assembly.** *A,* sequences of Tau isoforms and constructs assembled into fibrils in the presence of heparin are sketched in a *bar diagram*. The two hexapeptide motifs (*black bars*) involved in PHF core formation are located in repeat 2 and 3 (*R2* and *R3*). The position of the Lys^{280} deletion in hTau40ΔK280 and K18ΔK280 is indicated by *red dots*. *B,* EM image of K18ΔK280 fibrils with the typical appearance of PHFs. *C,* nonselective EM images of hTau40 fibril preparations show a heterogeneous mixture of fibril shapes. *D,* AFM topographs of the same fibril preparation confirm the heterogeneity of fibril structures but reveal details with superior contrast. Fibril morphologies differ in length, bending, internal twist, periodicity, and thickness (★ for thick fibrils (*bright yellow* on the color scale) and ○ for thin fibrils (*brown* on the color scale)). This structural heterogeneity was largely independent of the Tau isoform and construct from which the fibrils self-assembled (supplemental Figs. S1–S3). Notably, although the fibril thickness in EM images is given by the apparent width of the structure, it is reflected by the fibril height in AFM topographs. AFM topographs were recorded in imaging buffer (10 mM Tris-HCl, pH 7.4, 50 mM KCl) and exhibit a full color range that corresponds to vertical scale of 25 nm as indicated by the color scale bar. Length scale bars in *B*, *C*, and *D* correspond to 100 nm.

tence length of each fibril was calculated from the Gaussian variance of bending angles according to Ref. 27.

Fibril heights were measured from cross-sections perpendicular to the long fibril axis. Height profiles were taken along the longitudinal fibril axis. Fibril periodicities were determined from Fourier transformations (IGOR Pro version 5.04B, WaveMetrics Inc.) of topographs along the longitudinal fibril axis (ImageJ version 1.37 software). Gaussian fits to all apparent peaks in the Fourier spectra provided the periodicities further analyzed in histograms to determine the most probable periodicities (Fig. 3). For presentation, all topographs were tilted by 5° (ImageSXM 176-1C, Steve Barrett, Liverpool, UK) to allow perspective view.

RESULTS

Tau Proteins Assemble into Polymorphous Fibrils—In this work we characterize the structure of fibrils assembled *in vitro* from various Tau isoforms and constructs with different domain compositions (Fig. 1*A*). Assembly was initiated by the polyanionic cofactor heparin, which helps to overcome the kinetic nucleation barrier and reproduces Tau fibrils with *bona fide* PHF-like structures (28, 29). The longest isoform in the human central nervous system (CNS), hTau40, contains a repeat domain of four repeats (R1 to R4) and consists of 441 amino acids (aa). The three repeat isoform hTau23 lacks R2 and is 352 aa long. The deletion mutation ΔK280, which has been discovered in Tau-related dementia FTDP-17 (30), significantly enhances the speed of Tau aggregation into fibrils (31). Constructs containing only the repeat domains of hTau40, hTau23, and hTau40ΔK280 are named K18 (130 aa), K19 (99 aa), and K18ΔK280 (129 aa), respectively. Although considerably shorter, the repeat domain-only constructs form fibrils similar to the full-length proteins but are more prone to aggregation, presumably because they are lacking the N- and C-terminal

domains that protect the core against unfavorable interactions (7, 32). Randomly picked micrographs of all *in vitro* preparations showed an unexpected degree of polymorphic fibril appearances in both AFM and EM (Fig. 1, *C–D*). Compared with EM images, AFM topographs provided a superior contrast. The fibrils had different lengths and their morphology varied in bending, periodicity, twisting, thickness, and substructure. This heterogeneity was independent of the Tau isoform from which the fibrils self-assembled (Fig. 1 and supplemental Figs. S1–S3).

Next, we investigated whether the fibril morphologies depend on the electrolyte and pH of the buffer solution or on the properties of the supporting surface. We adsorbed Tau fibrils to different AFM supports in buffer solutions with electrolyte concentrations ranging between 50 and 500 mM NaCl or KCl and pH of 5.0, 6.0, 7.4, and 9.0. The AFM supports tested were hydrophobic HOPG, HOPG coated with positively charged poly-L-lysine, and hydrophilic mica. In all cases, we could not observe significant variations in the structural properties (thickness, bending, and twisting) of the fibrils (data not shown). Furthermore, we tested whether this polymorphism depends on sample preparation artifacts. Therefore, we imaged all fibrils of the different Tau isoforms in their native state (Fig. 1 and supplemental Figs. S2–S3) and in the fixed state, in which the fibrils were cross-linked before or after adsorption to the microscopy support using 0.5% glutaraldehyde. In all cases, the Tau fibrils imaged in buffer solution showed the same structural diversity. Thus, we conclude that the fibril polymorphism reflects an inherent property of Tau. We characterized the Tau fibril morphologies in more detail below.

Fibrils from Different Tau Proteins Form Equivalent Structural Classes—We first describe AFM topographs of fibrils prepared from the longest human four-repeat Tau isoform, hTau40, and the shortest three-repeat construct, K19 (Fig. 1*A* and Fig. 2). The fibrils revealed a diversity of appearances in terms of height, twist, coiling, and substructure, whereas the apparent width (measured across the fibrils) remained roughly comparable, about 40–60 nm. This enhanced width is explained by the broadening artifact that results from the non-linear so-called "stylus convolution" of the fibril with the AFM stylus (see "Experimental Procedures") (19). In contrast, AFM contours the sample height as well as height variations very accurately with a resolution of ≤0.5 nm (33, 34). We thus decided to judge the diameter of fibrils in AFM topographs from their height (Fig. 3). Fibrils assembled from both hTau40 and K19 could be categorized into three classes as follows: thick corrugated fibrils, thin corrugated fibrils, and thin smooth fibrils (supplemental Table S1).

Thick fibrils assembled from hTau40 had thicknesses (AFM heights) between 11.5 ± 1.3 nm (average $\pm$S.D.; $n = 39$) and 18.5 ± 1.7 nm ($n = 56$) (Fig. 3, *A–B* and supplemental Table S1). In the case of the repeat domain K19, the height of thick fibrils varied between 10.2 ± 1.2 nm ($n = 36$) and 15.9 ± 1.3 nm ($n = 29$) (Fig. 3, *C–D*). The pronounced corrugation along the longitudinal axis (★ in Figs. 1 and 2 and supplemental Figs. S2 and S3) indicates a twisted structure with a mean periodicity of 67.5 ± 2.0 nm ($n = 16$) for hTau40 and 60.4 ± 1.2 nm ($n = 20$) for K19 (Figs. 2 and 3 and

supplemental Table S2). Thick fibrils assembled from hTau40 ($\sim$18.5 nm) and K19 ($\sim$15.9 nm) showed a mean bending angle, q, of $2.2 \pm 1.3°$ ($n = 40$) and persistence length, l_p, of 2.4 ± 0.7 μm (supplemental Table S3). Accordingly, thick fibrils exhibited almost no bending and frequently broke into smaller fragments of variable lengths.

Thin fibrils showed large variations in bending and corrugation (Figs. 2 and 3). Corrugated hTau40 thin fibrils ranged in thickness from 9.8 ± 1.2 nm ($n = 137$) to 14.5 ± 1.8 nm ($n = 152$) (Fig. 3*B* and supplementary Table S1), a mean bending angle of $1.9 \pm 1.1°$ ($n = 34$), and a persistence length of 3.2 ± 0.6 μm (supplemental Table S3). The thickness of K19 fibrils ranged from 6.9 ± 0.8 nm ($n = 40$) to 13.4 ± 1.2 nm ($n = 39$). The mean twist periodicity along the longitudinal fibril axis was 47.8 ± 0.9 nm (hTau40; $n = 38$) and 46.3 ± 4.3 nm (K19; $n = 47$) (Fig. 2*O* and supplemental Table S2). In some cases, variable periodicities were observed in the same fibril (Fig. 2, *C* and *L*). The ability of Tau fibrils to bend appeared to be independent of their periodicity. Thin smooth fibrils from hTau40 and K19 that did not reveal obvious corrugations showed an average thickness of 11.0 ± 1.9 nm ($n = 140$) and 9.4 ± 1.0 nm ($n = 33$), respectively. Such fibrils were either straight ($q = 2.1 \pm 0.9°$, $l_p = 4.3 \pm 2.5$ μm, $n = 62$) or curved with wavy or spiral-like appearance ($q = 2.4 \pm 1.4°$, $l_p = 2.0 \pm 0.8$ mm, $n = 10$) (Fig. 1, *C* and *D* and Fig. 2, *A*, *D* and *E*). If the fibrils were fixed in solution with 0.5% glutaraldehyde prior to adsorption, long straight and large screw-like fibrils were observed (data not shown). We conclude that the wavy and spiral-like fibrils formed upon adsorption of screw-like structured fibrils to the support (Fig. 1, *C* and *D*, and Fig. 2, *A*, *D* and *H*). We found that in the case of hTau40, the thick fibrils made up $\sim$40% ($n = 183$) of all fibrils, whereas the remaining thin fibrils exhibited thicknesses between $\sim$10 and 11 nm. Thick and thin fibrils were observed for all Tau isoforms studied, although the abundance of thick fibrils was variable between 20 and 75% (supplemental Table S1). Comparing the periodicity and thickness of thick Tau fibrils characterized here by AFM with the periodicity of $\sim$80 nm and width of $\sim$22 nm reported for PHFs by EM (13, 14), it may be concluded that the thick Tau fibrils reflect the commonly reported PHF structure. This interpretation would be in agreement with previous AFM studies (17, 35). However, the coexistence of thin smooth, thin corrugated, and thick fibrils reassembled from the same Tau proteins suggests that these different structural classes may be gathered from Tau proteins showing different assemblies or conformations.

Fibrils from Different Tau Proteins Reveal Similar Subperiodicities—In addition to the coarse height variations of Tau fibrils, high resolution AFM topographs revealed corrugations of smaller magnitude with periodicities of 17.4 ± 2.7 nm ($n = 16$) and 17.2 ± 0.3 nm ($n = 11$) in thin smooth and thin twisted fibrils of hTau40 and K19 (Fig. 2, *B*, *D*, *E*, *H*, *I*, and *J* and supplemental Table S2), respectively. Similar observations were made for fibrils assembled from other Tau isoforms and constructs (supplemental Figs. S2 and S3 and supplemental Table S2). Occasionally, we observed similar periodic substructures in thick Tau fibrils. However, due to the strong corrugation of thick fibrils, their finer substructures could hardly be contoured by the scanning AFM stylus. The described vari-

Polymorphic Assembly and Stability of Human Tau Fibrils

ations in thickness, twist, and bending of Tau fibrils reflect their structural heterogeneity. In summary, all fibrils showed similar small height corrugations that indicated a periodic substructure of ~17–19 nm. Based on this common structural feature, it may be concluded that there is a uniform building block from

which Tau fibrils assemble. In the next experiments, we mechanically disassembled individual Tau fibrils to reveal further insight into their stability and architecture.

Mechanical Dissection of Tau Fibrils—To obtain topographs of unperturbed Tau fibrils, the forces applied by the scanning

periodicities (nm ± SD)			
		twist	stack
hTau40	thin	47.8 ± 0.9	17.4 ± 2.7
	thick	67.5 ± 2.0	
K19	thin	46.3 ± 4.3	17.2 ± 0.3
	thick	60.9 ± 1.2	
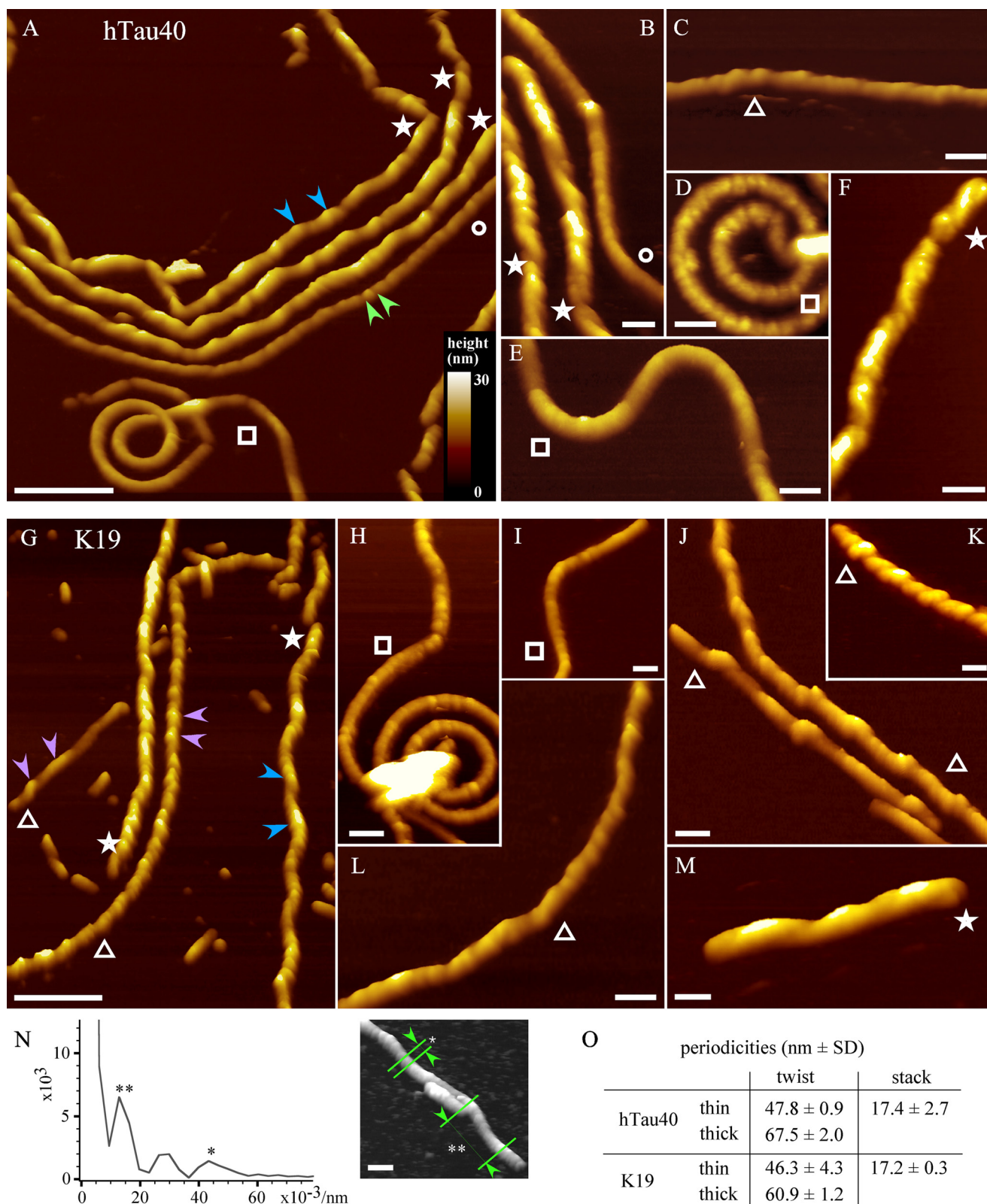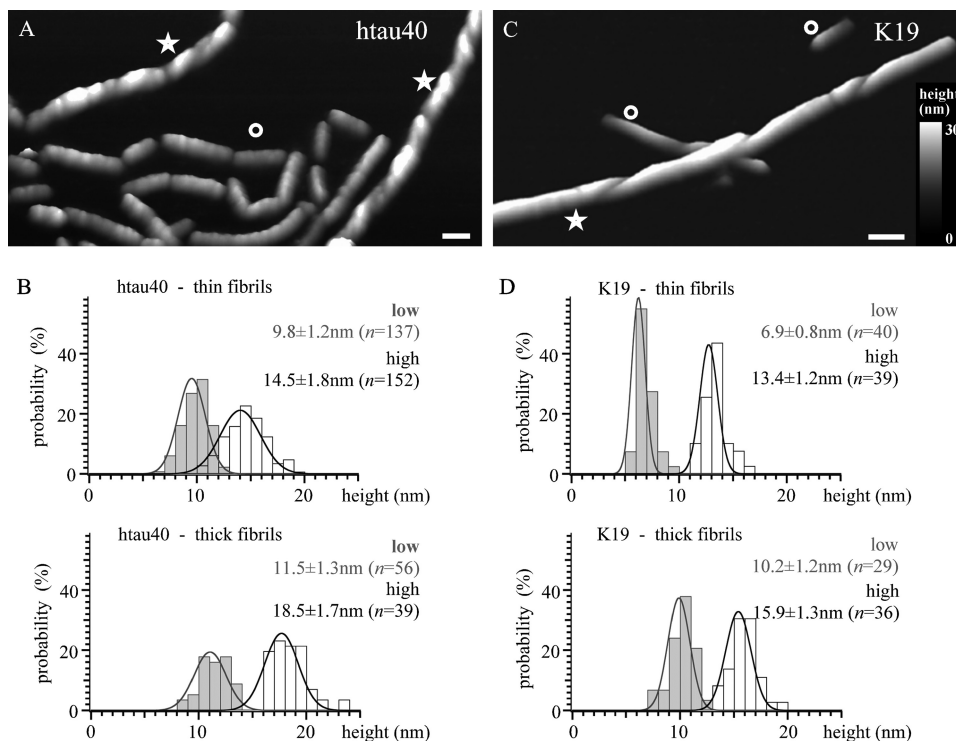
FIGURE 3. **Analysis of Tau fibril thickness.** Fibrils with a clear difference in thickness (height) coexist in the same preparation of hTau40 (*A*) and K19 (*C*). AFM topographs were taken to perform height measurements of thin (*A* and *C*, labeled ○) and thick fibrils (*A* and *C*, labeled ★) assembled from hTau40 (*B*) and K19 (*D*). The difference in height between thin and thick fibrils ranges from ~2 nm (lower heights) to ~4.5 nm (higher heights) for hTau40 fibrils and from ~2.5 nm (higher heights) to ~3 nm (lower heights) for K19 fibrils. Full color range corresponds to a vertical scale of 35 nm. Length of *scale bars* in *A* and *C* correspond to 50 nm.

AFM stylus had to be kept below 100 pN (Figs. 1–3). In the following experiments, we first imaged hTau40 fibrils at such minimal forces (Fig. 4). Then, we slightly increased the imaging forces to ~150–200 pN to apply mechanical stress to selected regions of Tau fibrils (force from *left-to-right* in Fig. 4, *A* and *B*). After this, the fibrils were re-imaged at minimal forces. The applied mechanical stress was sufficient to induce the stepwise disassembly of the fibrils into smaller fragments (Fig. 4, *arrowheads*). Other fibrils were simply displaced. High resolution topographs (Fig. 4, *D* and *E*) showed that the fragments of mechanically disassembled hTau40 fibrils were 9.0 ± 2.0 nm high ($n = 102$) (supplemental Fig. S4C) and remained connected by thread-like structures exhibiting heights of 2.6 ± 1.0 nm ($n = 74$). The lengths of the disassembled fragments were broadly distributed between 9 and 55 nm showing five preferred peaks around 14.9 ± 0.1, 21.3 ± 0.3, 26.2 ± 0.6, 36.0 ± 0.1, and 48.4 ± 1.5 nm ($n = 224$) (Fig. 4F). The shortest frag-

ment length (~15 nm) resembled the short periodicity of ~17 nm along the axis of the fibrils. The increments to longer fragments varied from 5 to 12 nm, for both hTau40 and K19, indicating similar mechanical constraints for both types of fibrils. Interestingly, sonication for ~10 min (120 Watt) prior to adsorption to mica induced structurally similar disassembly of Tau fibrils (data not shown). Such sonication-induced fragments could function as nucleation seeds for fibril re-assembly (32). However, chemical cross-linking with 0.5% glutaraldehyde prevented the mechanically induced disassembly of Tau fibrils even when applying much higher stressing forces (data not shown). Mechanically induced disassembly of Tau fibrils was observed for all Tau isoforms and occurred independently of ionic strength (up to 300 mM KCl or NaCl) and pH (from 5 to 9).
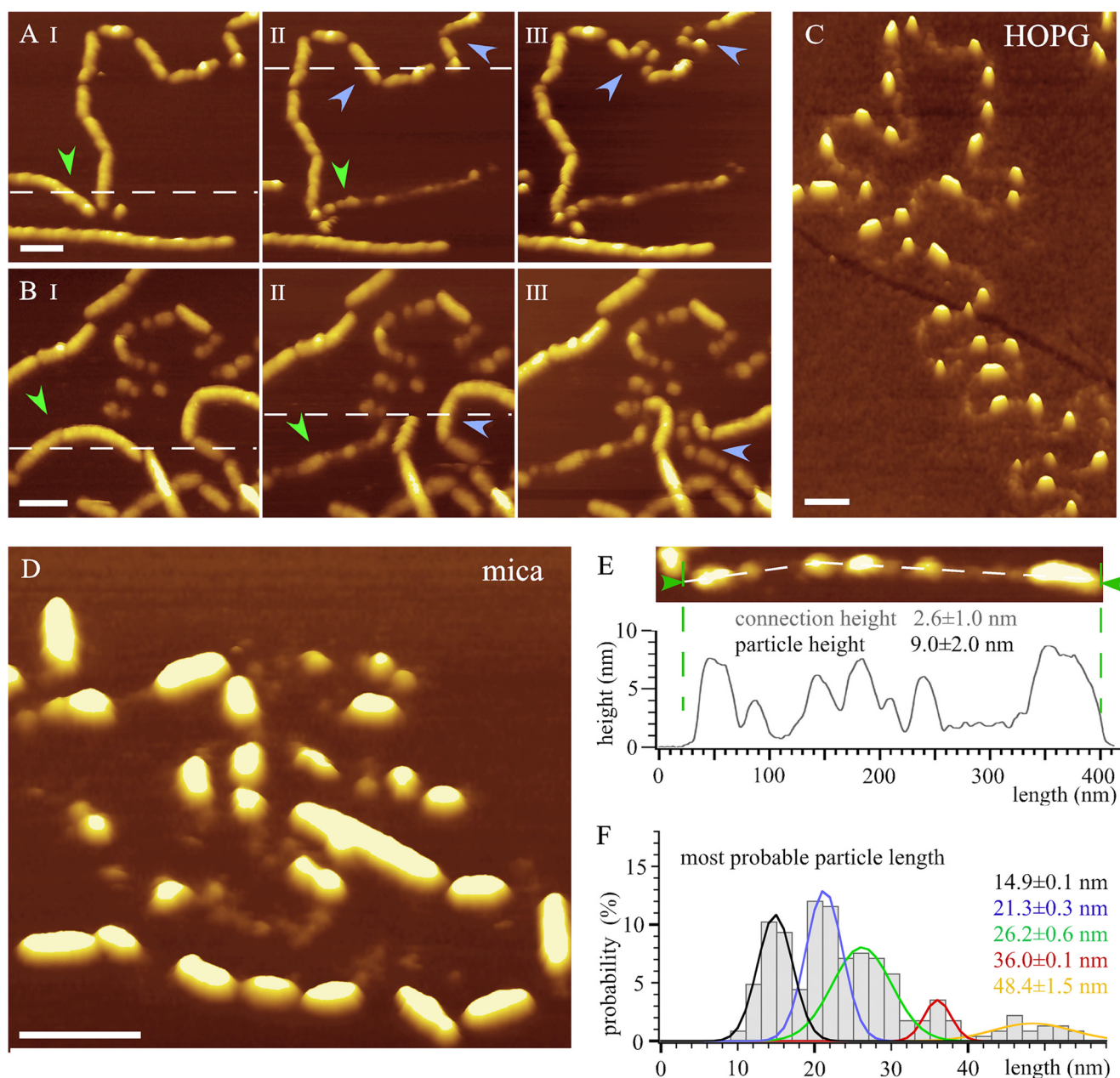
To mechanically disassemble thick Tau fibrils, we had to apply higher scanning forces (~300 pN). In most cases, these thick fibrils broke into ~200–500-nm-long fragments of thick Tau fibrils that showed sharp edges (supplemental Figs. S2H and S3K). Occasionally, mechanically stressed thick twisted Tau fibrils disassembled, similar to thin fibrils, into much smaller fragments. Our experiments showed that mechanical stress could induce the disassembly of Tau fibrils into shorter fragments. However, despite breakage, the fragments remained somehow connected by thread-like structures. But what were the interactions that hold the fragments in Tau fibrils together? We address this question and investigate interactions that contribute to Tau fibril stability below.

Hydrophobic and Electrostatic Interactions Stabilize Tau Fibrils—It has been proposed that the core of PHFs consists of stacked β-strands formed by the repeat domains of Tau (36) that are stabilized by hydrophobic interactions around the hexapeptide motifs (Fig. 1A), although the outer surface of Tau

FIGURE 2. **Morphologies of fibrils assembled from full-length Tau and repeat domain.** *A–F,* fibrils from hTau40. *G–M,* fibrils from the shortened Tau 3-repeat domain K19. With both Tau proteins, a variety of fibril morphologies can be observed by AFM. However, overall the collection of fibrillar structures is remarkably similar, despite the large size difference of hTau40 and K19 (441 *versus* 99 residues, respectively). There are thin straight fibrils (*A* and *B*, labeled ○), thin spiral or wave-like shapes (*A, D, E, H,* and *I,* labeled □), and thin fibrils with different degrees of internal twisting (*C, G, J, K,* and *L,* labeled △). Some fibrils are thicker (indicated by ★, *e.g. F* and *M*) than others. To discriminate thick and thin fibrils, their height was quantified from AFM topographs. The ratio of thick to thin fibrils (~20–75%) depends on the Tau protein and assembly conditions. Different twists can occur in the same fibril (*L*). Thin fibrils may appear as a stack of smaller subunits (*A,* green arrowheads, *B–E, H–J,* and *L,* with typical spacing of 15–20 nm). On top of this beaded substructure, thin fibrils can have an internal twist (*G,* purple arrowheads, *e.g. C* and *J*) of various periodicities. All thick fibrils show pronounced internal twisting (*e.g. A,* blue arrowheads, *B, F,* and *M*). Periodicities of hTau40 and K19 fibrils were obtained from Fourier transform spectra measured along the fibril axis and correspond to the maxima in the power spectrum (*asterisks*). *N,* Fourier transform spectrum obtained for a single thin hTau40 fibril, in this case showing a stack periodicity of 22 nm (*) and a twist periodicity of 77 nm (**). *O,* most probable periodicities for twisted thin ($n = 38$) and thick ($n = 12$) hTau40 fibrils and twisted thin ($n = 47$) and thick ($n = 20$) K19 fibrils were attained from Gaussian fits to periodicity distributions. The periodicities of stacked subunits in smooth thin fibrils of hTau40 ($n = 16$) and K19 ($n = 11$) were determined in the same way. AFM topographs were recorded in imaging buffer (10 mM Tris-HCl, pH 7.4, 50 mM KCl) and exhibit a full color range that corresponds to a vertical scale of 30 nm. Length scale bars equal 200 nm in *A* and *G* and 50 nm in *B–F* and *H–N*.

FIGURE 4. **Mechanically and chemically induced disassembly of Tau fibrils.** *A* and *B,* mechanical stress can induce the disassembly of hTau40 fibrils into smaller fragments. This phenomenon was observed for fibrils of every Tau protein when increasing the force applied to the AFM stylus to ∼150–200 pN. This disassembly emerges in the AFM fast scanning direction (*dashed horizontal lines* in topographs) where the lateral interaction forces between AFM stylus and fibril are highest. Repeatedly imaging the same surface area (*A, panels I–III,* and *B, panels I–III*) shows the consecutive fragmentation of hTau40 fibrils. Changes in fibril structure are indicated by *arrowheads* before and after fragmentation. *Green arrowheads* in *A* indicate the dislocation of a fibril accompanied by fragmentation and extension. *C,* spontaneous disassembly of hTau40 fibrils upon exposure to a hydrophobic surface (HOPG). As in the case of mechanical fragmentation, fibrils disassemble into smaller fragments typically 15–25 nm in length. *D* and *E,* high resolution AFM topographs of mechanically disassembled fibrils on mica highlight thread-like connections between the fragments. The cross-section plotted along a disassembled fibril (*E*) indicates a pronounced height difference between fragments (9.0 ± 2.0 nm; mean ± S.D.) and thread-like connections (2.6 ± 1.0 nm). *F,* histogram of fragment lengths (*n* = 224). The multimodal distribution shows three major peaks at 14.9, 21.3, and 26.2 nm (all maxima indicated on *right*). AFM topographs were recorded in imaging buffer and exhibit full color ranges that correspond to a vertical scale of 20 nm (*A* and *B*) or 10 nm (*C* and *E*). The length of all *scale bars* corresponds to 100 nm.

fibrils is largely charged or polar (37). The interaction of proteins with solid surfaces can induce conformational changes that destabilize the protein, often accompanied by a loss in activity (reviewed in Ref. 38). This is especially true for hydrophilic proteins adsorbed to hydrophobic surfaces, where the hydrophobic core of the native protein folds toward the hydrophobic support (39, 40) leading to malfunc-

tion and denaturation. We decided to investigate whether a similar effect would denature Tau fibrils when adsorbed to a hydrophobic surface. When adsorbing Tau fibrils in low salt (≤50 mM NaCl or KCl) to the hydrophobic surface of HOPG, the majority of fibrils spontaneously disassembled (Fig. 4C and supplemental Fig. S4B). This disassembly was similar to that observed upon applying mechanical stress. The disassem-

bled fibrils showed fragments that remained connected by thin thread-like chains having heights of 9.3 ± 2.3 nm ($n = 27$) and 1.5 ± 1.3 nm ($n = 21$), respectively (supplemental Fig. S4D). When the fibrils were exposed to HOPG for long times (>75 h), all fibrils disassembled, and the support was covered with a thin layer showing a height of 1.3 ± 0.2 nm ($n = 23$) (data not shown). Such fragmentation of Tau fibrils on HOPG was observed for full-length proteins and for repeat domain constructs at pH 7.4 at low ionic strength (≤ 50 mM NaCl or KCl) (Fig. 4C and supplemental Fig. S4, B–F). However, when increasing the electrolyte concentration to ≥ 200 mM KCl or NaCl, the fibrils stopped disassembling. By contrast, when adsorbed to hydrophilic mica, Tau fibrils were structurally stable for many hours (>72 h) in a broad pH range of 5–9, independently of the electrolyte composition and concentration. The disassembly of Tau fibrils was also inhibited when cross-linked by 0.5% glutaraldehyde before exposure to the hydrophobic support. Furthermore, coating the hydrophobic HOPG prior to fibril adsorption with either positively charged (poly-L-lysine), negatively charged (L-glutamate), or neutral polar (L-threonine) amino acids prevented Tau fibrils from disassembly (supplemental Fig. S4G). In the latter case, the fibril morphologies were similar to that of intact fibrils on mica and of fibrils that had been fixed with glutaraldehyde before adsorption. These observations suggest that the exposure of Tau fibrils to a hydrophobic environment competes with hydrophobic interactions that stabilize the fibril. If this competition of hydrophobic interactions is lost, the fibrils disassemble into smaller fragments.

DISCUSSION

Tau Fibrils Are Polymorphic but Show Common Properties— The observed polymorphism of Tau fibrils may resemble different ways of how Tau assembles into fibrils. The flexibility of the different fibril classes, as judged by their persistence length (supplemental Table S3), was found to be very similar to that observed for β-lactoglobulin amyloid fibrils (~ 1.6 μm) (41) and in the range of actin fibers (~ 15 μm) (42). We found that the persistence length of each fibril class, *i.e.* thin smooth, thin corrugated, and thick fibrils, remained unchanged for various buffer conditions and supporting surfaces. In addition the persistence length for each fibril class was the same among different Tau isoforms. These results, in combination with the rather high persistence length in the micromolar range, support the view that the different Tau fibrils resemble distinct, structurally well defined assemblies of low flexibility. Despite their rather large structural heterogeneity, Tau fibrils share common features. First, thick and thin fibrils exposed an ~ 17–19-nm periodicity. The protein mass per fibril length obtained from STEM measurements on purified unstained fibrils (63) suggested an average density of ~ 3.5 mol·nm^{-1} full-length hTau40 and ~ 4.5 mol·nm^{-1} in the fibrils. Accordingly, an ~ 17-nm subunit would consist of 17 nm·3.5 mol/nm ≈ 60 hTau40 molecules and 17 nm·4.5 mol/nm ≈ 77 K19 molecules. Such dimensions of a subunit seem reasonable when compared with oligomers of other amyloid-forming proteins like Aβ (~ 40 molecules Aβ (43)) or the prion protein (14–28 molecules PrP^{sc} (44)). Second, all thin and thick fibrils showed the same minimal height (thick-

ness) of ~ 9–11 nm. Third, all fibrils could disassemble into smaller fragments that remained connected by a thread-like structure. Fourth, hydrophobic interactions seem to play a major role for the integrity of the fibrils, regardless of the given Tau isoform and the presence of the N and C termini. Fifth, electrostatic interactions could be tuned to compensate destabilizing hydrophobic interactions. All fibrils assembled from Tau isoforms and constructs investigated in this work showed these features, suggesting that the assembly of Tau into differently shaped fibrils may follow common mechanisms.

To generate different fibril structures, different assembly mechanisms may coexist for the same Tau protein. Because different Tau isoforms and constructs form a similar polymorphic set of fibril structures that all contain β-stacked Tau repeat domains (45–47), it may be speculated that all Tau protein assemblies share common structural similarities. For the coexisting polymorphic fibril shapes one could think of different explanations. On the one hand, a variation in the β-stacking of Tau molecules could cause a set of different subunits, each of which assemble into a different fibril structure. Otherwise, Tau may assemble into structurally similar subunits that organize differently to form polymorphic fibril shapes. For MTs, it is known that minute differences in the tubulin binding angles result in different curvature of their protofilaments (48–50). Applying this principle to Tau fibrils, small variations in the Tau subunit conformations or interactions could result in fibrils that have different curvatures in their solution state, which, in turn, appear as different twisting degrees when adsorbed to a flat surface. For example, a noncurved flat ribbon would appear as a thin smooth fibril on the surface, although a slightly curved flat ribbon would adsorb as a thin corrugated fibril. Thick corrugated fibrils could be described as fibrils that are highly and regularly curved in solution and twist even after adsorption to the surface. Although all Tau isoforms and constructs showed a similar structural polymorphism, the frequency at which certain fibril morphologies were populated was characteristic for each Tau variant (supplemental Table S1). One may speculate that the structural polymorphism of Tau fibrils is related to the properties of the Tau protein (10). Several examples for different fibril morphologies were reported for Aβ and other amyloid fibrils (51–55). Similarly to Tau fibrils, these amyloid fibrils differ in twist and bending. Tau fibrils can also show differences in their crossover repeats, namely straight fibrils and PHFs, that can coexist in *in vitro* fibril preparations of different Tau proteins (56, 57). It has been discussed that this structural variability could reflect different protein assemblies. When AFM imaging fibrils of the FTDP-17 (frontotemporal dementia and parkinsonism linked to chromosome 17)-related deletion mutants (supplemental Fig. S3), hTau40ΔK280 and K18ΔK280, fibril morphologies and dimensions were similar to wild-type hTau40. However, the greater β-sheet propensity of the ΔK280 mutation increases the Tau aggregation rate (58) and changes the ratio of smooth and twisted thin fibrils (supplemental Fig. S3 and Table S1). For example, K18 assembles predominantly into thin smooth fibrils, but K18ΔK280 assembles into both thin smooth and thin twisted fibrils. Additionally, the formation of thick twisted fibrils is largely enhanced for K18ΔK280 (50% thick fibrils, see

supplemental Table S1) compared with wild-type K18 (20% thick fibrils). These alterations in the fibril morphology distributions are less pronounced when comparing hTau40 with hTau40ΔK280 (supplemental Table S1). From these results, it may be assumed that certain fibril morphologies contain higher β-sheet percentage than others. To test this hypothesis would require selecting Tau fibrils by their morphology and analyzing their specific β-sheet content by other methods, *i.e.* circular dichroism.

Thin and Thick Tau Fibrils, Flat and Twisted Ribbons?—One critical parameter to distinguish fibrils of different morphological classes is to measure their height in AFM topographs. It may be concluded that thick fibrils represent PHFs. Two alternative PHF models have been discussed in the literature. One model assumes a single flat ribbon structure with an internal twist around the fibril axis (59–61). The other model suggests two protofibrils twisted around each other, hence the name paired helical (13, 16, 17). The coexistence of thin and thick Tau fibrils is suggestive of the interpretation that PHFs consist of two strands. However, in our high resolution AFM topographs, the majority of thick fibrils (~95%) do not expose characteristic substructures that could be assigned to two smaller fibrils. In addition, a two-stranded fibril should show a much lower flexibility than single protofibrils. In contrast, the persistence length of thick fibrils was found to be slightly lower than that of thin smooth or thin twisted fibrils (supplemental Table S3), which indicates a higher flexibility of the thick fibrils. When breaking upon adsorption to a surface or mechanical stress, Tau fibrils never showed double ends as it would be expected when breaking up a two-stranded fibril. Moreover, when mechanically stressed, thin and thick fibrils disassembled into fragments that were connected by one thread-like chain. We therefore conclude that these thick fibrils are not composed of two individual fibrils.

Thick fibrils showed height corrugations ranging from ~11 to 19 nm (hTau40) and from ~10 to 16 nm (K19). The mean thin fibril height was ~11 nm for hTau40 and ~9 nm for K19. Thus, thick and thin fibrils show the same minimum height of ~9–11 nm. The thin fibrils clearly suggest that Tau assembles into flat ribbons. Apparently, these Tau ribbons can be corrugated, and in some cases we have observed the transition of a smooth thin ribbon into a corrugated thin ribbon. However, such a thin Tau ribbon, if twisted around its longitudinal axis, could easily form a thick twisted fibril. Thus, the polymorphic Tau fibrils would expose the same basic architecture of a ribbon providing a consistent explanation of the observed structures. Small differences in the interactions between the Tau subunits may induce changes in their packaging and lead either to flat, slightly corrugated, or twisted Tau ribbons or fibrils. In summary, our data suggest that the appearance of thin and thick Tau fibrils by AFM is based on similar ribbon-like structures. The periodicity and corrugation observed in the majority of thick Tau fibrils is likely to be explained by a twisted ribbon-like fibril (59, 62). If this twisted fibril would be stretched out it would show a similar height and width as a thin Tau fibril (reminiscent of a coiled telephone cord after stretching). The height and width of such a flat "thin" Tau ribbon would be ~9–11 and ~15–18 nm, respectively.

Surprisingly, the dimensions of the ribbons are nearly independent of the Tau protein from which it was assembled, even though the Tau proteins differed more than 4-fold in mass. Possible explanations are discussed below.

Fuzzy Coat—It is widely accepted that Tau assembly into fibrils is mediated by interactions of β-strands in their repeat domains (45, 58). However, the structure of the Tau domains outside the repeats in aggregated fibrils remains an open question. Limited digestion of PHFs removes these domains, leaving behind a PHF core built essentially from the repeat domains (60, 63). Thus, it has been suggested that the Tau termini form a fuzzy coat surrounding the PHF (20). However, the nature of this coat has remained elusive. We hoped to shed light on this issue by comparing Tau fibrils with different domain compositions. For example, in the case of full-length Tau, the repeat domain includes ~27% of the mass (~120/441 aa, see Fig. 1*A*), so that the cross-section dimensions of fibrils from the full-length protein should be almost four times larger than fibers from the repeat domain only. However, our topographs show that both full-length and short Tau constructs assemble into structurally similar thick and thin fibrils. The height difference between thick fibrils from hTau40 and K18 was only ~2 nm (supplemental Table S1) and even less when comparing thick fibrils of hTau23 *versus* K19 and hTau40ΔK280 *versus* K18ΔK280. Such small differences are in agreement with electron microscopy data showing the width difference between fibrils assembled from hTau40 and K18 is minute (1–2 nm) and poorly detectable (31). These differences in AFM height and corresponding EM width are too small to account for the "missing mass" of the Tau terminal domains. From structural studies, the Tau terminal domains are described as protruding from the fibril surface like a polymer brush (21, 64). This model is supported by AFM force spectroscopy measurements on a brush of Tau molecules that were projecting away from their anchoring surface (65). In this case, repulsive electrostatic forces between the protruding termini and the approaching AFM tip could be detected, which decreased with increasing salt concentrations in the surrounding medium. This is reminiscent with the behavior of a brush consisting of densely packed, unstructured poly-electrolyte chains.

The conformation and thus extension of surface-immobilized unstructured polypeptides in solution largely depends on their surface density (reviewed in Ref. 66). A dense packing enhances the polypeptide extension to form a polymer brush, although separation of neighboring polypeptides, large enough to prevent chain interactions, results in chain collapse onto the surface (67). According to this model of a polymer brush, there are different scenarios to explain how the unstructured Tau termini may establish the fuzzy coat of Tau fibrils.(i) A high packing density of Tau on the fibril surface would force their termini to fully protrude. In this case, the contribution of the termini to the fibril thickness would be that of extended polypeptide chains and much different for full-length Tau and terminally truncated Tau constructs. Assuming that every peptide of the N (~240 aa) and C termini (~70 aa) contributes ~0.3 nm to the polypeptide length, fibrils assembled from hTau40 would show a reasonably thick coat of ~20–70 nm. (ii) A medium or lower packing density of Tau molecules would allow

their termini to collapse onto the fibril surface. The thickness of such a collapsed layer would be in the range of the radius of gyration of the polypeptide in solution, R_g, and can be estimated using the freely jointed chain model for flexible polymers (68). For proteins, each peptide bond can be modeled as one subunit with a length of ~0.4 nm, and a Kuhn length b of 0.4–0.8 nm describes the elastic behavior of the polymer (69, 70). The height of an isolated unstructured collapsed polypeptide is then given by $H_{col} \approx b \cdot N^{3/5}$ (67), where N is the number of peptides in the peptide chain. A layer of collapsed Tau N-terminal domain (~240 aa) and C-terminal domain (~70 aa) on the fibril surface would show minimum heights of $H_{col, Nterm} \approx 0.4$ nm$\cdot 243^{3/5} \approx 10.8$ nm and $H_{col, Cterm} \approx 0.4$ nm$\cdot 69^{3/5} \approx 5.1$ nm, respectively. These values are much closer to the ~1–2 nm coat thickness detected in AFM and EM than the contribution expected for an extended polymer brush. However, these estimates are valid for isolated polymer chains on a surface and thus still underestimate the thickness of the polymer brush that would be generated by many Tau proteins assembled into a fibril (assuming ~4 Tau molecules per nm fibril length (63)). (iii) The third scenario assumes that the Tau termini protrude from the fibril surface at a similar medium to low density but show a stretched out conformation. In this case, the termini would form a loose but extended hydrophilic polymer brush. Such a soft brush may be too flexible to be imaged by AFM and stained for EM imaging. It has been assumed that during AFM imaging, loose polymer brushes may escape the AFM stylus (reviewed in Ref. 66). For the flexible termini of full-length Tau bound to MTs, a loose polymer brush model with a comparable low apparent polymer chain extension has been proposed (22). Tau stabilizes MTs by binding to their outer surface via several regions in the repeat domain, although the termini protrude brush-like (71), similar to the fuzzy coat that is thought to surround PHFs. AFM imaging of MTs that were coated with Tau molecules revealed a continuous ~1 nm thick layer on their outer surface (72), which indicates that the bound repeat domain of Tau but not the loose terminal polymer brush was detected. Accordingly, this phenomenon may explain the surprisingly small contribution of the fuzzy coat to the fibril diameter of ~2 nm. In conclusion, our data suggest that unstructured Tau termini protrude from the fibril surface into the surrounding medium to form a loose fur-like brush, which explains the nature of the so-called fuzzy coat.

Stability of Tau Fibrils—Mechanical as well as chemical stress induces Tau fibril disassembly into fragments that remain somehow connected by thread-like chains. Whereas thin Tau fibrils already disassembled at scanning forces of ~150–200 pN, thicker Tau fibrils required higher scanning forces of ~300 pN to disassemble. Thereby, thick fibrils tended to break into shorter fibrils, even though their flexibility was slightly higher compared with thin twisted or smooth fibrils. However, these fragments disassembled from thick fibrils could further fragment into small fragments that were connected by thread-like chains, such as observed for the disassembly of thin fibrils. Exposure to a hydrophobic surface induced spontaneous disassembly of Tau fibrils into "pearl chains." Thick fibrils first broke into smaller pieces that then further fragmented such as observed for thin fibrils. For adsorption times of ~30 min, the

number of Tau fibrils remaining intact was higher for thick ones (supplemental Fig. S4F, *arrowheads*). Upon exposure to the hydrophobic HOPG surface over longer times (>75 h), all thin and thick fibrils completely disassembled into thread-like chains. These results indicate that thicker Tau fibrils are more stable than the thinner ones but that the disassembling structures are similar. Furthermore, it can be concluded that chemically and mechanically induced disassembly of Tau fibrils follows similar ways and produces distinct structural entities.

Currently, the modes of toxicity of different assembly forms, namely monomers, oligomers, and fibrils, as well as their impact on *in vivo* aggregation are extensively discussed for Tau (73) and for other amyloidic proteins like the prion protein and amyloid-β (reviewed in Ref. 74). Recently, it was shown that a human mutant Tau domain, which is highly prone to aggregate, can induce the coaggregation of endogenous wild-type Tau in mice (75). Oligomeric Tau aggregates, when added to the culture medium, become endocytosed and then function as nucleation seeds for intracellular aggregation of endogenous Tau in cultured neural C17 cells (76). So far, no such propagation of aggregation on cells was observed for intact Tau fibrils. However, the mechanically or chemically induced fragmentation of fibrils into oligomers as we show here *in vitro* could also reflect a way to generate nucleation seeds for *in vivo* aggregation of Tau proteins.

Fragments and Thread-like Chains of Thick and Thin Fibrils Look Similar—The fragments have a size of ~15 nm (length) × ~9 nm (height) × 15–18 nm (width) and therefore are too large to reflect single Tau molecules. Therefore, they must reflect larger assemblies of Tau molecules. It may be speculated whether the thread-like connectors could be Tau termini. At this stage, we cannot state how many Tau molecules make up one oligomeric Tau fragment and how many termini may be required to form the thread-like connections between the fragments.

The current structural model of PHFs suggests a partial hydrophobic core of stacked β-strands and a mostly charged hydrophilic outer surface (21). From an entropic point of view, a protein exposed to a sufficiently hydrophobic surface unfolds and attaches its formerly hydrophobic interior to the surface (40). This unfolding minimizes the hydrophobic surface exposed to water. Such denaturation of proteins interacting with a hydrophobic surface is well known (77). Our experiments show that exposure to hydrophobic surfaces can be easily used to destabilize and disassemble Tau fibrils. However, coating the hydrophobic surface with polar or charged molecules inhibited the spontaneous fragmentation of Tau fibrils. We also observed that increasing the electrolyte concentration prevented Tau fibrils from destabilizing and disassembling when exposed to hydrophobic surfaces. With increasing electrolyte concentrations, both attractive and repulsive electrostatic interactions between surface charges become compensated by counter ions (78). Hydrophobic interactions remain mainly unaffected by the electrolyte. The fact that compensating of electrostatic interactions prevents Tau fibrils from hydrophobically induced denaturation suggests that the electrostatic interactions rather tend to destabilize Tau fibrils (79, 80). Such electrostatic contributions would not be restrained to the fuzzy

coat of the fibril surface because we observe the same phenomenon for full-length hTau40 and the terminally truncated Tau constructs. On the other hand, polyelectrolyte brushes extend in low salt conditions and collapse in environments with increased salt concentration (81). This reduction in chain extension was also observed for surface-immobilized soluble Tau by AFM (65). A collapse of the Tau termini in the fuzzy coat would increase the charge density on the fibril surface, which may be the mechanism behind the protection of the Tau fibrils against hydrophobic induced disassembly at higher and physiological relevant salt concentrations. The protective effect of the surface charge density that is generated by coating the hydrophobic HOPG surface with charged amino acids would strengthen this hypothesis. To examine the critical density of such a protective "charge coat" and its actual relevance for protecting the fibrils from disassembling is an interesting issue for prospective studies. However, all these results emphasize the key role of hydrophobic interactions to maintain the integrity of Tau fibrils. Stretching this idea further, chemically induced fibril destruction could also play a role *in vivo*. Following the suggested nucleation-elongation pathway of Tau aggregation (82), the production of smaller oligomeric aggregates, which can function as nucleation seeds (32) and can be transferred to other cells by unknown intermediate steps (83), may be a trigger of Tau aggregation in AD or other Tauopathy brains. In this context it could be of greatest interest to examine the physiological conditions that destabilize Tau fibrils and result in their fragmentation.

REFERENCES

1. Ballatore, C., Lee, V. M., and Trojanowski, J. Q. (2007) *Nat. Rev. Neurosci.* **8,** 663–672
2. Finder, V. H., and Glockshuber, R. (2007) *Neurodegener Dis.* **4,** 13–27
3. Iqbal, K., Liu, F., Gong, C. X., Alonso Adel, C., and Grundke-Iqbal, I. (2009) *Acta Neuropathol.* **118,** 53–69
4. Krebs, M. R., Domike, K. R., and Donald, A. M. (2009) *Biochem. Soc. Trans.* **37,** 682–686
5. Mandelkow, E., von Bergen, M., Biernat, J., and Mandelkow, E. M. (2007) *Brain Pathol.* **17,** 83–90
6. Minati, L., Edginton, T., Bruzzone, M. G., and Giaccone, G. (2009) *Am. J. Alzheimers Dis. Other Demen.* **24,** 95–121
7. Binder, L. I., Guillozet-Bongaarts, A. L., Garcia-Sierra, F., and Berry, R. W. (2005) *Biochim. Biophys. Acta* **1739,** 216–223
8. Bulic, B., Pickhardt, M., Schmidt, B., Mandelkow, E. M., Waldmann, H., and Mandelkow, E. (2009) *Angew. Chem. Int. Ed. Engl.* **48,** 1740–1752
9. Nelson, R., Sawaya, M. R., Balbirnie, M., Madsen, A. Ø., Riekel, C., Grothe, R., and Eisenberg, D. (2005) *Nature* **435,** 773–778
10. Jeganathan, S., von Bergen, M., Mandelkow, E. M., and Mandelkow, E. (2008) *Biochemistry* **47,** 10526–10539
11. Mukrasch, M. D., Biernat, J., von Bergen, M., Griesinger, C., Mandelkow, E., and Zweckstetter, M. (2005) *J. Biol. Chem.* **280,** 24978–24986
12. von Bergen, M., Barghorn, S., Biernat, J., Mandelkow, E. M., and Mandelkow, E. (2005) *Biochim. Biophys. Acta* **1739,** 158–166
13. Kidd, M. (1963) *Nature* **197,** 192–193
14. Crowther, R. A. (1991) *Proc. Natl. Acad. Sci. U.S.A.* **88,** 2288–2292
15. Ksiezak-Reding, H., Morgan, K., Mattiace, L. A., Davies, P., Liu, W. K.,
16. Yen, S. H., Weidenheim, K., and Dickson, D. W. (1994) *Am. J. Pathol.* **145,** 1496–1508
16. Pollanen, M. S., Markiewicz, P., and Goh, M. C. (1997) *J. Neuropathol. Exp. Neurol.* **56,** 79–85
17. Pollanen, M. S., Markiewicz, P., Bergeron, C., and Goh, M. C. (1994) *Am. J. Pathol.* **144,** 869–873
18. Moreno-Herrero, F., Pérez, M., Baró, A. M., and Avila, J. (2004) *Biophys. J.* **86,** 517–525
19. Allen, M. J., Hud, N. V., Balooch, M., Tench, R. J., Siekhaus, W. J., and Balhorn, R. (1992) *Ultramicroscopy* **42,** 1095–1100
20. Wischik, C. M., Novak, M., Thøgersen, H. C., Edwards, P. C., Runswick, M. J., Jakes, R., Walker, J. E., Milstein, C., Roth, M., and Klug, A. (1988) *Proc. Natl. Acad. Sci. U.S.A.* **85,** 4506–4510
21. Barghorn, S., Davies, P., and Mandelkow, E. (2004) *Biochemistry* **43,** 1694–1703
22. Santarella, R. A., Skiniotis, G., Goldie, K. N., Tittmann, P., Gross, H., Mandelkow, E. M., Mandelkow, E., and Hoenger, A. (2004) *J. Mol. Biol.* **339,** 539–553
23. Engel, A., and Müller, D. J. (2000) *Nat. Struct. Biol.* **7,** 715–718
24. Allison, D. P., Hinterdorfer, P., and Han, W. (2002) *Curr. Opin. Biotechnol.* **13,** 47–51
25. Müller, D. J., Sapra, K. T., Scheuring, S., Kedrov, A., Frederix, P. L., Fotiadis, D., and Engel, A. (2006) *Curr. Opin. Struct. Biol.* **16,** 489–495
26. Moreno-Herrero, F., Seidel, R., Johnson, S. M., Fire, A., and Dekker, N. H. (2006) *Nucleic Acids Res.* **34,** 3057–3066
27. Rivetti, C., and Codeluppi, S. (2001) *Ultramicroscopy* **87,** 55–66
28. Goedert, M., Jakes, R., Spillantini, M. G., Hasegawa, M., Smith, M. J., and Crowther, R. A. (1996) *Nature* **383,** 550–553
29. Pérez, M., Valpuesta, J. M., Medina, M., Montejo de Garcini, E., and Avila, J. (1996) *J. Neurochem.* **67,** 1183–1190
30. van Swieten, J. C., Bronner, I. F., Azmani, A., Severijnen, L. A., Kamphorst, W., Ravid, R., Rizzu, P., Willemsen, R., and Heutink, P. (2007) *J. Neuropathol. Exp. Neurol.* **66,** 17–25
31. Barghorn, S., Zheng-Fischhöfer, Q., Ackmann, M., Biernat, J., von Bergen, M., Mandelkow, E. M., and Mandelkow, E. (2000) *Biochemistry* **39,** 11714–11721
32. Friedhoff, P., von Bergen, M., Mandelkow, E. M., Davies, P., and Mandelkow, E. (1998) *Proc. Natl. Acad. Sci. U.S.A.* **95,** 15712–15717
33. Engel, A., Schoenenberger, C. A., and Müller, D. J. (1997) *Curr. Opin. Struct. Biol.* **7,** 279–284
34. Hansma, H. G., and Hoh, J. H. (1994) *Annu. Rev. Biophys. Biomol. Struct.* **23,** 115–139
35. Moreno-Herrero, F., Valpuesta, J. M., Pérez, M., Colchero, J., Barö, A. M., Avila, J., and Montejo De Garcini, E. (2001) *J. Alzheimers Dis.* **3,** 443–451
36. von Bergen, M., Friedhoff, P., Biernat, J., Heberle, J., Mandelkow, E. M., and Mandelkow, E. (2000) *Proc. Natl. Acad. Sci. U.S.A.* **97,** 5129–5134
37. Andronesi, O. C., von Bergen, M., Biernat, J., Seidel, K., Griesinger, C., Mandelkow, E., and Baldus, M. (2008) *J. Am. Chem. Soc.* **130,** 5922–5928
38. Nakanishi, K., Sakiyama, T., and Imamura, K. (2001) *J. Biosci. Bioeng.* **91,** 233–244
39. Kauzmann, W. (1959) *Adv. Protein Chem.* **14,** 1–63
40. Meyer, E. E., Rosenberg, K. J., and Israelachvili, J. (2006) *Proc. Natl. Acad. Sci. U.S.A.* **103,** 15739–15746
41. Sagis, L. M., Veerman, C., and van der Linden, E. (2004) *Langmuir* **20,** 924–927
42. Yanagida, T., Nakase, M., Nishiyama, K., and Oosawa, F. (1984) *Nature* **307,** 58–60
43. Orte, A., Birkett, N. R., Clarke, R. W., Devlin, G. L., Dobson, C. M., and Klenerman, D. (2008) *Proc. Natl. Acad. Sci. U.S.A.* **105,** 14424–14429
44. Silveira, J. R., Raymond, G. J., Hughson, A. G., Race, R. E., Sim, V. L., Hayes, S. F., and Caughey, B. (2005) *Nature* **437,** 257–261
45. Berriman, J., Serpell, L. C., Oberg, K. A., Fink, A. L., Goedert, M., and Crowther, R. A. (2003) *Proc. Natl. Acad. Sci. U.S.A.* **100,** 9034–9038
46. Goux, W. J., Kopplin, L., Nguyen, A. D., Leak, K., Rutkofsky, M., Shanmuganandam, V. D., Sharma, D., Inouye, H., and Kirschner, D. A. (2004) *J. Biol. Chem.* **279,** 26868–26875
47. Skrabana, R., Sevcik, J., and Novak, M. (2006) *Cell. Mol. Neurobiol.* **26,** 1085–1097

48. Gigant, B., Curmi, P. A., Martin-Barbey, C., Charbaut, E., Lachkar, S., Lebeau, L., Siavoshian, S., Sobel, A., and Knossow, M. (2000) *Cell* **102,** 809–816

49. Mandelkow, E. M., Mandelkow, E., and Milligan, R. A. (1991) *J. Cell Biol.* **114,** 977–991

50. Nogales, E., Wolf, S. G., and Downing, K. H. (1998) *Nature* **391,** 199–203

51. Fändrich, M., Meinhardt, J., and Grigorieff, N. (2009) *Prion* **3,** 89–93

52. Meinhardt, J., Sachse, C., Hortschansky, P., Grigorieff, N., and Fändrich, M. (2009) *J. Mol. Biol.* **386,** 869–877

53. Buée, L., and Delacourte, A. (1999) *Brain Pathol.* **9,** 681–693

54. Paravastu, A. K., Leapman, R. D., Yau, W. M., and Tycko, R. (2008) *Proc. Natl. Acad. Sci. U.S.A.* **105,** 18349–18354

55. Stromer, T., and Serpell, L. C. (2005) *Microsc. Res. Tech.* **67,** 210–217

56. Frost, B., Ollesch, J., Wille, H., and Diamond, M. I. (2009) *J. Biol. Chem.* **284,** 3546–3551

57. Kato, S., and Nakamura, H. (1990) *Acta Neuropathol.* **81,** 125–129

58. von Bergen, M., Barghorn, S., Li, L., Marx, A., Biernat, J., Mandelkow, E. M., and Mandelkow, E. (2001) *J. Biol. Chem.* **276,** 48165–48174

59. Ruben, G. C., Wang, J. Z., Iqbal, K., and Grundke-Iqbal, I. (2005) *Microsc. Res. Tech.* **67,** 175–195

60. Wischik, C. M., Novak, M., Edwards, P. C., Klug, A., Tichelaar, W., and Crowther, R. A. (1988) *Proc. Natl. Acad. Sci. U.S.A.* **85,** 4884–4888

61. Crowther, R. A. (1990) *Biochim. Biophys. Acta* **1096,** 1–9

62. Wischik, C. M., Crowther, R. A., Stewart, M., and Roth, M. (1985) *J. Cell Biol.* **100,** 1905–1912

63. von Bergen, M., Barghorn, S., Müller, S. A., Pickhardt, M., Biernat, J., Mandelkow, E. M., Davies, P., Aebi, U., and Mandelkow, E. (2006) *Biochemistry* **45,** 6446–6457

64. Dickson, D. W., Ksiezak-Reding, H., Liu, W. K., Davies, P., Crowe, A., and Yen, S. H. (1992) *Acta Neuropathol.* **84,** 596–605

65. Mukhopadhyay, R., and Hoh, J. H. (2001) *FEBS Lett.* **505,** 374–378

66. Bright, J. N., Woolf, T. B., and Hoh, J. H. (2001) *Prog. Biophys. Mol. Biol.* **76,** 131–173

67. de Gennes, P. G. (1980) *Macromolecules* **13,** 1069

68. Flory, P. J. (1969) *Statistical Mechanics of Chain Molecules,* pp. 432, Interscience Publisher, New York

69. Oesterhelt, F., Rief, M., and Gaub, H. E. (1999) *New J. Phys.* **1,** 6.1–6.11

70. Su, T., and Purohit, P. K. (2009) *Acta Biomater.* **5,** 1855–1863

71. Mukrasch, M. D., von Bergen, M., Biernat, J., Fischer, D., Griesinger, C., Mandelkow, E., and Zweckstetter, M. (2007) *J. Biol. Chem.* **282,** 12230–12239

72. Schaap, I. A., Hoffmann, B., Carrasco, C., Merkel, R., and Schmidt, C. F. (2007) *J. Struct. Biol.* **158,** 282–292

73. Congdon, E. E., and Duff, K. E. (2008) *J. Alzheimers Dis.* **14,** 453–457

74. Krammer, C., Schätzl, H. M., and Vorberg, I. (2009) *Prion* **3,** 206–212

75. Sydow, A., and Mandelkow, E. M. (2010) *Neurodegener. Dis.* **7,** 28–31

76. Frost, B., Jacks, R. L., and Diamond, M. I. (2009) *J. Biol. Chem.* **284,** 12845–12852

77. Gray, J. J. (2004) *Curr. Opin. Struct. Biol.* **14,** 110–115

78. Leckband, D., and Israelachvili, J. (2001) *Q. Rev. Biophys.* **34,** 105–267

79. Pace, C. N., Shirley, B. A., McNutt, M., and Gajiwala, K. (1996) *FASEB J.* **10,** 75–83

80. Lins, L., and Brasseur, R. (1995) *FASEB J.* **9,** 535–540

81. Moya, S., Azzaroni, O., Farhan, T., Osborne, V. L., and Huck, W. T. (2005) *Angew. Chem. Int. Ed. Engl.* **44,** 4578–4581

82. Congdon, E. E., Kim, S., Bonchak, J., Songrug, T., Matzavinos, A., and Kuret, J. (2008) *J. Biol. Chem.* **283,** 13806–13816

83. Brundin, P., Melki, R., and Kopito, R. (2010) *Nat. Rev. Mol. Cell Biol.* **11,** 301–307

Proline-directed Pseudo-phosphorylation at AT8 and PHF1 Epitopes Induces a Compaction of the Paperclip Folding of Tau and Generates a Pathological (MC-1) Conformation*[S]

Sadasivam Jeganathan, Antje Hascher[1]**, Subashchandrabose Chinnathambi, Jacek Biernat, Eva-Maria Mandelkow, and Eckhard Mandelkow**[2]

From the Max Planck Unit for Structural Molecular Biology, Notkestrasse 85, D-22607 Hamburg, Germany

Tau, a neuronal microtubule-associated protein that aggregates in Alzheimer disease is a natively unfolded protein. In solution, Tau adopts a "paperclip" conformation, whereby the N- and C-terminal domains approach each other and the repeat domain (Jeganathan, S., von Bergen, M., Brutlach, H., Steinhoff, H. J., and Mandelkow, E. (2006) *Biochemistry* 45, 2283–2293). In AD, Tau is in a hyperphosphorylated state. The consequences for microtubule binding or aggregation are a matter of debate. We therefore tested whether phosphorylation alters the conformation of Tau. To avoid the ambiguities of heterogeneous phosphorylation we cloned "pseudo-phosphorylation" mutants of Tau where combinations of Ser or Thr residues were converted into Glu. These mutations were combined with FRET pairs inserted in different locations to allow distance measurements. The results show that the paperclip conformation becomes tighter or looser, depending on the pseudo-phosphorylation state. In particular, pseudo-phosphorylation at the epitope of the diagnostic antibody AT8* (S199E + S202E + T205E) moves the N-terminal domain away from the C-terminal domain. Pseudo-phosphorylation at the PHF1 epitope (S396E + S404E) moves the C-terminal domain away from the repeat domain. In both cases the paperclip conformation is opened up. By contrast, the combination of AT8* and PHF1 sites leads to compaction of the paperclip, such that the N-terminus approaches the repeat domain. The compaction becomes even stronger by combining pseudo-phosphorylated AT8*, AT100, and PHF1 epitopes. This is accompanied by a strong increase in the reaction with conformation-dependent antibody MC1, suggesting the generation of a pathological conformation characteristic for Tau in AD. Furthermore, the compact paperclip conformation enhances the aggregation to paired helical filaments but has little influence on microtubule interactions. The data provide a framework for the global folding of Tau dependent on proline-directed phosphorylation in the domains flanking the repeats and the consequences for pathological properties of Tau.

Microtubules that serve as the tracks for motor proteins are important for the intracellular transport of vesicles, organelles, and protein complexes by motor proteins (2, 3). Microtubule dynamics are modulated by microtubule-associated proteins that bind to the surface of microtubules; among these, Tau protein is one of the major microtubule-associated proteins in neurons (4, 5). Its expression is strongly up-regulated during neuronal development to promote the generation of cell processes and to establish cell polarity (6). During this phase, Tau becomes sorted into the axon, and it diversifies into 6 different isoforms by alternative splicing (7, 8). In Alzheimer disease, Tau becomes hyperphosphorylated, missorted into the somatodendritic compartment, and aggregates into neurofibrillary tangles (9).

The numerous phosphorylation sites of Tau (10) can be broadly subdivided into three classes: (i) SP/TP motifs in the flanking regions of the repeat domain are targets of proline-directed kinases such as glycogen synthase kinase3β (11, 12), cyclin-dependent kinase 5 (CDK5) (13), or mitogen-activated kinase and its relatives (14). (ii) KXGS motifs in repeats are targets of non-proline directed kinases, such as MARK (15), SAD kinase (16), or PKA (17). (iii) Tyrosine residues at Tyr-18 and Tyr-394 are targets of Src family kinases such as fyn and c-Abl (18, 19). Phosphorylation at SP/TP motifs has only a moderate influence on Tau-microtubule interactions but is up-regulated in AD[3] and other tauopathies (3, 20). This characteristic feature can be recognized by various diagnostic antibodies (3, 21). Phosphorylation by certain non-proline directed kinases (*e.g.* by MARK or SADK at the KXGS motifs of the repeat domain, or Ser-214 by PKA) results in a strong reduction of the ability of Tau to bind to microtubules (15, 22–24) and inhibits the formation of PHFs (25). The region of Tau responsible for microtubule binding comprises the repeat domains (R1–R4) and the proline-rich flanking regions (Fig. 1). The repeat domain is also responsible for forming the core of the

---

[3] The abbreviations used are: AD, Alzheimer disease; DTT, dithiothreitol; FRET, fluorescence resonance energy transfer; GdnHCl, guanidine hydrochloride; IAEDANS, 5-((((2-iodoacetyl)amino)ethyl)amino)naphthalene-1-sulfonic acid; PHF, paired helical filaments; ThS, thioflavin S; BES, 2-[bis(2-hydroxyethyl)amino]ethanesulfonic acid; PIPES, 1,4-piperazinediethanesulfonic acid.

PHFs (26). The flanking domain upstream of the repeats contributes to MT binding, but can also bind to other proteins, *e.g.* Pin-1 (27) or protein phosphatase 2A (28). The N-terminal domain of Tau (~200 residues) projects away from the microtubule surface (29) and may serve as an anchor for other cell components such as kinases, membranes, or motor components (30).

In solution, Tau behaves as a "natively unfolded" or "intrinsically disordered" protein (31). NMR spectroscopy confirmed the paucity of secondary structural elements, but there are motifs in R2 and R3 showing inherent β-structure propensity that coincide with the hexapeptide motifs that nucleate PHF aggregation (26, 32). Several observations suggest that Tau cannot simply be a "random coil" in the strict sense. Hints for special conformational states come from the reactivities of antibodies such as Alz50, MC1, Tau-66, MN423, and SM134 that have discontinuous epitopes on Tau. Antibodies Alz50 and MC1 recognize conformations of Tau in brain tissue that occur at an early stage of AD. Their epitopes comprise residues near the N terminus and in the third repeat and this conformation is called "pathological conformation of Tau" as it precedes aggregation (33, 34). Similarly, Tau-66 reactivity depends on the elements upstream of the repeat domain and residues in repeat R3 (35), SMI34 reacts to a folded state of Tau wherein the repeat domain and one of the KSP motifs upstream or downstream from the repeats are required (36) and antibody MN423 requires a truncation site downstream of the repeats (at Glu-391) and the residues within the repeat domain (37). We recently characterized this globally folded state of Tau in solution by generating Tau variants containing FRET pairs at different positions and measuring their distance by the fluorescence energy transfer from the donor (tryptophan) to the acceptor (cysteine carrying a dansyl group). This study revealed a double hairpin or "paperclip" conformation where the C terminus was folded near the repeat domain, and the N terminus was folded back near the C terminus (1).

Given the results, the next question was whether phosphorylation at critical sites would have an influence on this global conformation of Tau and could induce the pathological state seen by the MC1 antibody. Ideally, it would be desirable to phosphorylate Tau by predetermined sites with 100% efficiency. This cannot be achieved due to the open structure of Tau, which makes many sites accessible to various kinases. Therefore, phosphorylation reactions generally result in a heterogeneous mixture of Tau molecules phosphorylated at different sites and to different extents. To circumvent this ambiguity we generated Glu mutants where phosphorylatable serine or threonine residues were replaced by glutamate. Although glutamate is not a perfect substitute for phosphorylation, it is a reasonable approximation (38), and the extent of "pseudo-phosphorylation" is by definition specific and complete. The effect of pseudo-phosphorylation on the aggregation and microtubule binding of Tau has also been studied (39, 40). But it has not been studied whether there are changes in the global folding of Tau that could be linked to its properties. We have therefore combined phospho-mutants with FRET donor/acceptor mutants to measure intramolecular distances. Here we report that phospho-

rylation at critical sites upstream or downstream of the repeats indeed modifies the global conformation of Tau so that the paperclip structure is either opened up or tightened. In the latter case the N-terminal domain approaches the repeats, which is reminiscent of the conformation recognized by conformation-dependent antibody MC1. This has consequences for the aggregation behavior of Tau.

EXPERIMENTAL PROCEDURES

Chemicals and Proteins—Chemicals of biochemical grade such as GdnHCl were purchased from Sigma. The fluorescent label 1,5-IAEDANS was obtained from Invitrogen. Point mutations were made in the htau40 coding sequence carried by plasmid pNG2 by site-directed mutagenesis using the QuikChange kit (Stratagene). The plasmids were sequenced on both strands to confirm the mutations. A number of mutants of the full-length Tau isoform htau40 (4R/2N) that carry mutations for FRET pairs, *i.e.* tryptophan (donor) and cysteine linked to IAEDANS (acceptor) at different positions, was used in the previous study (1). For the current study, the mutant for mapping the proximities between the N terminus and repeats (N-R) were chosen with tryptophan at residue 310 and cysteine at 17; the mutant for mapping the distance between repeats and the C terminus (R-C) were chosen with tryptophan at residue 432 and cysteine at either 291 or 322; the mutant for mapping the proximities between the N and C terminus (N-C) were chosen with tryptophan at residue 432 and cysteine at 17. These FRET pair mutations were combined with phosphomimic mutations (glutamic acid) (Fig. 1*B*), for example, phosphorylated epitopes of antibodies: AT8* (Ser-199, Ser-202, Thr-205) (41, 42), AT100 (Thr-212, Ser-214) (24, 43), and PHF1 (Ser-396, Ser-404) (44, 45). Thus to analyze the effect of mimicking phosphoepitopes (AT8*, AT100, and PHF1), constructs were made carrying Glu mutations and FRET pairs at different positions (*e.g.* N-R, R-C, and N-C). The expression of phosphomimic mutants were done using the BL21(DE3) *Escherichia coli* strain. The purification of Tau was usually done by making use of a heating step as described earlier (46). But FRET mutants of Tau were purified with modifications involving a stepwise ammonium sulfate precipitation but no heating step. Briefly, the cell lysate was initially brought to 25% $(NH_4)_2SO_4$ and then centrifuged for 45 min at $127,000 \times g$ to clear the supernatant. The supernatant was then adjusted to 55% saturated $(NH_4)_2SO_4$ to precipitate Tau protein and centrifuged for 45 min at $127,000 \times g$ to collect the pellet that was then dissolved and dialyzed against buffer. Further purification was carried out using the ion exchange column SP Sepharose, followed by a gel filtration column G200 (Amersham Biosciences). The purity of the proteins was analyzed by SDS-PAGE. As an example of terminology, Tau/N-$C_{AT8*+AT100+PHF1}$ will be used to denote the htau40 mutant carrying a combination of Glu mutations for epitopes of AT8*, AT100, and PHF1 with tryptophan at 432 and cysteine at 17 (N-C).

Labeling of Proteins—Protein in 4 M GdnHCl, phosphate-buffered saline buffer (~100 μM) was incubated with 10 M excess DTT for 10 min at 37 °C. DTT was then removed by size exclusion chromatography (Fast Desalting column, Amersham Biosciences) and the eluted protein was immediately supple-

mented with ~20 M excess IAEDANS (dissolved in *N,N*-dimethylformamide). The labeling reaction was allowed to proceed at room temperature for 2 h, or alternatively "solid state-based labeling" was used (47), which is achieved by reducing the protein with DTT, then precipitating with 70% $(NH_4)_2SO_4$, followed by dissolving the protein pellet with buffer containing IAEDANS. The solution was then dialyzed against phosphate-buffered saline and residual IAEDANS was removed by size exclusion chromatography. The concentration of protein was determined by absorption at 280 nm using the molar extinction coefficient $\in_{Tau}$ = 11,460 to 12,950 M^{-1} cm^{-1}, depending on the Tau mutants. The amount of bound IAEDANS was determined by the absorption at 336 nm ($\in_{IAEDANS}$ = 6,100 M^{-1} cm^{-1}) (48). The protein concentration was corrected for the contribution of the IAEDANS at 280 nm and the stoichiometry was calculated. Typically the labeling stoichiometry was 0.7–0.9. The distances calculated with or without correction for the fractional labeling ratio are within a difference of 10–15% (see below).

Fluorescence Spectroscopy—All steady state fluorescence measurements were performed with a Spex Fluoromax spectrophotometer (Polytec, Waldbronn, Germany), using 3 × 3-mm quartz microcuvettes from Hellma (Mühlheim, Germany) with 20 μl sample volumes. Protein was irradiated at 290 nm to excite tryptophan but not tyrosine. In all cases, the experimental parameters were as follows: scan range = 300–550 nm, excitation slit width = 4 nm, emission slit width = 6 nm, integration time = 0.25 s, and photomultiplier voltage = 950 V. Each time 3 spectra were scanned and averaged. A protein concentration of 4 μM was used and checked by SDS-PAGE as a control. In denaturation experiments with GdnHCl, the efficiency was calculated from emission intensities of labeled protein and unlabeled protein at the same GdnHCl concentration. The influence of various GdnHCl concentrations on the fluorimetric properties of tryptophan and IAEDANS was controlled with free dyes alone and in combination. The effects due to GdnHCl as a solvent were minor (<10%) in comparison to the FRET effects and the spectra were corrected for it. The FRET efficiency was measured by the energy transfer,

$$E_{FRET} = (1 - D_A/D)(1/f_A) \qquad \text{(Eq. 1)}$$

where D_A is the fluorescence intensity of the donor in the presence of the acceptor and D is the fluorescence intensity of donor in the absence of acceptor. The apparent efficiencies were normalized by f_A, the fractional labeling with acceptor, as shown in Equation 1. The distance R between donor and acceptor was calculated by the Förster equation,

$$E_{FRET} = [1 + (R/R_o)^6]^{-1} \qquad \text{(Eq. 2)}$$

where the Förster radius R_o is 22 Å for the Trp-IAEDANS pair (49). In the case of the tryptophan-IAEDANS pair, a small error in the labeling ratio would give distance values that are within acceptable error range even without a correction factor, due to the dependence of the efficiency on the 6th power of the distance. For example, if the measured efficiency is 0.5 with 100% labeling, then r = 22 Å. On the other hand, if the measured

FRET efficiency is 0.5 with only 80% labeling (f_A = 0.8) and the correction for fractional labeling is applied, then r = 20.2 Å. Note that in unfolded proteins the distance between a given FRET pair shows a wider distribution and the apparent FRET reflects this heterogeneity (50).

CD Spectroscopy—All measurements were carried out with a Jasco J-810 CD spectrometer (Jasco, Groß-Umstadt, Germany) in a cuvette with a path length of 0.1 cm. The scanning speed was 100 nm/min, bandwidth 0.1 nm, and a response time of 4 s. In each experiment, measurements were done at 20 °C and 4 spectra were summed and averaged. The CD spectra were normalized for the concentration at 214 nm using bovine serum albumin as a standard.

PHF Assembly—Aggregation was induced by incubating soluble Tau typically in the range of 50 μM in volumes of 20 μl at 37 °C in 20 mM BES, pH 7.4, plus 25 mM NaCl buffer with the anionic cofactor heparin 6000 (molar ratio of Tau to heparin = 4:1). The formation of aggregates was monitored by ThS fluorescence and confirmed by electron microscopy. For ThS fluorescence, 5 μl of 50 μM assembly reaction was diluted to 50 μl with NH_4Ac, pH 7.0, containing 20 μM ThS. Fluorescence measurements were done at 25 °C in a Tecan spectrofluorimeter (Crailsheim, Germany) with an excitation wavelength of 440 nm and an emission wavelength of 521 nm (slit width 7.5 nm each) in a black microtiter plate with 384 round wells (ThermoLabsystems, Dreieich, Germany). The background fluorescence was subtracted when needed. For electron microscopy, protein solutions were diluted to 1–10 μM and placed on 600 mesh carbon-coated copper grids for 45 s, washed twice with H_2O, and negatively stained with 2% uranyl acetate for 45 s. The samples were examined with a Philips CM12 electron microscope at 100 kV.

Microtubule Polymerization Assay—Microtubule assembly was monitored by UV light scattering at an angle of 90° at a wavelength of 350 nm in a black microtiter plate with 384 round wells (ThermoLabsystems) in a Tecan spectrofluorimeter in the presence and absence of Tau. 5 μM Tau was mixed with 30 μM tubulin dimer at 4 °C in microtubule assembly buffer (100 mM Na-PIPES, pH 6.9, 1 mM EGTA, 1 mM $MgSO_4$, 1 mM GTP, 1 mM DTT) in a final volume of 40 μl. The reaction was started by raising the temperature to 37 °C.

Western Blotting—The protein samples were added to SDS sample buffer and boiled at 95 °C for 5 min. Equal amounts of protein were loaded onto 10% SDS-polyacrylamide gels for subsequent electrophoresis. The proteins were transferred to a nitrocellulose membrane at 100 V for 40 min. After the transfer, the blot membrane was blocked with 5% milk and incubated overnight at 4 °C with the primary antibody (MC1 at 1:1000 dilution). After washing the unbound primary antibody, the secondary antibody (goat anti-mouse IgM conjugated to horseradish peroxidase at 1:1000 dilution) was incubated with the blot. The blot was then stripped of MC1 antibody and incubated with the pan-Tau antibody K9JA at 1:8000 dilutions (A0024, DAKO, Glostrup Denmark). Protein bands were visualized using chemiluminescence (ECL, Amersham Biosciences).
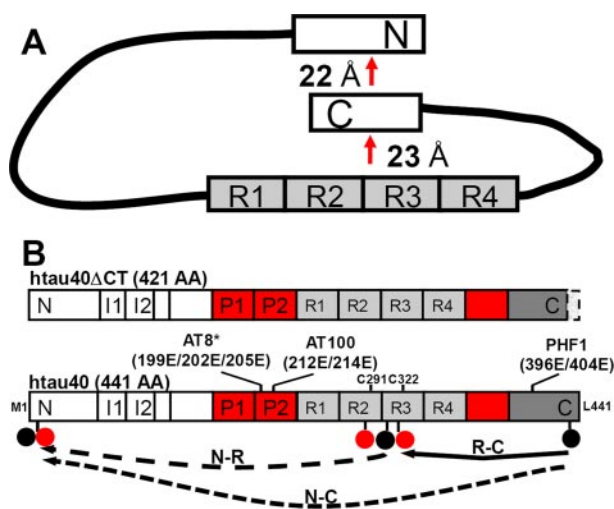
FIGURE 1. **Phosphomimic mutants of full-length Tau₄₄₁.** *A,* paperclip model of global folding of soluble Tau (1). The polypeptide chain of a full-length Tau is shown with the C-terminal domain folding into close vicinity of the repeat domain, and the N-terminal domain folding close to the C terminus but outside the FRET distance of the repeats. *B,* a set of mutants based on full-length Tau and TauΔCT (with deletion of C-terminal residues 422–441) carrying mutations of Glu at Ser-Pro/Thr-Pro motifs to mimic epitopes of antibodies AT8*, AT100, and PHF1. These mutants also contain single tryptophan mutations (FRET donor, *black circles*) and single cysteine sites (for labeling by IAEDANS as FRET acceptor, *red circles*) for measuring the distances of the N terminus to the repeat domain (N-R), repeats to C terminus (R-C), and N terminus to C terminus (N-C), indicated by *curved lines*.

RESULTS

Proteins and Phosphomimic Mutations—Tau is a natively unfolded protein that does not contain a significant amount of secondary structure (31). However, it is possible that there are global conformations defined by interactions between the different domains of Tau, as suggested by certain antibodies (*e.g.* Alz50, MC1) that are diagnostic of a pathological conformation and react with a discontinuous epitope comprising residues near the N terminus and the third repeat (33, 34). Indeed, as shown previously, Tau in solution adopts preferred long range interactions between the repeat domain and the C terminus and between the N and C terminus (paperclip conformation), as judged by FRET (1). For mapping FRET distances we inserted Trp as a donor and Cys-dansyl as an acceptor near the N terminus (*e.g.* residue Y18W or T17C-dansyl), near the C terminus (*e.g.* V432W), or within the repeats (Cys²⁹¹-dansyl in R2, Cys³²²-dansyl in R3 or Y310W in R3). In solution, the C-terminal domain of Tau is unexpectedly close (19–23 Å) to the repeat domain and therefore causes a pronounced FRET signal, whereas the N-terminal domain (residue 17) is not within the FRET range of the repeat domain, but close to the C-terminal tail where it causes FRET (21–24 Å, Fig. 1*A*).

Because the functions of Tau are regulated by phosphorylation we were interested whether this would influence the global conformation. In particular, we wanted to know whether phosphorylation could induce a state reminiscent of the pathological conformation seen by antibodies. To mimic the phosphorylation *in vitro*, we used pseudo-phosphorylation mutants by substituting Glu at the phosphorylatable residues. A series of Tau mutants based on the full-length isoform hTau40 were generated with certain pseudo-phosphorylation sites alone or

in combination. The choice of phosphorylation sites was based on the epitopes of antibodies that are characteristically elevated in AD (Fig. 1*B*). For example, the triple mutation S199E + S202E + T205E generates pseudo-phosphorylation at the epitope recognized by antibody AT8 (41, 42, 51). For brevity, we will refer to this mutant as the "AT8*" mutant (note: phosphorylated Ser²⁰² + Thr²⁰⁵ suffice for the reaction with antibody AT8, but Ser¹⁹⁹ is usually also phosphorylated in brain tissue and can be detected by the antibody, hence we chose the triple mutation and denote it as AT8*). Similarly, the "PHF1" mutant contains mutations S396E + S404E because phosphorylation at these sites generates the epitope for antibody PHF1 (44, 45) and the "AT100" mutant contains mutations T212E + S214E (24, 43). Together with the Glu mutations, FRET pairs were introduced into Tau to allow mapping of the distances between the N terminus and repeats (N-R), C terminus and repeats (R-C), or N and C terminus (N-C), for the different states of (pseudo-) phosphorylation.

Site-specific Pseudo-phosphorylation at Epitopes AT8 or PHF1 but Not AT100 Alters Long Range Interactions of Tau*— We first describe the effects of "single arm" pseudo-phosphorylation, either upstream of the R-domain (sites AT8* or AT100) or downstream (site PHF1). The phosphorylation of Tau at the AT100 epitope has been shown to reduce microtubule binding both *in vitro* and *in vivo* (22–24). To analyze the effect of pseudo-phosphorylation at the epitope AT100 on the global folding of Tau, we mutated Thr²¹² + Ser²¹⁴ into Glu and combined this with FRET pair mutations in the N, R, and C-terminal domains. For the unlabeled mutant Tau/N-R$_{AT100}$ (single tryptophan at 310, single cysteine at position 17, mutations T212E + S214E, and intrinsic Cys residues 291 and 322 mutated to Ala, no dansyl label), the tryptophan fluorescence emission has a maximum around 350 nm, indicating that the tryptophan residue is solvent-exposed (supplemental Fig. S1*A*, *black curve*) (52). The labeled mutant Tau/N-R$_{AT100}$ (as above, but Cys¹⁷-labeled with IAEDANS) resulted in a FRET efficiency of only 0.15 (supplemental Fig. S1*A*, *red curve*), showing that pseudo-phosphorylation at the AT100 epitope does not cause a change in the distance between the N and R domains, compared with the unphosphorylated Tau mutant (E = 0.19) (1). Similarly, no significant change in FRET efficiency was observed for Tau/R-C$_{AT100}$ or Tau/N-C$_{AT100}$, showing that the phosphomimic Glu²¹² + Glu²¹⁴ does not alter the paperclip folding of Tau (Table 1 and supplemental Fig. S1, *A–D*).

A different picture emerged with the mutant Tau/N-C$_{AT8*}$ (mimicking phosphorylation at Ser¹⁹⁹ + Ser²⁰² + Thr²⁰⁵, epitope AT8*), which resulted in a ~4-fold drop of the FRET efficiency between the N- and C-domains from 0.6 in the control to 0.14 (Fig. 2*C*). This indicates that the single-arm pseudo-phosphorylation at the AT8* epitope causes the N-domain to swing away from the C-domain, thus loosening the paperclip structure (Fig. 2*D*). However, the FRET between R- and C-domains (mutant Tau/R-C$_{AT8*}$, E = 0.44) did not change significantly from the unphosphorylated mutant showing that the C-domain remained close to the repeats, whereas the N-domain remained outside the FRET distance of the repeats (Fig. 2, *A* and *B*). Likewise, Glu mutations at Ser³⁹⁶ and Ser⁴⁰⁴ (to mimic the PHF1 epitope in the arm downstream of the repeats)

TABLE 1

Summary of results

FRET efficiencies (E) and the calculated FRET distances (R) are given for the Tau$_{40}$/Glu mutants mimicking phosphorylations that are epitopes of antibodies such as AT8*, AT100, and PHF1. The positions of donor (tryptophan), acceptor (IAEDANS linked to cysteine), and Glu mutations are given. Arrows up, down, or horizontal indicate an increase, decrease, or no significant change in the FRET efficiency between domains. (¶ values taken from ref 1)

Tau constructs (Antibody mimic)	Sites of Glu mutations	Folding	FRET pairs		FRET measured		Effect on the folding		
			W	DANS	E$_{FRET}$	R (Å)	N-R	R-C	N-C
Tau40[¶]		N-R	310	17	0.19	28.0	NA		
		R-C	432	322	0.29	25.6		NA	
		R-C	432	291	0.37	24.0		NA	
		N-C	432	17	0.59	20.8			NA
Tau40/E$_{AT100}$	212+214	N-R	310	17	0.15	29.4	→		
		R-C	432	322	0.31	25.1		→	
		N-C	432	17	0.50	22.0			→
Tau40/E$_{AT8*}$	199+202+205	N-R	310	17	0.16	28.9	→		
		R-C	432	322	0.44	22.9		→	
		N-C	432	17	0.14	30.0			↓
Tau40/E$_{PHF1}$	396+404	N-R	310	17	0.18	28.5	→		
		R-C	432	322	0.14	29.9		→	
		N-C	432	17	0.75	18.2			↑
Tau40/E$_{AT100+PHF1}$	212+214+396+404	N-R	310	17	0.34	24.6	↑		
		R-C	432	322	0.31	25.1		→	
		N-C	432	17	0.56	21.1			→
Tau40/E$_{AT8*+PHF1}$	199+202+205+ 396+404	N-R	310	17	0.41	23.4	↑		
		R-C	432	322	0.31	25.1		→	
		N-C	432	17	0.60	20.5			→
Tau40/ E$_{AT8*+AT100+PHF1}$	199+202+205+212+ 214+396+404	N-R	310	17	0.46	22.6	↑		
		R-C	432	322	0.60	20.6		↑	
		N-C	432	17	0.28	25.8			→
Tau40ΔCT		N-R	310	17	0.13	30.2	→	NA	NA
Tau40ΔCT/E$_{AT8}$	199+202+205	N-R	310	17	0.18	28.3	→	NA	NA
Tau40ΔCT/E$_{AT100}$	212+214	N-R	310	17	0.19	28.0	→	NA	NA
Tau40ΔCT/E$_{AT8*+AT100}$	199+202+205+ 212+214	N-R	310	17	0.16	29.0	→	NA	NA
Tau40ΔCT/ E$_{AT8*+AT100+PHF1}$	199+202+205+212+ 214+396+404	N-R	310	17	0.39	23.7	↑	NA	NA

caused an increase in the distance seen by FRET between the R-domain and C-domain, but at the same time a decrease in the distance between the C terminus to the N terminus (Fig. 2, *E–G*). Thus the FRET results show that phosphorylation mimic at the PHF1 site causes the C terminus to swing away from the repeats toward the N terminus, whereas the N terminus still remains outside the FRET distance from the repeats (Fig. 2*H*). This indicates that phosphorylations at sites recognized by AT8 or PHF1 epitopes, when present alone, open up the N- and C-terminal domains, respectively. As a result, the repeat

domain would become more exposed and might facilitate aggregation into paired helical filaments.

Combination of Pseudo-phosphorylation at AT8*, AT100, and PHF1 Epitopes Confers Pathological Folding to Tau—We next asked whether the conformation of Tau is affected by a combination of pseudo-phosphorylated epitopes. We tested the combination of Glu mutations at the AT100 plus PHF1 sites. Surprisingly, the "double arm" phosphorylation causes a compaction of the Tau molecule, in contrast to the single arm mutations described above that loosened up the paperclip con-
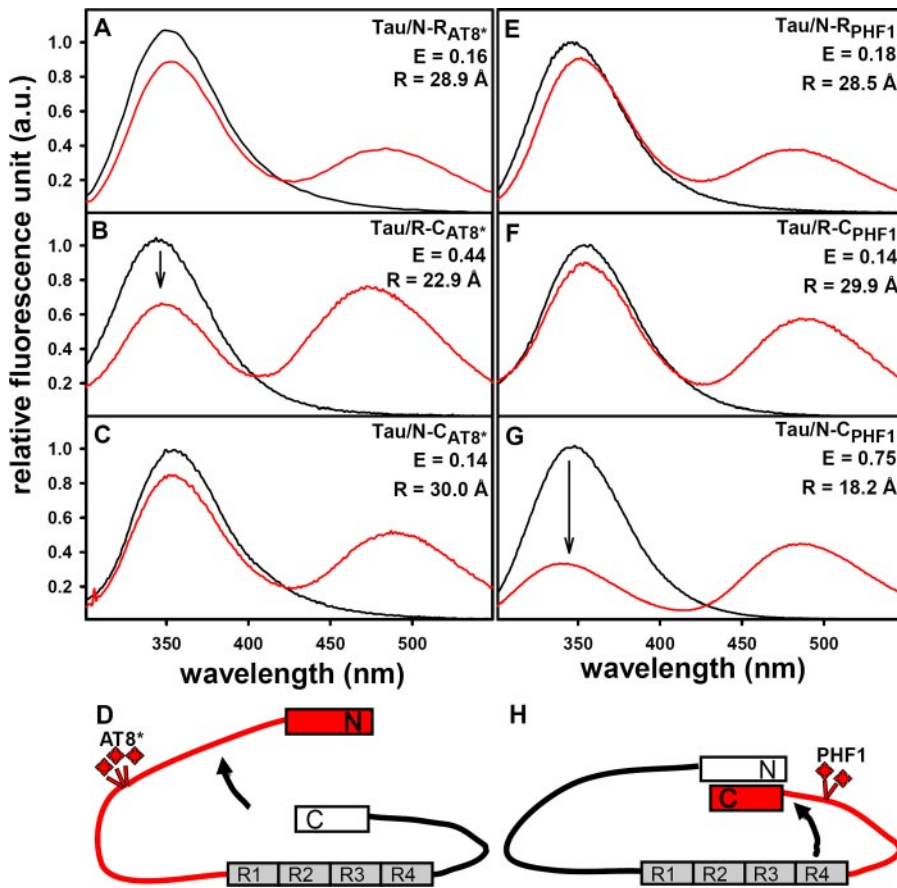
FIGURE 2. **FRET for Tau$_{441}$ mutants mimicking phosphorylation sites at AT8* and PHF1 epitopes.** Fluorescence emission spectra are shown for the mutant protein without label (*black*) and with IAEDANS label (*red*) for the following mutants: *A*, Tau/N-R$_{AT8*}$; *B*, Tau/R-C$_{AT8*}$; *C*, Tau/N-C$_{AT8*}$; *E*, Tau/N-R$_{PHF1}$; *F*, Tau/R-C$_{PHF1}$; and *G*, Tau/N-C$_{PHF1}$. *Panels D* and *H* show the model of changes in Tau folding upon pseudo-phosphorylation of AT8* and PHF1 sites, respectively. Note that mimicking phosphorylation at Ser^{199} + Ser^{202} + Thr^{205} (epitope AT8*) causes the N-domain to swing away from the C-domain, thus loosening the paperclip structure and Glu mutations at Ser^{396} + Ser^{404} (to mimic the PHF1 epitope in the arm downstream of the repeats) causes the C terminus to swing away from the repeats toward the N terminus. The protein concentration of 4 μM was excited at 290 nm and the emission was recorded from 300 to 550 nm with slit width of excitation 4 nm and emission 6 nm. The decrease of the tryptophan intensity at 350 nm was used for calculation of FRET efficiencies and subsequent distance calculations using Equation 2.

decreased efficiency (E = 0.28; Fig. 3*G*). Thus there appears to be a joint swinging of both termini toward the repeat domain. Overall, the triple epitope pseudo-phosphorylation of both arms at AT8*, AT100, and PHF1 causes a noticeable compaction of the molecule (Fig. 3*H*).

Cleavage of the C-terminal Domain Is Not a Requisite for the Folding of the N Terminus Close to the Repeats—The cleavage of the C-terminal tail by caspases is believed to favor Tau aggregation (53). To analyze if the deletion of the C-terminal tail allows the N-domain to approach the repeats (similar to the compaction by double-arm phosphorylation, see above), we created a Tau mutant lacking amino acids 422–441 with Trp at residue 310 and Cys-IAEDANS at residue 17 (denoted as TauΔCT/N-R). However, the FRET efficiency of TauΔCT/N-R remained low (E = 0.13, Fig. 4*A*), comparable with the full-length htau40 mutant. Thus the deletion of the C-terminal tail did not change the distance between the N- and R-domains. We then combined deletion of the C-terminal tail with single arm phosphorylation mutants (AT8* or AT100 epitopes). The mutants TauΔCT/N-R$_{AT8*}$, TauΔCT/N-R$_{AT100}$, or TauΔCT/N-R$_{AT8*+AT100}$ all resulted in efficiencies less than 20% showing that pseudo-phosphorylation upstream

of the repeats combined with C-terminal deletion are not sufficient to swing the N-domain close to the repeats (Table 1 and supplemental Fig. S3, *A–D*). However, the triple mutant TauΔCT/N-R$_{AT8*+AT100+PHF1}$ resulted in a higher efficiency (E = 0.39), indicating a compaction of the N-domain toward the repeats (Fig. 4, *B* and *C*).

GdnHCl Denaturation Decreases FRET Efficiencies—Some of the phosphomimic mutants of Tau, particularly the double arm combination of AT8* + PHF1 or AT100 + PHF1 or AT8* + AT100 + PHF1, showed a remarkably high FRET efficiency between Tau domains compared with unphosphorylated Tau, indicating a compaction of the Tau molecule. We therefore investigated the stability of these mutants and measured the change of FRET efficiency with increasing GdnHCl concentration. The efficiency of unphosphorylated Tau (Tau/C-R) decreased already at low GdnHCl concentration (<1.0 M), showing that the paperclip conformation is labile and can be easily perturbed (Fig. 5*A*). The same was true for the phosphomimic mutants Tau/N-R$_{AT8*+PHF1}$ and Tau/N-R$_{AT8*+AT100+PHF1}$ (Fig. 5*B*), revealing that Glu mutations did

formation. The FRET efficiencies for Tau/R-C$_{AT100+PHF1}$ (E = 0.31) and Tau/N-C$_{AT100+PHF1}$ (E = 0.56) were unchanged, but Tau/N-R$_{AT100+PHF1}$ showed a notable increase of efficiency from 0.14 to 0.34, indicating that the N-domain comes closer to the repeats (Fig. S2, *A–D*). To test whether this effect is epitope specific, we created mutants carrying other combinations of phosphomimics in both flanking regions of the repeats. Indeed, the combination of AT8* + PHF1 phosphomimics shows an even stronger effect of AT100 + PHF1 on the compaction of Tau by swinging the N-domain very close to the repeats, E = 0.41 for Tau/N-R$_{AT8*+PHF1}$ (Table 1 and Fig. 3, *A–D*). This corresponds to the pathological conformation detected by diagnostic antibodies MC1 or Alz50, reacting with a discontinuous epitope from the N-domain and the R-domain.
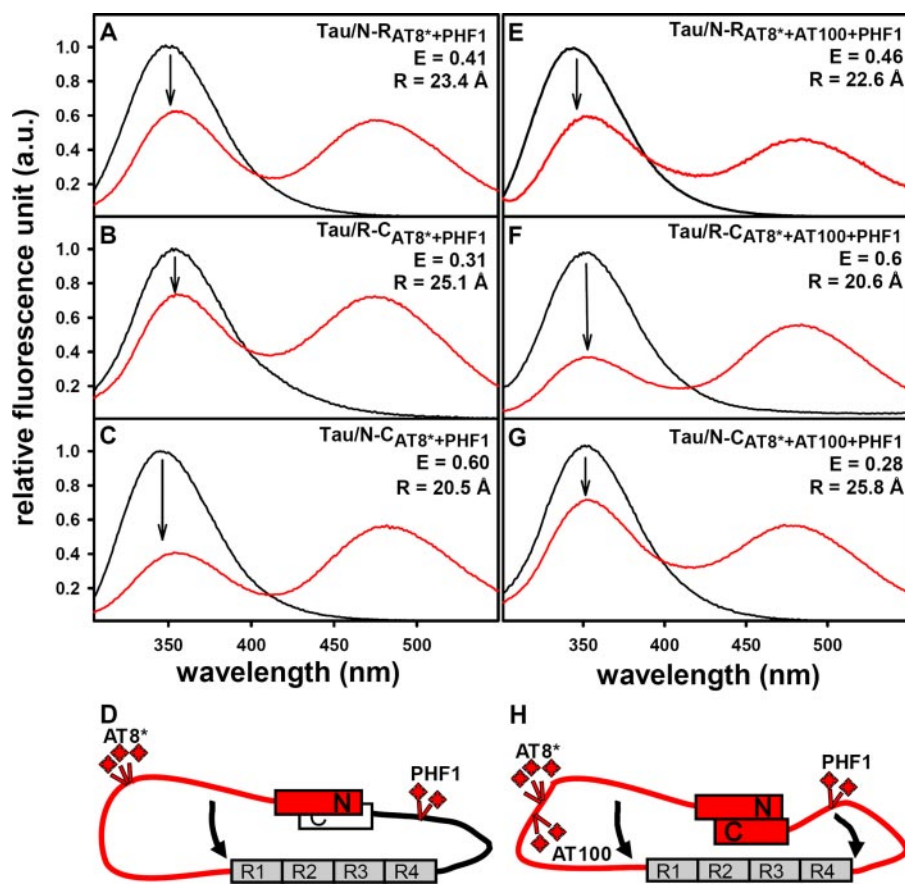
In the triple epitope mutant that bears double arm Glu mutations to mimic the epitopes of AT8*, AT100, and PHF1, the C terminus approaches the repeats very closely (with a high FRET efficiency of E = 0.6), whereas the N-terminal domain also approaches the repeats (E = 0.46, Fig. 3, *E* and *F*). At the same time the N-domain is still close to the C-domain, albeit with a

FIGURE 3. **FRET for Tau$_{441}$ mutants carrying epitopes of AT8* + PHF1 and AT8* + AT100 + PHF1.** Fluorescence emission spectra are shown for: *A*, Tau/N-R$_{AT8*+PHF1}$; *B*, Tau/R-C$_{AT8*+PHF1}$; *C*, Tau/N-C$_{AT8*+PHF1}$; *E*, Tau/N-R$_{AT8*+AT100+PHF1}$; *F*, Tau/R-C$_{AT8*+AT100+PHF1}$; and *G*, Tau/N-C$_{AT8*+AT100+PHF1}$. *Panels D* and *H* show the model of conformational change in Tau upon pseudo-phosphorylation of AT8* + PHF1 or AT8* + AT100 + PHF1. Note that mimicking the combination of pseudo-phosphorylation at epitopes AT8* + PHF1 causes the N-domain to come close to the repeats. The combination of mimicking epitopes AT8* + AT100 + PHF1 causes both the N and C terminus to swing close to repeats, thus tightening the paperclip structure.

we performed titration experiments. To 4 μM FRET mutant protein Tau/N-R$_{AT8*+PHF1}$ or Tau/N-R$_{AT8*+AT100+PHF1}$, increasing concentrations of non-fluorescent hTau40wt or Tau$_{AT8*+AT100+PHF1}$ (lack tryptophan, but has 5 tyrosine residues) were added up to 20 μM. The efficiency of the mutant proteins remained largely unchanged (supplemental Fig. S4*D*). Moreover, the addition of unlabeled mutant protein to labeled mutant protein only increased the tryptophan emission but not the IAEDANS emission (data not shown). These results showed that the FRET effects observed for the phosphomimics of Tau arise from intramolecular interactions.

Increased Aggregation Propensity and MC1 Antibody Reactivity Induced by Pseudo-phosphorylation—To relate the global conformational change of Tau induced by pseudophosphorylation to the functions of Tau we tested the propensity for aggregation, the ability to promote microtubule polymerization, and the reaction with antibody MC1, which is characteristic of a pathological conformation of Tau in AD. These properties were compared for wild-type Tau and the triple pseudo-phosphorylated mutant Tau$_{AT8*+AT100+PHF1}$, which shows the tightest compaction of the paperclip conformation. In the aggregation assay, Tau$_{AT8*+AT100+PHF1}$ showed a moderate but significant increase of ThS fluorescence (indicative of a higher extent of β-structure and aggregation) compared with Tau$_{wt}$ (Fig. 6*A*). This result suggests that the compaction due to pseudo-phosphorylation at both arms (AT8* + AT100 + PHF1) raises the tendency for aggregation (beyond the effect of polyanions alone). In contrast, the microtubule polymerizing ability of Tau$_{AT8*+AT100+PHF1}$ showed no difference in final extent and only a small retardation on assembly rate (Fig. 6*B*). This is consistent with the notion that the AD-like phosphorylation in the flanking domains has no or only a small effect on Tau-microtubule interactions (39, 54, 55). Third, we tested the reactivity of the Tau mutant proteins with antibody MC1 (Fig. 6*C*). There was a clear increase in signal for the triple-site mutant Tau/N-R$_{AT8*+AT100+PHF1}$. Remarkably, the increase became very pronounced with the C-terminal truncated version of the protein TauΔCT/N-R$_{AT8*+AT100+PHF1}$, compared with the unphosphorylated protein TauΔCT/N-R. Both of these observations suggest that the compaction of the molecule observed by FRET resembles the "pathological conformation" detected by the MC1 antibody.

not provide any additional stability to the paperclip conformation. In both cases, the FRET efficiency dropped to zero, showing that in the denatured state the N-, R-, and C-domains are outside the FRET range (Fig. 5*C*). This is consistent with their expected distances if one assumes a Gaussian polymer model for the denatured protein (see "Discussion").

CD Spectroscopy of Pseudo-phosphorylated and Fluorescently Labeled Tau—To confirm that neither the phosphomimic mutations nor the fluorescent labeling caused a change in the protein structure and functionality we performed CD spectroscopy. The CD spectra of the triple pseudo-phosphorylated mutant Tau$_{AT8*+AT100+PHF1}$ exhibited a minimum at about 200 nm, indicating a mostly random coil structure, similar to the spectra of wild-type Tau (supplemental Fig. S4*A*). The same was true for the pseudo-phosphorylated mutant carrying mutations for FRET pair (single tryptophan and single cysteine plus Glu mutations) and the fluorescently labeled proteins, indicating that the insertion of Glu residues and the fluorescent labels had no impact on the overall secondary structure of the protein as seen by CD (supplemental Fig. S4, *B* and *C*).

To rule out the possibility that the observed FRET for the Tau mutants might be due to the interactions between different molecules in the solution (rather than being intramolecular),

FIGURE 4. **FRET for TauΔCT mutants.** Fluorescence emission spectra are shown for TauΔCT/N-R (*A*) and TauΔCT/N-R$_{AT8*+AT100+PHF1}$ (*B*). Note that C-terminal deletion of residues 422–441 (TauΔCT) combined with pseudo-phosphorylation at epitopes AT8* + AT100 + PHF1, but not alone, exhibits a change in global conformation whereby the N terminus and the C terminus swing close to repeats.

DISCUSSION

Tau is a target of several kinases, it can be phosphorylated at multiple sites that leads to a decrease of Tau-microtubule binding and to altered microtubule dynamics. In AD, Tau is abnormally phosphorylated at many sites, mostly within the repeat domain (K*X*GS motifs) and in the flanking domains (mainly SP or TP motifs). The latter are of diagnostic value because certain antibodies against Alzheimer Tau recognize these motifs, including antibodies AT8, PHF1, and AT100 (24, 41, 45). Early clues to the conformation of Tau came from EM studies that showed Tau as an elongated rod (56, 57). Subsequent spectroscopic and x-ray studies revealed Tau as a natively unfolded protein (31). However, several observations suggested that there is a global conformation that is somehow related to Tau pathology. One evidence came from studies of PHF assembly showing that the repeat domain aggregated more readily than full-length Tau, consistent with a model whereby the domains outside the repeat domain protect the repeats from interacting with other molecules (5, 57). Another evidence came from monoclonal antibodies diagnostic of early stages of AD, which recognized a pathological folded conformation because the epitope was discontinuous (*e.g.* Alz50, MC1, SM134 (33, 34, 36, 58)). We therefore investigated the conformation by the FRET method and found that Tau in solution adopts a conformation reminiscent of a paperclip (1). This prompted the question whether the paperclip conformation was influenced by the state
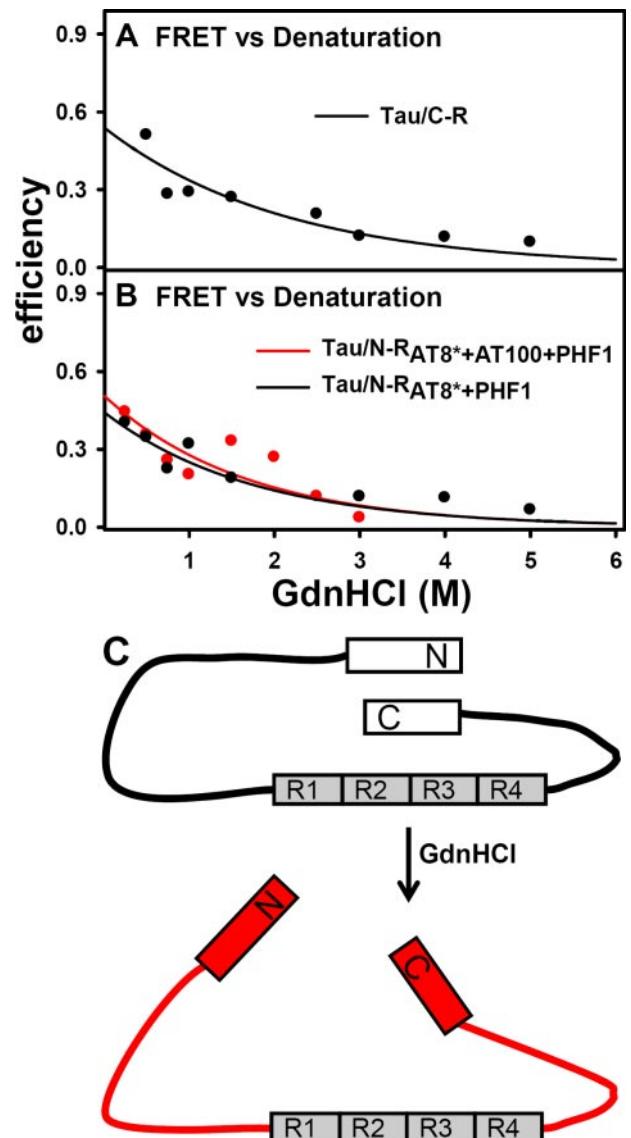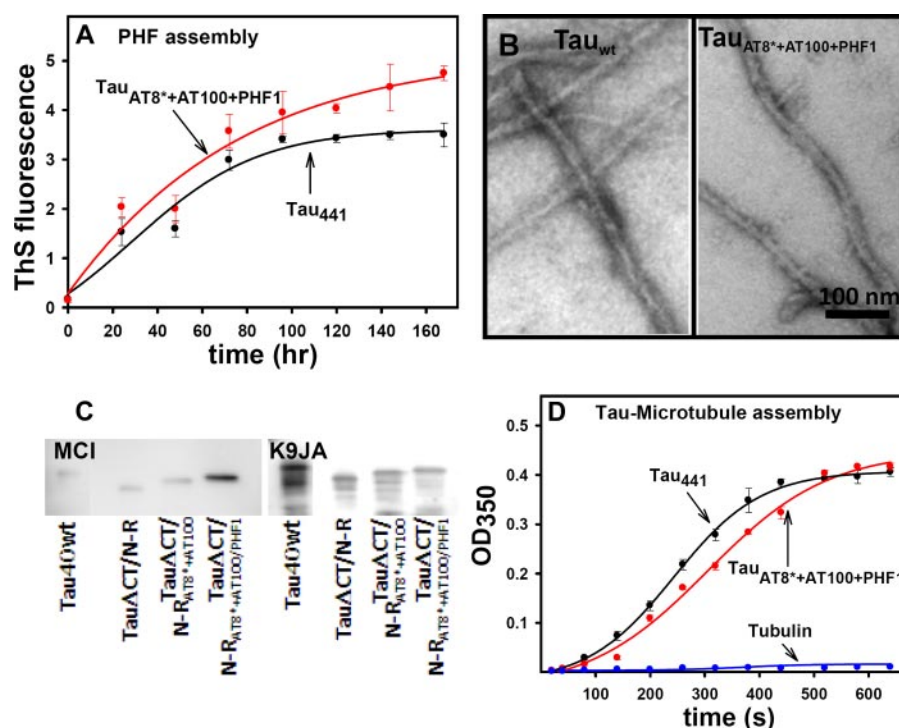

FIGURE 5. **Denaturation of phosphomimic mutants of Tau by GdnHCl.** The *curves* show the decrease in FRET efficiency against increasing GdnHCl concentration for the mutants Tau/R-C (*A*), Tau/N-R$_{AT8*+PHF1}$ (*B*), and Tau/N-R$_{AT8*+AT100+PHF1}$. The half-points of denaturation are low (~1–2 M GdnHCl) because the interactions within the natively unfolded Tau are weak. *Panel C* illustrates upon denaturation the interactions between domains are disrupted, resulting in a loss of FRET.

of phosphorylation. One could approach this issue by generating FRET pair mutants and phosphorylating Tau at the desired sites. However, because of the large number of phosphorylation sites and the incomplete extent of phosphorylation by kinases, this approach does not yield quantitative results. The alternative is to generate phospho-mimicking Ser/Thr to Glu mutations, which were combined with FRET pairs in the N-, R-, and C-domains (Table 1). For mutations, we chose epitopes of 3 well known antibodies known to become hyperphosphorylated early in AD (AT8*, PHF1, and AT100).

The results can be summarized by stating that single arm pseudo-phosphorylation, either upstream of the repeats at the AT8* epitope or downstream at the PHF1 epitope, loosens up the paperclip conformation, whereas double arm pseudo-phosphorylation (AT8* + PHF1) tightens the paperclip (Fig. 7). In

FIGURE 6. **Aggregation propensity, microtubule binding, and MC1 reactivity of phosphomimic mutants of Tau.** *A*, aggregation of Tau$_{wt}$ and Tau$_{AT8*+AT100+PHF1}$ monitored by ThS fluorescence. Aggregation was induced from 50 μM protein in 20 mM BES, pH 7.4, buffer with addition of heparin 6000 (molar ratio of Tau: heparin = 4:1) and DTT. The pseudo-phosphorylated protein reaches a higher level of ThS fluorescence, suggesting that the tighter paperclip conformation has a role in enhancing aggregation. *B*, electron micrographs of the filaments formed from Tau$_{wt}$ and Tau$_{AT8*+AT100+PHF1}$ in the presence of heparin. Both filaments are similar in morphology. *Scale bar* indicates 100 nm. *C*, Western blots showing reactivity of MC1 (conformational antibody whose discontinuous epitope comprises residues from the N-terminal and repeat domain, detecting the folding of the protein) and K9JA (pan-Tau polyclonal antibody raised against construct K9 of the C-terminal half of Tau) with phosphomimic mutants of Tau. Note that double arm pseudo-phosphorylation causes an increased MC1 reactivity. *D*, microtubule polymerization ability of Tau$_{wt}$ and Tau$_{AT8*+AT100+PHF1}$. Both proteins reach similar final levels, but the pseudo-phosphorylated protein shows a somewhat longer lag time.

hallmarks of natively unfolded proteins (*e.g.* minimum of CD spectra at 200 nm, supplemental Fig. S4). This is not a contradiction because CD spectroscopy reports on the local environment of residues, not on long-range interactions. In addition, denaturation studies show that the paperclip folding can be destroyed by GdnHCl, consistent with the view that certain (limited) stretches of secondary structure are responsible for generating the global folding, even though the protein is rather flexible on the level of residues. Such pockets of secondary structure have indeed been observed by NMR spectroscopy (32, 59).

If one models Tau as a random Gaussian coil, the mean distances between donor and acceptor would be expected to be ~88 Å for Tau/R-C (Cys^{322}–Trp^{432} in R- and C-domains) and ~143 Å for Tau/N-R (Cys^{17}–Trp^{310} in N- and R-domains), using the relation L$_m$ = 8.3 $\sqrt{N}$ Å, where *N* represents the intervening chain length (60). These values would be far outside the observable FRET distance, and therefore we can conclude that there must be some specific folding (*i.e.* paperclip) that brings the residues within FRET range. Conversely, the fact that FRET disappears upon exposure to GdnHCl supports the view that the polypeptide chain approaches a more random configuration, as expected for a denatured protein. The comparison illustrates the distinction between a "random" denatured protein and a natively unfolded protein with "global folding."

Perhaps the most provocative aspect of the results is the relationship between Alzheimer-like phosphorylation (at AT8*, AT100, and PHF1) epitopes, the compaction of the paperclip conformation, and the reactivity of Tau with antibodies that report on the pathological conformation of Tau in early stages of AD, such as MC1, Alz50, and others. This reaction is best observed in brain tissue and has been difficult to reproduce with Tau *in vitro*. However, the fact that the most compact conformations are also the ones showing the highest reactivity with MC1 (Fig. 6*C*) argues that the compaction of the paperclip conformation reflects the pathological state. The increase in MC1 reactivity becomes more pronounced when the C-terminal tail is absent, which argues that this tail normally opposes a close approach between the N terminus and the repeats (consistent with the paperclip model). As a caveat, we note that antibody Alz50 shows only a very weak reaction, both for wild-type soluble Tau and the phosphomimic mutants, even though the epitope comprises similar residues of Tau as antibody MC1

other words, the AT8* phosphomimic moves the N-terminal domain away from the C-terminal domain so that the FRET between the N and C terminus is decreased; the PHF1 phosphomimic moves the C-terminal domain away from the repeats and closer to the N-terminal domain; but the combination of both AT8* and PHF1 moves N-, R-, and C-domains closer to one another and causes a compaction of the paperclip fold so that even FRET between the N- and R-domains can now take place, which is normally not visible, and is a sign of the pathological conformation seen by the MC1 antibody. The double site AT100 (T212E + S214E) has no effect on the paperclip conformation as judged by FRET, even though phospho-Ser^{214} strongly reduces microtubule binding. However, AT100 in combination with AT8* and PHF1 accentuates the compaction of the paperclip, as seen by the strong FRET between the C-domain and the repeats, as well as between the N-domain and the repeats. Finally, the wide separation between N- and R-domains is not dependent on the C-terminal tail, because it is present even when the C-terminal tail of Tau is cleaved off (Fig. 4).
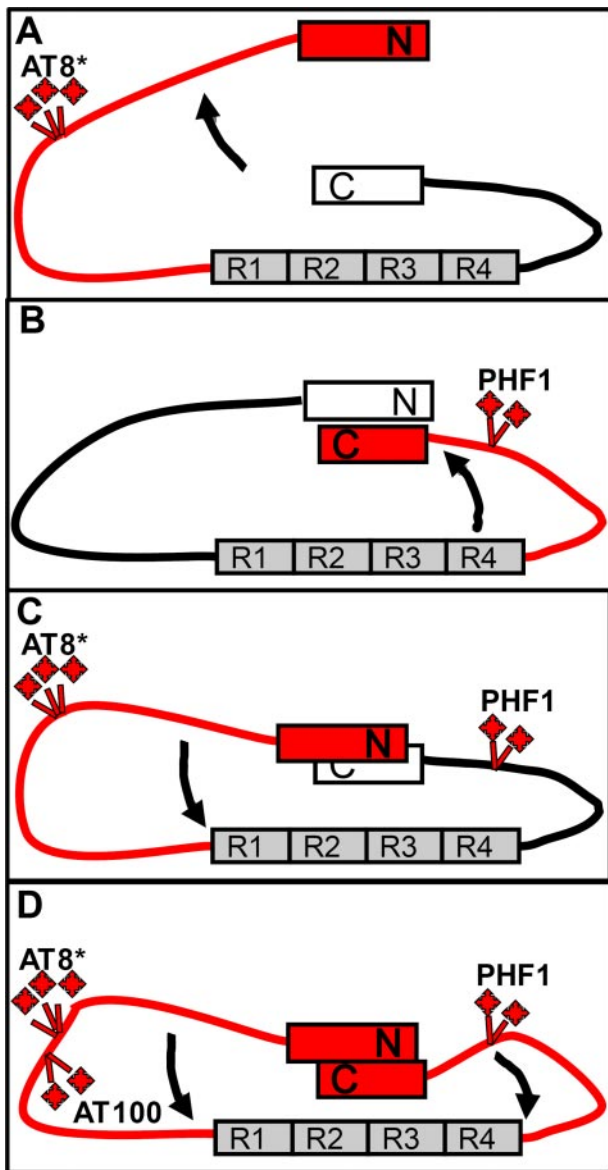
Altogether, the data support the view of a global conformation of Tau, which is regulated by phosphorylation at proline-directed sites in the microtubule-binding regions flanking the repeats. Nevertheless, all of the mutants show the spectroscopic

dues within FRET range. Conversely, the fact that FRET disappears upon exposure to GdnHCl supports the view that the polypeptide chain approaches a more random configuration, as expected for a denatured protein. The comparison illustrates the distinction between a "random" denatured protein and a natively unfolded protein with "global folding."

FIGURE 7. **Change in global conformation of Tau upon pseudo-phosphorylation.** *A*, pseudo-phosphorylation at epitope AT8* (S199E + S202E + T205E) loosens the paperclip structure by swinging the N-terminal domain away from the C-terminal domain. *B*, epitope PHF1 mimicking (S396E + S404E) also loosens the paperclip structure by swinging the C-terminal tail away from the repeats. *C*, combined mimicking of epitopes AT8* + PHF1 tightens the paperclip structure by swinging the N-terminal domain toward repeat domain. *D*, combined mimicking of epitopes AT8* + AT100 + PHF1 tightens the paperclip structure by swinging both the N- and C-terminal domains toward the repeat domain.

protective surroundings are removed, *e.g.* by cleavage or unfolding (63, 64). Contrary to these principles, we find that the compact pseudo-phosphorylated conformation forms aggregates somewhat more readily, whereas microtubule interactions show little change. A possible explanation is that the compactions of the paperclip takes place such that the amyloid-forming hexapeptide motifs in the repeat domain become exposed, which would then promote further aggregation. These issues must await further structural analysis, for example, by environment-sensitive tags.

REFERENCES

1. Jeganathan, S., von Bergen, M., Brutlach, H., Steinhoff, H. J., and Mandelkow, E. (2006) *Biochemistry* **45,** 2283–2293
2. Hirokawa, N., and Takemura, R. (2005) *Nat. Rev. Neurosci.* **6,** 201–214
3. Mandelkow, E., von Bergen, M., Biernat, J., and Mandelkow, E. M. (2007) *Brain Pathol.* **17,** 83–90
4. Garcia, M. L., and Cleveland, D. W. (2001) *Curr. Opin. Cell Biol.* **13,** 41–48
5. Binder, L. I., Guillozet-Bongaarts, A. L., Garcia-Sierra, F., and Berry, R. W. (2005) *Biochim. Biophys. Acta* **1739,** 216–223
6. Drubin, D. G., and Kirschner, M. W. (1986) *J. Cell Biol.* **103,** 2739–2746
7. Lee, G., Cowan, N., and Kirschner, M. (1988) *Science* **239,** 285–288
8. Goedert, M., Spillantini, M. G., Jakes, R., Rutherford, D., and Crowther, R. A. (1989) *Neuron* **3,** 519–526
9. Braak, H., and Braak, E. (1991) *Acta Neuropathol. (Berl.)* **82,** 239–259
10. Johnson, G. V., and Stoothoff, W. H. (2004) *J. Cell Sci.* **117,** 5721–5729
11. Hanger, D. P., Hughes, K., Woodgett, J. R., Brion, J. P., and Anderton, B. H. (1992) *Neurosci. Lett.* **147,** 58–62
12. Mandelkow, E. M., Drewes, G., Biernat, J., Gustke, N., Van Lint, J., Vandenheede, J. R., and Mandelkow, E. (1992) *FEBS Lett.* **314,** 315–321
13. Baumann, K., Mandelkow, E. M., Biernat, J., Piwnica-Worms, H., and Mandelkow, E. (1993) *FEBS Lett.* **336,** 417–424
14. Drewes, G., Lichtenberg-Kraag, B., Doring, F., Mandelkow, E. M., Biernat, J., Goris, J., Doree, M., and Mandelkow, E. (1992) *EMBO J.* **11,** 2131–2138
15. Drewes, G., Ebneth, A., Preuss, U., Mandelkow, E. M., and Mandelkow, E. (1997) *Cell* **89,** 297–308
16. Kishi, M., Pan, Y. A., Crump, J. G., and Sanes, J. R. (2005) *Science* **307,** 929–932
17. Drewes, G., Trinczek, B., Illenberger, S., Biernat, J., Schmitt-Ulms, G., Meyer, H. E., Mandelkow, E. M., and Mandelkow, E. (1995) *J. Biol. Chem.* **270,** 7679–7688
18. Bhaskar, K., Yen, S. H., and Lee, G. (2005) *J. Biol. Chem.* **280,** 35119–35125
19. Derkinderen, P., Scales, T. M., Hanger, D. P., Leung, K. Y., Byers, H. L., Ward, M. A., Lenz, C., Price, C., Bird, I. N., Perera, T., Kellie, S., Williamson, R., Noble, W., Van Etten, R. A., Leroy, K., Brion, J. P., Reynolds, C. H., and Anderton, B. H. (2005) *J. Neurosci.* **25,** 6584–6593
20. Gong, C. X., Liu, F., Grundke-Iqbal, I., and Iqbal, K. (2005) *J. Neural. Transm.* **112,** 813–838
21. Augustinack, J. C., Schneider, A., Mandelkow, E. M., and Hyman, B. T. (2002) *Acta Neuropathol. (Berl.)* **103,** 26–35
22. Brandt, R., Lee, G., Teplow, D. B., Shalloway, D., and Abdel-Ghany, M. (1994) *J. Biol. Chem.* **269,** 11776–11782
23. Illenberger, S., Zheng-Fischhofer, Q., Preuss, U., Stamer, K., Baumann, K., Trinczek, B., Biernat, J., Godemann, R., Mandelkow, E. M., and Mandelkow, E. (1998) *Mol. Biol. Cell* **9,** 1495–1512
24. Zheng-Fischhofer, Q., Biernat, J., Mandelkow, E. M., Illenberger, S., Godemann, R., and Mandelkow, E. (1998) *Eur. J. Biochem.* **252,** 542–552
25. Schneider, A., Biernat, J., von Bergen, M., Mandelkow, E., and Mandelkow, E. M. (1999) *Biochemistry* **38,** 3549–3558
26. von Bergen, M., Friedhoff, P., Biernat, J., Heberle, J., Mandelkow, E. M.,

(34). In the case of neurons, we speculate that multiple phosphorylation plus stabilization by other interactions may lead to the enhanced visibility of the pathological conformation seen in brain tissue.

Whether or not this conformation promotes aggregation directly or some other intermediate state (*e.g.* oligomers of Tau) remains open at present. From a structural perspective, the folding of the N- and C-domains over the repeat domain would be expected to protect against aggregation, and indeed Tau forms aggregates more readily when the non-repeat domains are cleaved off (5, 26, 57, 61, 62). This is reminiscent of other amyloid aggregation processes that are enabled only when the

and Mandelkow, E. (2000) *Proc. Natl. Acad. Sci. U. S. A.* **97,** 5129–5134

27. Smet, C., Sambo, A. V., Wieruszeski, J. M., Leroy, A., Landrieu, I., Buee, L., and Lippens, G. (2004) *Biochemistry* **43,** 2032–2040

28. Sontag, E., Nunbhakdi-Craig, V., Lee, G., Brandt, R., Kamibayashi, C., Kuret, J., White, C. L., 3rd, Mumby, M. C., and Bloom, G. S. (1999) *J. Biol. Chem.* **274,** 25490–25498

29. Chen, J., Kanai, Y., Cowan, N. J., and Hirokawa, N. (1992) *Nature* **360,** 674–677

30. Magnani, E., Fan, J., Gasparini, L., Golding, M., Williams, M., Schiavo, G., Goedert, M., Amos, L. A., and Spillantini, M. G. (2007) *EMBO J.* **26,** 4546–4554

31. Schweers, O., Schonbrunn-Hanebeck, E., Marx, A., and Mandelkow, E. (1994) *J. Biol. Chem.* **269,** 24290–24297

32. Mukrasch, M. D., Biernat, J., von Bergen, M., Griesinger, C., Mandelkow, E., and Zweckstetter, M. (2005) *J. Biol. Chem.* **280,** 24978–24986

33. Carmel, G., Mager, E. M., Binder, L. I., and Kuret, J. (1996) *J. Biol. Chem.* **271,** 32789–32795

34. Jicha, G. A., Bowser, R., Kazam, I. G., and Davies, P. (1997) *J. Neurosci. Res.* **48,** 128–132

35. Ghoshal, N., Garcia-Sierra, F., Fu, Y., Beckett, L. A., Mufson, E. J., Kuret, J., Berry, R. W., and Binder, L. I. (2001) *J. Neurochem.* **77,** 1372–1385

36. Lichtenberg-Kraag, B., Mandelkow, E. M., Biernat, J., Steiner, B., Schroter, C., Gustke, N., Meyer, H. E., and Mandelkow, E. (1992) *Proc. Natl. Acad. Sci. U. S. A.* **89,** 5384–5388

37. Skrabana, R., Kontsek, P., Mederlyova, A., Iqbal, K., and Novak, M. (2004) *FEBS Lett.* **568,** 178–182

38. Huang, W., and Erikson, R. L. (1994) *Proc. Natl. Acad. Sci. U. S. A.* **91,** 8960–8963

39. Leger, J., Kempf, M., Lee, G., and Brandt, R. (1997) *J. Biol. Chem.* **272,** 8441–8446

40. Haase, C., Stieler, J. T., Arendt, T., and Holzer, M. (2004) *J. Neurochem.* **88,** 1509–1520

41. Biernat, J., Mandelkow, E. M., Schröter, C., Lichtenberg-Kraag, B., Steiner, B., Berling, B., Meyer, H. E., Mercken, M., Vandermeeren, A., Goedert, M., and Mandelkow, E. (1992) *EMBO J.* **11,** 1593–1597

42. Goedert, M., Jakes, R., and Vanmechelen, E. (1995) *Neurosci. Lett.* **189,** 167–169

43. Hoffmann, R., Lee, V. M., Leight, S., Varga, I., and Otvos, L., Jr. (1997) *Biochemistry* **36,** 8114–8124

44. Greenberg, S. G., Davies, P., Schein, J. D., and Binder, L. I. (1992) *J. Biol. Chem.* **267,** 564–569

45. Otvos, L., Jr., Feiner, L., Lang, E., Szendrei, G. I., Goedert, M., and Lee, V. M. (1994) *J. Neurosci. Res.* **39,** 669–673

46. Barghorn, S., Biernat, J., and Mandelkow, E. (2005) *Methods Mol. Biol.* **299,** 35–51

47. Kim, Y., Ho, S. O., Gassman, N. R., Korlann, Y., Landorf, E. V., Collart, F. R., and Weiss, S. (2008) *Bioconjug. Chem.* **19,** 786–791

48. Hudson, E. N., and Weber, G. (1973) *Biochemistry* **12,** 4154–4161

49. Matsumoto, S., and Hammes, G. G. (1975) *Biochemistry* **14,** 214–224

50. Schuler, B., Lipman, E. A., and Eaton, W. A. (2002) *Nature* **419,** 743–747

51. Porzig, R., Singer, D., and Hoffmann, R. (2007) *Biochem. Biophys. Res. Commun.* **358,** 644–649

52. Eftink, M. R. (1991) *Methods Biochem. Anal* **35,** 127–205

53. Gamblin, T. C., Berry, R. W., and Binder, L. I. (2003) *Biochemistry* **42,** 15009–15017

54. Biernat, J., Gustke, N., Drewes, G., Mandelkow, E. M., and Mandelkow, E. (1993) *Neuron* **11,** 153–163

55. Cho, J. H., and Johnson, G. V. (2003) *J. Biol. Chem.* **278,** 187–193

56. Hirokawa, N., Shiomura, Y., and Okabe, S. (1988) *J. Cell Biol.* **107,** 1449–1459

57. Wille, H., Drewes, G., Biernat, J., Mandelkow, E. M., and Mandelkow, E. (1992) *J. Cell Biol.* **118,** 573–584

58. Dickson, D., Crystal, H., Bevona, C., Honer, W., Vincent, I., and Davies, P. (1995) *Neurobiol. Aging* **16,** 285–304

59. Mukrasch, M. D., von Bergen, M., Biernat, J., Fischer, D., Griesinger, C., Mandelkow, E., and Zweckstetter, M. (2007) *J. Biol. Chem.* **282,** 12230–12239

60. Fitzkee, N. C., and Rose, G. D. (2004) *Proc. Natl. Acad. Sci. U. S. A.* **101,** 12497–12502

61. Kampers, T., Pangalos, M., Geerts, H., Wiech, H., and Mandelkow, E. (1999) *FEBS Lett.* **451,** 39–44

62. Berry, R. W., Abraha, A., Lagalwar, S., LaPointe, N., Gamblin, T. C., Cryns, V. L., and Binder, L. I. (2003) *Biochemistry* **42,** 8325–8331

63. Dobson, C. M. (1999) *Trends Biochem. Sci.* **24,** 329–332

64. Uversky, V. N. (2007) *J. Neurochem.* **103,** 17–37

Curriculum Vitae

Name	:	Subashchandrabose Chinnathambi
Home address	:	Veerappalli, Thiriyalam post, Jolarpet (via), Vellore (dt)
		Tamil Nadu, India, 635851.
Date of Birth	:	22.05.1981
Nationality	:	Indian

University studies

1999-2002	:	Bachelor of Science (Microbiology), University of Madras
		Tamil Nadu, India.
2002-2004	:	Master of Science (Microbiology),
		Bharathidasan University, Trichirappalli, Tamil Nadu, India.
2005-2007	:	Junior research fellow in Prof. H.S.Savithri's lab,
		Indian Institute of Science, Dept of Biochemistry, Bangalore,
		Karnataka, India.

Doctoral study

05.2007- 09. 2011	:	Max-Planck-Unit for Structural Molecular Biology
		C/o DESY Hamburg, Germany, 22607.
Advisor	:	Prof. Eckhard Mandelkow
Title	:	**Influence of phosphorylation on the pathological conformation of human microtubule associated protein Tau**

Publications:

1) Pappachan, A., **Subashchandrabose, Chinnathambi**[#], Satheshkumar, P.S., Savithri, H.S., and Murthy, M.R. (2008). Structure of recombinant capsids formed by the beta-annulus deletion mutant rCP (Delta48-59) of Sesbania mosaic virus. Virology *375*, 190-196. (# second author; cover page).

2) Jeganathan, S., Hascher, A., **Subashchandrabose, Chinnathambi**, Biernat, J., Mandelkow, E.M., and Mandelkow, E. (2008). Proline-directed pseudo-phosphorylation at AT8 and PHF1 epitopes induces a compaction of the paperclip folding of Tau and generates a pathological (MC-1) conformation. J Biol Chem *283*, 32066-32076.

3) Pappachan, A., **Subashchandrabose, Chinnathambi**[#], Satheshkumar, P.S., Savithri, H.S., and Murthy, M.R. (2009). A single point mutation disrupts the capsid assembly in Sesbania Mosaic Virus resulting in a stable isolated dimer. Virology *392*, 215-221. (# second author; cover page).

4) Wegmann, S., Jung, Y.J., **Subashchandrabose, Chinnathambi** #., Mandelkow, E.M., Mandelkow, E., and Muller, D.J. (2010). Human Tau isoforms assemble into ribbon-like fibrils that display polymorphic structure and stability. J Biol Chem *285*, 27302-27313.

5) Shkumatov, A.V.*, **Subashchandrabose, Chinnathambi***, Mandelkow, E., and Svergun, D.I. (2011). Structural memory of natively unfolded tau protein detected by small-angle X-ray scattering. Proteins. (* equal first author).

6) Sadasivam Jeganathan*, **Subashchandrabose, Chinnathambi***, Mandelkow Eva., and Mandelkow, E.,(2011). Conformations of Microtubule-Associated Protein Tau mapped by fluorescence resonance energy transfer (FRET). Methods in Molecular biology, In press (* equal first author).

7) Stefan Bibow , Marco Mukrasch , **<u>Subashchandrabose Chinnathambi</u>** , Jacek Biernat , Christian Griesinger , Eckhard Mandelkow , and Markus Zweckstetter (2011). The Dynamic Structure of Filamentous Tau. *Angewandte Chemistry, International Edition, 50, 11520-11524*

8) Giovanni Coppola[*], **<u>Subashchandrabose Chinnathambi</u>**[*], et al., The Rare p.A152T Variant in MAPT is a Risk Factor for Neurodegenerative Disease, **Submitted** (*equal first author).

9) Venita Daebel, **<u>Subashchandrabose Chinnathambi</u>**[#]., Jacek Biernat, Antoine Loquet, Henrik Müller, Marc Baldus, Christian Griesinger, Eckhard Mandelkow, Vinesh Vijayan and Adam Lange Structural model of the core of Alzheimer-like paired helical filaments revealed by solid-state NMR. **Submitted**

Declaration (Erklärung)

I declare that I have carried out this thesis by myself and have not used external help except where explicitly indicated. This thesis is not submitted to any other university. I did not make any earlier attempt to submit this work as a doctoral thesis.

Subashchandrabose Chinnathambi

July, 2011

Hamburg

Hiermit erkläre ich, dass ich die vorliegende Arbeit selbständig und ohne fremde Hilfe verfasst, andere als die angegebenen Quellen und Hilfsmittel nicht benutzt und die den verwendeten Werken wörtlich oder inhaltlich entnommenen Stellen als solche kenntlich gemacht habe.

Ferner versichere ich, dass ich diese Dissertation noch an keiner anderen Universität eingereicht habe, um ein Promotionsverfahren eröffnen zu lassen. Hiermit erkläre ich auch, dass ich keine anderen früheren Versuche gemacht habe, die Arbeit zur Promotion einzureichen.

Subashchandrabose Chinnathambi

July, 2011

Hamburg